

Hygrothermal Performance of Structural Insulated Panels and Attics for Inuit
Communities

Ahmad Kayello

A Thesis

In the Department

of

Building, Civil and Environmental Engineering

Presented in Partial Fulfillment of the Requirements

For the Degree of

Doctor of Philosophy (Building Engineering) at

Concordia University

Montreal, Quebec, Canada

November 2018

© Ahmad Kayello, 2018

CONCORDIA UNIVERSITY
SCHOOL OF GRADUATE STUDIES

This is to certify that the thesis prepared

By: Ahmad Kayello

Entitled: Hygrothermal Performance of Structural Insulated Panels and Attics for Inuit Communities

and submitted in partial fulfillment of the requirements for the degree of

Doctor Of Philosophy (Building Engineering)

complies with the regulations of the University and meets the accepted standards with respect to originality and quality.

Signed by the final examining committee:

_____	Chair
Dr. Andrea Schiffauerova	
_____	External Examiner
Dr. Zaiyi Liao	
_____	External to Program
Dr. Yong Zeng	
_____	Examiner
Dr. Radu Grigore Zmeureanu	
_____	Examiner
Dr. Liangzhu Wang	
_____	Thesis Co-Supervisor
Dr. Hua Ge	
_____	Thesis Co-Supervisor
Dr. Andreas Athienitis	

Approved by _____
Dr. Fariborz Haghighat, Graduate Program Director

December 3, 2018

Dr. Amir Asif, Dean
Gina Cody School of Engineering and Computer Science

Abstract

Hygrothermal Performance of Structural Insulated Panels and Attics for Inuit Communities

Ahmad Kayello, Ph.D.

Concordia University, 2018

The extreme climate and remoteness of Inuit communities bring unique challenges to sustainable living. Homelessness and housing shortages are still common, underlining the need for the construction of durable, sustainable, and affordable housing. The building envelope is highly susceptible to moisture damage and deterioration if not well designed and constructed, especially in the Arctic. This thesis focuses on the heat, air, and moisture performance of structural insulated panels (SIPs) and attics in Arctic climates.

A full-scale SIP test hut with an attic is constructed in an environmental chamber. Eight types of SIP joints were monitored with thermocouples, with at least 6 thermocouples per joint. The SIPs were subjected to temperature differences of up to 62 °C and pressure differences up to 15 Pa. The attic of the test hut is divided into two bays, one is unvented and the other is ventilated mechanically. Imposed external temperature conditions reflect typical conditions observed in Inuit communities, and small pumps are used to deliver controlled rates of air leakage from the indoor space to the attics. The attic bays are monitored with temperature, relative humidity, and moisture content sensors.

Using hygrothermal simulation software WUFI Plus, a model is developed and verified with the experimental results. The model is then used to simulate the performance of

attics utilizing various ventilation strategies, including unvented and novel building integrated photovoltaic/thermal system (BIPV/T) ventilation methods, subjected to climatic conditions of three Inuit communities. The BIPV/T system uses solar energy to generate electricity while preheating outdoor air for attic ventilation. Various rates of air leakage are applied to examine the sensitivity of the attics under each ventilation strategy. Mold index is used to evaluate the long-term performance and suitability of each strategy.

It is found that while SIPs can be insulating and airtight, they are most susceptible to air leakage and moisture damage at the joints since they rely heavily on adhesive tape to prevent air movement. Complex joints where three panels meet are more leaky than joints where two panels meet. These joints are also more difficult to seal with tape. Joints above the neutral pressure plane are especially vulnerable to moisture damage since indoor air tends to exfiltrate through those joints.

Attics in Arctic climates can avoid mold growth with ventilation rates as low as 1 ACH, whether provided naturally or mechanically. Unvented attics are risky, though they can perform well if air leakage rates are kept within passive house standards. Also, diffusion vents improve the performance of unvented attics significantly. BIPV/T mechanical ventilation can dramatically improve attic hygrothermal performance while generating useful electrical and thermal energy, even at very high latitudes.

Acknowledgements

Firstly, I acknowledge that we are on unceded Kanienkehaka and Anishinaabe territory that has been unjustly taken by colonial powers through genocide and coercion to establish the state of so-called “Canada”. The issues we face today cannot be addressed properly without acknowledging history and putting our current problems in context. The Inuit are a truly wonderful people that have endured so much pain and suffering at the hands of the colonial regime, and they are still suffering the consequences of events that transpired in the last century. Our role as the “privileged” and “educated” is to remember the past and empower those who have been systematically oppressed, by helping them reclaim their culture, way of life, and sovereignty, hard as it may be.

I would like to thank the late Dr. Fazio who put me on this journey and saw in me what I could not. Thank you Mom, Dad, and Lima for your love and support all these years. Thank you to my love Christine Ghawi for the endless inspiration and uncompromising hope that you bring into my life. Thank you to my friends and family for being there for me: Seri Kombarji, Samer Kombarji, Maha Al Zaben, Ida Koraitem, Angel Lam, Colin Beattie, Stijn Van Nieuwenhove, Stephanie Van Goethem, Julian Maass, Carole Rickmouni, Clément Belleudy, Dan Baril, Firouzeh Souri, German Molina, Edvinas Bigaila, Costa Kapsis, and so many more. Thank you to everyone whose efforts were indispensable in making this project come to life: Dr. Jiwu Rao, Dr. Hua Ge, Dr. Andreas Athienitis, , Jeff Armstrong, Sara Wyss, Luc Demers, the late Jacques Payer, Olga Soarez, Lyne Dee, Guy Gosselin, Robbie Dale, Joe Hrib, and the helpful crew from Concordia Distribution.

Table of Contents

List of Figures	x
List of Tables	xv
List of Acronyms	xvii
CHAPTER 1 Introduction	1
1.1 Objective and Scope	3
1.2 Thesis Outline	3
CHAPTER 2 Literature Review	5
2.1 The Canadian North	5
2.1.1 Housing	5
2.1.2 Outdoor climate.....	7
2.1.3 Indoor Conditions.....	11
2.2 SIPs	11
2.2.1 Research on SIPs	12
2.2.2 SIPs in Extreme Cold Climates	16
2.2.3 Conclusion on SIPs and joints.....	19
2.3 Performance of Attics in Cold Climates	19
2.3.1 Research on Hygrothermal Performance of Attics	22
2.3.2 Attics in Extreme Cold Canada.....	29
2.3.3 Integrating Renewable Energy Technologies.....	31
2.3.4 Conclusion on Attics	31

CHAPTER 3	Experimental Setup – Methodology	33
3.1	Test Setup	35
3.1.1	Test Hut	35
3.1.2	Environmental Chamber	44
3.2	Instrumentation	45
3.2.1	Instrumentation Locations	47
3.2.2	Information on Sensors and Monitoring Methods	59
3.3	Equipment	63
3.3.1	Heating in Test Hut	63
3.3.2	Humidity Control in Test Hut	64
3.3.3	Air Pumps for Pressurization, Depressurization, and Attic Ventilation	66
3.3.4	Air Pumps for Attic Air Leakage	66
3.3.5	DC Power Supply Units	68
3.3.6	Electrical switching box (power supply)	68
3.3.7	Other	68
3.4	Test Procedure	69
3.4.1	SIP Joint Tests	69
3.4.2	Attic Tests	70
CHAPTER 4	Experimental Results	72
4.1	SIP Joints	72
4.1.1	-20°C and -40°C Exterior Temperatures	72
4.1.2	Temperature profiles at -20°C with pressurization and with tape seal	75
4.1.3	Temperature profiles at -20°C with and without tape seal	77
4.1.4	Other observations	79
4.2	Attic Tests	80

4.2.1	Test 1: -40 °C Outdoor Temperature	80
4.2.2	Test 2: -25 °C, -7 °C, 6 °C Outdoor Temperature	87
CHAPTER 5 Hygrothermal Simulation.....		94
5.1	SIP Joints.....	94
5.1.1	Methodology	94
5.1.2	Results	95
5.2	Comparison of Attic Experimental Results with Simulation.....	101
5.2.1	Methodology	101
5.2.2	Results	103
5.3	Long Term Performance of Attics Under Actual Climate Conditions	106
5.3.1	Methodology	106
5.3.2	Results	118
CHAPTER 6 Conclusion		132
6.1	SIP Joints.....	132
6.2	Attics	133
6.3	Contributions	136
6.4	Recommendations for Future Work	137
References		140
Appendix A Complete SIP Joint Results		158
Appendix B Complete Attic Simulation Results		173
Appendix C Airtightness Tests.....		183
Appendix D Electric MC Measurement Setup.....		185
Appendix E Collaboration in Development of Heat-Airflow Model.....		189

Appendix F Attic Hygrothermal Model Sensitivity Analysis	192
Appendix G Natural Ventilation CFD Analysis Results	197

List of Figures

Figure 2.1 Mean monthly temperature in five most populated Inuit communities in Canada, 1981–2010 (Environment Canada, 2013). Population indicated in legend obtained from 2011 Census of Population (Statistics Canada, 2014).....	8
Figure 2.2 Mean temperature data for Iqaluit, Nunavut from 1981–2010 (Environment Canada, 2013) and hourly temperature from a typical meteorological year.....	9
Figure 2.3 Mean absolute and relative humidity data for Iqaluit, Nunavut from 1981–2010 (Environment Canada, 2013) and hourly relative humidity from a typical meteorological year.....	10
Figure 2.4 Types of attic spaces.....	21
Figure 3.1 Test hut in environmental chamber	36
Figure 3.2 Three-dimensional rendering of test hut.....	37
Figure 3.3 Insulated I-joint connection	39
Figure 3.4 Insulated caps are used to fill most SIP joints. An example of installed thermocouples is also shown	40
Figure 3.5 Three-dimensional rendering of test hut with roof cutaway	41
Figure 3.6 vents in soffit of ventilated attic	42
Figure 3.7 HVAC system air supply in the environmental chamber	45
Figure 3.8 Instrumentation in the environmental chamber	48

Figure 3.9 Joint types monitored in this study	50
Figure 3.10 Sensor placement for joint type H (dimensions in mm).....	53
Figure 3.11 Sensor placement for joint types F, J, and L (dimensions in mm)	53
Figure 3.12 Sensor placement for joint types G, I, K, and M.....	54
Figure 3.13 Plan of test hut in environmental chamber showing location of monitored joints and other sensors	55
Figure 3.14 Section of attic bay with sensor locations	56
Figure 3.15 Three-dimensional view of an attic bay with sensor locations.....	57
Figure 3.16 Heaters used to heat the test hut	63
Figure 3.17 Humidifiers used in the test hut: evaporative (left) and atomizer (right)	64
Figure 3.18 Dehumidifier used in the test hut.....	64
Figure 3.19 Sample pump delivering air to attic spaces	66
Figure 3.20 Locations of air injection in the attic corresponding to each test	67
Figure 3.21 Air flow meter	68
Figure 4.1 Temperature profile of joint L with -20 °C exterior temperature with tape seal	75
Figure 4.2 Temperature profile of joint G with -20 °C exterior temperature with tape seal	76

Figure 4.3 Temperature profile of joint M with -20 °C exterior temperature with tape seal	77
Figure 4.4 Temperature profile of joint H with and without tape seal	78
Figure 4.5 Temperature profile of joint G with and without tape seal	79
Figure 4.6 Top-down view of joint M _A showing moisture accumulation	79
Figure 4.7 Temperature conditions for test 1: -40 °C outdoor temperature.....	80
Figure 4.8 RH conditions for test 1: -40 °C outdoor temperature.....	81
Figure 4.9 Humidity ratio trend in test 1: -40 °C outdoor temperature.....	83
Figure 4.10 Moisture content readings for test 1: -40 °C outdoor temperature	85
Figure 4.11 Temperature conditions for test 2: -25, -7, and 6 °C outdoor temperature....	87
Figure 4.12 RH conditions for test 2: -25, -7, and 6 °C outdoor temperature.....	88
Figure 4.13 Humidity ratio conditions for test 2: -25, -7, and 6 °C outdoor temperature.	90
Figure 4.14 Moisture content readings for test 2: -25, -7, and 6 °C outdoor temperature	92
Figure 5.1 Temperature profile of Joint L with values obtained from 2D simulation.....	96
Figure 5.2 Temperature profile of Joint M with values obtained from 3D simulation.....	97
Figure 5.3 Temperature profile of Joint K with values obtained from 3D simulation	97
Figure 5.4 Model of test hut in WUFI Plus	102

Figure 5.5 Measured and simulated temperature in the attics for test 2: -25, -7, and 6 °C outdoor temperature	104
Figure 5.6 Measured and simulated RH in the UA for test 2: -25, -7, and 6 °C outdoor temperature	104
Figure 5.7 Experimental and simulated RH conditions in the VA for test 2: -25, -7, and 6 °C outdoor temperature	105
Figure 5.8 WUFI Plus model of house and attic.....	107
Figure 5.9 Monthly average weather conditions in three Inuit communities	108
Figure 5.10 Roof ridge section with diffusion vent	109
Figure 5.11 Section of house showing attic ventilation path and filter media.....	110
Figure 5.12 Relative humidity in unvented attics with medium air leakage in Iqaluit...	118
Figure 5.13 Relative humidity in mechanically ventilated attics with medium air leakage in Iqaluit	119
Figure 5.14 Relative humidity in naturally ventilated attics with medium air leakage in Iqaluit	120
Figure 5.15 Relative humidity in BIPV/T naturally ventilated attics with medium air leakage in Iqaluit.....	121
Figure 5.16 Relative humidity in BIPV/T mechanically ventilated attics with medium air leakage in Iqaluit.....	122

Figure 5.17 Sheathing moisture content in select attics with medium air leakage in Iqaluit	123
Figure 5.18 Mold index in unvented attics in Iqaluit.....	125
Figure 5.19 Mold index in unvented attics with diffusion vents	125
Figure 5.20 Total monthly electrical energy generated with BIPV/T cladding.....	130
Figure 5.21 Total monthly thermal energy collected from BIPV/T cladding.....	131
Effect of porous membrane of ventilation rates.....	199
Effect of heat conduction and solar radiation on ventilation rate	200

List of Tables

Table 3.1 Building envelope characteristics of constructed SIP houses and test huts.....	38
Table 3.2 Sensors used to gather hygrothermal data	46
Table 3.3 Sensors in environmental chamber	47
Table 3.4 Sensors in test hut interior space.....	49
Table 3.5 Sensors in SIP joints	51
Table 3.6 Sensors used in each attic bay.....	56
Table 3.7 Pressure transducers used in this test.....	62
Table 3.8 Summary of SIP Joint tests.....	69
Table 3.9 Summary of Attic tests	71
Table 4.1 Steady state temperature values and differences for joint F at -20 °C and -40 °C with tape seal but without pressurization.....	73
Table 4.2 Steady state temperature values and differences for joint M at -20 °C and -40 °C with tape seal but without pressurization.....	74
Table 5.1 Thermal properties of simulated materials (Kumaran et al., 2002)	95
Table 5.2 RMSD values between experimental and simulation results.....	99
Table 5.3 Envelope elements connected to each attic bay as modeled in WUFI Plus ...	103
Table 5.4 Inuit communities investigated in this study	108

Table 5.5 Summary of Simulations	112
Table 5.6 Summary of Model Setup and Boundary Conditions.....	117
Table 5.7 Maximum mold index attained in each attic during 3-year simulation	127
Table 5.8 Total annual energy values, normalized with living area	131
Table 6.1 Summary of comments for each ventilation strategy	135

List of Acronyms

ACH – air changes per hour	OSB – oriented strand board
ASTM – American Society for Testing and Materials	PCM – phase change material
BIPV/T – building integrated photovoltaic and thermal	PIR – polyisocyanurate
CMHC – Canada Mortgage and Housing Corporation	PU – polyurethane
DAS – data acquisition system	PV – Photovoltaic
EC – environmental chamber	RH – relative humidity
EPS – expanded polystyrene	RMSD – root mean square deviation
GN – Government of Nunavut	RTD – resistance temperature detectors
GNT – Government of Northwest Territories	SIP – structural insulated panel
HAM – heat, air, and moisture	SBPO – spunbonded polyolefin
HVAC – heating, ventilation, and air conditioning	SPF – spruce-pine-fir
IGU – insulated glazing unit	T – temperature
IR – infrared	TC – thermocouple
IRC – Institute for Research in Construction	TH – test hut
ISR – Inuvialuit Settlement Region	VB – vapor barrier
LST – local standard time	WUFI – Wärme und Feuchte instationär
NBCC – National Building Code of Canada	XPS – extruded polystyrene
NECCB – National Energy Code of Canada for Buildings	
NHC – Nunavut Housing Corporation	

CHAPTER 1 Introduction

Shelter is one of the basic necessities of human living. Traditional indigenous peoples around the world have all developed sustainable building methods that use local materials, are appropriate for the local environment, and have virtually no negative ecological effects. The Inuit were such a nation, prior to colonization, who constructed sustainable forms of shelter such as the igloo. With their self-sufficient way of life, the Inuit were autonomous, free, and happy, especially compared to today.

Colonization in North America has had profound, detrimental effects on indigenous peoples, their culture, and the environment. In addition to genocide, mass displacements, and assimilation, the indigenous peoples have been stripped of their autonomy and are reliant on their colonizers for their livelihood. In the case of the Inuit, this process began quite recently in the 20th century. Permanent, wood frame construction for housing was introduced, which provided an immediate comfort, at the expense of self-sufficiency and self-reliance. Wood frame houses were essentially imported from the south and were not designed with the Arctic climate and culture in mind. A domino effect of issues ensued.

Whereas traditional housing required only body heat and animal oils for heating, wood frame housing requires non-renewable fossil fuels which must be imported at high costs. Lack of local skilled labor means the communities did not have the ability to build or repair these homes, and so labor would also be imported. The houses would often fail prematurely because of their poor design. Housing shortages and homelessness quickly became a chronic problem in most Inuit communities, and still is. This housing crisis, along with many other conditions imposed on the Inuit, has led to high rates of

depression, domestic violence, a wide array health issues, and suicide in these communities.

The solution, unfortunately, is not as simple as reverting to traditional ways of life, partly due to the influence of residential schools and assimilation on people's knowledge and affinity to their own culture and partly due to the apparent, immediate convenience and comfort of modern living. Efforts to improve the conditions in these communities should in the least empower locals to be able to construct and repair their own homes. Within the paradigm of permanent wood frame housing, the current status quo, new housing construction can benefit the communities if they are

- Designed to last, accounting for the extreme Arctic climate and lifestyle.
- Easy and quick to build such that the locals can learn how to build their own homes and rely less on imported labor.
- Energy efficient and well insulated. This will reduce consumption of fossil fuels, which are virtually the only source of energy used in Inuit communities.
- Simple and incorporate robust technologies that are easy to use, maintain, and repair.
- Inexpensive and use as little material as possible. Fewer materials also mean less shipping costs.
- Minimize reliance on fossil fuels and incorporate renewable energy technologies, particularly solar.

Of course, a crucial element to the effectiveness of a plan for improvement would be to involve the communities in generating ideas and empowering them to determine their own future. Such facilities are not well in place yet, but are warranted.

In recent years there have been some efforts to address the housing crisis, accounting for the points mentioned above. In 2009, 142 houses made of structural insulated panels (SIP)

were built in several communities across Nunavut. The design of the houses was simple, they were easy to build and could be done so quickly, and were well insulated. More recent versions of the SIP house incorporate an unvented attic, which prevent fine blowing snow from entering the attic space and damaging the building.

These developments in Arctic/Northern housing sound promising, but lack testing and evaluation. Industry is interested in the long-term feasibility of SIP systems and various attic designs, therefore in-depth studies are warranted.

1.1 Objective and Scope

In brief, the objectives of this thesis are as follows:

- To investigate experimentally the hygrothermal performance of SIPs subjected to Arctic climatic conditions.
- To investigate experimentally the comparative hygrothermal performance of unvented and ventilated attics subjected to Arctic climatic conditions.
- To investigate using hygrothermal simulations the comparative hygrothermal performance of attics of various ventilation strategies subjected to extreme cold climates.
- Explore the use of photovoltaic panels as cladding material that can also provide heated air to remove moisture from attic spaces.

The above objectives discussed in more detail in the following chapters.

1.2 Thesis Outline

Chapter 2 presents a literature review pertaining to the situation in the Arctic and Inuit communities, research on SIPs and joints in construction, and research on attics and attic ventilation. Chapter 3 details the experimental setup. Chapter 4 presents the results from

the experiment. Chapter 5 includes the hygrothermal simulation methodology and results for the SIPs and attics. Chapter 6 presents the conclusions, contributions, and suggested future work.

CHAPTER 2 Literature Review

To address durability issues of northern Canadian housing, a careful examination of the history and current state of the Inuit communities is done. SIPs and attics used in extreme cold climates are of particular interest, so a review of SIPs and attics is also carried out with a focus on hygrothermal aspects.

2.1 The Canadian North

Inuit Nunangat is an Inuktitut (Inuit language) term defined as the Inuit homeland in Canada, currently containing 53 communities. Inuit Nunangat (homeland) includes the Inuvialuit Settlement Region (ISR) in the Northwest Territories (6 communities), Nunavut (28 communities), Nunavik in northern Quebec (14 communities), and Nunatsiavut in northern Labrador (5 communities). These communities represent roughly 0.15% of the total population in Canada (Statistics Canada, 2014). Half of the Inuit population in Inuit Nunangat reside in Nunavut. All Inuit communities are accessible only by air or sea, with the exception of Inuvik, NT, which can also be accessed via the Dempster Highway.

2.1.1 Housing

Inuit communities undergo many challenges to sustain themselves, where housing is one of the major problems. Permanent housing in Inuit communities began in the mid-1950s as a result of a number of factors including the introductions of compulsory schooling, the end of the fur trade, and outbreak of infectious diseases (Tester, 2009). This almost

immediately sparked the housing crisis, where NHC was confronted with problems of suitability, adequacy, and affordability (Tester, 2009).

There are many challenges to living in the north today. All the materials needed to construct wood frame houses cannot be obtained locally, so they must be shipped from southern Canada. The same goes for skilled labor, which is flown over from the south. These imply high costs for housing construction. Also, residential electrical energy prices are 1.5 to 10 times more expensive than in southern regions of Canada (QEC, 2018). In fact, there is an almost complete dependence on fossil fuels for energy; diesel generators are used to produce electricity. Residential construction costs are 1.3 to 3.6 times higher than in larger southern cities (NRCC, 1997). Construction and mechanical equipment is often in short supply. Machines that break down cannot be quickly repaired since it would take weeks to obtain the parts and expertise necessary.

Housing shortage and crowding is an issue in many communities, as recent statistics suggests. Crowding in homes is defined as having more than one person per room (Statistics Canada, 2008), where rooms include bedrooms, kitchens, and living rooms. A survey of 1,901 Inuit households in Nunavut, ISR, and Nunatsiavut showed that 30% of Nunavut households were crowded (Minich et al., 2011). Crowding was found to be more prevalent in houses with children. One-fifth of Inuit homes surveyed provided shelter to the homeless.

Existing houses have exhibited numerous, systemic issues caused by poor design and construction. In a study on Inuit housing, it was found that 40% of surveyed homes were in need of major repairs while 20% reported mold problems (Minich et al., 2011).

Accelerated deterioration of these houses is caused by a number of factors including the extreme conditions, substandard building materials and construction, culturally inappropriate housing designs, and overcrowding (Minich et al., 2011). A large part of the solution is ensuring that new housing construction is durable, easy and quick to build, energy efficient, inexpensive, and culturally appropriate (Thirunavukarasu et al., 2015).

In 2009, Nunavut Housing Corporation's effort to address the housing issue saw 142 pre-engineered SIP houses constructed in several communities across Nunavut. The SIP system was chosen since houses can be built very quickly and easily. These SIP houses were single-family, single story, detached homes with cathedral ceilings measuring around 100 m² each. Since then, the SIP housing system has been modified to improve upon the earlier designs. A prototype SIP Duplex built in Iqaluit in 2012 uses wall and floor SIPs, but replaced the SIP cathedral roof for a truss roof with an unvented attic. The attic was chosen over the cathedral ceiling primarily because it can be better insulated. The attic was unvented to prevent fine snow from being blown into the attic and causing moisture damage. However, its hygrothermal performance is not well understood, so there is interest in understanding the long-term feasibility of using unvented attics. The indoor, outdoor, and attic conditions of this house are monitored as a part of an ongoing field study on attic venting (Baril et. al, 2013).

2.1.2 Outdoor climate

Whereas the southern Canadian cities are generally considered to be located in cold climate zones, the climate in Inuit communities is generally regarded as extreme cold. The number of heating degree-days in these communities is not less than 8500

(Environment Canada, 2013). There are communities at higher latitudes that are even colder, with up to 12,000 or so heating degree-days (Environment Canada, 2013).

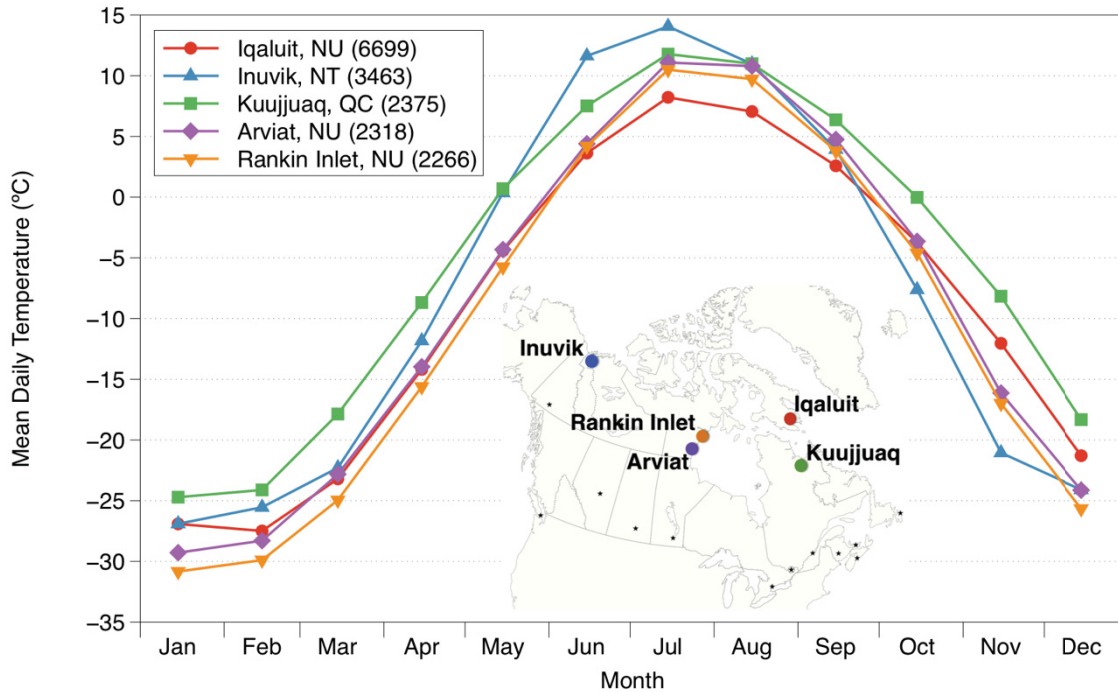


Figure 2.1 Mean monthly temperature in five most populated Inuit communities in Canada, 1981–2010 (Environment Canada, 2013). Population indicated in legend obtained from 2011 Census of Population (Statistics Canada, 2014)

Figure 2.1 shows the average monthly temperature conditions in the five most populated Inuit communities in Canada. The conditions in these communities is quite similar year round, the difference in their average monthly temperatures is up to 8 °C. Roughly 6 to 8 months a year, the temperatures are below freezing. Average monthly temperatures can go below -30 °C in the winter, and January is generally the coldest month. These communities are rather cool in the summer, where the average temperatures in the warmest month, July, are below 15 °C. It is interesting to note that increasing latitudes do not necessarily provide colder temperatures. Inuvik, located in northwest Canada with a latitude of 68°, is the northernmost community of the five and has a relatively warm climate. Rankin Inlet, located in central Canada with a latitude of 62°, is the coldest of the

five. Iqaluit is the most populated city, almost twice as much as the runner-up, and has a relatively average climate year-round, which makes it a good representative location for northern climate conditions.

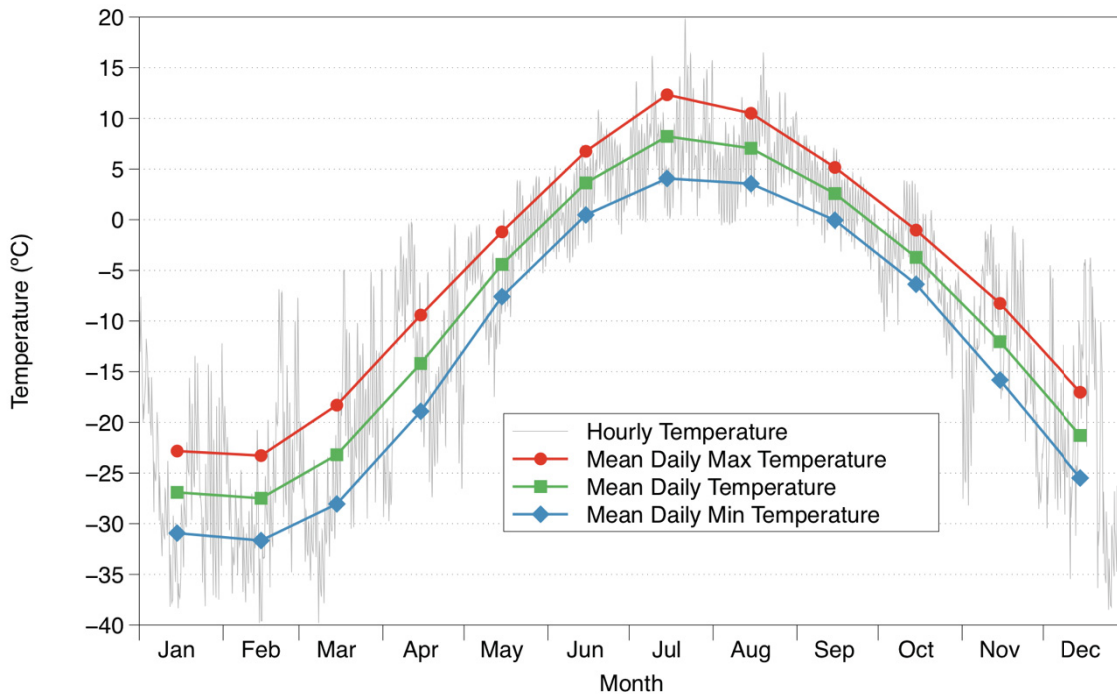


Figure 2.2 Mean temperature data for Iqaluit, Nunavut from 1981–2010 (Environment Canada, 2013) and hourly temperature from a typical meteorological year

Figure 2.2 shows the average and hourly temperature conditions in Iqaluit. In the summer, the outdoor temperature generally does not exceed 20 °C, while in the winter it can go as low as -40 °C. In fact, the design outdoor winter temperature for Iqaluit is -40 °C (NRCC, 2010; ASHRAE, 2013a).

Northern communities tend to have high relative humidity conditions year round, largely due to the proximity of these communities to large bodies of water. Figure 2.3 shows the average monthly relative humidity and moisture content conditions in Iqaluit, as well as hourly relative humidity conditions. The average monthly relative humidity is over 60% year round, and is generally higher in summer than in winter. The average relative

humidity in winter is between 60% and 70%, while in summer it is closer to 80%. The relative humidity regularly exceeds 90%, especially in the summer, approaching 100% at times. The air moisture content is extremely low in the winter due to the limited capacity for water vapor in the air at cold temperatures. Higher moisture content conditions can be seen in the summer and shoulder seasons, July having the highest values.

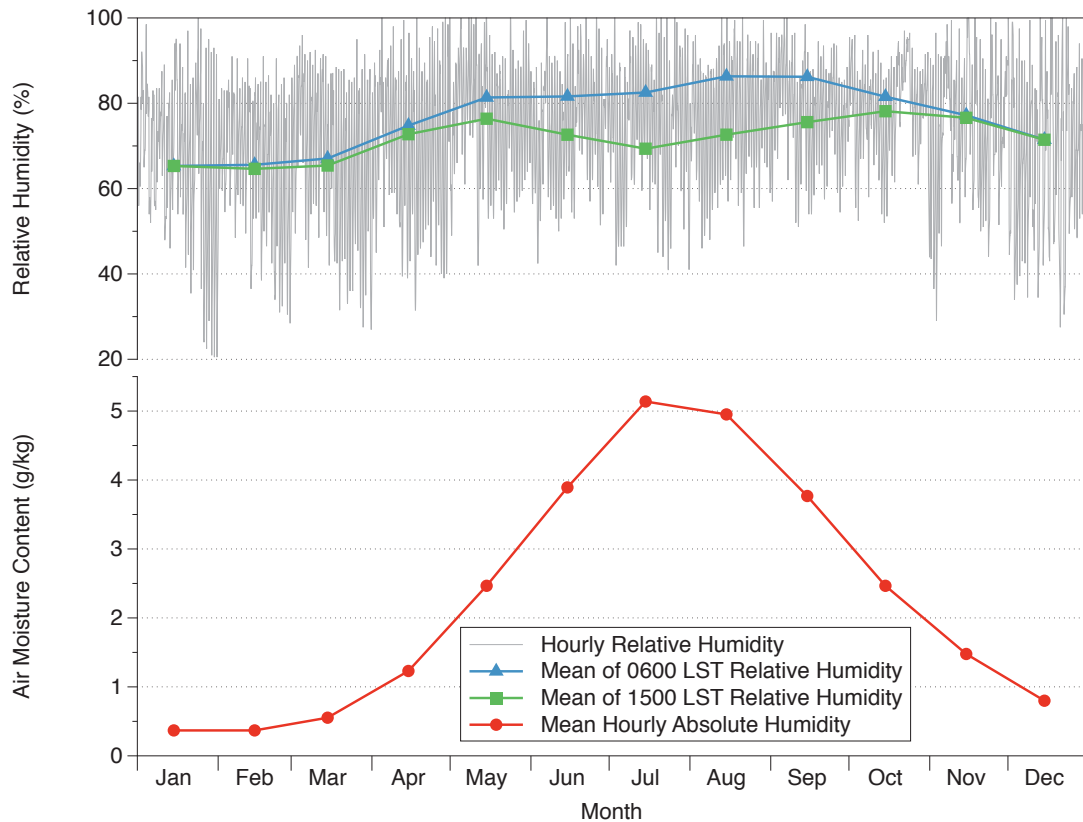


Figure 2.3 Mean absolute and relative humidity data for Iqaluit, Nunavut from 1981–2010 (Environment Canada, 2013) and hourly relative humidity from a typical meteorological year

Interestingly, although snowfall is much heavier in the north than in southern Canada, the roof loads are not as high. In fact, snow is readily blown off of roofs because of strong, undisturbed winds. However, snow in the Canadian north is very fine (often called “icing sugar snow”) and tends to blow into tiny openings in buildings and accumulate.

2.1.3 Indoor Conditions

Indoor conditions in Inuit houses are often quite warm and dry in the winter. A survey of houses in northern Canada showed that high occupancy does not automatically imply high indoor relative humidity or moisture related problems in a house (Rouseau et al., 2007). In Inuvik, where the climate is extremely cold and dry, reported problems in public housing include formation of dew, frost, and mold growth on windows. Average indoor temperature was found to be 25.5 °C in winter (Rouseau et al., 2007). The average relative humidity was consistently below 30%, indicating very dry conditions; this is primarily due to the houses being very leaky. The bath and kitchen areas do get high relative humidity peaks, however.

2.2 SIPs

Structural insulated panels (SIP) building envelope systems are intended for high performance housing and lightweight commercial construction. SIPs are made of a rigid, insulating core material sandwiched between two layers of structural board, bound using an adhesive. The insulating core is often made of expanded polystyrene (EPS), extruded polystyrene (XPS), polyisocyanurate (PIR), or polyurethane (PU). The structural boards are commonly made of plywood, oriented strand board (OSB), sheet metal, or cement. As the name suggests, SIPs provide the structural support and thermal insulation for a building, but can also act as the air and vapor barrier. The thickness of SIPs generally depends on the insulation requirements of the building. The term SIP can be used interchangeably with sandwich panel.

The concept of the SIP originated in 1935 at Forest Products Laboratory in Madison, Wisconsin (Smith, 2010). The aim was to develop housing that was energy efficient and low-cost, while minimizing use of resources. Test houses made of SIPs were built and monitored for over three decades. By 1952, SIPs became commercially available, but were not widely accessible and affordable until the 1960s (Smith, 2010). Though SIPs have been shown to perform very well as a building envelope system, they have yet to become universally adopted.

2.2.1 Research on SIPs

SIPs have been subject to countless studies across many engineering disciplines. The majority of the research conducted on SIPs relates to their structural performance. The structural aspects of SIPs have been investigated experimentally and using models for decades and continue to be studied in the 21st century (Ha & Fazio, 1978; Taylor et al., 1997; Mousa & Uddin, 2012; Smakosz & Tejchman, 2014). One of the major benefits of SIPs is their accelerated and simplified construction. Mullens and Arif (2006) studied the influence of SIPs on the residential construction process by comparing the erection of a SIP house and a similar wood-frame house. SIPs required 66% less site framing labor for walls and roofs as compared to wood-framing; cycle times were reduced by a similar magnitude. Though they increase costs, features such as cut-to-size and pre-installed splines have significant positive impact on the construction process (Mullens and Arif, 2006). The SIP system is often considered in the design and evaluation of high performance and net-zero energy buildings, both on the field and with computer-aided simulation (Christian, 2007; Horvat et al., 2009; Broniek, 2010; Hales & Howard, 2013).

SIPs have also been evaluated under extreme situations. Mousa and Uddin (2013) tested experimentally the effects of floodwater exposure to the structural performance of composite SIPs, concluding that the strength degradations were small and that SIPs would survive a flood event. One study compares the performance of different wall systems for single-family homes under various hazard conditions (Memari, 2012). Findings include that SIPs perform rather well with earthquakes and tornadoes, less so with hurricanes and floods, and poorly with fire. The high flammability of the polystyrene core is one of the main factors for the poor performance of SIPs in fires. Another study looks at the influence of the SIP design on its fire performance through experimental testing (Collier & Baker, 2011). Using SIPs with metal facings, the authors found that maintaining the integrity of the metal skins and the fasteners sealing the panels' joints had a significant positive impact on the fire performance of the SIPs (Collier & Baker, 2011). One study assesses the integration of phase change materials (PCM) with SIPs to increase and locate the thermal mass within the SIPs, thereby reducing heat transfer (Medina et al., 2008).

SIPs have also been examined with regards to their hygrothermal performance, though not nearly to the same extent as their structural performance. Pankratz and Holm (2004) investigated the use of hygrothermal simulation software to aid in the design of a novel SIP, ensuring good performance with regards to building physics. The constructed SIP was then monitored on the field and the results agree well with simulation, which showed that simulation can be used to develop hygrothermally safe construction. Another study by Pratinthong et al. (2005) subjects steel faced SIPs with either PU, rock wool, or glass wool insulation to outdoor climates of French Guiana and Finland for one year. These

two climates represent hot and cold climates, respectively. Condensation was found on the inner steel facing in French Guiana and on the outer steel facing in Finland. PU insulation had the best thermal and moisture performance of the three.

Existing studies through both experiments (Cunningham, 1993; Desmarais et al., 2000; Simonson et al., 2005; Rao et al., 2009; Slanina & Šilarová, 2009; Langmans et al., 2012; Alev & Kalamees, 2016; Goto et al., 2016) and modeling (Ojanen & Kumaran, 1996; Jansens & Hens, 2003; Saber et al., 2012; Younes & Abi Shdid, 2013; Belleudy et al., 2015) indicate that imperfections and consequential air leakage in the building envelope have significant impact on the hygrothermal performance of building envelopes. Similarly, the weak spots of SIPs, and prefabricated envelope systems in general, are often the joints, not the main section of the panel or panelized system. Thermal bridging and air leakage at the joints of prefabricated constructions have become more important with regards to hygrothermal performance, though studies are scarce. Panjehpour et al. (2013) reviewed the current status of SIPs as a building material. They conclude that improving the thermal performance and airtightness of SIP joints is a key milestone for the future of SIPs.

Abdou (1997) conducted an experiment to evaluate the thermal performance of 25.4 mm (1") and 76.2 mm (3") fiber-reinforced plastic panels, a type of SIP. Thermocouples and test plates were used to find the heat flux through the center of the panels as well as the joints, with and without the joint sealant. The thermal resistance values at the joints were found to be lower than at the center of the panel. Also, the overall R-values of the panels increases by 5-46% after the joints had been sealed, which shows how significant the influence of air leakage can be and that the tightness of the joints without sealant can vary

considerably. The study is limited to one type of joint and does not consider the effects of air pressure differences. Also the testing temperatures range between 27 to 58 °C.

One field study by Asiz et al. (2008) recognizes the importance of the heat, air, and moisture performance of joints in prefabricated construction. In this study, a house in New Brunswick composed of prefabricated, panelized wood-frame walls is monitored for two years with temperature, relative humidity, and differential pressure sensors at the joint and the clear areas of the panels. Findings include that the air leakage occurred mainly at the joints and that the leaking air contributed to drying of the joint materials. Little evidence of moisture accumulation in the joints was found. The authors also remark on the lack of existing studies on the hygrothermal performance of prefabricated construction.

Newell & Newell (2011) investigated the cost-effectiveness of sealing the SIP joints of a net-zero house, known as Equinox House. They measured the air leakage rate of the building at 50 Pa at several stages during the caulking process. The ACH of the house at 50 Pa before and after caulking the joints were 3.0 and 0.5, respectively, indicating a heavy reliance on the joint sealing for airtightness. The additions of drywall further improved the airtightness from 0.5 to 0.4 ACH at 50 Pa. They also indicate lack of information on the air leakage characteristics of specific SIP joints, such wall to wall, wall to floor, and wall to roof.

Okamoto et al. (2012) conducted an experiment to study the thermal performance and condensation potential of a vertical joint in a wood-frame assembly. The wall was configured such that rigid insulation is placed on the exterior of the sheathing and no

insulation is placed between the studs. Thermocouples were installed along the thickness of the joint and at five different heights. The gap between the exterior insulation panels is varied between 0 to 10 mm, though the sheathing remained continuous. The outdoor and indoor temperature were 8 °C and 33 °C respectively. The thermal resistance of the joint was found to decrease with increasing gap thickness. With a 10 mm gap and no Spun-bonded Polyolefin (SBPO) on the exterior of the insulation, the thermal resistance of the joint decreases by 30%. Condensation was found not to be an issue if the indoor relative humidity was below 80%.

2.2.2 SIPs in Extreme Cold Climates

Recent efforts have been made to build sustainable housing for the North made of structural insulated panels (SIP). SIP houses can be built quickly and easily (Mullens & Arif, 2006), and a number of studies have identified SIP construction as one of the suggested high performance building envelopes for the Arctic (CMHC, 2001; Saïd, 2006; Cornick et al., 2009; Adams et al. 2013).

A field evaluation of SIPs as an alternative to wood frame construction in the north was performed in Repulse Bay, Nunavut (CMHC, 2001). The SIP system required 45% less time to construct compared to a wood frame house, and semi-skilled worker readily acquired the skills needed to build with SIPs. The cost of the materials and transportation for SIPs was comparable to wood frame construction, higher by only 2.4%. The SIP system weighed about 35% less than equivalent wood frame construction, and generated significantly less on-site waste. The SIP house was found to be very airtight, achieving 0.49 ACH at 50 Pa. The R-2000 requirement is 1.5 at 50 Pa, and the Passive House

requirement is 0.6 at 50 Pa (Passive House Institute, 2016). The locals that reside in the SIP house expressed satisfaction with the house as well.

At Summit Station, Greenland, an administration building composed mainly of SIPs was examined for its thermal performance after more than 20 years of service (Barna et al., 2012). The wall SIPs were 127 mm thick, constituting of a PIR insulation core and OSB facings. An IR camera was used to inspect the thermal performance of the envelope, while data loggers recorded temperature and relative humidity data indoors. Variations in indoor humidity were found to coincide with occupant activity, such as showering and cooking, and were not a function of the number of occupants (Barna et al., 2012). IR imagery showed that the joints between the walls and the roof exhibited noticeable thermal bridging, less so elsewhere. Using both IR imagery and a blower door, the air leakage characteristics were investigated. The joints between the wall SIPs were found to leak very little air, even after the building had been lifted on its steel supports several times over the years. Given its age, the building was found to perform very well.

There have also been reports of SIP houses failing in Arctic climates. SIP houses built in Juneau, Alaska encountered moisture problems in their roofs only six years after construction (SIPA, 2002). Improper sealing of the joints allowed warm, moist air to migrate through the joints and condense at the exterior facing. The occurrence emphasizes the importance of design and workmanship for these building systems to perform as expected.

The thermal performance of SIPs and SIP joints in extreme cold climates has been investigated experimentally recently at Concordia University (Wyss, 2011; Wyss et al.,

2015). An inverted SIP test hut, where the cold conditions are reproduced inside the test hut and exterior conditions are the ambient room conditions, provided the experimental setup. The SIPs in this system were designed for the Canadian north and are 304.8 mm (1') thick, containing an EPS insulation core and OSB facings. Several thermocouples were installed along the thickness of the SIPs, both near the center of the panel and at the joint between two aligned wall SIPs. These joints incorporate a wooden I-joist spline, which is thermally broken. The wood based materials in the SIPs were instrumented with moisture content sensors as well. Tests were conducted where the conditions inside the inverted test hut are brought down to -10 °C, -20 °C, and -30 °C, and for each of those temperatures thermal steady-state conditions were attained. The results showed that the design of the joint with the incorporated thermal break was effective in attenuating heat losses. The author also indicates that air leakage, not conduction, is the most significant cause of heat losses through the joints, and that air leakage caused by defects and cracks in the joints are the most likely failure mechanism for this system. However, tests with pressure differentials were not conducted in the study. The findings from the moisture content sensors were inconclusive since the change in the moisture content of the wooden materials in the SIPs changed extremely slowly and no significant variations were found during the testing periods, which lasted a few days each. The author's suggestions for future work include studying the panels at lower temperatures, carrying out tests with higher indoor relative humidity levels to reflect overcrowding in homes, and to test other connections like wall-to-roof and wall-to-floor, which are not possible with the inverted test hut setup.

There has also been research in combining SIPs with BIPV/T technology to produce highly insulating and energy generating envelope assemblies for northern climates (Chen et al., 2012a; Chen et al., 2012b).

2.2.3 Conclusion on SIPs and joints

Literature indicates that there are significant gaps with the evaluation of SIPs. Though it is known that SIPs are most susceptible to heat, air, and moisture problems at the joints, there have been no studies investigating the performance of the many joints formed by a SIP assembly. Since the SIP system is being implemented in Arctic climates, they need to be evaluated under corresponding conditions. The study by Wyss et al. (2015) is the most in depth with regards to SIP joints in extreme cold climates. However, it examines only one joint, without pressurization. The authors suggest that other joints should be tested as well. This study aims to evaluate the suitability of SIPS in extreme cold climates by experimentally evaluating the hygrothermal performance of SIP joints under large temperature differences, as well as pressure differences.

2.3 Performance of Attics in Cold Climates

By general definition, the attic is the space below a sloped roof of a building, usually a house. The space exists because of the need to have a sloped roof, primarily for snow shedding but also for architectural reasons. The attic space may or may not be separated from the space below it with a horizontal partition. If it is not, the sloped roof itself becomes the ceiling and the thermal, vapor, air, and moisture barriers are placed at the plane of the roof. This is called a **cathedral ceiling**. If the four barriers are in that same location, but the attic is separated from the space below with a horizontal partition, it is

called a **cathedralized attic**. A cathedralized attic is either directly or indirectly conditioned. The roof construction of cathedral ceilings or cathedralized attics can be vented or unvented, but space below the roof is effectively part of the indoor space and is never vented. Where the moisture barrier is on the plane of the sloped roof, and the three other barriers are located at the plane separating the attic from the space below, it is called an **unconditioned attic**. In this thesis, an unconditioned attic is simply referred to as an **attic**. Attics can be **vented** or **unvented**. A vented attic can be passively ventilated, where wind and stack effect drive air exchange between the unconditioned attic and outdoor air, or mechanically ventilated, where a fan is used to actively ventilate the attic with outdoor air. Generally, an unvented attic has no intentional vents but background air exchange can still occur. An unvented attic can also be sealed, such that the unconditioned attic itself is separated from the outdoor space with an air barrier. Figure 2.4 illustrates the various attic types.

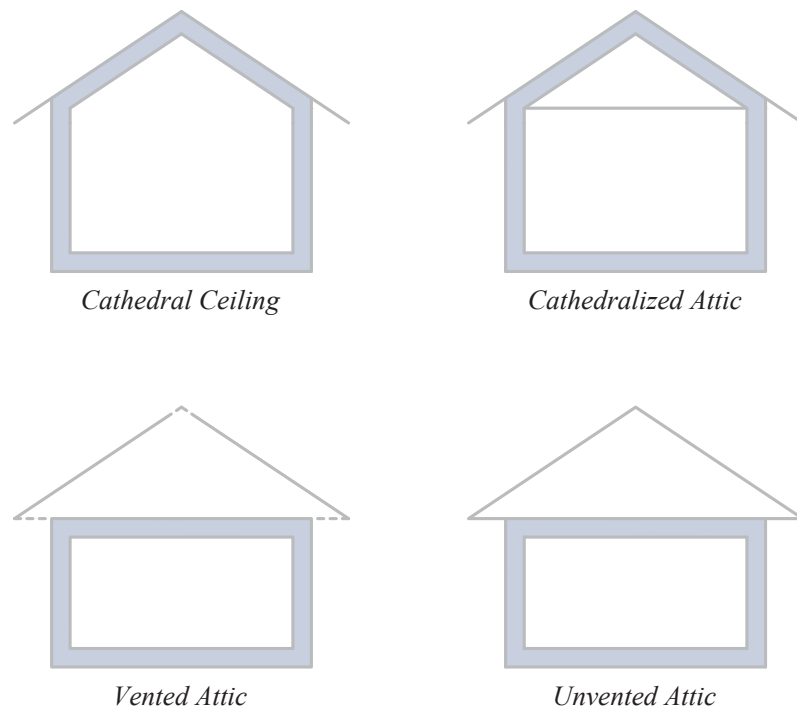


Figure 2.4 Types of attic spaces

The reason for clarifying the terminology is because of the inconsistency and use of misleading terms in literature, an issue also addressed by Lstiburek (2014). Cathedralized attics are sometimes referred to as unvented attics (Pallin et al., 2013) (Lstiburek, 2006). Attics, or unconditioned attics, are sometimes called cold attics (Blom, 2001; Nik et al., 2012; Harderup & Arfvidsson, 2013) because they are unheated; this term can be misleading because in warmer seasons or climates, the attic space can be warmer than the outdoors. Even attics in the Arctic experience temperatures above 25 °C (Baril et. al, 2013).

Ventilating attics has become common practice in nearly all climates. The benefits of attic venting include moisture control, reduction of cooling loads in hot climates, avoiding ice dams in cold climates, and extending the service life of the roofing materials by lowering their temperatures. By reducing the moisture levels in the attic, biological

degradation of wood based materials through mold or decay is decreased. Attic ventilation removes heat build-up in the winter that can melt snow on the roof, causing ice dams and icicles. Ice dams, in turn, can lead to infiltration of the melting water into the attic.

Most attics are vented such that ventilation occurs passively. The drivers for passive ventilation are the pressure differences caused by wind and stack effects (Forest & Walker, 1992), where wind is the main driver (Forest & Walker, 1993). The ventilation rate is actually highly dependent on wind speed and wind orientation (Forest & Walker, 1992; Walker & Forest, 1995; Fugler, 1999). Stack effect, on the other hand, utilizes the buoyancy of the warmer attic air and the temperature difference between the attic and the outdoor air. If an attic is highly insulated, however, the heat build-up becomes a non-issue and ventilation is not needed for that purpose. Ventilation would still be needed to remove the moisture entering the attic from the indoor space. Actually, higher ceiling insulation levels and lack of sufficient ventilation caused by the chimney effect are the main reasons for moisture and mold damage in attics in Sweden (Harderup & Arfvidsson, 2013). Passive attic ventilation often occurs through soffit vents, roof vents, ridge vents and gable vents. Using soffit vents in conjunction with ridge vents is generally the most effective venting strategy (Forgues, 1985).

2.3.1 Research on Hygrothermal Performance of Attics

The earliest hygrothermal studies on attics and attic venting have been performed as early as the 1930s. Experimental studies by Rowley et al. (1939) provided the first documented

evidence of reduced condensation by attic ventilation. Scaled-down test houses with either no ventilation, natural ventilation, or mechanical ventilation of the attics were tested in a conditioned room. Mechanical and natural ventilation effectively eliminated condensation when the exterior temperature was -23°C , and reducing ventilation produced condensation. They also recommended indoor humidity control as a way to reduce attic condensation. In 1948, Britton, unaware of Rowley's work, conducted tests on vented and unvented flat roof assemblies in a climatic chamber over several weeks (Rose, 1995; TenWolde & Rose, 1999). The results provided further support for attic ventilation, while highlighting the importance of airtightness and vapor barriers. Also in 1948, Jordan et al. performed field tests on three attics in Wisconsin during the winter (TenWolde & Rose, 1999). In all three houses, higher indoor humidity conditions corresponded with higher attic humidity conditions (TenWolde & Rose, 1999) suggesting a strong relationship between the two zones. In fact, Jordan et al. concluded that moisture in the attic is more a function of indoor humidity than of vapor barriers or ventilation (Rose, 1995). The authors also suggest that higher attic ventilation rates may be needed in highly insulated attic, even if a vapor barrier is installed (Rose, 1995). The 1:300 attic ventilation rule of thumb, which states that for every 300 square units attic floor area there should be 1 square unit of attic vent, first appeared in 1942 in "Property Standards and Minimum Construction Requirements for Dwellings" published by the United States' Federal Housing Authority without any explanation or attribution (Rose, 1995). This rule is currently used in many codes and standards, such as in Quebec (2018), even though it is unfounded. In 1949, a publication called "Condensation Control in Modern Buildings" was released, based primarily on the work by Jordan et al. and Britton; it served as a basis

for nearly all standards and regulations thereafter (Rose, 1995). Since then, there have been many studies on the thermal and hygrothermal performance of attics. Some studies examine unventilated attics as well.

Importance of Airtightness

By far, attic ventilation is the most closely watched and regulated moisture control mechanism compared to airtightness and vapor barriers (Rose, 1995), but many studies suggest that airtightness cannot be overlooked and demands to be regulated. Early research on attic moisture performance generally concluded that moisture problems in the attic can be avoided using a vapor retarder (TenWolde & Rose, 1999). Later research would show that air infiltration is the major source of moisture in attics and that a vapor barrier is not an effective way of managing attic moisture (Hinrichs, 1962; Dutt, 1979). Most moisture enters the attic from the indoor space via air leakage (Forgues, 1985). A study on the hygrothermal performance of exterior walls in winter (Madison, WI) using computer simulation showed that the vapor barrier is only effective if air leakage is eliminated (Burch & TenWolde, 1993). In fact, vapor diffusion is only significant in the absence of air leakage (Rose, 1995). One study showed that the amount of moisture accumulating in the building envelope was directly linked to rate of air exfiltration (Ojanen & Kumaran, 1996). A long-term field study of attics in Edmonton and Vancouver noted that higher indoor relative humidity conditions corresponded with higher attic moisture levels, regardless of the attic ventilation rate (Sheltair Scientific, 1997). Essentially, minimizing heat and moisture transport from the indoor space to the attic is the most effect method of preventing moisture problems (Fugler, 1999). Also, the

initial moisture in the construction materials, known as construction damp, should not be overlooked (Nik et al., 2012).

Attic Ventilation

The purported benefits of attic venting have also been questioned. The 1:300 rule has generally been found to be effective in houses where the ceiling exhibits significant air leakage (Fugler, 1999). Though rarely exacerbating moisture problems, attic venting has been shown to play a relatively small part in the control of attic moisture (Fugler, 1999). In cool, marine climates, attic venting has been shown to increase the moisture levels in wood members, and so lower ventilation rates, below that provided by the 1:300 standard, are being suggested (Fugler, 1999). The University of Alberta (Forest & Berg, 1993) predicted through a validated computer model that generally the 1:300 code requirement provides too much ventilation in Canadian marine climates (Vancouver, Halifax, St. John's) and the dominant moisture source for the attic is the outdoor air. Furthermore, they predicted that the ceiling airtightness had little impact on the sheathing moisture contents and virtually did not affect the quantity of moisture deposited by condensation. They suggested that sheathing moisture content can be reduced by sealing the attic or at least substantially reducing vent area by not installing any vents and relying only on the background leakage of the attic envelope. A long-term field study of attics in a cool, marine climate (British Columbia) was conducted to identify the contributing factors for moisture problems and mold growth (Roppel et al., 2013). They conclude that providing adequate venting and ensuring an airtight ceiling are not sufficient to control moisture and limit mold growth in such climates, and that more ventilation does not solve problem.

With unvented attics, the indoor air becomes more influential than the outdoor air (Fugler, 1999) and the air tightness of the ceiling becomes all the more important. Forest and Walker (1993) performed a two-year field study on two test houses in cold climate, where one had no intentional vents and the other had traditional soffit and ridge vents; the study was also extended with simulations using a validated model. Their results showed that where the ceiling allows for significant air leakage, the unvented attic will have higher moisture levels in the materials than the vented attic. However, if the attic is airtight, increasing the attic ventilation will result in higher moisture levels in the attic materials. Rose (1992) conducted a two-year field study of residential attics in Illinois, where temperature and moisture conditions in vented and unvented attics and cathedral ceilings were monitored. It was found that after two winters, unvented and vented attics exhibited similar moisture performance when the ceiling was airtight. Samuelson (1998) performed a year-long field experiment in Sweden with an attic divided into similarly sized bays. The bays were either unvented, naturally ventilated, or mechanically ventilated; either mineral wool or cellulose was used as insulation. It was found that if there is no air leakage from the indoor space to the attic, the climate in the attic becomes drier with less ventilation.

Harderup and Arfvidsson (2013) conducted a study with field measurements and simulations to evaluate the moisture performance of attics in Sweden. They found evidence that reduced ventilation rates decrease the risk of moisture damage. It is suggested that ventilation is needed during the construction phase, but that decreased ventilation during operation can have good results provided that the ceiling's airtightness can be guaranteed for the life of the building. Ojanen (2001) performed a long-term field

study to evaluate the performance of a sealed attic with a vapor-permeable moisture barrier, also called underlay, in Finnish climate. An attic divided into five sections provided the test setup; the attic bays were either ventilated or sealed, with either concrete tile or steel plate roofing. Measurements were obtained from temperature, relative humidity, and moisture content sensors as well as gravimetric sample. The air leakage from the indoor space to the attics was controlled. The moisture performance of the sealed attics performed as well as the ventilated attics. The sealed attics dried just as well as the ventilated attic in winter and exhibited better drying efficiency in the summer. Also, Essah et al. (2009) performed simulations which suggest that if a vapor-permeable underlay is used and the ceiling is relatively airtight, attic ventilation is not necessary.

In very cold climates, ventilating attics with outdoor air is not an effective way of removing moisture due to the low capacity of the air to absorb moisture (Forgues, 1985; Samuelson, 1998; Fugler, 1999). Actually, the wood members in the attic have more moisture removal and storage capacity than the cold winter air (Fugler, 1999). Also, most of the moisture that enters the attic will quickly condense on cold surfaces such as the sheathing or the cold side of the insulation. However, ventilation does help when the outdoor temperature gets warmer and can absorb more moisture (Forgues, 1985).

Because the outdoor conditions do not always assist with drying the attic space, it can be beneficial to ventilate the attic only when the conditions are favorable. Hagentoft and Sasic Kalagasidis (2010) performed field experiments on houses in Stockholm, Sweden along with hygrothermal simulation to study the performance of attics that are sealed and fitted with adaptive ventilation systems. This ventilation system only runs when the outdoor air has potential to dry the attic. Results show that adaptive ventilation reduces

the risk of mold growth and provides more stable and lower relative humidity levels during the winter than the cold attics with traditional ventilation design. Adaptive ventilation has been suggested as the most effective method of avoiding mold growth in attics (Nik et al., 2012)

Studies Using Hygrothermal Simulation

Thermal models were being developed and validated as early as the late 1970s, and moisture models were being attempted since the 1980s (Rose, 1995). Burch et al. (1984) validated an attic condensation model with data collected from a short-term experiment with a small test house in a climatic chamber. The test house was pressurized and holes were made in the ceiling to simulate air leakage into the attic space from the indoor space. The authors noted that, unexpectedly, no condensation was not observed during the 12-day test, where the outdoor temperature would be as low as -12 °C, and that it would take the order of months for the wood materials in the attic to attain moisture equilibrium with the attic air.

Today, the hygrothermal performance of attics can be simulated using a wide array of validated software including WUFI Plus (Antretter et al., 2011), DELPHIN (Grunewald, 2007), and HAM-Tools (Essah et al., 2009; Hagentoft & Sasic Kalagasidis, 2010; Nik et al., 2012; Harderup & Arfvidsson, 2013). Though all models have their limitations, they have been shown to effectively evaluate the hygrothermal performance of attics (Nik et al., 2012). In conjunction with hygrothermal simulations, a standard model for measuring mold growth is often used as a criterion for the performance of attics (Hagentoft & Sasic Kalagasidis, 2010; Nik et al., 2012). This model (Hukka & Viitanen, 1999; ASHRAE,

2016a) predicts mold growth potential as a function of temperature, relative humidity, and time. Generally, colder climates decrease the likeliness for mold growth (Nik et al., 2012), but it is still a possible problem in the warmer seasons.

2.3.2 Attics in Extreme Cold Canada

The principal issue with ventilated attics in the north is that fine, blowing snow infiltrates into the attic space and accumulated (Forgues, 1985; Lstiburek, 2009). This snow eventually melts, wetting the attic materials and increasing the overall humidity level in the attic. The added moisture can result in reduced performance of the insulation as well as mold growth and decay. Seeing that the main reason for venting is to remove excess moisture in the attic, this phenomenon is highly counterproductive to the cause. Conventional techniques of venting are not suitable for the Canadian north (Forgues, 1985).

In Nunvaut, cathedral ceilings are preferred over attics mainly to avoid the issues related to venting, since common knowledge dictates that truss roofs need to be vented. In Nunavik, however, houses generally have attics. These attics are ventilated using a unique design tailored for northern climates. Instead of allowing the outdoor air to enter the attic directly through soffit vents, the attic vents are actually placed at the bottom of the cladding allowing the air to travel up between the cladding and the sheathing before reaching the attic space. Along this passage, polyester filter membranes are installed to filter the snow particles out and let the air through such that the attic can be ventilated without the threat of snow accumulation. This system is implemented in many houses in Nunavik with many variations on the design. The effectiveness of this system has not yet

been proven, though there are ongoing field studies being conducted that indicate good performance (Baril et al., 2013; Ge et al., 2018).

Another way of dealing with snow infiltration involves the concept of an expansion chamber applied to the soffit, such that the drop in pressure in the chamber will prevent snow from penetrating further into the attic (Lstiburek, 2009). Thiis et al. (2007) used a full-scale test house in a wind tunnel with artificial snow to examine the snow infiltration into attics with various soffit designs and geometries. Some of the soffits were divided into small compartments to induce lower pressure differences. The authors found that the soffit design had a significant impact on snow accumulation in the attic, the position and design of the opening is probably the most important factor (Thiis et al., 2007)

There are a number of reasons favoring the use of attics over cathedral ceilings. Attics have more insulation and the surface area is smaller, both of which aid in reducing heat losses (Less et al., 2016). Attics are also associated with reduced cost. Cathedral ceilings are inherently more susceptible to moisture damage than attics because of the isolated conditions between the rafters (TenWolde & Rose, 1999). In general vented attics perform better than vented cathedral ceilings in cold climates (Goldberg et al., 1999).

Design recommendation for attics in Arctic climates exist, but are not well substantiated. The Government of Nunavut's Good Building Practices Guideline suggests that providing adequate ventilation is important to avoid condensation, but snow infiltration through required ventilation openings is difficult to avoid (GN, 2005). The Government of Northwest Territories's Good Building Practice for Northern Facilities states that attics should be naturally ventilated to keep the insulation dry after retaining moisture from

drifting snow and water, and that the water that accumulated should be drained to the exterior (GNT, 2011).

2.3.3 Integrating Renewable Energy Technologies

Implementing renewable energy technologies is of key interest in the Arctic to offset heavy fossil fuel dependency. Building-integrated photovoltaic/thermal (BIPV/T) systems generate solar power while heating outdoor air to be used as preheated ventilation air or as a source of useful heat. The photovoltaic panels are cooled in the process, making them more efficient, and the preheated air can be used for ventilating the house, ideally combined with a heat recovery or energy recovery ventilator (Beattie et al., 2015). Chen et al. (2012a) assessed the potential for implementing photovoltaic and solar thermal systems on vertical faces in high latitude locations experimentally and using simulation. It was found that significant amounts of heat ($>2\text{MJ/m}^2$) and electrical energy ($\sim 1000\text{ kWh/kW}$) can be harvested. One way the heated air can be used, at least partially, is attic ventilation, since the air would have a higher capacity to dry the attic (Kayello et al., 2017a). Because BIPV/T ventilation can slightly increase attic temperature, this kind of ventilation strategy may not be as useful in locations where there is heavy snowfall and ice damming is common. In the Arctic/Northern regions, however, snow loads are generally low.

2.3.4 Conclusion on Attics

Attics and their hygrothermal performance have been researched for almost a century, and continue to garner interest from researchers as building designs evolve. Minimizing air leakage is key in keeping moisture levels low in attics, especially if they are unvented.

Moisture transport via vapor diffusion is only significant if the ceiling is airtight. Attic ventilation is often beneficial in removing moisture that can accumulate in attics, though in humid climates and in cases where the building materials are dry ventilation may add moisture. Drifting snow presents a unique challenge in the north, where snow can accumulate in indoor spaces through small cracks in the envelope. This makes conventional attics impossible to use in those climates. Special ventilation designs and unvented attics have been implemented in the Arctic, though studies on their performance are few and limited. This thesis aims to investigate the suitability of various attic venting strategies for Arctic climates.

CHAPTER 3 Experimental Setup – Methodology

A test is developed such that the experiment fulfills the objectives of the study within a concise timeframe. A full-scale test hut (TH) composed of SIPs provides the subject of the experiment. The TH is fitted with an attic space, too. The TH is constructed in an environmental chamber (EC), which can control the temperature and humidity conditions using an HVAC system. The temperature and humidity conditions inside the TH are controlled separately by another HVAC system. As a reminder, experimental objectives are listed below:

- To investigate experimentally the hygrothermal performance of SIPs subjected to Arctic climatic conditions.
- To investigate experimentally the comparative hygrothermal performance of unvented and ventilated attics subjected to Arctic climatic conditions.

For the SIPs, it is important to understand how they perform not only subjected to large temperature differences, but also to air pressure differences. This way, the test will address the air leakage, the phenomenon most critical to the hygrothermal performance of SIPs. Also, SIPs are often sealed at the joints with tape, which can degrade and lose its sealing properties over time. So, the SIPs are tested with and without the sealant tape.

The tests with SIPs can be summarized as such:

- Subject the SIPs with tape seals to -20 °C outside temperature with no pressure differences.
- Subject the SIPs with tape seals to -40 °C outside temperature with no pressure differences.
- Subject the SIPs with tape seals to -20 °C outside temperature with pressure differences +15, +5, -5, and -15 Pa.

- Subject the SIPs without tape seals to -20 °C outside temperature with no pressure differences.
- Subject the SIPs without tape seals to -20 °C outside temperature with pressure differences +5 and -5 Pa

To evaluate unvented and ventilated attics simultaneously, the attic space of the TH is divided into two symmetrical bays, where one is unvented and the other is mechanically ventilated. Sampler pumps, which can supply air at controlled rates, are used to emulate air leakage from the interior of the TH to the attic bays. For hygrothermal tests, long-term tests are preferred since moisture transfer occurs very slowly, compared to heat transfer. However, due to limitations imposed by the EC HVAC system, including lab scheduling and repairs, tests on the attic bays are kept simple and are relatively brief.

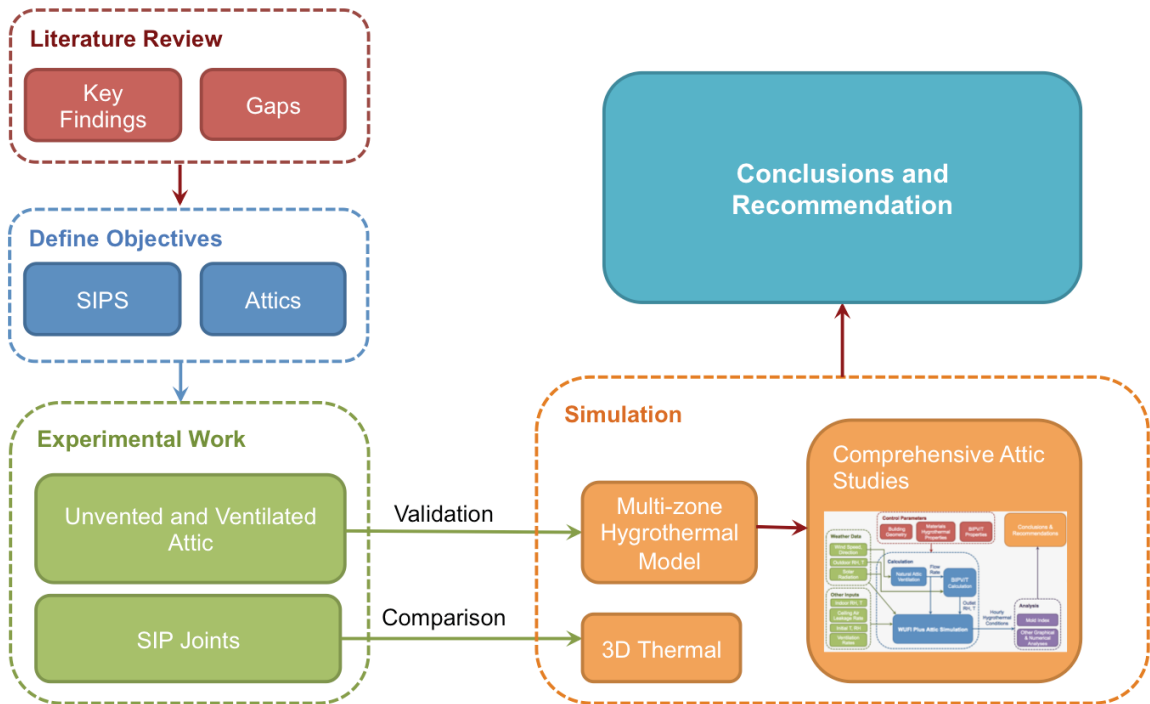


Figure 3.1 Project methodology

To place the experimental work in context of the entire thesis, see Figure 3.1 for a flow chart of the project methodology. The results from the experimental work are compared with those from simulation. The validated attic simulation model is used to conduct extensive studies on the performance of attics in extreme cold climates.

3.1 Test Setup

A full-scale TH constructed in an environmental chamber provides the setup for the experiment. The TH design is based on that of the prototype SIP duplex built in Iqaluit Nunavut. The TH walls and floor are composed of SIPs while the roof consists of trusses supporting an attic insulated at the ceiling level.

3.1.1 Test Hut

Based on a rectangular cuboid shape, the TH measures 4.27 m by 3.05 m (14' by 10') in length and width. Four casters support the TH and allow for repositioning of the TH within the EC. Figure 3.2 shows the TH in the environmental chamber where it is pushed back under the mechanical system. The TH design, shown in Figure 3.3, is based on the prototype SIP duplex built in Iqaluit, Nunavut. The SIP Duplex design is based on, and improves upon, the 142 SIP houses that were constructed across Nunavut to address the housing crisis.

Table 3.1 compares the insulation and airtightness characteristics of the SIP houses and test huts related to this study. The last column of the table shows the values recommended by the Government of Nunavut (GN, 2005).



Figure 3.2 Test hut in environmental chamber

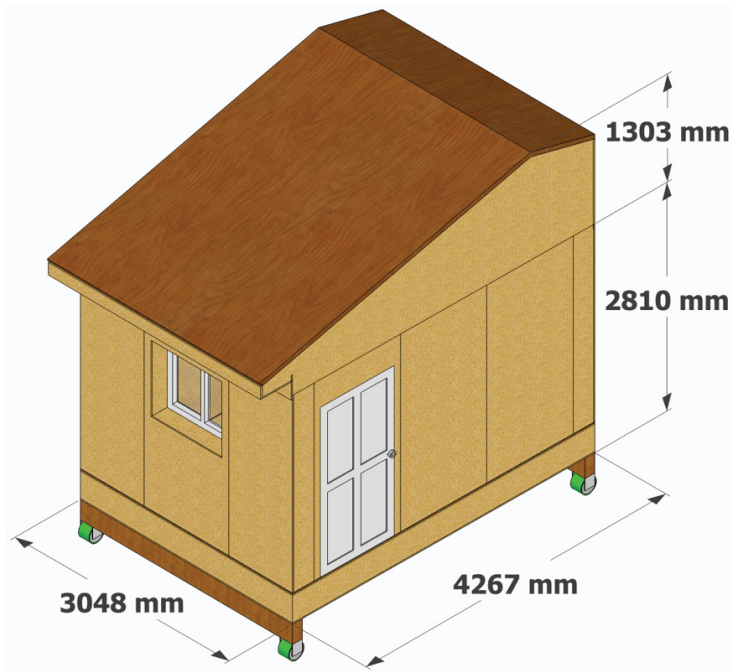


Figure 3.3 Three-dimensional rendering of test hut

Table 3.1 Building envelope characteristics of constructed SIP houses and test huts

	SIP Houses	Inverted Test Hut (Wyss et al., 2011)	SIP Duplex	New Test Hut	Nunavut Guideline (GN, 2005)
Units Constructed	142	1	1	1	-
Location	Distributed across Nunavut	BEP Lab, Concordia University	Iqaluit, Nunavut	SSEC Lab, Concordia University	-
Wall R-Value (m²K/W)	7.0	7.0	7.0	7.0	4.9
Ceiling R-Value (m²K/W)	8.8	8.8	12.3	12.3	7.0
Floor R-Value (m²K/W)	8.8	8.8	8.8	8.8	7.0
Airtightness @ 50 Pa (ACH)	0.5	2.4	0.6	1.1	<1.5
Floor Area (m²)	~100	5	170	12	-
Other Details	Cathedral ceiling using SIPs	Flat roof using SIPs	Attic spaces with trusses	Attic spaces with trusses	-

SIPs

The TH contains 12 wall SIPs and 3 floor SIPs. The wall SIPs are generally 2.44 m (8') in height and 1.22 m (4') in width. Four of the wall SIPs in the TH are only 0.91 m (3') to prevent the TH from being too wide for the EC. The floor SIPs are 4.27 m (14') long and run the length test hut.

The SIPs are composed of an expanded polystyrene (EPS) insulation core layer sandwiched between OSB panels on either side. The EPS layer is 275 mm (10 13/16") thick for the wall SIPs and 341 mm (13 7/16") thick for the floor SIPs. The OSB facings are each 15 mm (19/32") thick. On all four edges of a wall SIP, the EPS is recessed 44 mm (1 3/4") into the panel. The empty spaces formed from these recessions in the insulation are filled with one of two framing elements, depending on the location (Figure 3.4 and Figure 3.5).



Figure 3.4 Insulated I-joist connection

Between two aligned SIPs, the framing element is an I-joist with a thermal break as shown in Figure 3.4 and Figure 3.11. The I-joists provide rigidity to the connected SIPs to the joint. The web of the I-joist is OSB while the flanges are spruce-pine-fir (SPF). The I-joist is in direct contact with the exterior OSB facing, while there is a 32 mm (1 1/4") EPS thermal break between the I-joist and the interior OSB facing. EPS occupies the areas on either side of the web. The entire framing element is installed on one of the SIPs in the manufacturing process, forming the male end of the tongue-and-groove fitting. The opposing SIP edge is left empty in manufacturing, forming the female end.

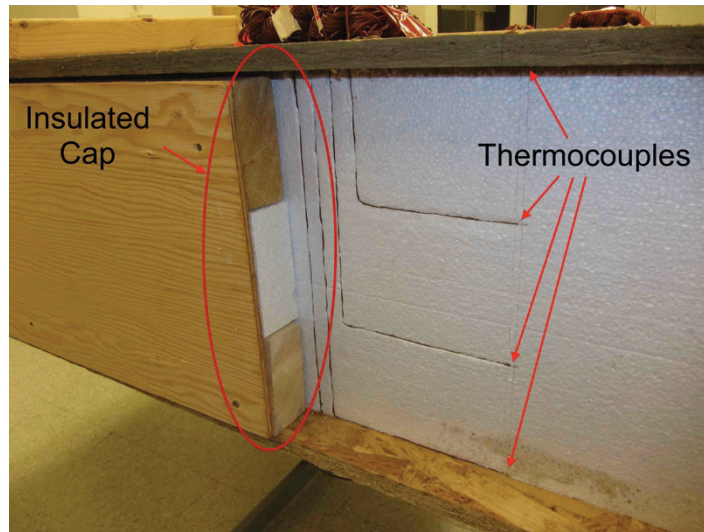


Figure 3.5 Insulated caps are used to fill most SIP joints. An example of installed thermocouples is also shown

In all other instances, insulated caps are used at the edges of SIPs, shown in Figure 3.5 and Figure 3.13. The insulated caps are all identical and are installed on the SIPs during construction. The insulated caps consist of a 275 mm (10 13/16") wide plywood board, 6 mm thick (1/4"). Attached to the plywood board are two two-by-fours flushed with both ends of the plywood. The space between the two-by-fours is filled with EPS, which acts as a thermal break.

The interior joints between SIPs, as well as the SIPs and the ceiling, are sealed using SIGA Rissan tape (60 mm wide). This tape provides the continuity of the air barrier.

Attics

The roof of the TH contains an attic space. Six identical SPF trusses provide the structure of the roof. The trusses are designed such that the ridge of the roof is off-center, allowing for more vertical space in the attic while maintaining the 3/12 roof slope. The roof sheathing is made of 13 mm (1/2") plywood sheets fastened to the top chord of the trusses.

Directly below the trusses, 38 mm (1.5") thick rigid polyisocyanurate (PIR) insulation is fastened to the bottom chords. The PIR boards have aluminum facings, so they act as a vapor barrier and as a thermal break for the ceiling. The joints between the PIR board are sealed with sheathing tape on the inside face to ensure continuity of the air barrier. Cellulose is blown into the attic, carried by the PIR, and acts as the main insulating layer of the ceiling. The thickness of the cellulose layer is roughly between 356 mm and 381 mm (14" and 15"). It is important to note that cellulose settles over time as well. OSB boards 15 mm (19/32") thick are used for the gables and the vertical attic wall on the east façade.

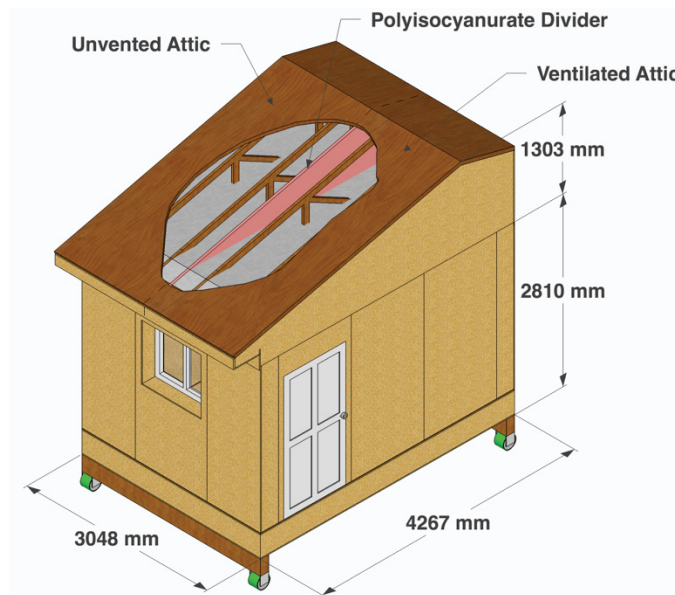


Figure 3.6 Three-dimensional rendering of test hut with roof cutaway



Figure 3.7 vents in soffit of ventilated attic

The attic space is divided into two symmetrical attic bays, separated by 38 mm (1.5”) of PIR. The north attic is sealed and unvented, whereas the south bay is vented with five 38 mm (1.5”) holes in the soffit (see Figure 3.7) and ventilated mechanically with a pump, as described later in this chapter. Before blowing in the cellulose insulation and installing the roof sheathing, the PIR is sealed at the bottom (to the ceiling PIR) and at the sides using sheathing tape. The PIR is then sealed to the roof sheathing using silicone sealant. On the east face of the attic, a transparent acrylic sheet is installed to provide a window to look into each attic bay. A sheet of rigid extruded polystyrene (XPS) is installed on the exterior of the attic bay windows to prevent frost formation on the inside surface. Each XPS board is fixed on a vertical hinge such to allow for easy viewing access to each attic bay. A 13 mm (1/2”) orifice is made in the ceiling PIR of each attic bay, which serves as the entry point for controlled air leakage, as described later in this chapter.

The TH contains additional features that are indirectly related to the main tests of this project. Two of the wall SIPs contain windows, while one wall SIP contains the only door. The window insulated glazing units (IGUs) are triple-glazed with low-e coatings and argon gas fill. The window frames are made of fiberglass. The window on the west

façade is fixed and the window on the east façade is an awning window. The door has a polyurethane core for improved thermal performance. The gap between the window frame and the framing in the wall SIP is sealed with PU. The same goes for the gap between the doorframe and the framing in the wall SIP. These windows add a realistic element to the TH as they are potential weak points in the building envelope, both thermally and in terms of airtightness. It is worth noting that houses in the north typically have a cold porch, which separates the main living space from the outdoors thus preventing any single door from being the sole isolator of the indoor and outdoor environment.

Spunbonded polyolefin (SBPO) acts as the building's vapor permeable moisture barrier. It is included in the experimental setup since it is the main air barrier for the attic space, effectively making it a sealed attic. Without it, air can readily transfer through the joints between the plywood sheathing panels. It is expected to provide additional airtightness to the house overall, but its lack of continuity around the entire building, especially the bottom of the house, makes it unsuitable as the main air barrier. The SBPO seams are sealed with sheathing tape.

The TH is not fitted with exterior or interior finishing since it is not a necessary component for the test. The actual finished house would have wood siding and a 25 mm (1") air space between the SBPO and the cladding. The interior walls and ceiling would be finished with gypsum board on furring strips. Flooring would be added as well. Finally, the roof would be finished with metal roofing with a ventilated cavity beneath.

3.1.2 Environmental Chamber

The EC is part of the Solar Simulator-Environmental Chamber facility located in the basement of the Concordia University's Hall Building. The internal dimensions of the EC measure 4.66 m by 8.77 m by 7.17 m (15.3' by 28.8' by 23.5') in width, length, and height, respectively. The enclosure of the EC is insulated to minimize heat transfer, and access ports provide passages for cables, wires, and piping through the EC enclosure. The west wall of the EC contains high transmittance window for use with a mobile solar simulator. The EC is fitted with a number of sensors for temperature, relative humidity, and pressure differential; EC sensors relevant to this test are presented in the next section.

The primary function of the EC is to accurately reproduce and maintain particular climatic conditions with regards to temperature and relative humidity. The EC can maintain temperatures as low as -40 °C and as high as 50 °C. Above 2 °C, the EC can be humidified and dehumidified as needed. Below 2 °C, the EC can only be dehumidified so that frost formation is kept at a minimum. The HVAC system of the EC is essentially a rooftop AHU. Two compressors are used for cooling. The smaller compressor is used for temperatures as low as 5 °C while the larger compressor is used for temperatures between -40 °C and 5 °C.

The HVAC system of the EC is controlled using a computer located in the control room in the SSEC. The program used is Insight by Siemens. The temperature and relative humidity conditions in the EC are controlled by with setpoints, which can be constant or time-dependent.

Figure 3.8 shows the HVAC air supply. The conditioned air can be supplied into the EC through vents that are directed either westward or downwards. For this experiment, the air was directed downwards to avoid localized cooling of the TH near the air supply and maximize mixing.









Figure 3.8 HVAC system air supply in the environmental chamber

3.2 Instrumentation

To continuously monitor the hygrothermal conditions in the various locations about the test hut and the environmental chamber, sensors wired to data acquisition systems (DAS) are used. Some of the instrumentation cannot be monitored continuously and involves manual readings. The DASs collect data from sensors and stores them on a hard disk. The main parameters monitored include temperature, relative humidity (RH), and moisture content (MC). Temperature sensors include thermocouples (TC) and temperature sensors

embedded within RH probes. The sensors used to gather hygrothermal data for the experiments are listed in Table 3.2.

Table 3.2 Sensors used to gather hygrothermal data

Sensor	Count	Parameters	Type	Accuracy	Picture
Thermocouple (Pelican Wire Company)	146 (Sensor letters A, C, F-M, R-U, V, W)	T	Type T, 30 gauge	±0.5 °C	
P-L-1/10-1/8-6-0-T3 (Omega Engineering, Inc.)	1	T	RTD	±0.04 °C	N/A
HMT 330 (Vaisala)	6	RH	Capacitive (HUMIDICAP® 180)	±3% RH	
		T	RTD (Pt100 RTD F0.1 IEC 60751)	±0.5 °C	
HMT 120 (Vaisala)	2	RH	Capacitive (HUMIDICAP® 180)	±4% RH	
		T	RTD (Pt1000 RTD 1/3 Class B IEC 751)	±0.2 °C	
HMT 310 (Vaisala)	2	RH	Capacitive (HUMIDICAP® 180R)	±3% RH	
		T	RTD (Pt100 IEC751/3 class B)	±0.5 °C	
HygroFlex1 (Rotronic)	2	RH	Capacitive (Hygromer® IN-1)	±3% RH at 23 °C	
		T	Thermistor	±0.3 °C at 23 °C	
Steel Screws	12 (pairs)	MC	10 mm screws	Unknown/ Varies	

3.2.1 Instrumentation Locations

The instrumentation for this experiment is arranged to provide as much information as possible on key aspects of the building using a limited number of sensors. As a basic requirement, the temperature and humidity conditions in the EC and TH air space are monitored. A larger number of sensors are installed in the SIP joints and in the two attic bays since they are the main focus of this project.

Environmental Chamber

Table 3.3 Sensors in environmental chamber

Sensor Name	Sensor	Parameters	Description
A1	TC	T	EC air space, west of TH, 2 m above ground
A2			EC air space, north of TH, 2 m above ground
A3			EC air space, east of TH, 2 m above ground
A4			EC air space, south of TH, 2 m above ground
A5			EC air space, above roof ridge of TH
B1	HygroFlex1	RH+T	EC air space, south-east of TH, 2 m above ground
B2			EC air space, north-west of TH, 2 m above ground

The temperature and relative humidity conditions in the EC air space were monitored. The location of these sensors is shown in Figure 3.9. Sensors A1 through A5 are installed on five sides of the TH such that the tip is about 15 cm (6") away from the building. These sensors indicate the level of homogeneity of the air in the EC and variations of temperature experience around the TH. B1 and B2 are installed on the south and north EC walls, respectively.

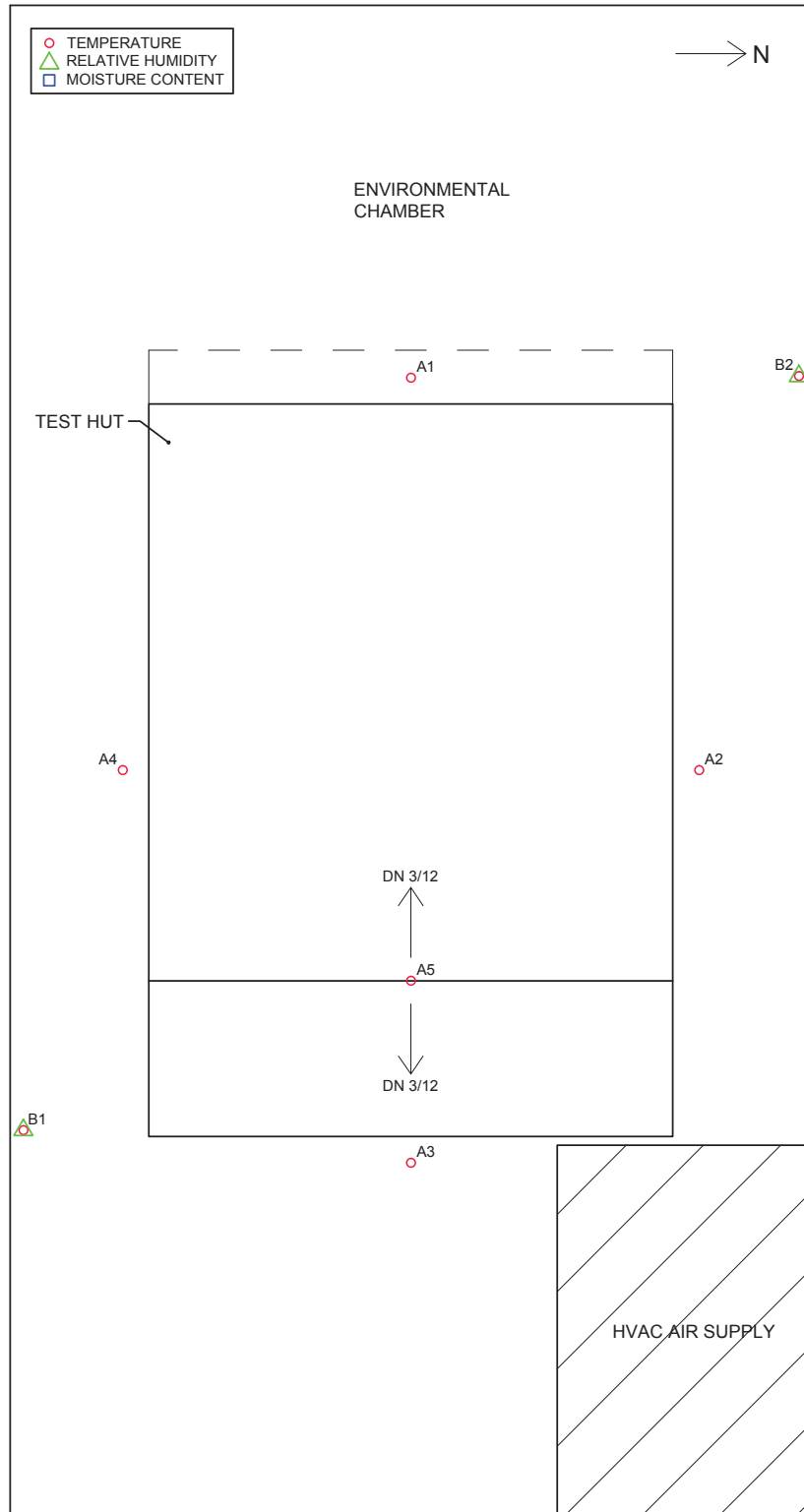


Figure 3.9 Instrumentation in the environmental chamber

Test Hut Interior

Table 3.4 Sensors in test hut interior space

Sensor Name	Sensor	Parameters	Description
C1	TC	T	TH air space, center of room, mid-height
C2			TH air space, center of room, 5 cm below ceiling
D1	HMT310	RH+T	TH air space, center of room, mid-height
D2			TH air space, center of room, mid-height. Used for RH control system.

The interior of the TH is also monitored for temperature and relative humidity. Sensors C1, D1, and D2 are installed in the same location in the center of the room to show whether the readings are consistent among the sensors. Sensor C2 provides a temperature reading near the ceiling to indicate the level of thermal stratification. Sensor D2 is used as the feedback signal for the humidity control system in the TH.

SIP Joints

To fully enclose a SIP house, the SIPs are connected to each other in a number of ways, forming a variety of different connections. In addition, there are more joints and connections formed when doors and windows are installed within a SIP. For this study, the focus is on the main joints and connections associated with wall SIPs.

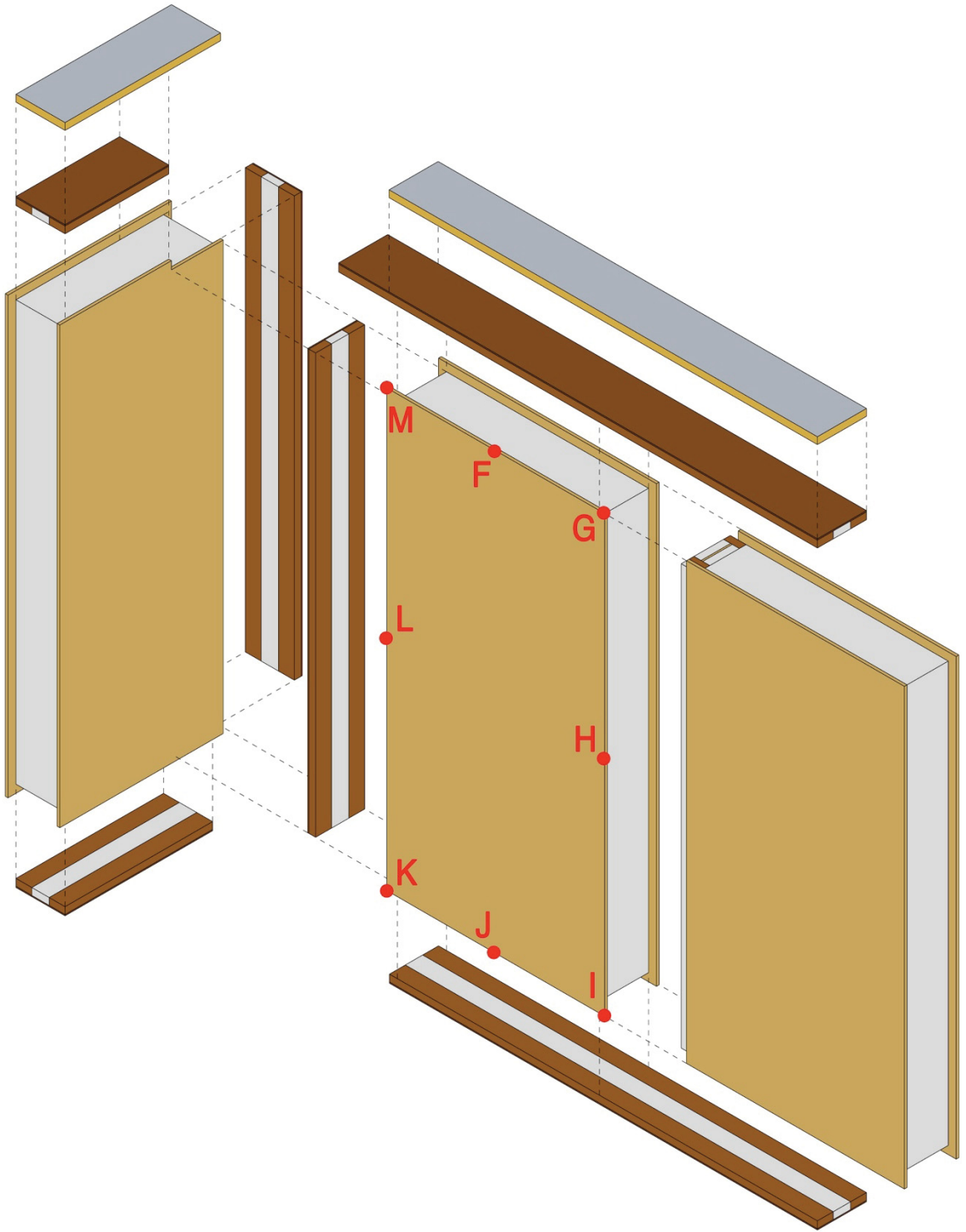


Figure 3.10 Joint types monitored in this study

There are 8 types of wall SIP joints in the construction of a SIP house:

- Wall SIP and ceiling (F)
- Two aligned wall SIPs and ceiling (G)
- Two aligned wall SIPs (H)
- Two aligned wall SIPs and floor SIP (I)
- Wall SIP and floor SIP (J)
- Two perpendicular wall SIPs and floor (K)
- Two perpendicular wall SIPs (L)
- Two perpendicular wall SIPs and ceiling (M)

Table 3.5 Sensors in SIP joints

Sensor Group Name	Sensor	Parameters	Description
F	TC	T	Joint between wall SIP and ceiling, with 6 sensors at each joint. 3 incidences of this joint are monitored: <ul style="list-style-type: none"> • F_A: wall SIP #4 and ceiling • F_B: wall SIP #5 and ceiling • F_C: wall SIP #6 and ceiling
G			Joint between two aligned wall SIPs and ceiling, with 6 sensors at each joint. 2 incidences of this joint are monitored: <ul style="list-style-type: none"> • G_A: wall SIPs #4 and #5 and ceiling • G_B: wall SIPs #5 and #6 and ceiling
H			Joint between two aligned wall SIPs, with 7 sensors at each joint. 2 incidences of this joint are monitored: <ul style="list-style-type: none"> • H_A: wall SIPs #4 and #5 • H_B: wall SIPs #5 and #6
I			Joint between two aligned wall SIPs and floor SIP, with 6 sensors at each joint. 2 incidences of this joint are monitored: <ul style="list-style-type: none"> • I_A: wall SIPs #4 and #5 and floor SIP • I_B: wall SIPs #5 and #6 and floor SIP
J			Joint between wall SIP and floor SIP, with 6 sensors at each joint. 3 incidences of this joint are monitored: <ul style="list-style-type: none"> • J_A: wall SIP #4 and floor SIP • J_B: wall SIP #5 and floor SIP • J_C: wall SIP #6 and floor SIP
K			Joint between two perpendicular wall SIPs and floor SIP, with 6 sensors at each joint. 2 incidences of this joint are monitored: <ul style="list-style-type: none"> • K_A: wall SIPs #3 and #4 and floor SIP • K_B: wall SIPs #6 and #7 and floor SIP
L			Joint between two perpendicular wall SIPs, with 6 sensors at each joint. 2 incidences of this joint are monitored: <ul style="list-style-type: none"> • L_A: wall SIPs #3 and #4 • L_B: wall SIPs #7 and #7

M			Joint between two perpendicular wall SIPs and ceiling, with 6 sensors at each joint. 2 incidences of this joint are monitored: <ul style="list-style-type: none"> • M_A: wall SIPs #3 and #4 and ceiling • M_B: wall SIPs #6 and #7 and ceiling
----------	--	--	---

In this experiment, each of these 8 types of joints is monitored with several TCs along the thickness of the panel (Table 3.5). For redundancy, at least two incidences of each joint type are monitored, resulting in a total of 18 monitored joints (3 incidences of joints type F and J are monitored; while 2 incidences of the other six joint types are monitored).

For each joint, the TCs are installed on the female end of the SIP. One TC is placed on the inside surface of the SIP and another on the outside surface. Several TCs are placed in the core section of the joint, where the EPS is located. In joints of type H, shown in Figure 3.11, 5 TCs are placed in the core section, and the sensor distribution along the thickness reflects the location of the material interfaces of the corresponding male end; in the case of joint type H, the male end is the I-joist with the thermal break. In all other joint types, 4 TCs are placed in the core section, and the sensor distribution reflects the material interfaces of the insulated caps that fit into these joint, as shown in Figure 3.12 and Figure 3.13. It is worth noting that the two different framing elements (the I-joist and the insulated cap) both meet at joint types G and I, but the sensor distribution only reflects that of the insulated cap. Figure 3.14 shows a plan view of the test hut within the environmental chamber and the general location of the sensors. The sensors are installed in the wall SIPs labeled #4, #5, and #6.

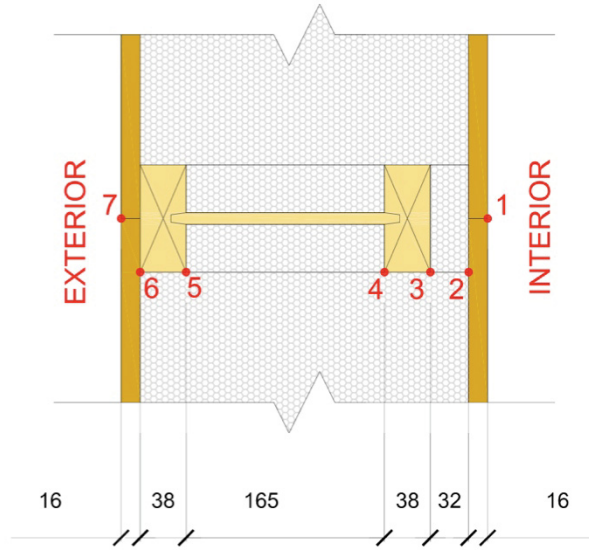


Figure 3.11 Sensor placement for joint type H (dimensions in mm)

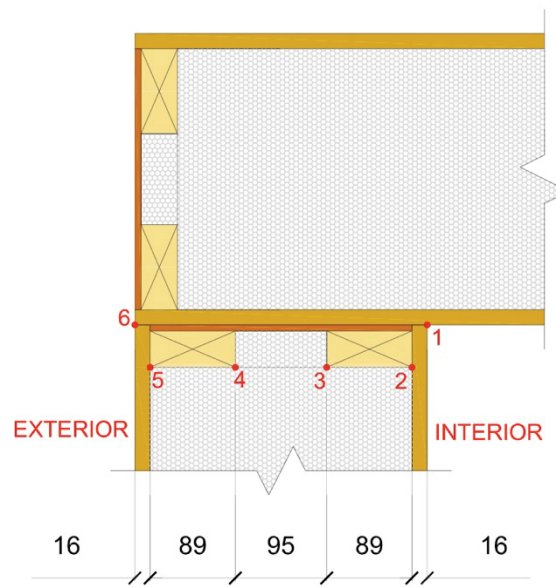


Figure 3.12 Sensor placement for joint types F, J, and L (dimensions in mm)

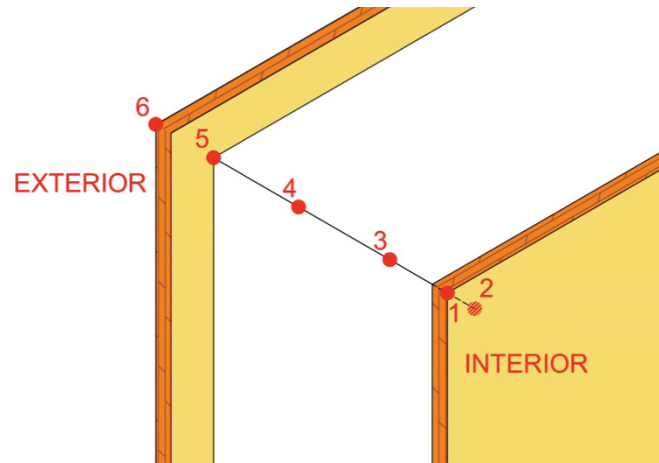


Figure 3.13 Sensor placement for joint types G, I, K, and M

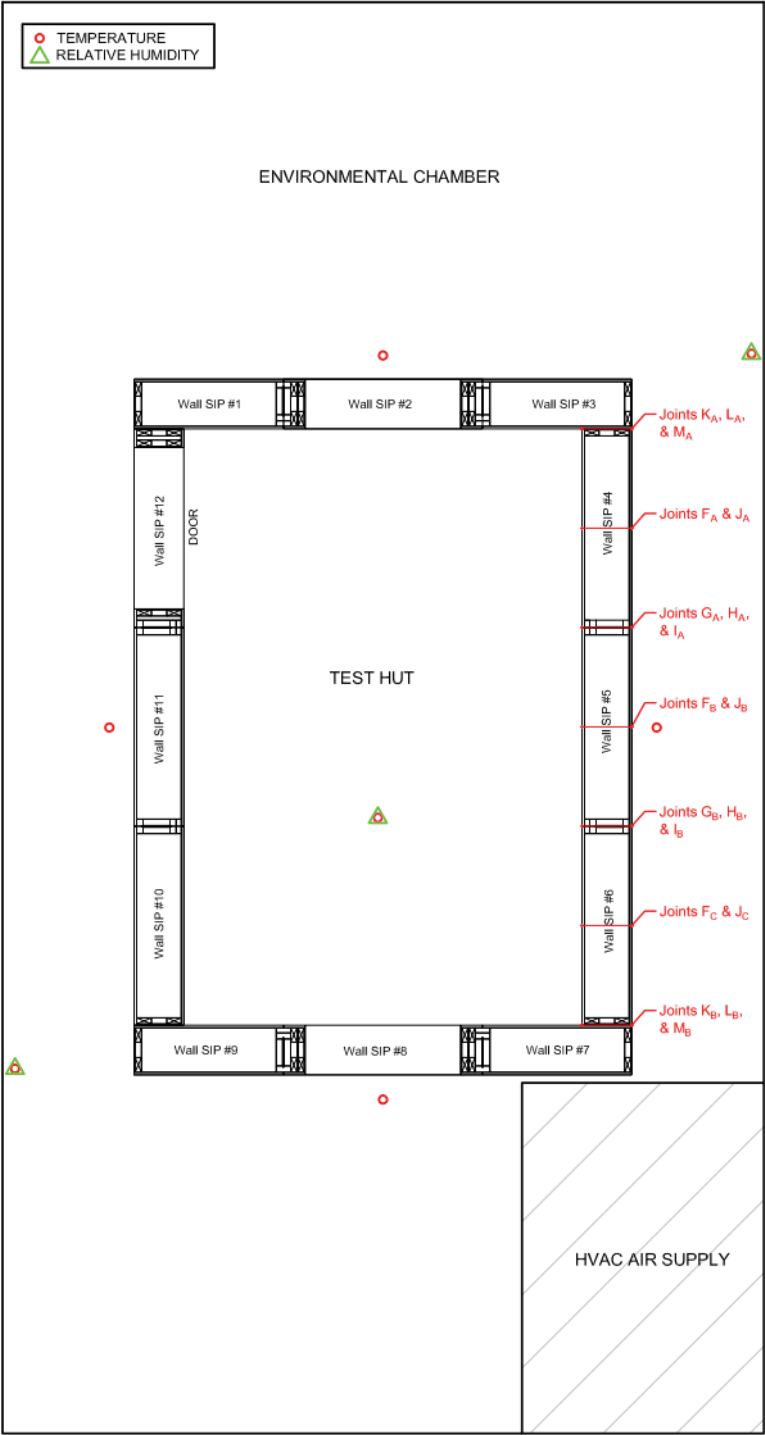


Figure 3.14 Plan of test hut in environmental chamber showing location of monitored joints and other sensors

With this sensor configuration, a temperature profile can be attained for each joint. The temperature profile will vary depending on the indoor and outdoor conditions, the thermal performance of the joint, the amount and path of air leakage at the joint, and time. By subjecting the TH to various temperature and pressure differences, a number of temperature profiles can be attained, which will indicate the thermal and air performance of each joint. The letter designation for the sensors and joints can be seen in a number of forms, and they are explained in the following example. The letter F alone would refer to the joint type, F_A refers to instance A of that joint type (as indicated in Figure 3.14), F1 refers to the thermocouples on the interior surface from all three instances of the joint F, and F_A1 refers to the thermocouple on the inside surface of joint F_A .

Unvented and Ventilated Attics

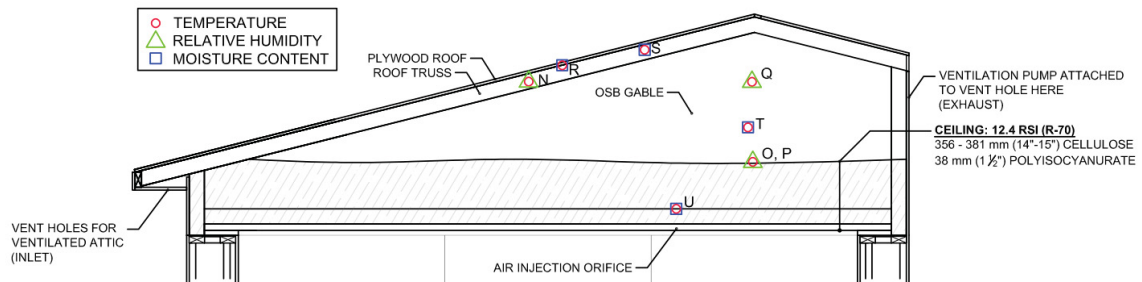


Figure 3.15 Section of attic bay with sensor locations

Table 3.6 Sensors used in each attic bay

Sensor Name	Sensor	Parameters	Description
N	HMT330	RH+T	Directly under roof sheathing
O			Directly above cellulose, on vertical axis of orifice in PIR
P			Directly above cellulose, 52 cm away from vertical axis of orifice in PIR
Q	HMT120		Attic air space
R	Steel screws & TC	MC+T	Underside of plywood sheathing
S			Top chord of truss
T			Inside of OSB gable
U			Bottom chord of truss, adjacent to orifice in PIR

In the attics, temperature, relative humidity, and moisture content sensors are used to provide an in-depth view of thermal and moisture performance of each attic. The unvented and vented attic bays are symmetrical and have identical, symmetrical instrumentation as well. This setup facilitates direct comparison of the measurements from the two attic bays. Figure 3.15 and Figure 3.16 show two views of an attic bay and the sensor locations, and Table 3.6 lists those sensors.

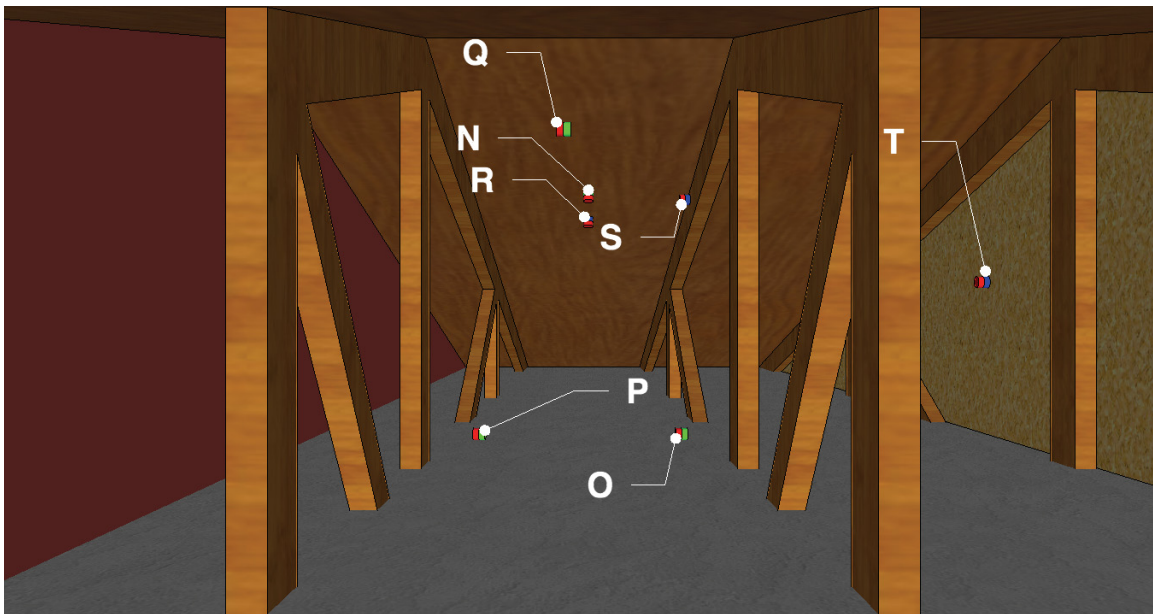


Figure 3.16 Three-dimensional view of an attic bay with sensor locations

Four RH+T sensors are installed in each attic bay. The first of them, N, is located flush with the underside of the sheathing. The underside of the sheathing is one of the locations most susceptible to condensation because it is often the coldest surface in the attic. Sensors O and P are located just above the cellulose insulation; sensor O is directly above an orifice in the PIR where air is injected, while sensor P is 52 cm away from the vertical axis of the orifice. In extreme cold temperatures, the exfiltrating indoor air can condense and freeze in the ceiling insulation before reaching the attic air space. When the frost melts, the surrounding insulation becomes damp and wet. Sensors O and P therefore

provide information on the local behavior of moisture and temperature, where sensor O represents a location that is affected by air leakage and sensor P is in a relatively undisturbed location. The last RH+T sensor is sensor Q, located in the attic air space below the ridge.

Four MC+T sensors are installed in wooden materials in the attic most likely to experience elevated moisture conditions. Sensor R is on the underside of the plywood sheathing, adjacent to the RH+T sensor N. Sensor S is located on the top chord of one of the SPF trusses in the attic. Sensor T is on the inside face of the OSB gable, which, like the sheathing, is expected to be a cold surface in the attic. Sensor U is installed on the bottom chord of a SPF truss, adjacent to the orifice in the PIR. This location is susceptible to the frost that may accumulate in the cellulose and melt, potentially getting absorbed by the wood truss.

With regards to sensor designation for the sensors in the attics, the subscript U refers to the unvented attic, while V refers to the vented attic. For example, N_U is the RH+T sensor on the underside of the sheathing in the unvented attic.

TCs are also installed within the cellulose insulation over and around the air leakage orifice. Their arrangement provides a temperature profile of the cellulose insulation and details on the effect of air leakage on the cellulose, the approximate location of frost formation in the cellulose, and the melting of the frost as well. The results were used to verify a heat-airflow model developed by Belleudy et al. (2015). See Appendix E for more details.

The wiring for all the attic sensors is brought out through a sealed opening in the gable, so as not to compromise the air barrier of the ceiling.

3.2.2 Information on Sensors and Monitoring Methods

Each piece of instrumentation has unique characteristics, as well as a specific installation and monitoring procedure. 51 mm (2") holes are drilled in the test hut to allow wires, tubes, and flexible piping to pass through the TH envelope.

Thermocouples

For measuring temperature in this experiment, thermocouples (TCs) are used extensively as they are reliable, low profile, and inexpensive. TCs are made of two dissimilar metal wires and produce a voltage when there is a temperature difference between the contact point of the two metals and a reference spot in the circuit. Type T, 30 gauge TCs are used in this experiment and they are composed of copper and constantan, insulated with a brown PVC jacket. These TCs can operate between -270 °C to 400 °C. TCs are calibrated to an accurate temperature sensor.

Because of the high thermal conductance of the TC metals, readings may be inaccurate if the insulated wire near the tip is exposed to significantly different temperature than the tip itself. Where possible, a minimum of 25 to 50 mm of the insulated wire should follow an isothermal line. For TCs installed on surfaces, a 100 mm segment of wire is placed in contact with the surface.

TCs placed on the joint surfaces are installed prior to assembly of the test hut. Small holes are drilled in the interior OSB such that the TC wires are fed through them. These

holes are then sealed so the air tightness of the joint is not affected. The TCs are embedded in the EPS such that they do not protrude and affect the performance of the joints. Each TC wire follows the plane of the wall, the direction of minimal change in temperature, for at least 100 mm from the thermocouple junction to maintain accuracy in the readings. In two-dimensional joints, this portion of TC wire runs along an isothermal line. In three-dimensional joints, there are no isothermal lines for the wires to follow; however, the wires will follow a line of least expected temperature variation, which is parallel to the SIP facings.

TCs installed on material surfaces are done after the test hut is constructed. A small bead of high thermal conductivity compound is placed on the material surface such that the TC tip is inserted into the bead. The tip is then covered and held in place using masking tape. 100 mm of the insulated wire is taped along the surface.

Resistance Temperature Detectors

One resistance temperature detector (RTD) is used. RTDs utilize a fine-coiled metal wire with a known resistance as a function of temperature. This allows for obtaining the temperature at the location of the metal wire by measuring its resistance. RTDs are known for their high accuracy and repeatability.

Relative Humidity Sensors

Twelve relative humidity (RH) sensors are used. Ten of these sensors are made by Vaisala and utilize a capacitive thin-film polymer sensor. The dielectric properties and capacitance of the sensor changes as the relative humidity changes, and the DAS measures converts the measured capacitance to a relative humidity reading. For the HMT

330 and HMT 120 devices, the sensor is connected to the transmitter by a 5 m cable, allowing the transmitters to be stationed in a conditioned space while the sensors can be installed in harsher conditions. The two HMT 120 devices have the sensors built-in with the transmitter, so they cannot be placed in areas where the temperature drops below 0 °C.

Moisture Content Sensors

Moisture content (MC) sensors are homemade using steel screws soldered onto wires. Typically, the sensor pins can be insulated pins, stainless steel nails, or screws (Straube et al., 2002). Screws were used to ensure contact and pressure in the wood material. When possible, the screws were installed in clear wood, parallel to the grain, and about one inch apart (Straube et al., 2002); this is where OSB presents a complication since the wood is randomly oriented. The uninsulated screws measure the highest moisture content in their path (Straube et al., 2002). Since high moisture content is expected near the surface of wood material, screws are used to measure “surface” moisture content. TCs are used at each MC sensor location to provide the temperature reading required to make corrections. More information on the setup and calibration of the MC sensors can be found in Appendix D.





Gravimetry

Gravimetry is a reliable method to obtain MC readings at any MC. Gravimetric samples of the interior OSB could be taken to compare with the results from the moisture content pins. However, the samples cannot be collected while the experiments are running, at least not too often, because that will involve opening the doors to the EC and the test-hut, briefly disturbing the indoor and outdoor conditions. This is even more serious for the

attic, where small amounts of air leakage can have a severe impact on the attic condition. This technique was only used to compare with the readings from the electric readings as the system was being developed (see Appendix D).

Pressure Transducers

Table 3.7 Pressure transducers used in this test

Model	Specifications	Picture
PX655-05DI (Omega Engineering, Inc.)	Requires external power Range: 0–125 Pa Accuracy: 0.25% full scale [0.31 Pa]	
HM28D3B10000 (Love Controls)	Battery powered, hand held Range: 0–2500 Pa Accuracy: 0.2% full scale	
HHP-2000 (Omega Engineering, Inc.)	Battery powered, hand held Range: 0–2500 Pa Accuracy: 0.15% rdg + 0.15% full scale + 1 digit	
DG-700 (The Energy Conservatory)	Battery powered, hand held Range: -1250–1250 Pa Accuracy: greater of 1% and 0.15 Pa	

Four pressure transducers are used, and they are the only ones available. The PX655-05DI has the smallest range, but all the readings are expected to be well within that range. It is also the most accurate of the sensors, and so it is preferred and first-choice pressure transducer of the lot. When more than one transducer is needed at a time, the choice is based on the practicality and accuracy needed.

The DG-700 is mainly intended for use with a blower door, which was used to conduct air tightness tests (see Appendix C).

3.3 Equipment

In addition to the instrumentation, various pieces of equipment were needed to ensure the experiment runs as intended.

3.3.1 Heating in Test Hut

Two heating devices are used to maintain the temperature conditions in the TH: a 1 kW baseboard heater and a 1 kW heating element in a duct installed in series with a duct fan (Figure 3.17). A PID controller and an RTD sensor are used in conjunction with the heaters such that the heat output is automatically controlled between 0 – 100% capacity.

Electronic equipment in the room provides additional heat gains that cannot be controlled. This presents the issue of overheating in the TH since it is so insulated. There is not cooling system in the TH to overcome this issue. It was found, however, that below 5 °C, overheating was unlikely to occur.



Figure 3.17 Heaters used to heat the test hut

3.3.2 Humidity Control in Test Hut



Figure 3.18 Humidifiers used in the test hut: evaporative (left) and atomizer (right)



Figure 3.19 Dehumidifier used in the test hut

To control the humidity in the TH, both humidifying and dehumidifying systems were installed. Two types of humidifiers were used (Figure 3.18). An evaporative humidifier, model HM-3500 by Holmes, adds moisture to the air at slow rate. It uses a fan to pull air through a moist wick thereby humidifying the air and dispersing the moist air in the TH. The other humidifier is atomizer, model 707U by Hermidifier. It supplies moisture at a high rate, up to 1 kg/h. It works on the concept of centrifugal atomization, where water

droplets are broken down into a fine mist. A fan is added to the atomizer to help disperse the moisture in the TH.

Dehumidification is taken care of using a Wood's dehumidifier (Figure 3.19). The dehumidifier essentially utilizes a refrigeration cycle, where condensation that occurs on evaporator coils is collected and heat is rejected into the TH through the condenser coils. This rejected heat significantly adds to the heat gains in the TH and increases the likeliness of overheating when the EC temperature is above 0 °C.

To manage the water requirements of the humidity control system, a water tank is installed in the TH. The tank is filled with water and acts a reservoir for the humidification and dehumidification systems. Two, small fish tank pumps supply water to each of the two humidifiers so that they do not dry up. Also, the condensate from the dehumidifier is piped directly back into the water tank via a flexible tube.

An RH+T sensor (sensor D2) provides feedback for the humidity control system. The sensor is connected to a DAS, controlled by LabVIEW in a laptop located in the control room. Through the DAS, an electrical switch box is controlled such that the power supply to the humidifiers, dehumidifier, fan, and water pumps are turned on or off as needed. The set point relative humidity is implemented in LabVIEW and can be programmed such that the setpoint follows a particular daily schedule. The minimum difference between the measured and setpoint relative humidity that engages a humidifier or dehumidifier can be changed as needed. Typically, this minimum difference is larger for the atomizer humidifier than the evaporative humidifier because the atomizer humidifies

the TH very quickly and is less effective at managing humidity within a small relative humidity band.

3.3.3 Air Pumps for Pressurization, Depressurization, and Attic Ventilation

Two large air pumps with a capacity of 45 cfm are used in the test setup. They are equipped with laminar flow element devices for accurate flow rate measurements. These air pumps are used to pressurize and depressurize the various zones of the test hut to test for air leakage. One air pump is also used to ventilate one of the attic bays at a constant flow rate during the experiment.

3.3.4 Air Pumps for Attic Air Leakage



Figure 3.20 Sample pump delivering air to attic spaces

Sample pumps (Figure 3.20) are used to introduce a controlled air leakage rate from the indoor space to the attic. Universal sample pump to be used to control airflow into the attic. This implies that the attic be completely sealed of all leaks to ensure that all the air entering the attic is delivered by the sample pump. The sample pump can provide flow rates between 750 and 5000 ml/min, or 0.045 and 0.3 m³/h, or 0.0075 and 0.05 ACH if we consider the attic volume to be 6 m³, approximated from geometry. The sample pump

runs on a rechargeable battery that provides 8 hours of continuous operation on each charge. However, this amount of time is not sufficient for the purposes of the experiment, so the pump must be connected directly to a 6V DC power source. Also, an exhaust port fitting is needed to ensure airtightness of the exhaust port and proper air supply.

Two 13 mm (1/2") orifices are made in the ceiling PIR of each attic bay, which serves as the entry points for the tubes. There are two air injection locations: one is located 5 cm away from sensor U at the top of the PIR insulation, beneath the cellulose, and the other is midway between the trusses, at the top of the cellulose, as shown in Figure 3.21. Locations of air injection in the attic corresponding to each test. Plastic tubes measuring 13 mm in diameter are attached to the pump to direct air injection to those locations.

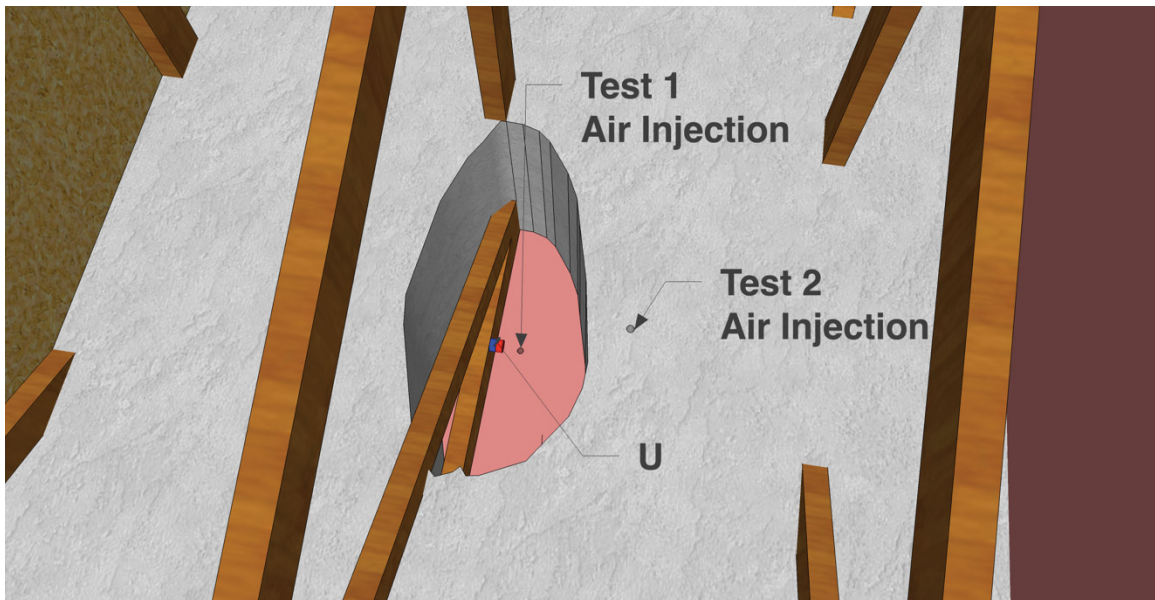


Figure 3.21 Locations of air injection in the attic corresponding to each test



Figure 3.22 Air flow meter

The sample pump flow rates are verified manually using a flow meter (DryCal[®] DC-Lite, Figure 3.22). It utilizes dry piston technology and infrared sensors to obtain volumetric flow rates. It measures flow rates between 100 mL/min – 7 L/min with $\pm 1\%$ accuracy.

3.3.5 DC Power Supply Units

DC Power supply units were used power a number of devices and sensors, including the electric moisture content measuring system, the air leakage pumps, and some of the RH+T sensors.

3.3.6 Electrical switching box (power supply)

All electronic equipment in the test hut is powered using this switching box except for the heating, one of the interior lights, and the light in each attic bay.

3.3.7 Other

An incandescent light bulb is installed in each attic bay that can be turned on so that photos of the attic can be taken from the exterior of the test hut.

3.4 Test Procedure

The materials composing the test hut must initially be preconditioned in the indoor environment of the university to ensure that the panels are all at roughly the same initial conditions before testing begins. The materials are inspected to verify that their moisture content values are within an acceptable range. So as to not encumber the EC, the preconditioning of the materials will occur outside the lab, in room H-0015. The temperature in this room is kept at 22 °C while the relative humidity is around 20 %.

3.4.1 SIP Joint Tests

It is important to understand how the SIP joints perform not only subjected to large temperature differences, but also to air pressure differences. This way, air leakage, the phenomenon most critical to the hygrothermal performance of SIPs, is addressed. Also, SIPs are often sealed at the joints with tape, which can degrade and lose its sealing properties over time. Thus, the SIPs are tested with and without the tape. The tests carried out are summarized in Table 3.8.

Table 3.8 Summary of SIP Joint tests

Test	Interior Temperature	Exterior Temperature	Pressurization (Pa)	Tape on joints
1	22	-20	None	Yes
2	22	-40	None	Yes
3	22	-20	+15, +5, -5, -15	Yes
4	22	-20	None, +5, -5	No

Steady-state conditions for temperature readings defined in similar fashion to ASTM C177-04 (2004), which states that thermal steady-state is reached when the temperatures of the cold and hot sides of the specimen and the power to the conditioning equipment are stable within the error limits of the measuring equipment and that these conditions exist

for at least four time intervals of 30 min or longer. For the experiments described here, steady-state conditions are attained for all temperature readings.

3.4.2 Attic Tests

Two tests were performed on the attics, each test lasting at least 20 consecutive days. The first test subjects the attics to extreme winter conditions, while the second test subjects them to typical winter, spring, and summer conditions. The tests are summarized in Table 3.9.

For test 1, the UA and VA are subjected to $-40\text{ }^{\circ}\text{C}$ outdoor conditions with two air leakage flow rates, 2 L/min and 5 L/min. This is equivalent to $0.4\text{ L/m}^2\text{min}$ and $1.0\text{ L/m}^2\text{min}$, and roughly equivalent to a building with 1.0 ACH at 50 Pa, considering that 30% of the air leakage goes through the ceiling (ASHRAE, 2013a) and the n-factor (Sherman, 1987) is 20 and 10 respectively. The air is delivered from the indoor space to the bottom of the cellulose insulation, as shown in Figure 3.21. After an 11-day period of $-40\text{ }^{\circ}\text{C}$ outdoor conditions, the EC HVAC system is turned off to allow any frost accumulation to melt.

For test 2, the attics are subjected to three sets of outdoor conditions consecutively: winter conditions ($-25\text{ }^{\circ}\text{C}$), shoulder season conditions ($-7\text{ }^{\circ}\text{C}$), and then summer conditions ($6\text{ }^{\circ}\text{C}$). These conditions are typical average seasonal temperatures for Arctic communities. Air is injected directly into the air space of the attic, as shown in Figure 3.21, at a rate of 5 L/min for a few days in each period. The sequence of EC temperatures was reproduced as intended. The VA is ventilated at a rate of 5 cfm ($\sim 140\text{ L/min}$) in both

tests, equivalent to 3 ACH, which is with the typical range for attics (Walker & Forest, 1995).

For test 1, the RH in the test maintained at 40%, with an hour-long period of high humidity (80%) every twelve hours simulating activities that significantly humidify the air like showering or cooking. For test 2, the RH is kept at 40% throughout the duration of the test.

Table 3.9 Summary of Attic tests

Parameter	Test Conditions	
	Test 1: -40 °C Outdoor Temperature	Test 2: -25, -7, and 6 °C Outdoor Temperature
Duration of test	22 days	20 days
TH Temperature	22 °C	22 °C
TH RH	40%, 1 hour period at 80% every 12 hours	40%
EC Temperature	-40 °C for 11 days then EC HVAC system is turned off	-25 °C for 5 days then -7 °C for 5 days then 6 °C for 7 days
EC RH	Not controlled, EC dehumidified as needed to protect HVAC system	Not controlled, EC dehumidified as needed to protect HVAC system
VA ventilation rate	140 L/min (3 ACH)	140 L/min (3 ACH)
Air injection rate into attic	2 L/min then 5 L/min	5 L/min
Air injection location in attic	Bottom of cellulose insulation	Directly into attic air space

CHAPTER 4 Experimental Results

This chapter presented the results obtained from the SIP and attics tests.

4.1 SIP Joints

The results are presented in three subsections. First, the steady-state results obtained at -20 °C and -40 °C, without pressurization and with the tape seal, are presented in tabular form. The second and third subsections go over the effect of pressurization with the tape seal and without tape seal, respectively; the results are presented in graphical form. The complete set of tabulated and graphical results can be found in Appendix A.

4.1.1 -20°C and -40°C Exterior Temperatures

The steady-state results at -20 °C and -40 °C are presented in this section. The following tables show the temperatures obtained at all incidences for each joint type. The differences between the temperature readings at each location are shown. Since the uncertainty of the temperature readings is 0.5 °C, differences greater than 0.5 °C are in bold. The percentage difference is calculated using the following equation:

$$\%Difference = \frac{T_1 - T_2}{T_{in} - T_{out}} \times 100 \quad (4.1)$$

T_1 and T_2 are temperature readings in the same location in a joint, but at different incidences of that type of joint. T_{in} and T_{out} are the temperatures in the test hut and the environmental chamber, respectively.

Table 4.1 shows the temperature readings for joint type F, as an example. The largest temperature difference observed is 0.66 °C at F5 at -20 °C, and 2.93 °C at -40 °C, at F5 as

well. At -20 °C, the small temperature differences indicate that the three incidences of the joint behave very similarly in response to the temperature gradient. At -40 °C, the larger temperature gradient leads to larger temperature differences between the readings as expected. However, the percentage difference values under -40 °C conditions are considerably larger than those under -20 °C, indicating that the effect is not linear. This phenomenon can be explained in part by the fact that the larger temperature gradient increases the stack effect pressures on the building envelope. Higher pressures on the envelope imply higher air leakage rates and, therefore, greater temperature changes in the envelope. Because the patterns of air leakage are complex and unpredictable, joints are affected to varying degrees with a high degree of uncertainty. Identical joints, therefore, perform differently under the same temperature conditions because of these complex joint imperfections that define how air leaks through them. Though air leakage is a significant contributor to the temperature differences in the readings, other factors include imperfections in the envelope geometry and, to a lesser extent, the inaccuracy of sensor placement.

Joints H, J, and L, which, like joint F, are formed by the intersection of two envelope elements, perform very similarly to joint F. The largest percentage difference in these joints is 3% at -20 °C and 7% at -40 °C.

Table 4.1 Steady state temperature values and differences for joint F at -20 °C and -40 °C with tape seal but without pressurization

	Sensor	Temperature (°C)			Difference (Max-Min)	Percentage Difference
		F _A	F _B	F _C		
-20 °C	F1	18.26	18.25	18.05	0.22	0.52
	F2	17.58	17.36	17.67	0.30	0.72
	F3	7.23	7.16	7.52	0.36	0.86
	F4	-6.44	-6.36	-6.20	0.24	0.57
	F5	-16.36	-15.70	-16.29	0.66	1.57
	F6	-17.62	-16.97	-16.97	0.65	1.55

-40 °C	F1	17.47	18.72	18.51	1.25	2.02
	F2	16.46	17.34	17.57	1.11	1.80
	F3	2.75	3.97	2.77	1.22	1.97
	F4	-16.40	-15.92	-17.80	1.88	3.04
	F5	-30.51	-30.53	-33.44	2.93	4.72
	F6	-32.94	-32.53	-34.95	2.41	3.89

Joints G, I, K, and M, which are formed by the intersection of three joint elements, are more complex joints making them less likely to be airtight. Table 4.2 shows the results for joint M, the intersection of two perpendicular walls and the ceiling. It can be seen that at both -20 °C and -40 °C, the difference in the temperature readings at the two incidences of joint M are almost always above 0.5 °C. The readings at M4 exhibit the largest discrepancy as it is the point location within the joint most sensitive to temperature changes due to exfiltration. This difference indicates that the two incidences of joint M are behaving quite differently. As mentioned earlier, this is due to a combination of air leakage caused by stack effect and imperfections in the envelope geometry. However, these results do not show how leaky the joints are. Pressurization and depressurization tests are needed for this purpose, as demonstrated in the following subsection.

Table 4.2 Steady state temperature values and differences for joint M at -20 °C and -40 °C with tape seal but without pressurization

	Sensor	Temperature (°C)		Difference (M _A -M _B)	Percentage Difference
		M _A	M _B		
-20 °C	M1	18.04	16.48	1.56	3.71
	M2	16.89	15.92	0.97	2.31
	M3	10.27	6.96	3.31	7.88
	M4	1.73	-4.29	6.02	14.34
	M5	-13.01	-15.72	2.71	6.45
	M6	-16.17	-17.15	0.98	2.34
-40 °C	M1	17.54	16.61	0.94	1.51
	M2	15.74	15.74	0.01	0.01
	M3	7.24	5.38	1.86	3.00
	M4	-0.41	-6.48	6.07	9.78
	M5	-25.59	-28.36	2.78	4.48
	M6	-29.69	-33.35	3.67	5.91

4.1.2 Temperature profiles at -20°C with pressurization and with tape seal

Figure 4.1 shows the temperature profile of joint L at -20°C, as an example. It is located at the intersection of two perpendicular walls. Because there is a combination of wood and insulating materials in the joint, the lines are not perfectly straight. When pressure differences are imposed on the joint, there are noticeable changes in temperature but not significant. This joint is rather airtight and simple to seal as well because of its geometry. Joints F, H, and J perform similarly as well.

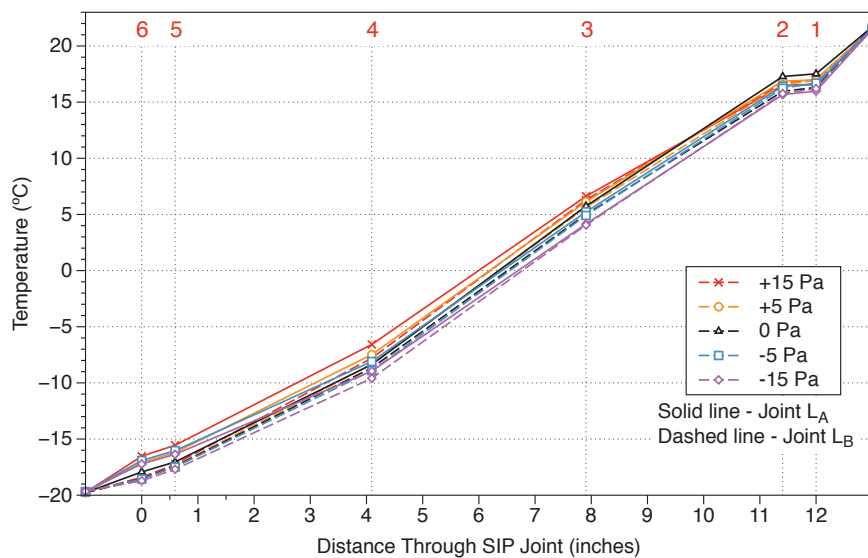


Figure 4.1 Temperature profile of joint L with -20 °C exterior temperature with tape seal

Figure 4.2 shows the temperature profile for joint G, at the intersection of two parallel walls and the ceiling. The effects of air leakage on temperature are more pronounced and indicate higher rates of air leakage in the vicinity of that joint. Temperature changes of up to 4 °C occur in the joint due to a 5 Pa pressure difference exerted on the envelope, and up to 7 °C with 15 Pa.

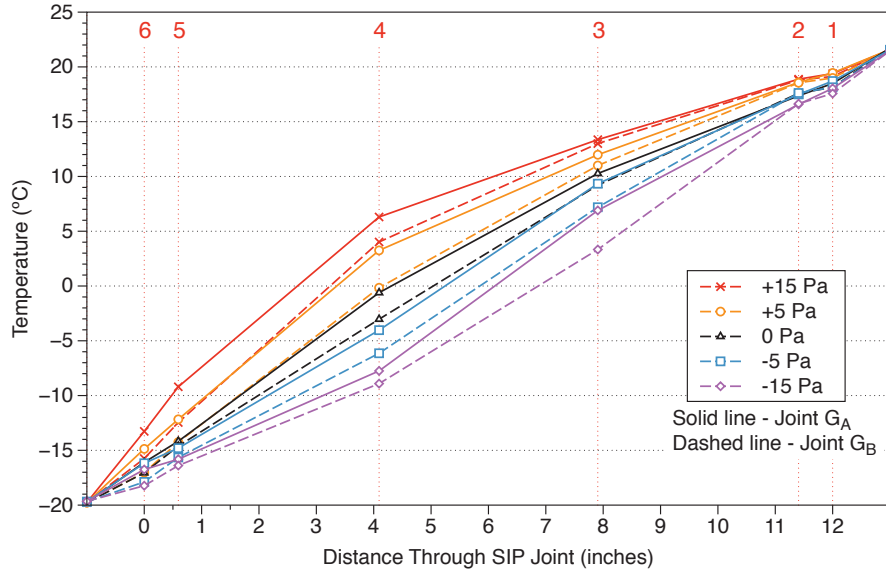


Figure 4.2 Temperature profile of joint G with -20 °C exterior temperature with tape seal

Figure 4.3 shows the temperature profile for joint M, at the intersection of two perpendicular walls and the ceiling. Compared to other joints, the amount of air leakage found here is higher, as demonstrated by the large temperature changes caused by pressure differences across the envelope. It can also be seen that the two identical joints seem to perform very differently even with no pressure differential. This indicates inconsistencies and imperfections in the joint construction. Even with regards to air leakage, it can be seen that incidence B of the joint is significantly more leaky than A. The temperature reading at M_B3 changes by 6 °C under 15 Pa of depressurization, while at M_A3 the change is 17 °C under the same conditions.

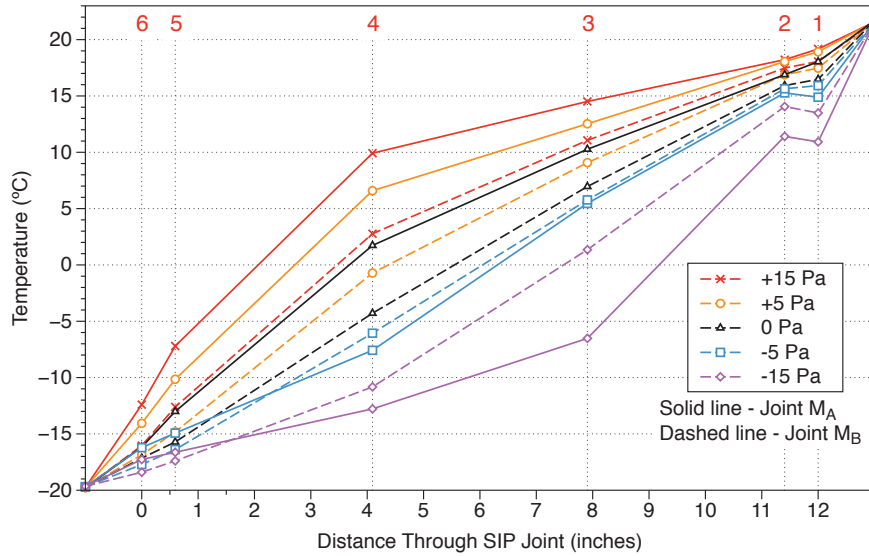


Figure 4.3 Temperature profile of joint M with -20 °C exterior temperature with tape seal

4.1.3 Temperature profiles at -20°C with and without tape seal

The continuity of the air barrier in this SIP system is maintained by tape at the joints. However, the long-term durability of tape is questionable. This subsection examines how reliant this wall system is on the tape for air tightness. Figure 4.4 shows the temperature profile for joint H with and without the tape seal. It is clear that the joint is relatively airtight with the tape in place. Without the tape, instance H_B of the joint is not significantly affected since the temperature profile does not change considerably. The profile at instance H_A, however, is affected significantly by the removal of the tape. Even without any pressurization, air leaks at this joint to the exterior. This indicates that the neutral plane is below the midway height of the SIPs.

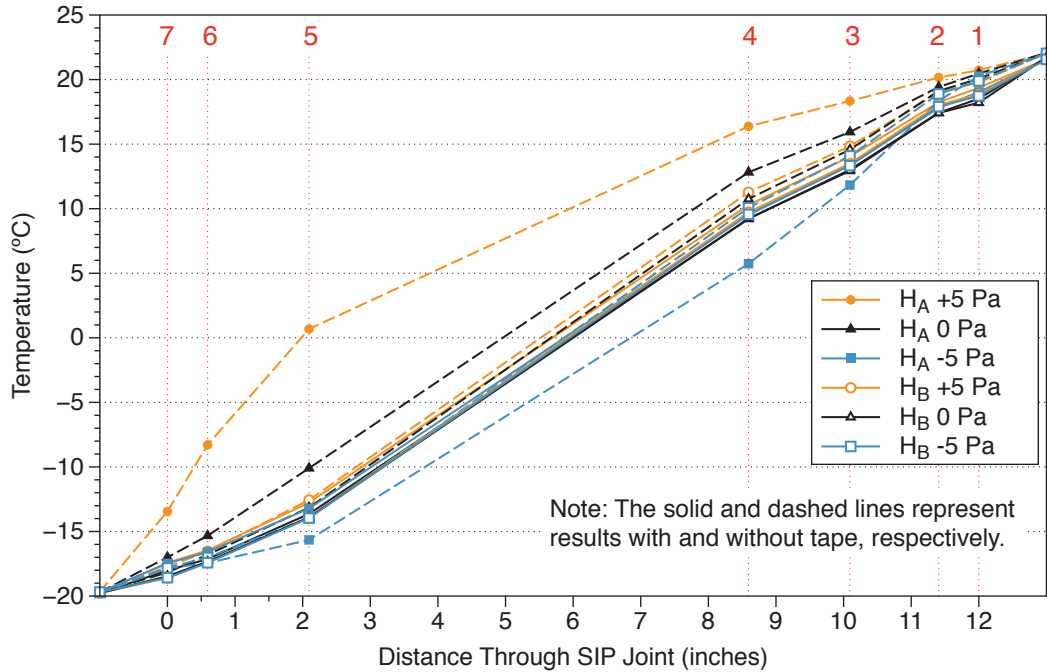


Figure 4.4 Temperature profile of joint H with and without tape seal

Figure 4.5 shows the temperature profile for joint G, the intersection of parallel SIPs and the ceiling, with and without the tape seal. At this joint, the tape has played a big role in minimizing air leakage. At G_A4, 5 Pa of pressurization causes a 4 °C temperature change with tape, and a 12 °C temperature change without tape. In general, joints at the intersection of three envelope elements are found to have a more significant reliance on the tape. At the same time, these locations are more difficult to seal with tape.

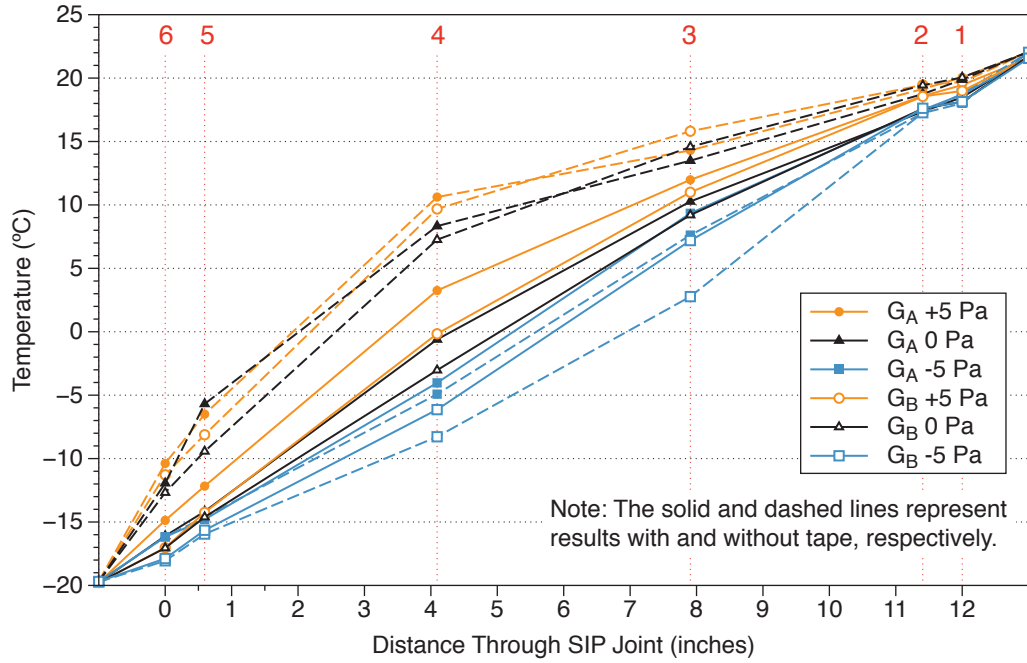


Figure 4.5 Temperature profile of joint G with and without tape seal

4.1.4 Other observations



Figure 4.6 Top-down view of joint M_A showing moisture accumulation

Upon dismantling the experimental setup, the authors noted that the tops of the insulated caps on the wall SIPs were stained, indicating moisture accumulation at those locations. They tend to be on the exterior portion of the SIP rather than the interior. These locations correspond to joints F, G, and M. Figure 4.6 shows the moisture accumulated in joint M_A. No moisture accumulation was found in any of the other 5 joint types.

4.2 Attic Tests

The attic test results are presented in two subsections. The first is for test 1, which was carried out with an outdoor temperature of -40 °C. The second subsection is for test 2, which was carried with -25 °C, -7 °C, and 6 °C, outdoor temperatures.

4.2.1 Test 1: -40 °C Outdoor Temperature

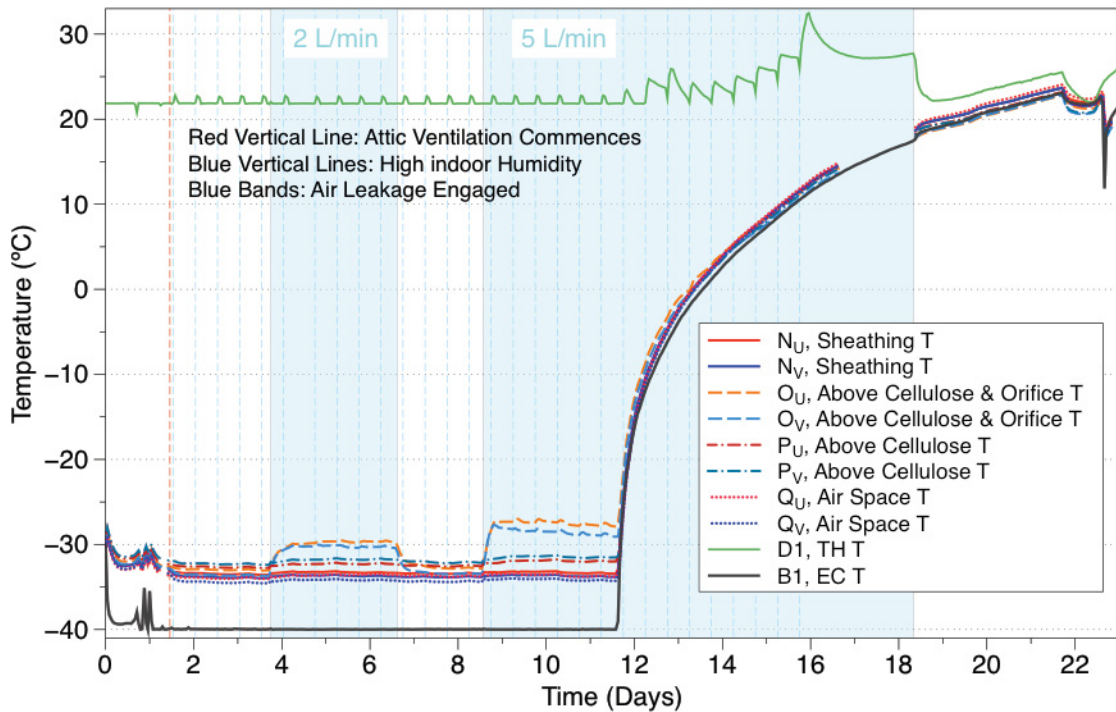


Figure 4.7 Temperature conditions for test 1: -40 °C outdoor temperature

Figure 4.7 shows the temperature conditions in the attics, EC, and TH for test 1. The heat gains in the TH that occur every 12 hours are caused by the dehumidifier that is initiated after period of high humidity are created. Temperatures in both attics are almost identical. On average, the UA temperature is 0.5 °C higher than in the VA, while the maximum difference between these two attics is 0.9 °C. The temperature above the cellulose and orifice is slightly higher in the unvented attic when air is leaking (<2 °C). When the EC temperature is -40 °C and the TH temperature is 22 °C, the attic air temperatures are between -32 °C and -34 °C. For both the UA and VA, the temperature observed under the sheathing is higher than that of the air space. However, the difference, in both attics, is generally less than 0.5 °C, which is within the measurement error. As the temperature of the EC goes up after the compressor is switched off, the TH begins to overheat due to the heat generation by the dehumidifier and electrical devices.

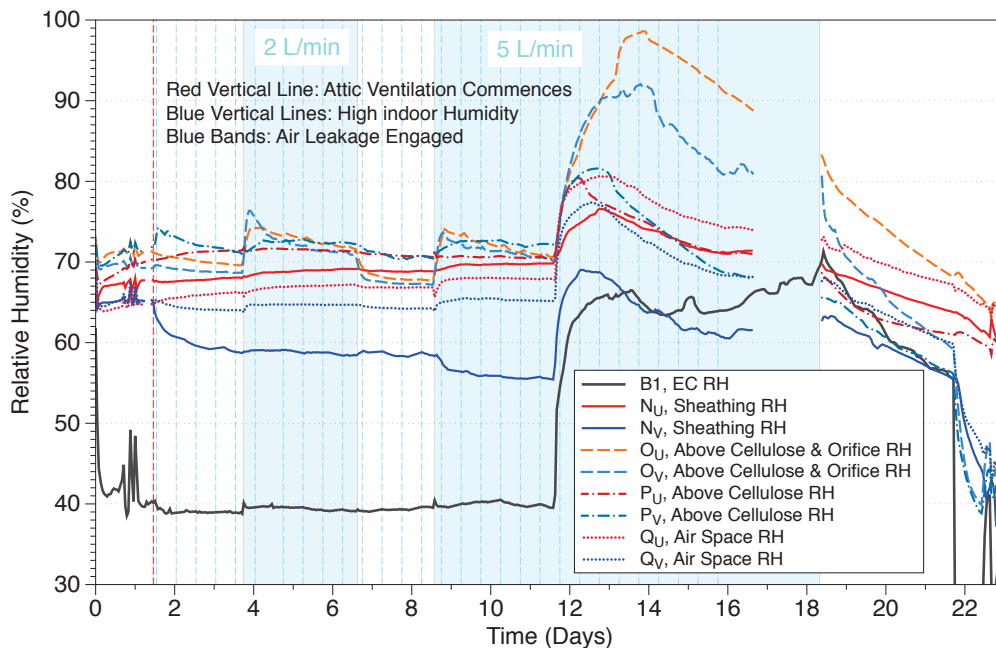


Figure 4.8 RH conditions for test 1: -40 °C outdoor temperature

Given that the temperature readings are similar in the two attics, the RH readings can be compared too. Figure 4.8 shows the RH conditions in the attics and EC for test 1. The lines represent data obtained by the sensors detailed in Chapter 3. Note that the indoor RH is kept at 40% and elevated to 80% every 12 hours for an hour. Those instances are indicated by the vertical blue lines on Figure 4.8. As soon as the ventilation is initiated for the VA, the RH reading at the sheathing, N_v , is directly affected and drops about 5% over the course of a day, while the temperature drops slightly by 2 °C as shown in Figure 4.7. Sensors O, P, and Q in the VA also decrease slightly by 3% or less. This is reasonable, given that the outdoor air is drier, as shown in Figure 4.9 by the humidity ratio, and ventilation dries the attic air. The greater change at sheathing location, N_v , is due to the air ventilation path. When the air leakage is engaged, all the RH readings increase slightly, except for the VA sheathing RH, which is mostly unaffected. Actually, the second time the air leakage is engaged, the VA sheathing RH slightly drops by 3%. It is possibly due to the formation of ice on the surface of sheathing. As shown in Figure 4.9, humidity ratio is more or less constant during this period, when ice forms on the sheathing surface it release heat, which may increase the local surface temperature, consequently lower the local RH. When the air injection started, the RH increases and the level of RH following the order of O, P, Q, N. As shown in Figure 3.21, sensor O is directly above the injection orifice, sensor P is above cellulose insulation but 52 cm away from the orifice, Q is in the air 30 cm below the roof ridge, and N is close to the sheathing. The closer to the air injection, the greater the increase of RH. The response is quick, stabilizing within a day, indicating that the air injection and ventilation have reached equilibrium. Though the RH conditions in the UA and VA are almost the same at

the beginning of the test, the UA RH is 3% higher than that of the VA by day 11. Larger differences are observed in the sheathing underside readings. By day 11, the RH in the VA sheathing is 14% less than the RH in the UA. Again, this is because sensor N_V is located along the ventilation path. While the EC is kept at $-40\text{ }^\circ\text{C}$, the EC air is consistently drier than the attic space, since the T and RH are both lower. Above the cellulose, the readings from the two attics are similar. After the EC HVAC system is turned off and the temperature begins to increase, the RH in above the cellulose and orifices increase to 92% in the VA and 99% in the UA. This is caused by the melting of the frost that has accumulated in the cellulose during the cold phase of the test. However, the cellulose does dry over the course of a few days. The RH in the sheathing of both attics increases for about one day after the EC HVAC system is turned off, but decreases after that. Generally, the RH readings in the VA decrease more rapidly than those of the UA.

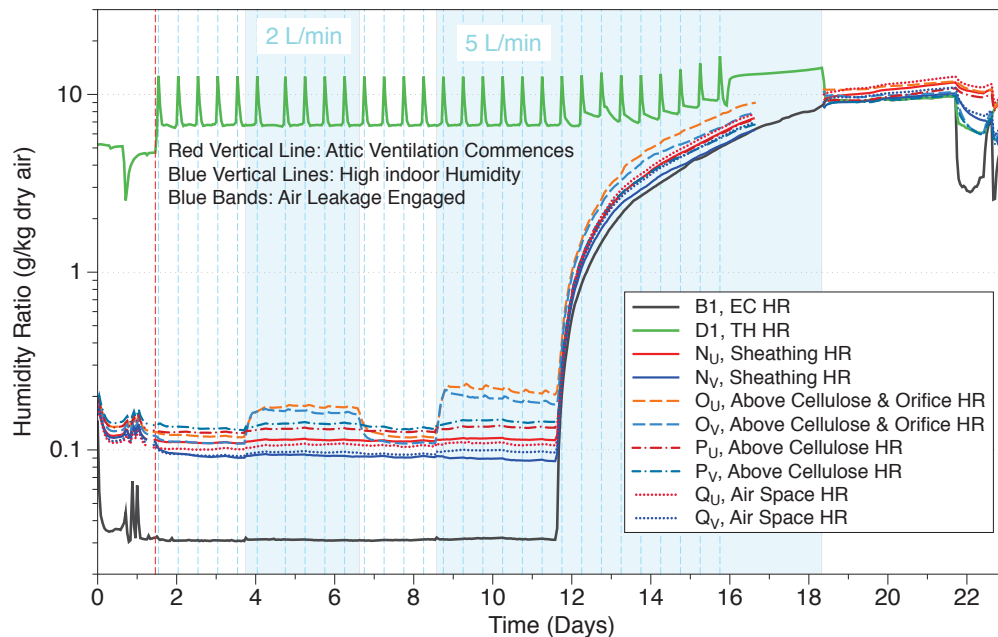


Figure 4.9 Humidity ratio trend in test 1: $-40\text{ }^\circ\text{C}$ outdoor temperature

Figure 4.9 shows the trend in the humidity ratio in the EC, TH, and attics for test 1. Throughout the entire test, the EC HR is consistently lower than the conditions of either attic. At temperatures below freezing, there is no control of EC humidity conditions, aside from ensuring that humidity is sufficiently low to avoid moisture problems with the EC HVAC system. This low EC HR provides an advantage for the VA. In reality, the outdoor conditions of communities in the Canadian north tend to be more humid. The average RH is around 65-70% in the winter and around 80-85% in the summer, where the shoulder seasons lie somewhere in between. The HRs in attic air (Q), close to sheathing surface (N), and above cellulose insulation (P) do not change noticeably although slightly increases with the injection of air leakage from indoor. The only noticeable HR increase with the injection of air leakage is at location above the cellulose and orifice (point O). This trend indicates 1) non-uniform distribution of moisture in attic air, higher moisture level close to the air injection location; 2) most of the moisture introduced into attic has been absorbed by cellulose insulation; and 3) under extreme cold conditions attic ventilation does not remove significant amount of moisture. In general, HR levels observed in the UA are slightly higher than those in the VA.

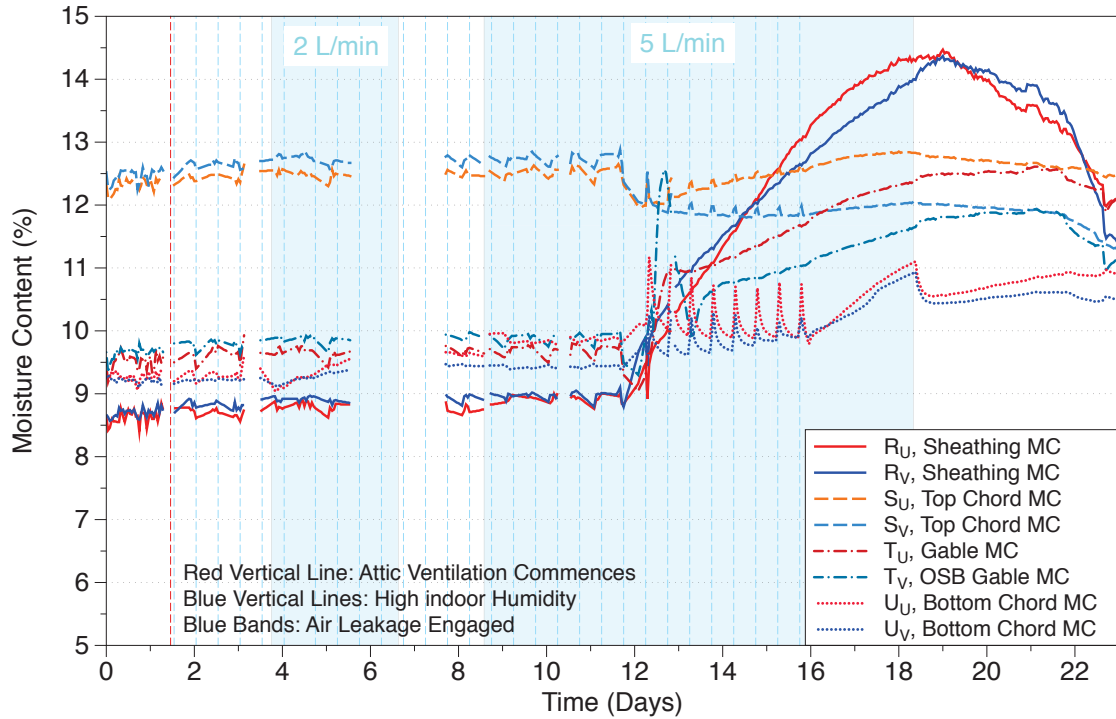


Figure 4.10 Moisture content readings for test 1: -40 °C outdoor temperature

Figure 4.10 shows the moisture content readings for the attics in test 1. During the cold phase of the test, the MC values do not change significantly, but there is generally a slight increase of less 1%. After the warming of the EC, the readings are more responsive to the environmental changes. The readings at the bottom chord near the orifice are directly affected by the air leakage and changes in the humidity of the leaked air. These changes are momentary and do not have lasting effects within a short test period. This may not be true in the long term, as moisture tends to accumulate slowly in materials over time. For the sheathing, a temporary increase in the MC readings is observed. Starting at about 9% MC at the end of the cold phase for both attics, the readings increase to over 14% in 6 days, then decrease to about 12%. UA Bottom chord MC increases from 9.5% at the beginning of the test to 10.5% at the end. UA Sheathing MC increases from 8.5% to 12%. The more significant increase of MCs in plywood sheathing and bottom chord is mostly

due to the melting of frost under milder conditions. The VA generally exhibits lower reading of MC, although the differences are not great, often less than 1%, which is an indication that attic ventilation helps removal of moisture under milder conditions.

With this test, it is found that at extreme temperature (-40 °C), ventilation has an insignificant effect on the moisture in the attic when air leaks at the bottom of the insulation, even if the air moisture content outside is less than that of the attic. This is partially because most of the water in the leaking air condenses and freezes in the cellulose insulation. The bursts of high indoor RH have a temporary and small effect on the RH readings in the attics. The major effect is that there will be more frost in the cellulose that will melt in the warmer seasons. At warmer temperatures, the VA performs better than UA as the frost melts. The RH readings in VA are all lower than that in the UA. The RH outside is quite low during these warm temperatures, which has a significant effect on the VA's drying capacity.

4.2.2 Test 2: -25 °C, -7 °C, 6 °C Outdoor Temperature

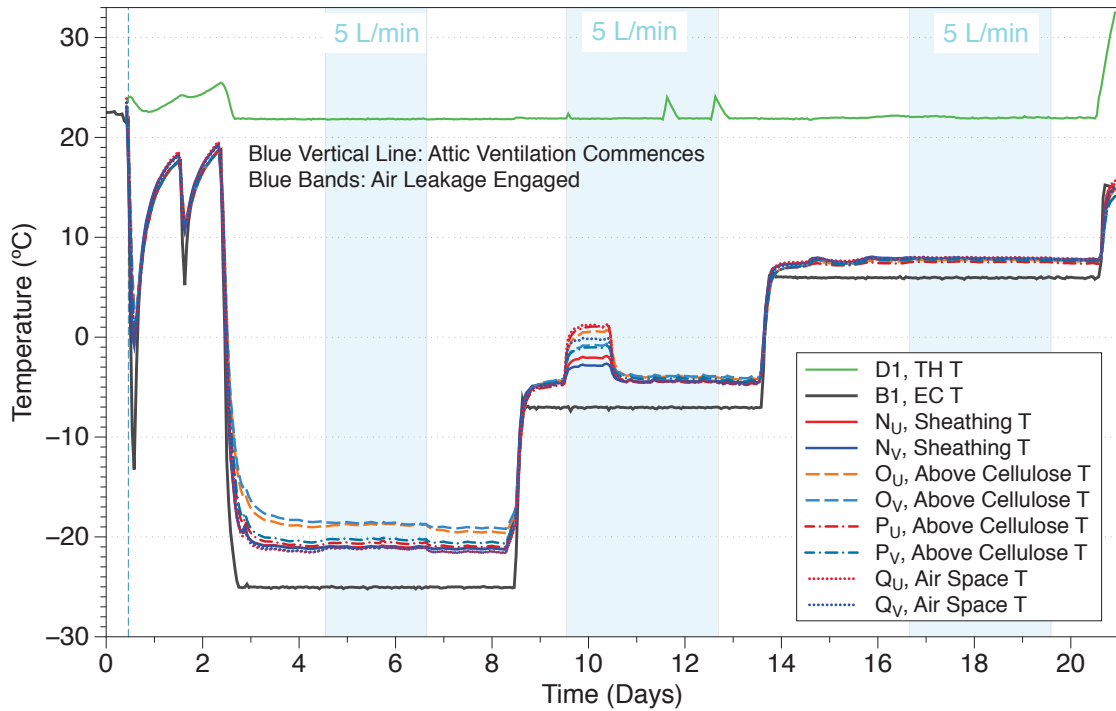


Figure 4.11 Temperature conditions for test 2: -25, -7, and 6 °C outdoor temperature

Figure 4.11 shows the temperature conditions in the EC, TH, and attics for test 2. The three stages of the test are shown clearly. On the ninth day of the test, however, a day-long elevation of the temperature in the attics is caused by lights in the attics being left on unintentionally. Otherwise the temperature difference between the UA and VA is generally less than 0.2 °C throughout the test.

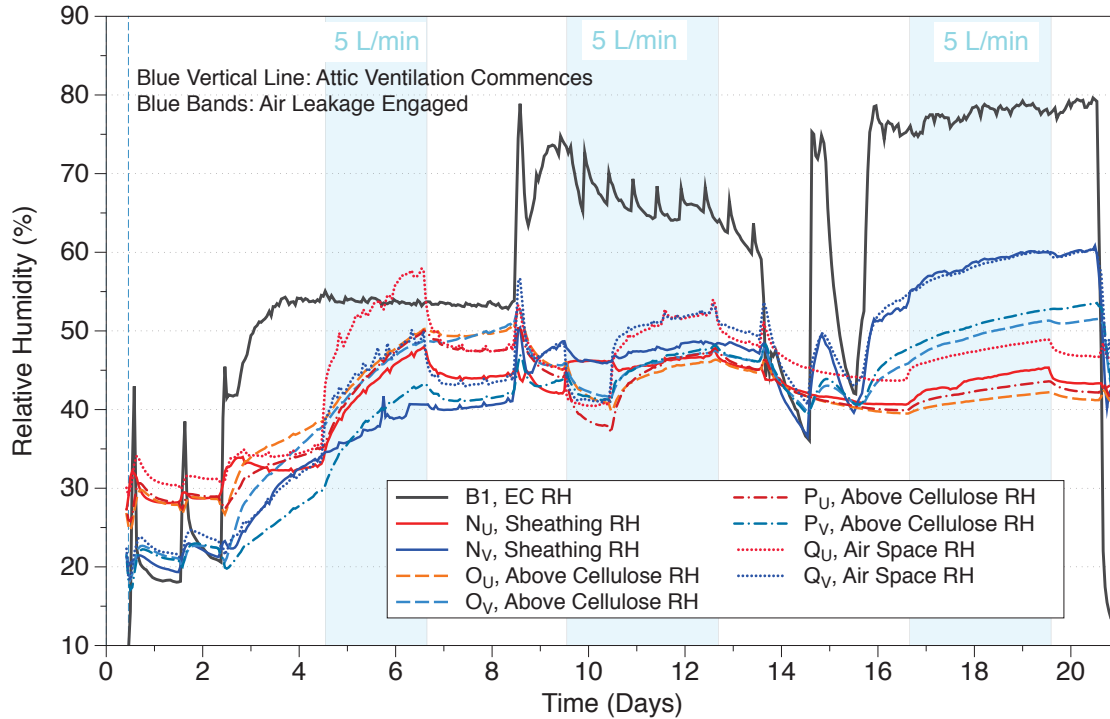


Figure 4.12 RH conditions for test 2: -25, -7, and 6 °C outdoor temperature

Figure 4.12 shows the RH conditions in the EC and attics for test 2. The EC RH conditions cannot be compared with those of the attic since the temperature conditions are not the same. However, the range of the EC RH conditions in this test is rather representative of the conditions that would be experienced in the Arctic (between 50 and 80%). The initial RH conditions of the attics are rather dry (<40%), so the RH levels in the TH attained throughout this short-term test are understandably not high (<60%). Nevertheless, the relative performance of the attic can be compared. During the first phase of the test when the outdoor temperature is -25 °C, the UA exhibits higher RH levels than the VA overall, up to 8% difference in the air space RH. The UA is immediately and directly affected by the air leakage, where the air space RH increases by 23% in two days, while the VA RH increases by 17% in the same period. In the second phase of the test when the EC temperature is -7 °C, the two attics respond similarly. The

VA RH levels are slightly higher overall (less than 2% difference). In both attics the RH levels increase at a rate of less than 1% per day when air leakage is engaged. The RH levels immediately begin to decrease when there is no air leakage. In the third phase of the test when the EC temperature is 6 °C, the VA RH levels are significantly higher than those of the UA. Compared to the UA, the VA air space RH is up to 11% higher and the VA sheathing RH is up to 15% higher. Clearly, because of the high ventilation rate in the VA, the humidity conditions in the VA are strongly influenced by the high RH levels in EC during this period. Therefore, the VA is gaining moisture from the EC, whereas the UA RH level is more stable. The other observation in test 2 is that compared to test 1, RH at monitored locations in the attic increases noticeably with the injection of air leakage given that the moist indoor air is introduced directly into the attic and therefore the RH of attic air, close to the sheathing surface and above the cellulose responded to that increase. This can be seen in the humidity ratio (Figure 4.13) and moisture content (Figure 4.14) as well.

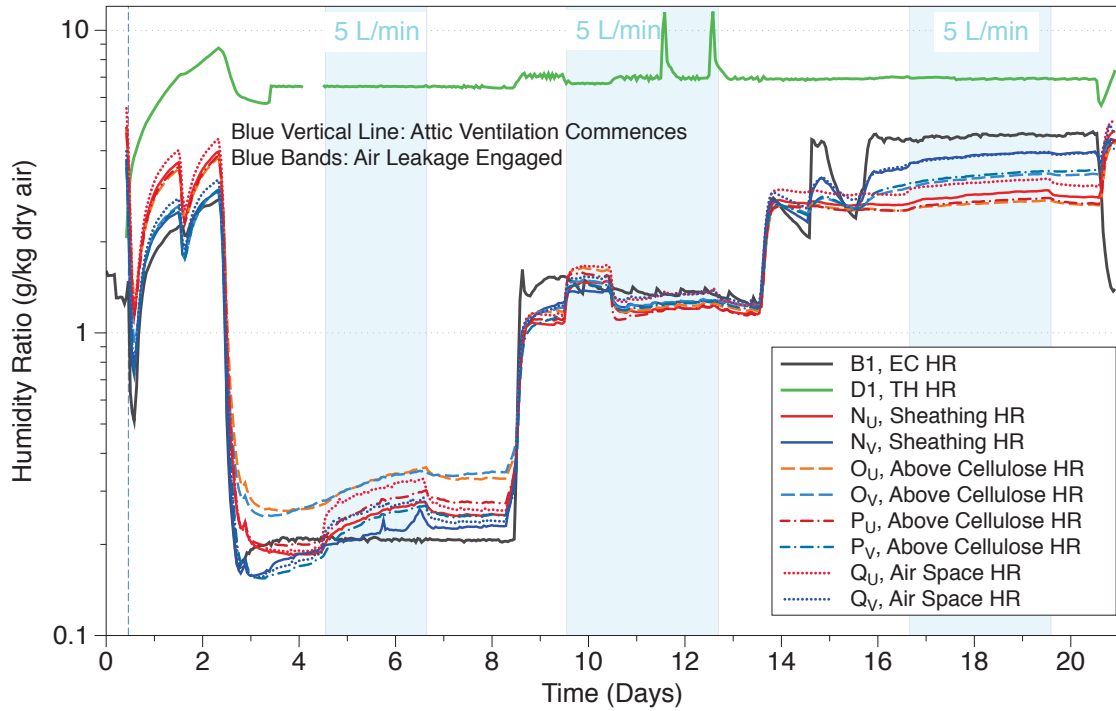


Figure 4.13 Humidity ratio conditions for test 2: -25, -7, and 6 °C outdoor temperature

Figure 4.13 shows the humidity ratio in the EC, TH, and attics for test 2. The initial humidity ratio conditions at this temperature are quite similar in both attics. At first, without air leakage, the humidity conditions in the UA are stable for the first two days at about 0.18 g/kg. The VA sees increasing levels of humidity during that same period from 0.16 g/kg to 0.18 g/kg. The increasing humidity conditions can be attributed to the higher HR conditions in the EC during that period (between 0.19 g/kg and 0.21 g/kg). When air leakage commences, the humidity conditions increase in both attics, more so in the UA. In the 2 days with air leakage, the UA air space HR increases from 0.20 g/kg to 0.33 g/kg. The VA HR increases from 0.19 g/kg to 0.28 g/kg. The lower HR conditions in the EC during this period (between 0.20 g/kg to 0.21 g/kg) allow the VA to maintain lower levels of humidity than the UA.

Once air leakage is removed, the HR in both attic air spaces decrease sharply for about a half day. The UA air space HR stabilizes around 0.26 g/kg while the VA stabilizes around 0.24 g/kg. When the EC conditions are changed to -7 °C, the HR in the attics increase as the materials release moisture into the air. The HR in the UA reaches about 1.15 g/kg and does not increase further. The HR in the VA, on the other hand, keeps increasing to about 1.22 g/kg, at which point air leakage is initiated. The EC HR conditions are well above those of the attics during this period, which would explain the increasing humidity levels in the VA.

The start of the air leakage coincides with the lights in the attic bays being turned on. The elevated temperatures in the attic bays caused by the lights generates higher HR levels than would be expected if the lights had not been activated. Therefore, the initial change in HR conditions caused by air leakage cannot be identified. After the lights had been deactivated, the HR conditions in both attics decrease quickly. The initial conditions for this test are very dry and the short duration of the test did not allow for significant wetting and moisture accumulation in the attics. With a more long-term test, the attics would attain higher levels of moisture and approach more closely the steady state conditions. Higher air leakage rates would also accelerate the wetting process, though moisture transport through the materials would still require much time and very high air leakage rates may not be realistic.

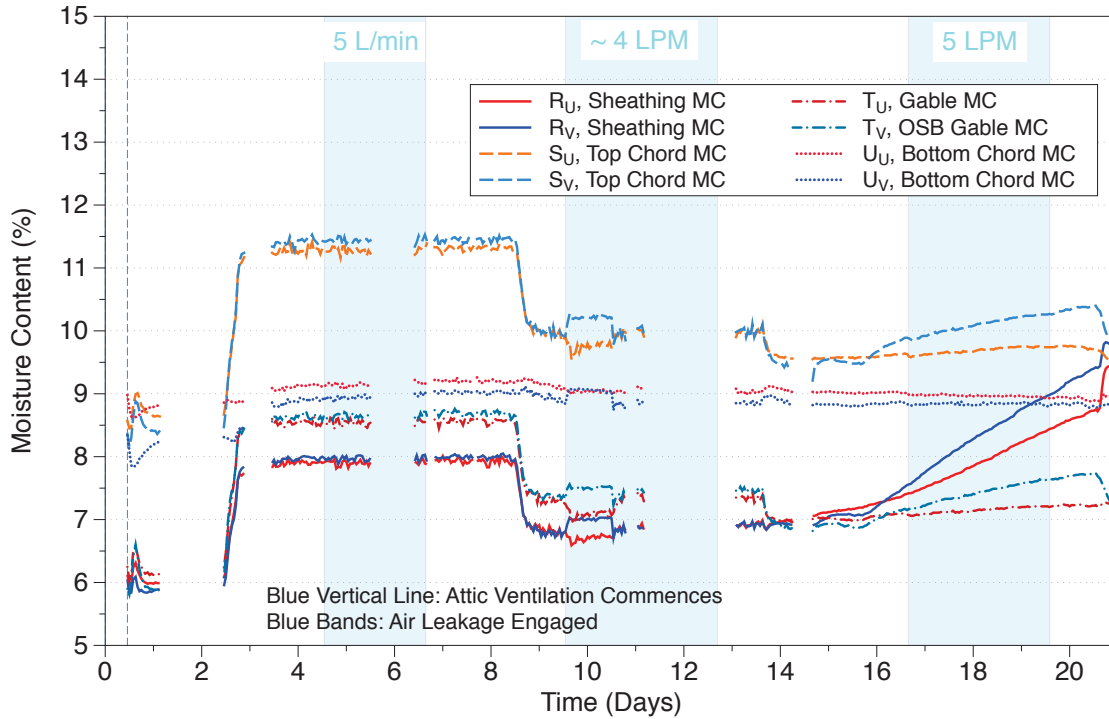


Figure 4.14 Moisture content readings for test 2: -25, -7, and 6 °C outdoor temperature

Figure 4.14 shows the MC readings in the attics for test 2. When the EC temperature is -25 °C, the moisture readings increase by up to 2-3%. This increase only occurs for the sensors that are exposed to the cold temperature in the attic, since the MC readings at the bottom chords are not affected in this way given that the air leakage is introduced directly into the attic air. When the EC temperature is -7 °C, the MC readings decrease and stabilize at levels around 1-1.5% higher than those at the beginning of the test. The MC level in plywood and top chord in VA is slightly higher than that in UA (within 0.5%) due to the slightly higher HR in the EC compared to the attic as shown in Fig. 13 for this period. When the EC temperature is 6 °C, MC readings begin to increase, except for the bottom truss chords. The sheathing MC increases from 7% to 9.5% in the VA and from 7% to 9% in the UA over the course of 6 days. Similar results are observed in the top truss chords and the gables, where the MC readings in the VA increase more rapidly than

in the UA. The increase of MC in plywood sheathing and top chord in VA is higher than that in UA due to the moisture brought in by ventilation during this test period, as shown in Figure 4.13, where the humidity ratio in EC is higher than in the attic. This trend shows that attic ventilation brought moisture in when outdoor humidity ratio is higher than the attic.

The limitation of this experiment do not allow for the results to be generalized. Hygrothermal simulation may be able to extent the findings to more general cases. Short periods (1-2 hours) of high indoor humidity have shown not to have a significant effect on the conditions in the attics in both air leakage cases, where the air is supplied directly into the air space and where the air is supplied at the bottom of the cellulose. These short bursts of high humidity do not pose significant dangers to the attics in the long term, even if periodically. The existence of chronic air leakage, caused by stack effect and other sources of pressure differentials, at any reasonable indoor RH condition is more detrimental to the attic performance.

CHAPTER 5 Hygrothermal Simulation

This chapter covers the simulation component of this project. The first section pertains to thermal simulations of SIP joints while the second section pertains to hygrothermal simulations of attics. In each section, the first subsection presents the methodology, while the second presents the results.

5.1 SIP Joints

5.1.1 Methodology

Two- and three-dimensional thermal simulations are performed to obtain reference temperature profiles for the joints. Minor defects and imperfections in the wall assembly mean that joints do not fit perfectly together and some degree of air leakage is bound to occur. The 8 joint types tested are simulated separately, and the geometry applied is that of the ideal case (perfect-fitting, no air leakage). Joints F, H, J, and L are simulated in two dimensions since those joints are formed by the meeting of two components that are essentially extrusions of a two-dimensional section. Joints G, I, K, and M are simulated in three dimensions since they are formed by the meeting of three components. All simulations are performed using COMSOL Multiphysics (COMSOL, 2016).

The thermal properties of the materials used are listed in Table 5.1 and are obtained from Kumaran et al. (2002). The exterior and interior film coefficients are assumptions, and the interior tape seal and exterior SBPO layer are excluded from the simulation. The interior and exterior air temperatures in the simulation are set to 22 °C and -20 °C,

respectively. The temperature values at the sensor locations obtained through simulation are compared with the experimental results.

Table 5.1 Thermal properties of simulated materials (Kumaran et al., 2002)

Material	Thermal Conductivity (W/m·K)
Wood (I-joist flange)	0.11
OSB	0.102
EPS	0.0379
Thermal Conductance (W/m²K)	
Exterior film coefficient	12
Interior film coefficient	4

5.1.2 Results

Though the experimental results reveal much about the performance of the joints under temperature and pressure differences, none of the cases tested represent the ideal scenario for any of the joints. Minor defects and imperfections in the wall assembly mean that joints do not fit perfectly together and some degree of air leakage is bound to occur. Two- and three-dimensional thermal simulations are, therefore, performed to obtain reference temperature profiles for the joints. This subsection compares the experimental results with the thermal simulations. Figure 5.1 shows the temperature profile for joint L with both the experimental and values from 2D simulation. Good agreement is observed generally. Discrepancies greater than the instrumentation bias can be attributed to imperfections in wall assembly, discrepancies in the material properties, as well as the modest amount of air leakage that occurs due to stack effect. Good agreement is observed for all the joints simulated in two dimensions.

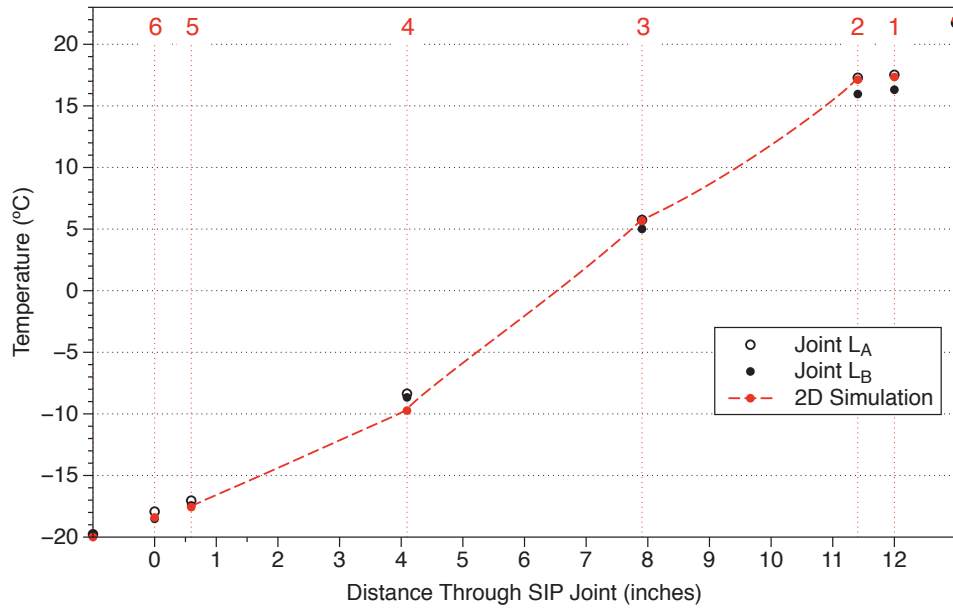


Figure 5.1 Temperature profile of Joint L with values obtained from 2D simulation

Figure 5.2 shows the temperature profile for joint M with both the experimental and simulated values. Large discrepancies are observed especially at sensor M_{4A}, where the difference is about 13 °C. As was seen before, joint M leaks air even without mechanical pressurization. Stack effect causes the air exfiltration at joint M, warming the joint. This is the main reason for the large discrepancy. At joint K, stack effect causes the air to infiltrate and cool the joint. Figure 5.3 shows the temperature profile of joint K. In this case, the experimental readings are lower than those obtained by simulation.

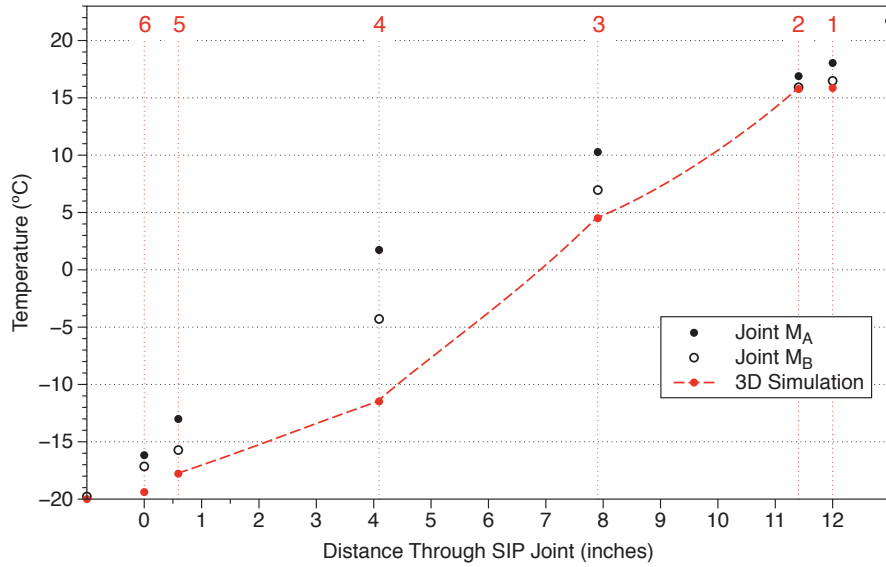


Figure 5.2 Temperature profile of Joint M with values obtained from 3D simulation

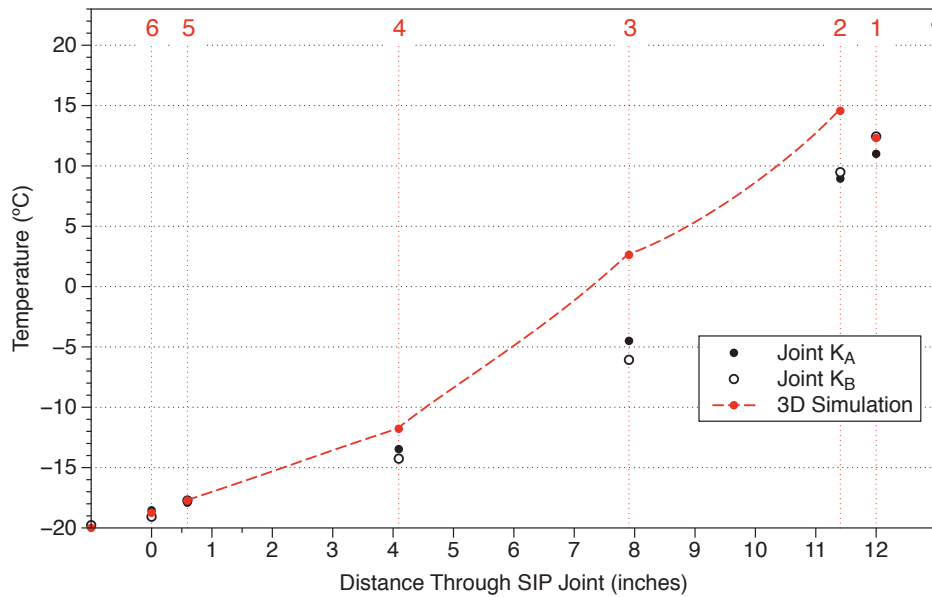


Figure 5.3 Temperature profile of Joint K with values obtained from 3D simulation

The results as shown in Figure 5.1 to Figure 5.3 clearly show the difference in performance between the various joints and that the experimental temperature profiles can differ greatly from the simulated, ideal case scenarios. To present the results in a

concise and meaningful way, root-mean-square deviation (RMSD) calculation comparing the experimental results with the simulated results are carried out using the following equation:

$$RMSD = \sqrt{\frac{\sum_{t=1}^n (T_{simulation,t} - T_{experiment,t})^2}{n}} \quad (5.1)$$

Where $T_{simulation}$ and $T_{experiment}$ are the temperature values at the sensor locations obtained by simulation and experiment, respectively; t designates the sensor number in each joint; and n is the total number of sensor in each joint (7 for joint H, 6 otherwise). This calculation is done for all 18 joints, under all air pressurization conditions tested, with and without tape, subjected to -20 °C exterior temperatures. The RMSD values are tabulated in Table 5.2. The greater the RMSD value, the more the experimental temperature profile differs from that of the simulation. A graded color scale is applied to the table for convenience.

The results with the tape seal show how the joints would perform under normal operating conditions. Joints F, H, J, and L have the low values for RMSD (up to 4.07 °C) and are not affected by pressurization significantly. These joints are also formed by the connection of only two envelope elements, which makes them easier to fit together and seal. The RMSD values for those joints are consistently below 2.6 °C, except for F_A and F_B under +15 Pa of pressurization. Joints H and L perform better than F and J overall. Part of the reason for this is that F and J are subjected to greater pressures from stack effect, since joint F, the top joint, exhibits higher RMSD values under pressurization and joint J, the bottom joint, exhibits higher RMSD values under depressurization.

Joints G, I, K and M stand out as being the leakier joints when compared to the simulation results. Even without any pressurization, the RMSD values are at least 2.9 °C. Because of stack effect joint G and M, which are top joints, are more affected by pressurization while joints I and K, which are bottom joints, are more affected by depressurization. The two instances of each of these joints generally exhibit similar performance, with the possible exception of joint M. The RMSD values for joint M_A are significantly higher than those of joint M_B, and the highest of all the joints too. This may be an indication of improper sealing at that joint.

Table 5.2 RMSD values between experimental and simulation results

RMSD values between experimental and simulation results (°C)					
Air pressure in test hut (Pa)					
	-15	-5	0	+5	+15
Joint	With tape seal				
F _A	2.05	1.70	1.36	2.33	3.85
F _B	1.55	1.35	1.61	2.24	4.07
F _C	2.05	1.34	1.55	1.71	2.60
G _A	1.49	2.62	3.99	5.91	7.77
G _B	2.17	1.58	2.90	4.12	6.20
H _A	1.54	1.53	1.60	1.41	2.04
H _B	1.40	1.27	1.60	1.18	1.14
I _A	7.95	6.70	6.81	5.27	2.89
I _B	5.29	4.12	3.57	2.71	1.74
J _A	2.31	1.53	2.10	1.07	1.18
J _B	2.45	1.81	1.97	1.42	1.20
J _C	1.84	1.78	1.75	1.51	0.70
K _A	7.44	5.36	3.81	2.07	3.20
K _B	6.97	5.53	4.24	2.46	4.10
L _A	1.27	1.19	0.64	1.23	1.80
L _B	0.99	0.64	0.82	0.64	0.87
M _A	5.36	2.43	6.42	9.06	11.08
M _B	1.83	2.44	3.35	5.10	6.97
	Without tape seal				
F _A		1.86	3.78	5.44	
F _B		1.26	5.67	7.59	
F _C		2.35	5.10	7.06	
G _A		2.38	9.26	10.13	
G _B		2.26	8.28	9.62	
H _A		2.29	2.42	7.69	
H _B		0.89	0.94	1.26	
I _A		10.28	7.26	6.02	
I _B		7.93	4.11	4.17	

J_A		1.94	1.15	1.37
J_B		4.28	1.31	4.74
J_C		2.13	0.84	0.62
K_A		12.64	9.39	16.18
K_B		11.04	6.56	8.21
L_A		1.93	1.65	4.02
L_B		3.25	1.34	3.11
M_A		4.65	11.54	12.79
M_B		5.28	12.34	13.02

When the tape is removed, the inherent capabilities of the SIP system to control air leakage are examined. Generally, the joints rely heavily on the tape to minimize air leakage. However, some joints like H_B, J_A, and J_C maintain their airtightness even without tape. Whereas different incidences of a joint type perform rather similarly with tape, this is much less the case without tape. The RMSD value for joint H_B at +5 Pa is 1.18 °C with tape and 1.26 °C without tape, while for joint H_A, the value is 1.41 °C with tape and 7.69 °C without tape. This inconsistency between like joints can also be seen in joints I, J, and K. Interestingly, joints M_A and M_B, which performed very differently with tape, behave very similarly without tape. This supports the notion that the tape seal was not applied properly for M_A. Joint K_A, which performed well with tape and +5 Pa (RMSD = 2.07), exhibited the worst performance of all joints without tape (RMSD = 16.18). Overall, it can be said that joints F, H, J, and L perform better than G, I, K, and M, with or without the tape seal.

The high reliance on the tape exhibited by most of the joints indicates that there is a need to improve the manufacturing standards of the SIPs, or even that the overall design should be revised. Because the ability of the tape to maintain a good seal over a long period is not easy to guarantee, improving the mechanical connection of the SIP elements can be very beneficial.

Analyses show that the most critical joints, based on hygrothermal risk, are joints F, G, and M, the top joints. Not only do all these joint exhibit substantial air leakage under pressurization, they are subjected to a considerable amount of stack effect pressure when indoor and outdoor temperature differences are high, causing exfiltration. Exfiltration is more risky than infiltration in this case because the warm, humid air is on the interior side, and condensation and frost accumulation are very likely to occur under typical Arctic fall, winter, and spring conditions. The authors recommend that special attention be given when sealing the joint between the top of the SIP wall and the ceiling, and that a more robust method of sealing be implemented there.

5.2 Comparison of Attic Experimental Results with Simulation

5.2.1 Methodology

A model of the experimental setup is created in WUFI Plus (Antretter et al., 2011) to compare the experimental and simulation results for validation. The model is then used to perform more complex and long-term simulations in real outdoor climates. The TH geometry is used to build the model. Figure 5.4 shows the three-dimensional model of the TH in WUFI Plus. One-dimensional heat and moisture transfer is considered for each of the envelope elements, therefore edge effects and thermal bridges are not considered. The test conditions imposed on the attics in the experiment, including the EC temperature and RH conditions, and TH temperature and RH conditions, are used as boundary conditions in the simulation. The material properties are taken from WUFI Plus, since they are conventional materials.

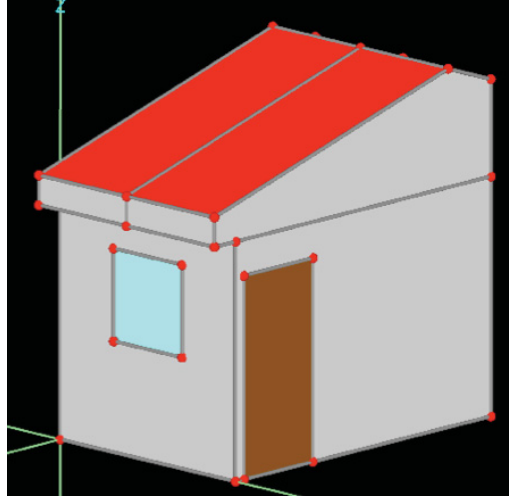


Figure 5.4 Model of test hut in WUFI Plus

Some of the main assumptions are presented below:

- Radiation between attic interior surfaces not considered
- Radiation between exterior surfaces and EC surfaces not considered
- All heat and moisture transfer assumed to be one-dimensional. Three-dimensional effect of trusses not considered.
- Unvented attic assumed to have an air leakage rate of 0.1 ACH based on air tightness tests performed in the lab.
- Time step: 1 hr
- Initial moisture conditions of materials: 30% RH for the UA and 25% for the VA, based on RH readings.
- To account for the moisture buffering effect of the wooden trusses, 2 m² of 38 mm thick wood is added to each attic as a component within the attic zone. These numbers are calculated based on the number of trusses in each attic and their geometry.

Table 5.3 Envelope elements connected to each attic bay as modeled in WUFI Plus

Envelope Element	Assembly	Connects attic bay to
Roof	13 mm Plywood Spun Bonded Polyolefin Membrane	Environmental Chamber
Gable, Attic Walls, & Soffit	15 mm OSB Spun Bonded Polyolefin Membrane	Environmental Chamber
Attic Separator	38 mm Polyisocyanurate	Other attic bay
Ceiling	330 mm Cellulose 38 mm Polyisocyanurate	Test Hut Interior

5.2.2 Results

Figure 5.5 shows the temperature conditions in the attics obtained by simulation and measurements for test 2. The trend obtained by simulation resembles that of the experiment very well. The discrepancies between the simulation and experimental results are found to be greater at more extreme low temperatures than warmer temperatures. This may be due to the mismatch of the real and simulated material thermal properties. The largest temperature differences are about 3 °C, while the root mean square error is 1.0 °C.

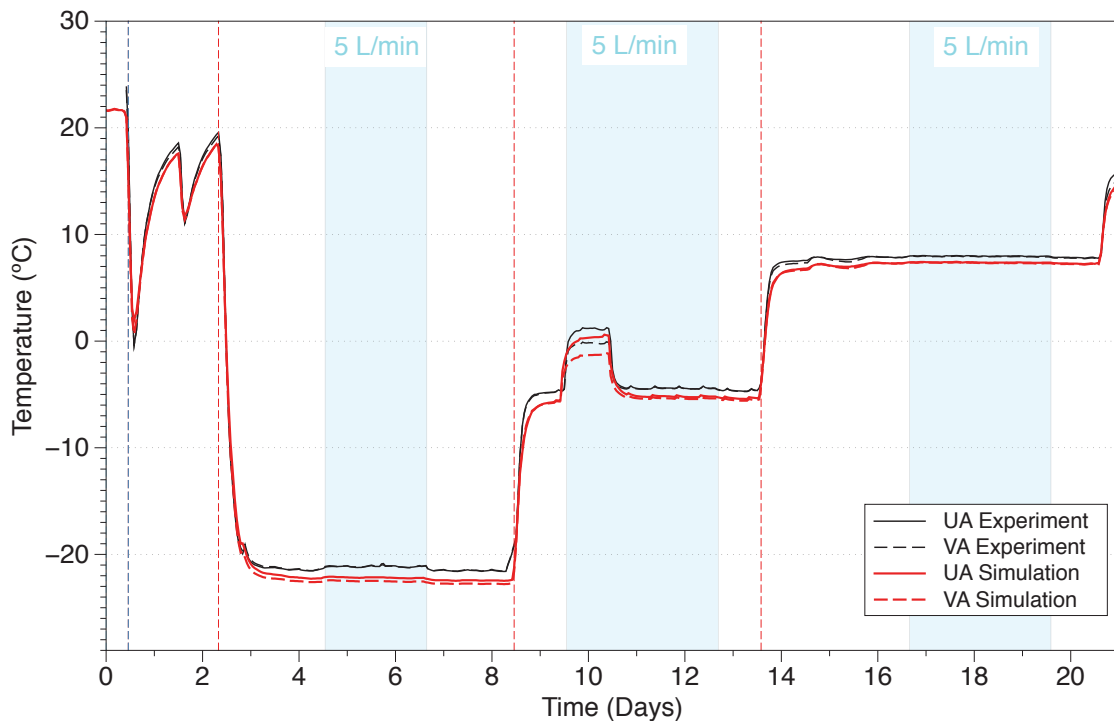


Figure 5.5 Measured and simulated temperature in the attics for test 2: -25, -7, and 6 °C outdoor temperature

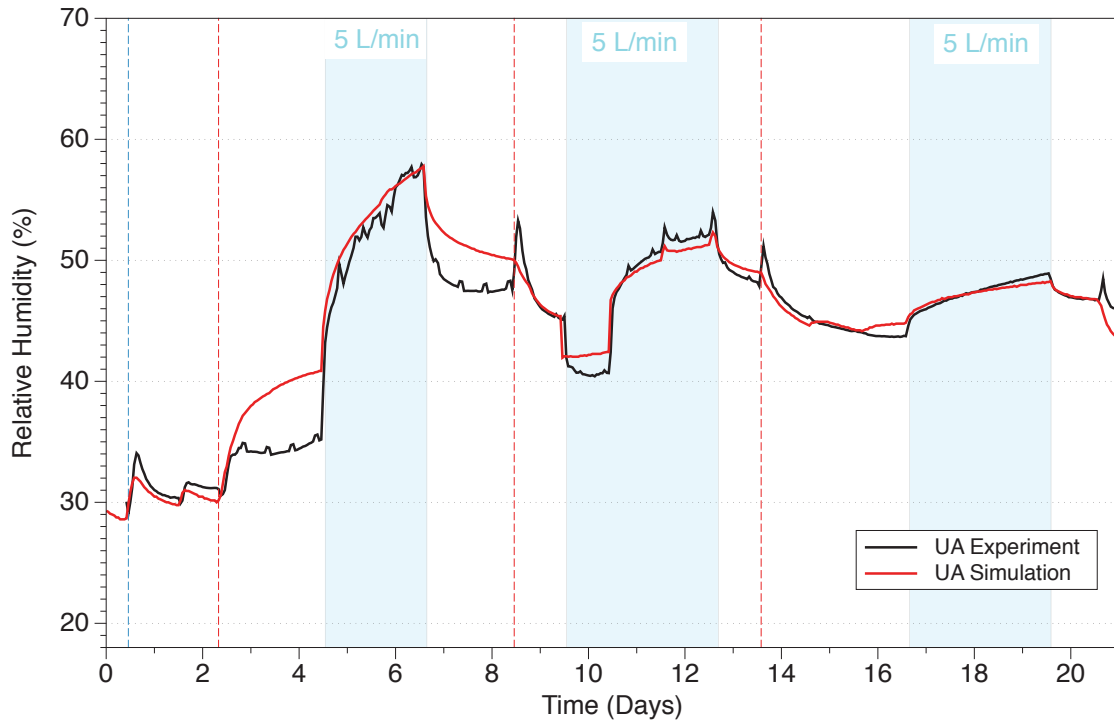


Figure 5.6 Measured and simulated RH in the UA for test 2: -25, -7, and 6 °C outdoor temperature

Figure 5.6 and Figure 5.7 show the RH conditions in the UA and VA, respectively, obtained by simulation and experiment. Similar to the temperature results, the trend obtained here by simulation has good agreement with the experimental results. For the UA results, the largest difference between the simulation and experimental results is less than 6%, while the root mean square error is 2.0%, which is less than the measurement uncertainty ($\pm 3\%$). For the VA, The largest difference is less than 7%, and the root mean square error is 2.0%, which is also less than the measurement uncertainty ($\pm 3\%$). The results show that the WUFI Plus model can be used to simulate the hygrothermal performance of unconditioned attics. Appendix F includes a short sensitivity analysis of the model.

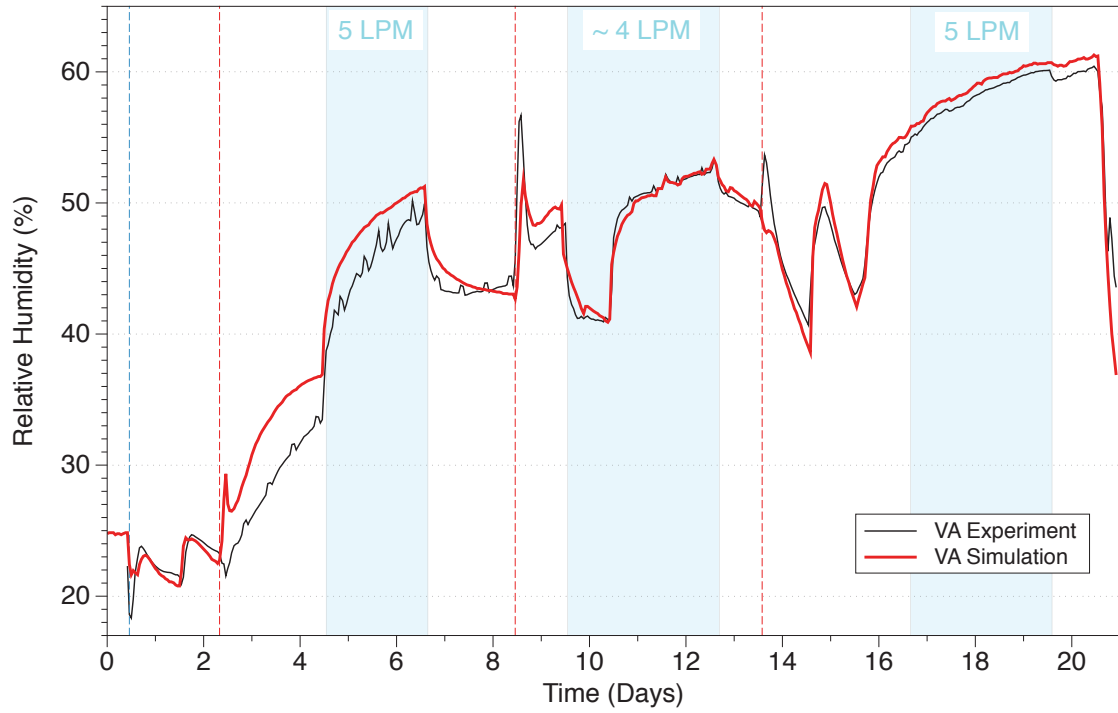


Figure 5.7 Experimental and simulated RH conditions in the VA for test 2: -25, -7, and 6 °C outdoor temperature

5.3 Long Term Performance of Attics Under Actual Climate Conditions

5.3.1 Methodology

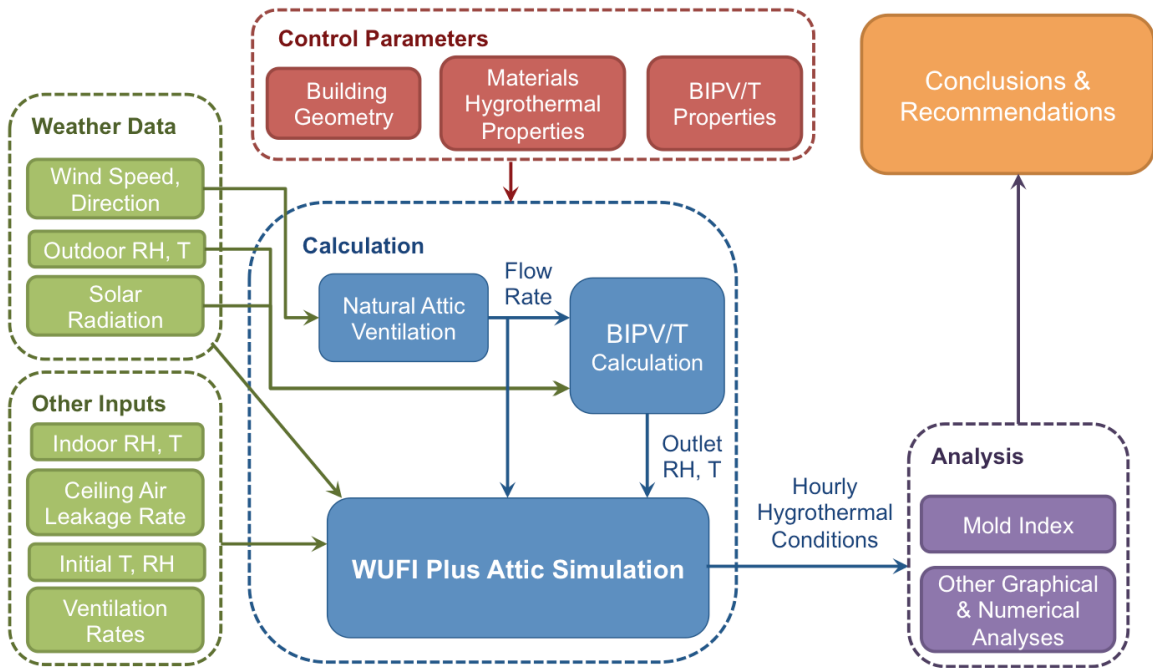


Figure 5.8 Simulation Methodology

Various attic ventilation strategies are evaluated using hygrothermal simulation. The methodology is summarized in Figure 5.7 and detailed in this subsection. WUFI Plus is used to create and simulate heat, air, and moisture transfer in the multi-zone model. The model was used to simulate the hygrothermal conditions of an experiment conducted in an environmental chamber using a full-scale test hut, described in (Kayello et al, 2013; Belleudy et al., 2015; Kayello et al., 2017b). A one-story house measuring 12 m by 8 m serves as the subject of this study (Figure 5.9). The long side of the house is south facing. The house has a gable roof with a 3/12 slope, typical of northern construction. The indoor

space is treated as one zone with constant temperature and relative humidity (22 °C, 40% RH). The attic space is treated as a single zone with passive response.

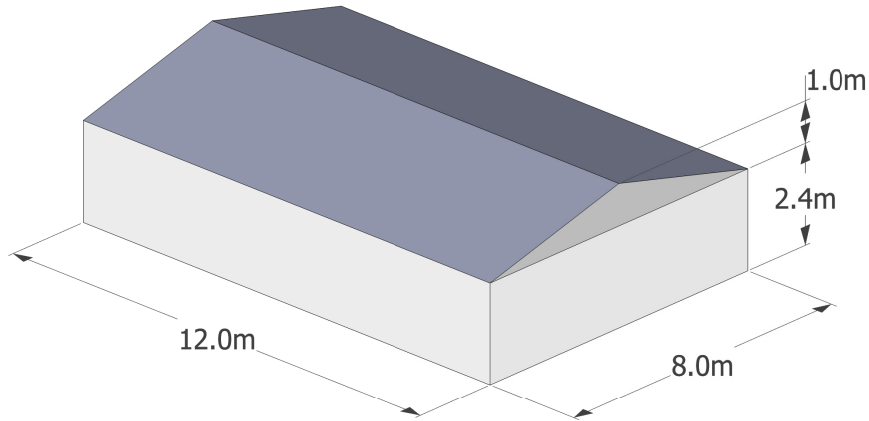


Figure 5.9 WUFI Plus model of house and attic

Figure 5.10 shows the monthly average weather conditions in the three Inuit communities studied. These locations were chosen to account for the variability in weather conditions within Arctic communities. Iqaluit, NU is the most populated Inuit community and the capital of Nunavut. Kuujuaq is the largest community in Nunavik (Northern Quebec) and is warmer than Iqaluit. Resolute, NU is the northern-most Inuit community and so is considerably colder than Iqaluit and receives no sunlight three months a year. Table 5.4 lists some general information on each community. Though the heating degree days value varies significantly between the communities, they are all considered to be in ASHRAE climate zone 8 (ASHRAE, 2013a).

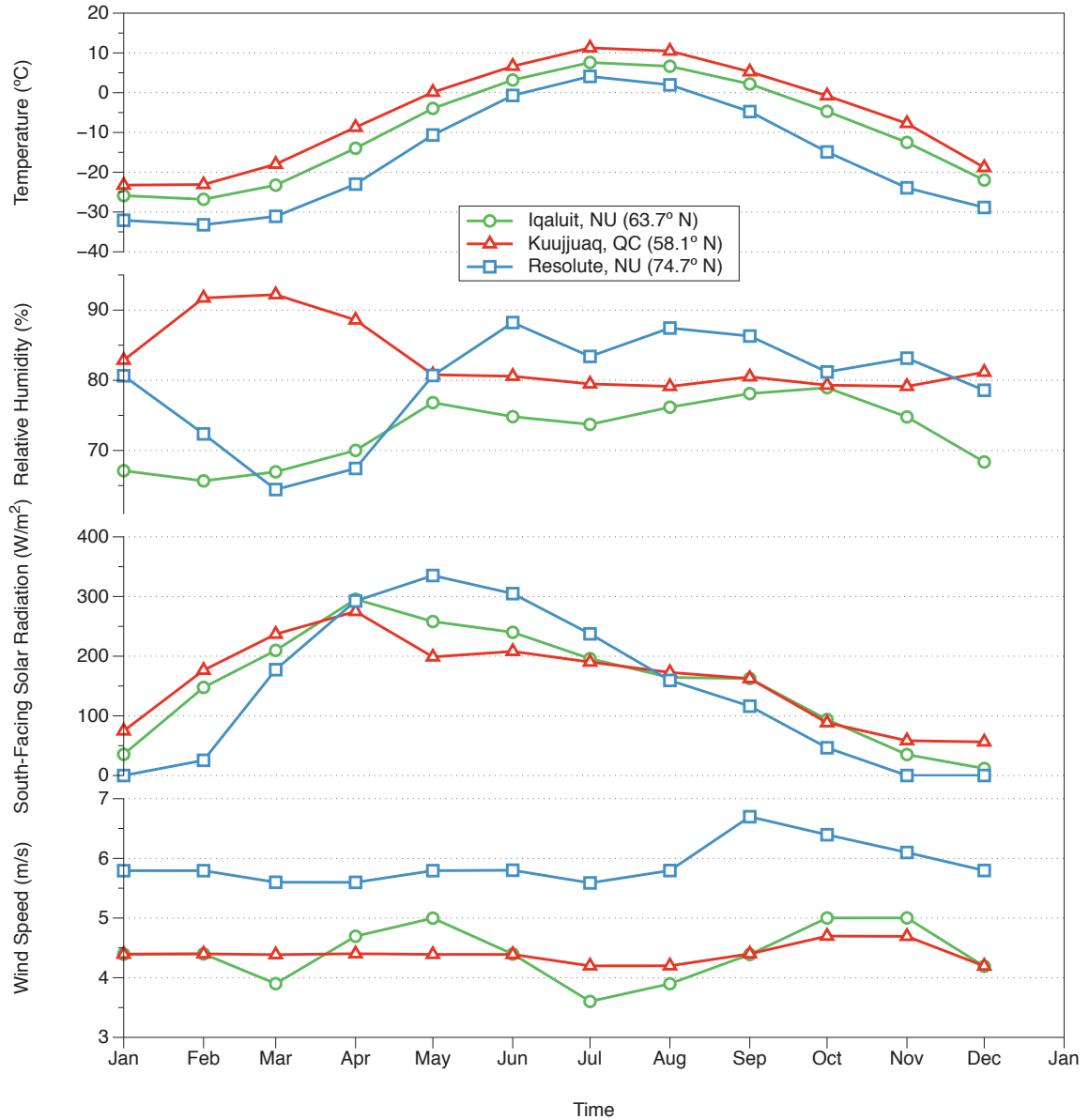


Figure 5.10 Monthly average weather conditions in three Inuit communities

Table 5.4 Inuit communities investigated in this study

	Iqaluit, NU	Kuujuaq, QC	Resolute, NU
Latitude	63.7° N	58.1° N	74.7° N
Heating Degree Days	9931	8520	12273
ASHRAE Climate Zone	8	8	8
Population	6699	2375	214

Several attic ventilation strategies are examined in this study. The unvented attic is sealed to prevent air exchange, only a small background air change rate of 0.05 ACH is considered. Under the unvented configuration three ceiling levels are simulated (7 RSI, 9 RSI, and 12 RSI) to examine the effect of varying the ceiling insulation level; 9 RSI is the default insulation level used in all other cases. 7 RSI is the minimum thermal resistance recommended by the Government of Nunavut (2005). Also under the unvented configuration, a roof diffusion vent is implemented in one of the cases. The diffusion vent is 0.3 m wide and it is located on either side of the eave, spanning the length of the roof. The roofing at the ridge is raised such that filtered outdoor air is allowed to enter under the ridge, and attic moisture is allowed to diffuse through a layer of spun-bonded polyolefin (Figure 5.11).

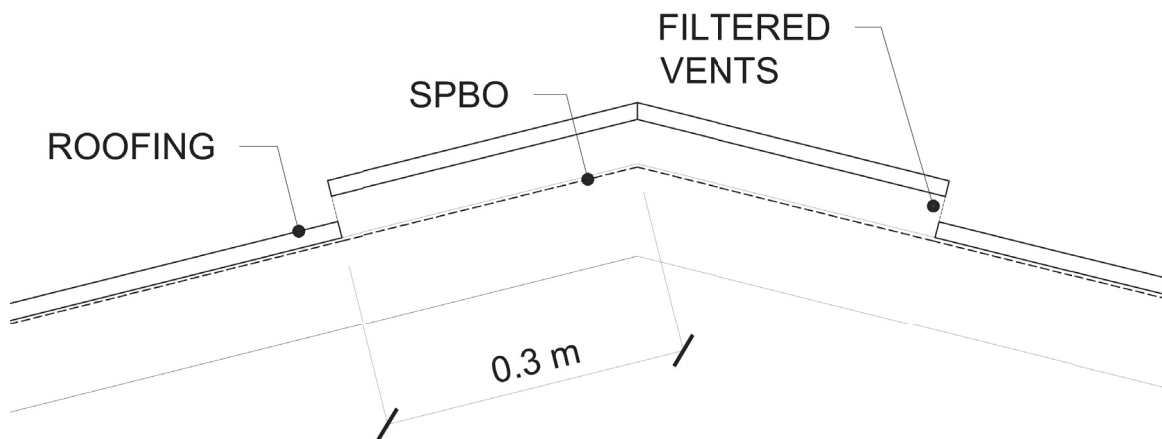


Figure 5.11 Roof ridge section with diffusion vent

The mechanically ventilated attic is ventilated using an electrical fan at a constant rate (1 ACH, 3 ACH, and 6 ACH). In this case, and in all cases with ventilation, the attic ventilation air drawn from an opening at the bottom of the facade, going through a snow

filter membrane behind the cladding before reaching the attic, as shown in Figure 5.12. This way, it is assumed that there is no snow infiltration. This method of ventilating the attic is used in Inuit communities in Nunavik. In this configuration, the temperature and moisture conditions of the air entering the attic are assumed to be the same as the outdoor conditions. Year-round ventilation as well as seasonal ventilation, where ventilation only occurs April through September, are considered.

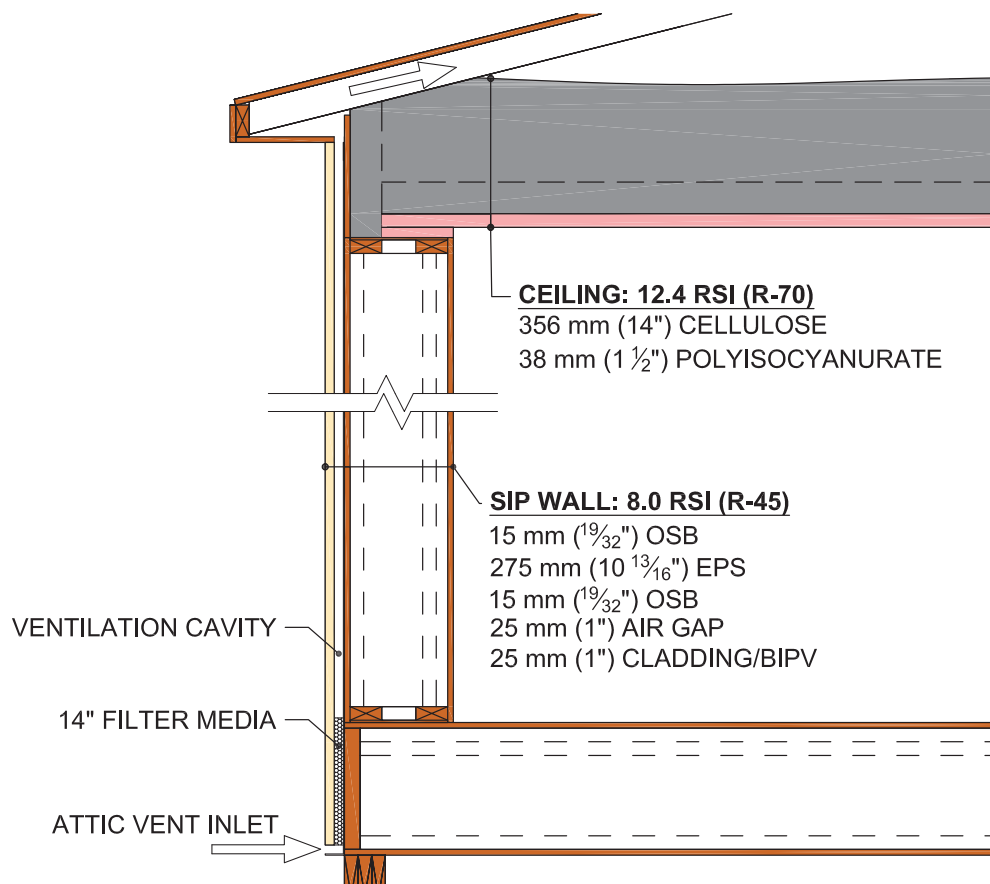


Figure 5.12 Section of house showing attic ventilation path and filter media

With the naturally ventilated attic, the ventilation rate is dependent on wind speed and direction. The correlation between ventilation rate and wind conditions is based on computational fluid dynamics simulations performed accounting for the use of the cavity

behind the cladding with a filter membrane as an attic ventilation path (Kayello et al., 2016). The study accounts for wind speeds between 1 m/s and 10 m/s, and at 0°, 45°, and 90° from normal. To calculate the airflow rate in the cavity at any wind speed and angle, symmetry is assumed across the two axes and the data is simply interpolated linearly. The temperature and moisture conditions of the air entering the inlet of the air cavity are assumed to be the same as the outdoor conditions. To account for variations in the air permeability characteristics of the filter membrane, several ventilation rates are implemented by multiplying the original ventilation rate obtained from CFD simulation by 0.25, 0.5, and 2.

The BIPV/T naturally ventilated attic is ventilated as with the naturally ventilated case, though in this case the cladding is replaced with a BIPV/T system. The temperature of the air entering the attic is therefore affected by the BIPV/T system, though the ventilation rate is strictly wind-dependent. It is assumed, based on the results obtained by Kayello et al. (2016), that the buoyancy driven air is negligible.

The BIPV/T mechanically ventilated attic uses an electrical fan to draw outdoor air through the BIPV/T cladding cavity. In this configuration, the BIPV/T system generates electricity while the air drawn in the cavity cools the solar panels, increasing their efficiency. The air that ventilates the attic is therefore heated by the BIPV/T system and consequently has a higher capacity to dry the attic. For this case, the fan ventilates the attic at a rate of 11.4 ACH, corresponding to a speed of 0.5 m/s in façade air cavity, only when there is solar radiation incident on the panels. At night, the fan turns off and ventilation is prevented. It is assumed that the air entering the attic is warmed by the BIPV/T system, but the humidity ratio is the same as the outdoors.

Table 5.5 Summary of Simulations

Location	Ventilation Configuration		Ventilation Method	Ventilation Rate	# of cases
Iqaluit	Unvented	7 RSI Ceiling	Background ventilation	0.05 ACH	1
		9 RSI Ceiling*			1
		12 RSI Ceiling			1
		Diffusion Port			1
	Mechanical Ventilation	Year-Round	Constant ventilation	1, 3, and 6 ACH	3
		Seasonal	Constant ventilation from April 1 st to October 1 st	1, 3, and 6 ACH	3
	Natural Ventilation	-	Wind dependent	1x: 7.5 ACH† 2x: 15.1 ACH† 0.5x: 3.8 ACH† 0.25x: 1.9 ACH†	4
	BIPV/T Natural Ventilation	-	Wind dependent	1x: 7.5 ACH† 0.25x: 1.9 ACH†	2
	BIPV/T Mechanical Ventilation	Year-round	11.4 ACH ventilation in the daytime	5.6 ACH†	1
		Seasonal	11.4 ACH ventilation in the daytime from April 1 st to October 1 st	3.9 ACH†	1
Seasonal, 30%		3.4 ACH ventilation in the daytime from April 1 st to October 1 st	1.2 ACH†	1	
Kuujuuaq	Unvented	9 RSI Ceiling*	Background ventilation	0.05 ACH	1
		Diffusion Port			1
	Mechanical Ventilation	Year-Round	Constant ventilation	1 and 3 ACH	2
		Seasonal	Constant ventilation from April 1 st to October 1 st	1, 3, and 6 ACH	3
	Natural Ventilation	-	Wind dependent (1x, 0.25x)	1x: 7.4 ACH† 0.25x: 1.8 ACH†	2
	BIPV/T Natural Ventilation	-	Wind dependent (1x, 0.25x)	1x: 7.4 ACH† 0.25x: 1.8 ACH†	2
	BIPV/T Mechanical Ventilation	Year-round	11.4 ACH ventilation in the daytime	5.7 ACH†	1
		Seasonal	11.4 ACH ventilation in the daytime from April 1 st to October 1 st	3.6 ACH†	1
		Seasonal, 30%	3.4 ACH ventilation in the daytime from April 1 st to October 1 st	1.1 ACH†	1
	Resolute	Unvented	9 RSI Ceiling*	Background ventilation	0.05 ACH
Diffusion Port			1		
Mechanical Ventilation		Year-Round	Constant ventilation	1 and 3 ACH	2
		Seasonal	Constant ventilation from April 1 st to October 1 st	1, 3, and 6 ACH	3
Natural Ventilation		-	Wind dependent (1x, 0.25x)	1x: 11.4 ACH† 0.25x: 2.9 ACH†	2
BIPV/T Natural Ventilation		-	Wind dependent (1x, 0.25x)	1x: 11.4 ACH† 0.25x: 2.9 ACH†	2
BIPV/T		Year-round	11.4 ACH ventilation in the	5.7 ACH†	1

	Mechanical Ventilation		daytime		
		Seasonal	11.4 ACH ventilation in the daytime from April 1 st to October 1 st	4.9 ACH†	1
		Seasonal, 30%	3.4 ACH ventilation in the daytime from April 1 st to October 1 st	1.5 ACH†	1
				Total	47
* Default ceiling thermal resistance used in all cases					
† Annual Average					

The hourly outlet temperature conditions for the BIPV/T airflow are needed for the hygrothermal simulation. Using a weather files for each community, which includes hourly temperature, relative humidity, wind speed, and solar radiation, the required values are calculated as follows. The equation below (Athienitis et al., 2004) is applied to determine the air temperature in a cavity of finite length and width.

$$T_a(x) = \frac{T_w + T_b}{2} + \left[T_o - \frac{T_w + T_b}{2} \right] \cdot e^{\frac{-2x}{A}} \quad (5.2)$$

$$A = \frac{Mc\rho}{Wh} \quad (5.3)$$

Where T_a is the temperature of the air in the cavity, T_w is the BIPV/Cladding temperature, T_b is the back plate/sheathing temperature, T_o is the outdoor temperature, x is the upward vertical distance from the bottom of the vented cavity, M is the volume flow rate, c is the specific heat of air, ρ is the air density, W is the width of the wall, and h is the cavity surface convective heat transfer coefficient. An initial guess is made for the cavity wall temperatures to execute the equation and find the mean air temperature in the cavity. That value is used in the energy balance equations below to check if the initial guesses for wall temperatures are reasonable, making this an iterative process.

$$T_w = \frac{U_o T_o + U_c T_{a(mean)} + U_r T_b + S \alpha A_{wall} (1 - \eta)}{U_o + U_c + U_r} \quad (5.4)$$

Above is the energy balance equation for the BIPV/T cladding, where U_o is the outdoor heat transfer coefficient, U_c is the cavity convection coefficient, U_r is the cavity radiation coefficient, S is the incident solar radiation on the BIPV panels (obtained from the weather file), α is the absorptance of the panels (0.95), A_{wall} is the area of the panels, and η is the electrical efficiency of the panels.

$$T_b = \frac{U_c T_{a(mean)} + U_r T_w + U_w T_r}{U_c + U_r + U_w} \quad (5.5)$$

Above is the energy balance equation for the backplate/sheathing, where U_w is the conductance of the wall and T_r is the indoor temperature. These balance equations are solved iteratively until the error in the temperature value is less than 0.001 °C.

The value of U_c is determined using correlations for calculating the Nusselt number for BIPV/T system, obtained by Candanedo et. al (2011), shown below:

$$U_c = \left(\frac{k Nu}{D_h} \right) A_{wall} \quad (5.6)$$

$$Nu = 0.052 Re^{0.78} Pr^{0.4} \quad (5.7)$$

where k is the thermal conductivity of the air, D_h is the hydraulic diameter, Re is the Reynolds number, and Pr is the Prandtl number. U_r is calculated with the following, linearized equation:

$$U_r = \frac{4\sigma \left(\frac{T_w + T_b}{2} \right)^3}{1/\epsilon_w + 1/\epsilon_b - 1} A_{wall} \quad (5.8)$$

where σ is the Stefan-Boltzmann constant, while ε_w and ε_b are the emissivity values for the BIPV and the backplate/sheathing, assumed to be 0.9. U_o is calculated with the following equation, combining convective and radiative components:

$$U_o = (h_o + h_{ro})A_{wall} \quad (5.9)$$

The value of h_o , the convective component, is obtained using correlations provided by Test at al. (1981):

$$h_o = 8.55 + 2.56V_{wind} \quad (5.10)$$

Where V_{wind} is the wind speed. h_{ro} is the calculated in a similar fashion as U_r , exchanging T_b for T_o and omitting A_{wall} . The electrical efficiency of the BIPV system is that of typical poly-Si panels (PikeResearch, 2012) which is temperature dependent:

$$\eta = 0.15 [1 - 0.45(T_w - 20)] \quad (5.11)$$

The electrical energy production is calculated as follows.

$$E_{PV} = S\alpha\eta A_{wall} \quad (5.12)$$

The heat gained by the air flowing behind the BIPV/T system is calculated using the value of T_a at the outlet, which is the inlet of the attic.

$$Q = \dot{m}c_p(T_{a(outlet)} - T_o) \quad (5.13)$$

where \dot{m} is the flow rate and c_p is the specific heat of air.

Hygrothermal simulations with WUFI Plus provide the hourly temperature and relative humidity conditions in each attic, for a total of three years. An important criterion in comparing the performance of the attics is the mold growth index developed by Hukka & Viitanen (1999). The mold growth index uses temperature and relative humidity

conditions to determine the potential for mold growth on wood-based materials. The mold growth index is represented by a number between 0 and 6, where 0 indicates no mold growth and 6 indicates 100% mold coverage on a material. A mold growth index of 1 indicates the first stage of mold growth has been reached, while a mold growth index of 3 signifies mold growth that can be detected visually, implying system failure (ASHRAE, 2016). For every time step in the simulation, a change in the mold growth index is calculated based on ASHRAE standard 160 (ASHRAE, 2016). The temperature and relative humidity conditions of the inner surface of the north roof sheathing are used for this calculation. The initial value given to the mold growth index is 0. The value of the mold index is provided by the following equation:

$$\frac{dM}{dt} = \frac{k_1 k_2}{168 \exp(-0.68 \ln T_s - 13.9 \ln RH_s + 0.14W + 66.02)} \quad (5.14)$$

M is mold is the mold growth index, T_s and RH_s are the wood surface temperature and relative humidity, W is a factor accounting for the sensitivity of the wood material (assumed very sensitive), and k_1 and k_2 are coefficient that vary depending on the stage of the mold growth.

Table 5.6 lists some of the simulation details. In terms of the envelope assemblies, the ceiling is composed of a sheet of polyisocyanurate (PIR) topped with loose fill cellulose insulation. The default ceiling thermal resistance used throughout the simulation is 9 RSI, though 7 RSI and 12 RSI are also used in the unvented case to study its effect. The roof is composed of a sheet of plywood covered with spun-bonded polyolefin, with metal roofing attached to 1” strapping. The indoor conditions are at a constant 22 °C, 40% relative humidity. The initial conditions of the attic space and materials are set to -20 °C,

since the simulation starts in January, and 80% relative humidity, which is typical for wood based materials. Four rates of air leakage are implemented: none; low, representing passive house standards (0.6 ACH@50Pa) (Passive House Institute, 2016); medium, representing Nunavut’s recommendation for airtightness (1.5 ACH@50Pa) (GN, 2005), and high, which is twice the government recommended value (3.0 ACH@50Pa). The values are obtained by taking the air changes per hour at 50 Pa, dividing by an n-factor of 14.0 to approximate the natural air changes per hour (Sherman, 1987). 30% of the air leaking is assumed to occur through the ceiling into the attic (ASHRAE, 2013a). The final values are listed in Table 5.6.

Table 5.6 Summary of Model Setup and Boundary Conditions

Parameter	Description
Building Dimensions	L: 12 m (faces south) W: 8 m Floor Area: 96 m ² Wall height: 2.4 m Roof Slope: 3/12
Attic Volume	48 m ³
Wall Thermal Resistance	8 RSI
Ceiling Assembly	275 mm of cellulose insulation and foil-faced 33 mm PIR (equivalent to 9 RSI)*
Roof Assembly	Plywood, Spun-bonded Polyolefin, Air Space, Metal Roofing
Air Leakage Rate	No Air Leakage: 0 m ³ /h Low Air Leakage: 2.96 m ³ /h (0.031 m ³ /h/m ²) Medium Air Leakage: 7.4 m ³ /h (0.077 m ³ /h/m ²) High Air Leakage: 14.8 m ³ /h (0.154 m ³ /h/m ²)
BIPV/T	1 inch cavity 0.5 m/s air velocity in the cavity
Attic Initial Conditions	-20 °C, 80% RH
Indoor Conditions	22 °C, 40% RH
Outdoor Conditions	Typical Meteorological Year (TMY2) weather files for Iqaluit, Kuujuaq, and Resolute
Time step	1 hr
Simulation Duration	3 years starting January 1 st
*In cases with 7 RSI and 12 RSI ceilings, thickness of cellulose layer varies	

5.3.2 Results

The simulations were carried out successfully and the results are presented below in three subsections: relative humidity and sheathing moisture, mold index, and energy generation.

Relative humidity and sheathing moisture

The monthly average relative humidity conditions in the attic air spaces is presented in this subsection to show how the different ventilation strategies affect the attics in each season over the course of three years. Only the results from the medium air leakage cases in Iqaluit, NU are shown due to space restrictions. The complete results can be found in Appendix B.

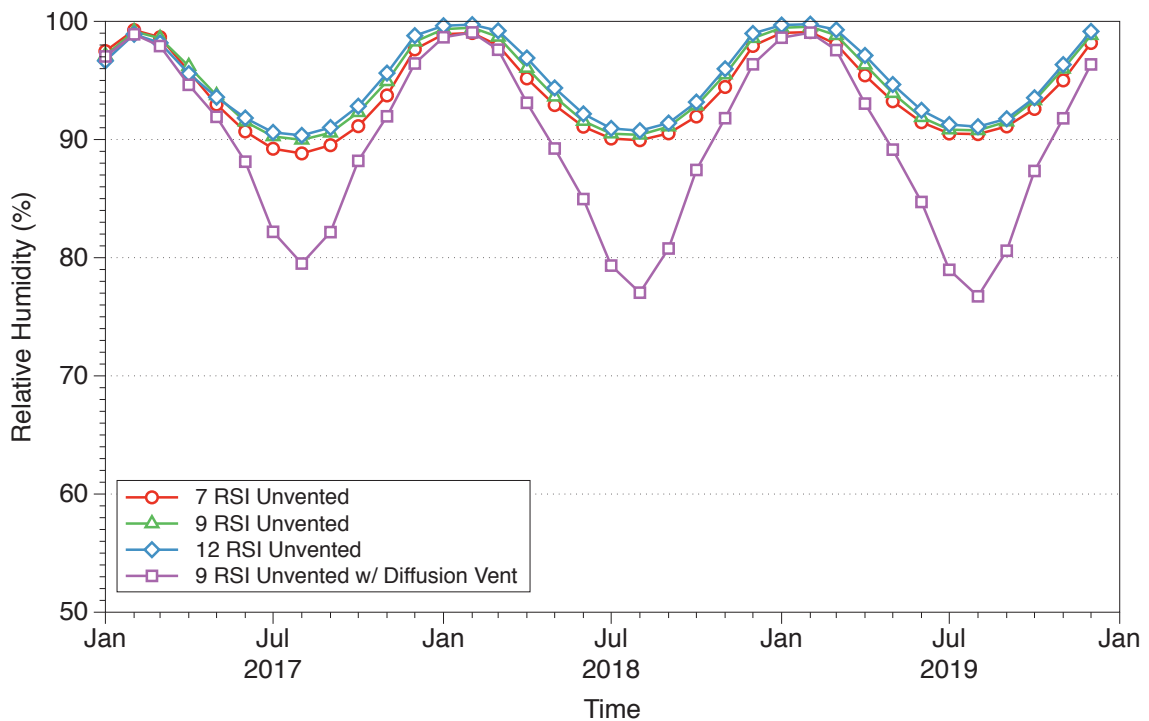


Figure 5.13 Relative humidity in unvented attics with medium air leakage in Iqaluit

Figure 5.13 shows the RH conditions in the unvented attics. Without a diffusion vent, the RH remains above 90% and reaches close to 100% in winter. Changing the ceiling insulation level between 7 RSI and 12 RSI does not impact attic hygrothermal performance significantly. The incorporation of a diffusion vent effectively reduces the overall RH of the attic. The greatest benefit is observed in the warmer seasons, where the RH level decreases sooner in the season, reaching less than 80% by August.

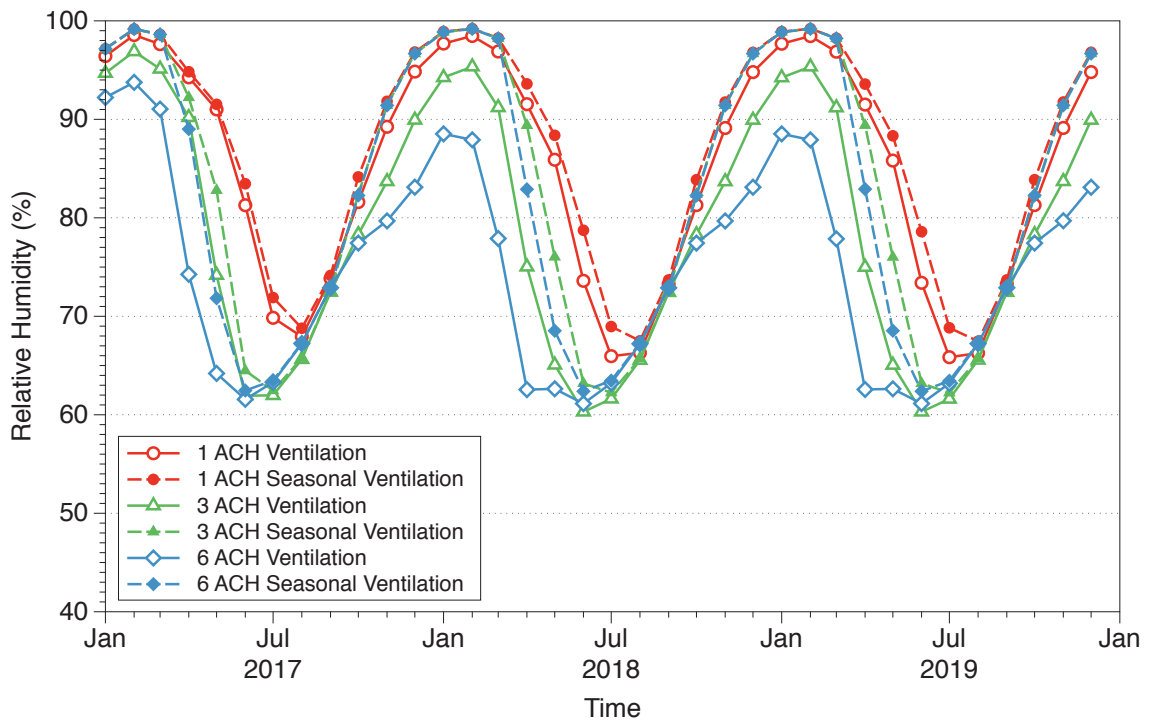


Figure 5.14 Relative humidity in mechanically ventilated attics with medium air leakage in Iqaluit

Figure 5.14 shows the RH levels in mechanically ventilated attics. Compared the unvented attics, the RH levels in these ventilated attics are much lower, especially in the warmer months. 1 ACH ventilation, both year-round and seasonal, can reduce RH levels in the summer to less than 70%. Ventilation rates of 3 ACH and 6 ACH, both year-round

and seasonal, dry the attics quicker in the spring time and achieve RH levels lower than 65% in the summer time. High rates of ventilation are needed to lower the RH levels in the winter, though it is not critical since the temperatures are too cold for mold growth. RH levels above 80% are dangerous when temperatures exceed 0 °C. Higher ventilation rates means the RH levels drop sooner in the spring, minimizing mold growth potential.

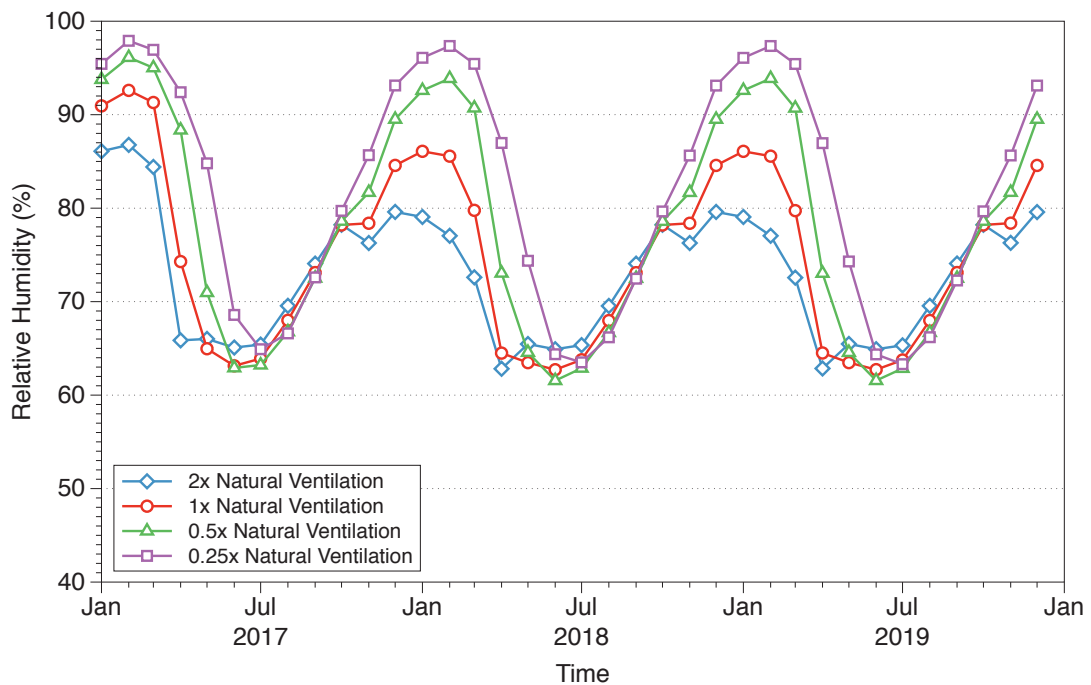


Figure 5.15 Relative humidity in naturally ventilated attics with medium air leakage in Iqaluit

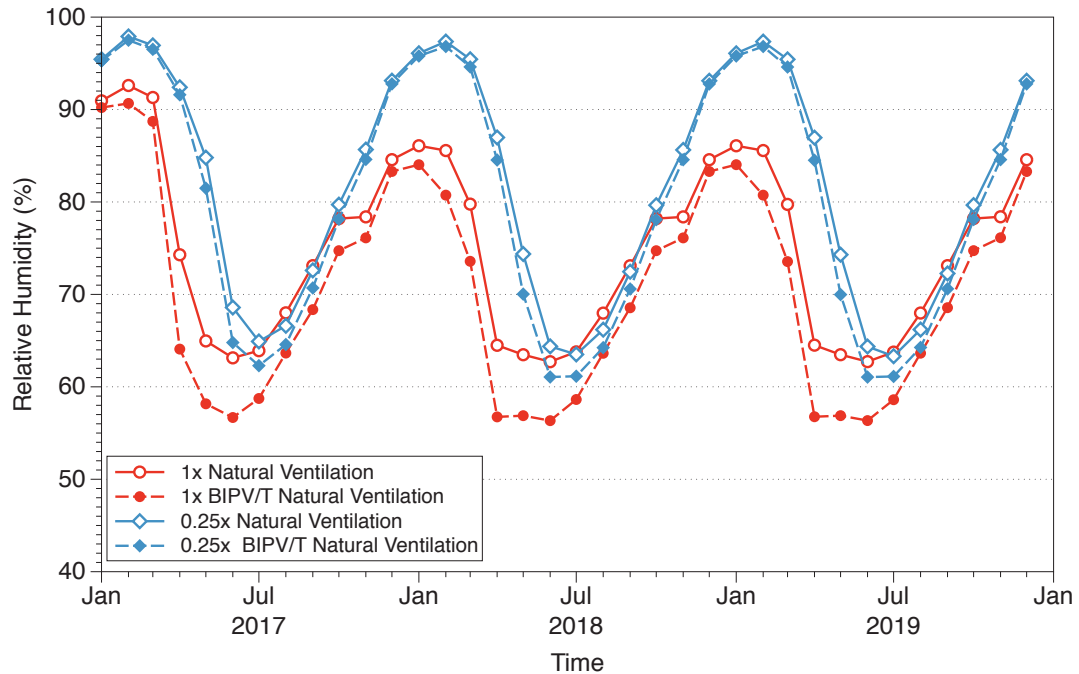


Figure 5.16 Relative humidity in BIPV/T naturally ventilated attics with medium air leakage in Iqaluit. Natural ventilation is effective at maintaining low RH levels in the attic, as shown in Figure 5.15. Even at 0.25x the base ventilation rate such that the annual average rate is 1.9 ACH, the average monthly RH decreases to less 70% by June. This is comparable in performance to the mechanically ventilated case with 3 ACH. High ventilation rates (2x, 15.1 ACH annual average) can keep the monthly RH levels in the winter below 80%, though it is probably unnecessary for simply deterring mold. Figure 5.16 shows the RH levels in BIPV/T naturally ventilated attics. The addition of a BIPV/T system to naturally ventilated attics results in lower overall RH levels. The effectiveness of the BIPV/T is increased with higher ventilation rates and in the warmer seasons when there is more sun. At the base rate of ventilation (1x, 7.5 ACH annual average) the RH levels in the summer are around 7% less in the case with the BIPV/T system.

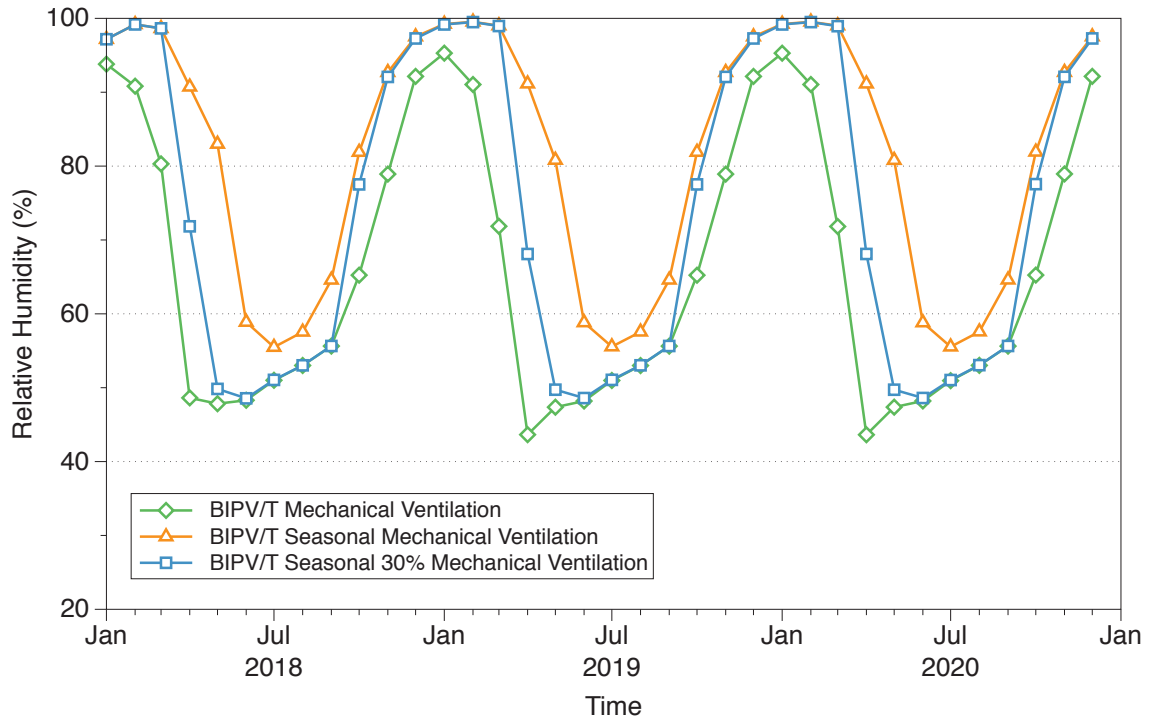


Figure 5.17 Relative humidity in BIPV/T mechanically ventilated attics with medium air leakage in Iqaluit. Combining mechanical ventilation with a BIPV/T system can markedly improve attic hygrothermal performance, as shown in Figure 5.17. When ventilation is used year-round, the RH levels reach a maximum monthly value of 95% in the winter and decrease to less than 50% as early as April. If ventilation is only engaged seasonally, high RH levels, up to 100%, are observed in winter but decrease to less than 70% by April, which is the first month in the year that ventilation is engaged. Even when only 30% of the seasonal airflow is used to ventilate the attic, the RH levels in the attic are kept below 60% in June, July, and August.

The sheathing moisture content in select cases with medium air leakage is shown in Figure 5.18. Note how the unvented attic has a delayed and limited capacity to dry in the warm season compared to the other cases, leading to accumulated moisture over the years.

The incorporation of diffusion vents improves sheathing moisture performance drastically, keeping the moisture content below 24% in winter and as low as 12% in the summer. In the other cases where some type of ventilation is implemented, the moisture content decreases to below 10% in the summer. Higher moisture content levels in winter, up to 27%, are observed in the cases where seasonal ventilation is implemented, but this does not limit that capacity of these attics to keep the moisture levels low in the warmer months. High ventilation rates in winter, as in the case of 3 ACH mechanical ventilation, can keep moisture content levels below 20% year-round, further limiting the possibility of decay in the long term.

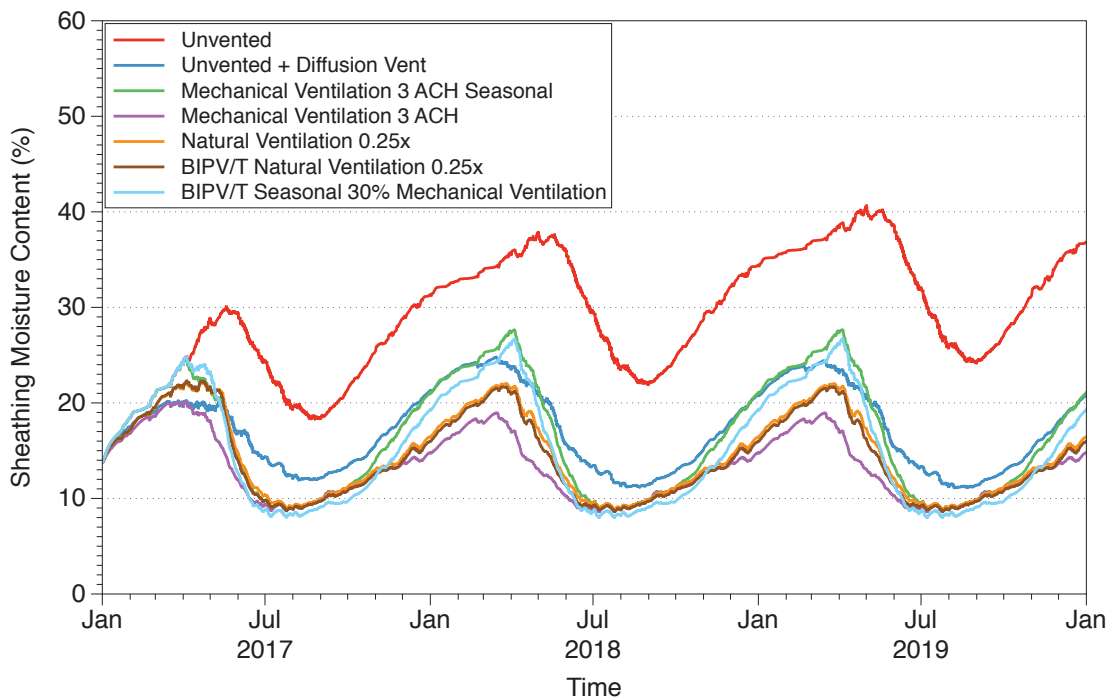


Figure 5.18 Sheathing moisture content in select attics with medium air leakage in Iqaluit

Mold Index

The mold index is a good indicator of potential damage caused by high levels of moisture as it takes into account temperature conditions needed for mold to grow. Figure 5.19 shows the mold index calculated over a three-year period for the unvented case in Iqaluit. Note that the mold index is initially zero and does not increase until April when the temperatures are high enough for mold to form. Regardless of the amount of air leakage, the unvented attics with medium and high air leakage levels reach a mold index of 3 in the first summer, indicating system failure. With low rates of air leakage, the mold index exceeds 2 in the first summer but the peak decreases in the following years. This shows the importance of having the materials as dry as possible throughout the construction process. Figure 5.20 shows the effect of the diffusion vent on mold index. The improvement is significant: mold index remains below 2 even at high rates of air leakage, and below 1 with medium air leakage. This shows that it is important for unvented attics to be able to diffuse built-up moisture in order to minimize mold growth in the summer.

Unvented attic at low air leakage rate, initial conditions matter because the MI trend is going down. MI decreases in all cases except unvented medium and high air leakage.

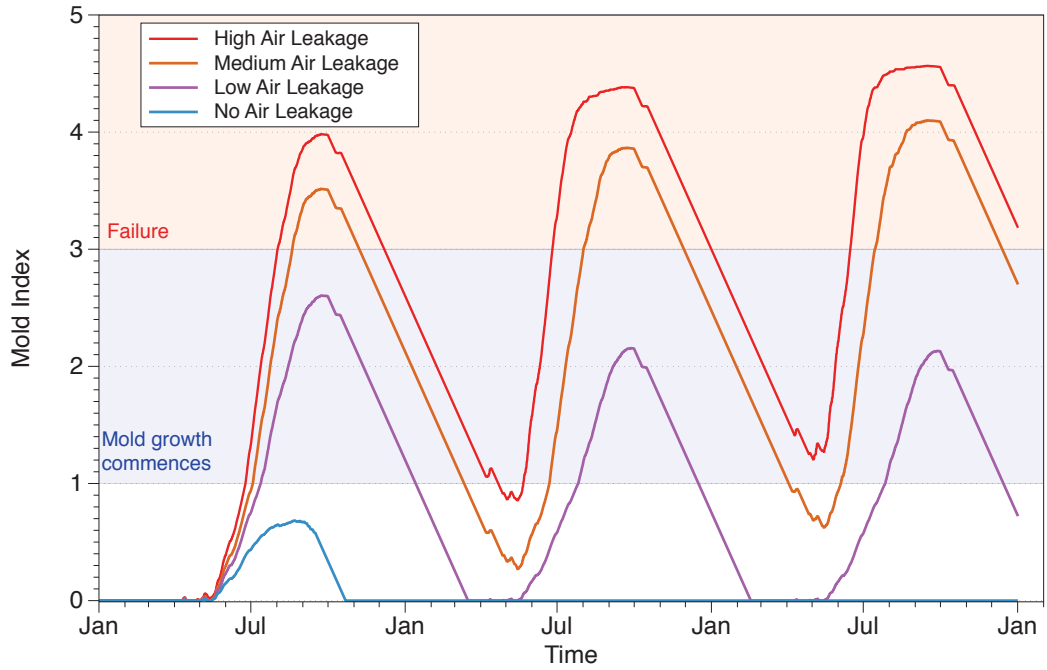


Figure 5.19 Mold index in unvented attics in Iqaluit

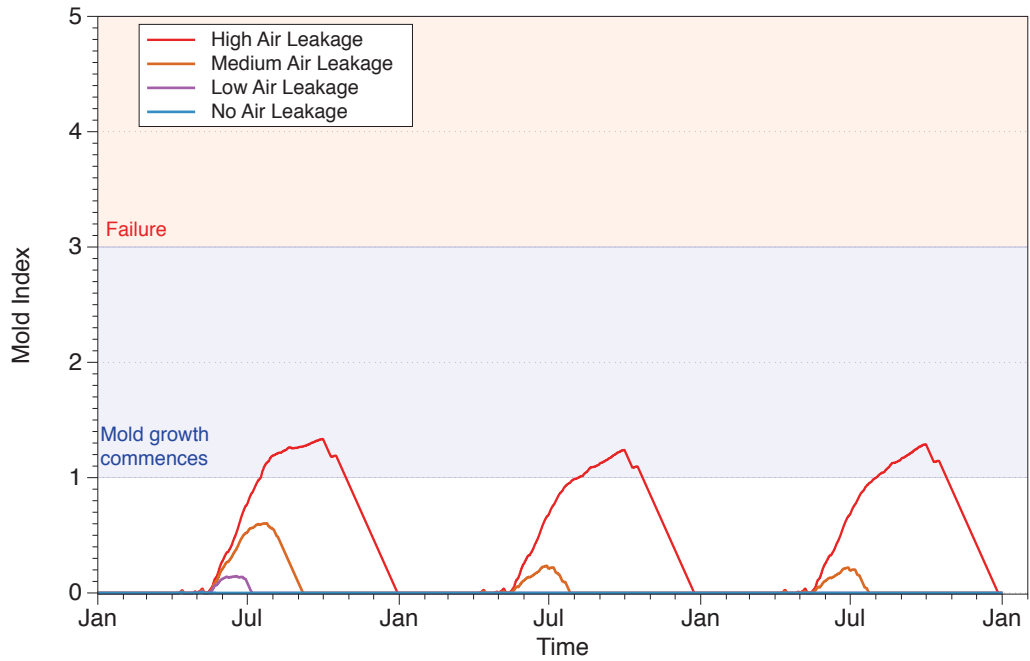


Figure 5.20 Mold index in unvented attics with diffusion vents

Table 5.7 summarizes the mold index results obtained from all cases in the three communities studied. It displays the highest value of mold index attained during the three-year simulation period. The unvented attics remain below a mold index value of 3 so long as the air leakage rate is low. This compares well with the field measurements obtained in Iqaluit, where an unvented attic exhibited high levels of moisture and mold index values of around 3 (Ge et al., 2018). The addition of a diffusion vents reduces the risk of mold growth dramatically, more successfully in Iqaluit and Kuujuaq where it is relatively warmer. Attics with diffusion vents in all communities can tolerate even a high rate of air leakage without failure.

A constant rate of ventilation can be effective at preventing mold growth. A rate of 1 ACH year-round prevents mold growth in all three communities, even with high rates of air leakage. Actually, the 1 ACH ventilation rate can be applied only from April through September in all three communities without any risk of mold growth. With a ventilation rate of 3 ACH, the mold index remains below 0.1 in all three communities. Natural ventilation yields positive results as well. In all cases the mold index is kept below 0.1. This includes cases where the ventilation rate is reduced by a factor of 4, resulting in average annual air change rates of less than 3 ACH and as low as 1.8 ACH. The incorporation of a BIPV/T system with natural ventilation slightly improves the mold index results while generating electricity. The maximum mold index is reduced by 0.1 up to 0.2. However, since all the cases of natural ventilation are shown to be mold free (<1), the improvement in performance is insignificant.

In the cases where the attic is ventilated mechanically with the use of the BIPV/T system, the mold index is kept very low (<0.13). This includes cases where ventilation occurs

only April through September and where only 30% of the BIPV/T air is used for attic ventilation. In fact the mold index is lowest in Resolute and highest in Kuujuaq. This is due to the fact that, in Resolute, the days are longer in the summer, the incidence angle is closer to normal, and ventilation occurs only in the daytime.

Table 5.7 Maximum mold index attained in each attic during 3-year simulation

		No Air Leakage	Low Air Leakage	Medium Air Leakage	High Air Leakage
Iqaluit					
Unvented	7 RSI	0.27	2.03	4.04	4.57
	9 RSI	0.68	2.61	4.10	4.57
	12 RSI	1.66	2.87	4.12	5.13
	w/ Diffusion Port	0.01	0.15	0.60	1.34
Mechanical Ventilation	1 ACH	0.01	0.01	0.14	0.42
	3 ACH	0.00	0.00	0.00	0.01
	6 ACH	0.00	0.00	0.00	0.00
	1 ACH Seasonal	0.01	0.05	0.19	0.47
	3 ACH Seasonal	0.00	0.00	0.00	0.01
	6 ACH Seasonal	0.00	0.00	0.00	0.00
Natural Ventilation	1/4 Ventilation	0.00	0.00	0.02	0.04
	1/2 Ventilation	0.00	0.00	0.00	0.01
	Full Ventilation	0.00	0.00	0.00	0.00
	2x Ventilation	0.00	0.00	0.00	0.00
BIPV/T Natural Ventilation	1/4 Ventilation	0.00	0.00	0.02	0.03
	Full Ventilation	0.00	0.00	0.00	0.00
BIPV/T Mech Ventilation	Year round	0.00	0.00	0.00	0.00
	Seasonal	0.00	0.00	0.00	0.01
	30% Seasonal	0.01	0.01	0.02	0.03
Kuujuaq					
Unvented	9 RSI	0.83	2.65	4.13	4.46
	w/ Diffusion Port	0.05	0.07	0.48	0.97
Mechanical Ventilation	1 ACH	0.04	0.05	0.25	0.60
	3 ACH	0.00	0.02	0.03	0.05
	1 ACH Seasonal	0.04	0.06	0.37	0.71
	3 ACH Seasonal	0.02	0.03	0.05	0.07
	6 ACH Seasonal	0.01	0.01	0.03	0.04
Natural Ventilation	1/4 Ventilation	0.02	0.05	0.07	0.09
	Full Ventilation	0.00	0.00	0.00	0.01
BIPV/T Natural	1/4 Ventilation	0.02	0.05	0.07	0.09

Ventilation					
	Full Ventilation	0.00	0.00	0.00	0.01
BIPV/T Mech Ventilation	Year round	0.00	0.00	0.00	0.00
	Seasonal	0.00	0.00	0.01	0.03
	30% Seasonal	0.05	0.07	0.10	0.13
Resolute					
Unvented	9 RSI	0.78	1.74	3.04	4.16
	w/ Diffusion Port	0.03	0.58	1.25	2.34
Mechanical Ventilation	1 ACH	0.00	0.05	0.34	0.78
	3 ACH	0.00	0.00	0.00	0.01
	1 ACH Seasonal	0.01	0.08	0.36	0.83
	3 ACH Seasonal	0.00	0.00	0.01	0.01
	6 ACH Seasonal	0.01	0.01	0.01	0.01
Natural Ventilation	1/4 Ventilation	0.00	0.00	0.01	0.02
	Full Ventilation	0.02	0.02	0.02	0.02
BIPV/T Natural Ventilation	1/4 Ventilation	0.00	0.00	0.01	0.03
	Full Ventilation	0.01	0.01	0.01	0.01
BIPV/T Mech Ventilation	Year round	0.00	0.00	0.00	0.00
	Seasonal	0.00	0.00	0.00	0.00
	30% Seasonal	0.00	0.00	0.01	0.01

Energy Generation

The BIPV/T system with mechanical ventilation generates both electrical and thermal energy that can be used by the building. The electrical energy can be used for appliances, lights, and plug-loads. As a reminder, the BIPV/T system covers the entire south façade of the building and measures 3.4 m in height and 12 m in length for a total area of 40.8 m², equivalent to about 6 kW. Figure 5.21 shows the total monthly electrical energy generated by the BIPV/T system, which covers the entire 12 m length of the south facing façade. The curves have a concave-down shape since there is more solar energy available in the summer time. In Kuujuaq, electricity is generated year-round where the least production occurs in November (260 kWh) and the highest in April (1180 kWh). Though there is more daylight hours in the summer, the incidence angle and cloudiness reduce

overall energy production. The curve is similar for Iqaluit, though less energy is generated in the winter and more in the summer. This phenomenon is observed more dramatically in Resolute where no energy is generated November through January, while peak production occurs in May (1523 kWh). The total annual electrical energy generation in each community, normalized with livable building area (96 m^2), can be found in Table 5.8. The BIPV/T system produces the most electricity annually in Kuujuaq (86.1 kWh/m^2) and the least in Resolute (79.5 kWh/m^2), though the values are comparable. Resolute suffers the disadvantage of over-producing in the summer and under-producing in the winter, more so than Iqaluit and Kuujuaq. An energy efficient house can use less than 40 kWh/m^2 per year for lighting, appliances and plug loads (CMHC, 2017). The power requirement of the fan used to draw the air behind the BIPV/T cladding would be on the order of 10 W , and the annual energy use less than 1 kWh/m^2 . Therefore this BIPV/T system can potentially supply all the electrical requirements of an Arctic house. However, electrical energy demand is not uniform throughout the year since much more lighting is needed in the winter than in the summer. The cost of electrical energy in the Arctic is very high: 57¢/kWh is the lowest rate of all communities in Nunavut (QEC, 2018). At this rate, the BIPV/T system is able to generate more than $4,500\text{\$}$ worth of electrical energy annually for the building considered. Overproduction of electrical energy in the summer season means that much of this would not be used and therefore would be wasted; maximum savings can be realized if seasonal storage is implemented, and if the electrical energy can be sold to the grid. Since electricity in the north is produced using fossil fuels, which also need to be delivered by sea from the south,

offsetting the electrical loads with solar power would be very beneficial to the long term sustainability of northern housing.

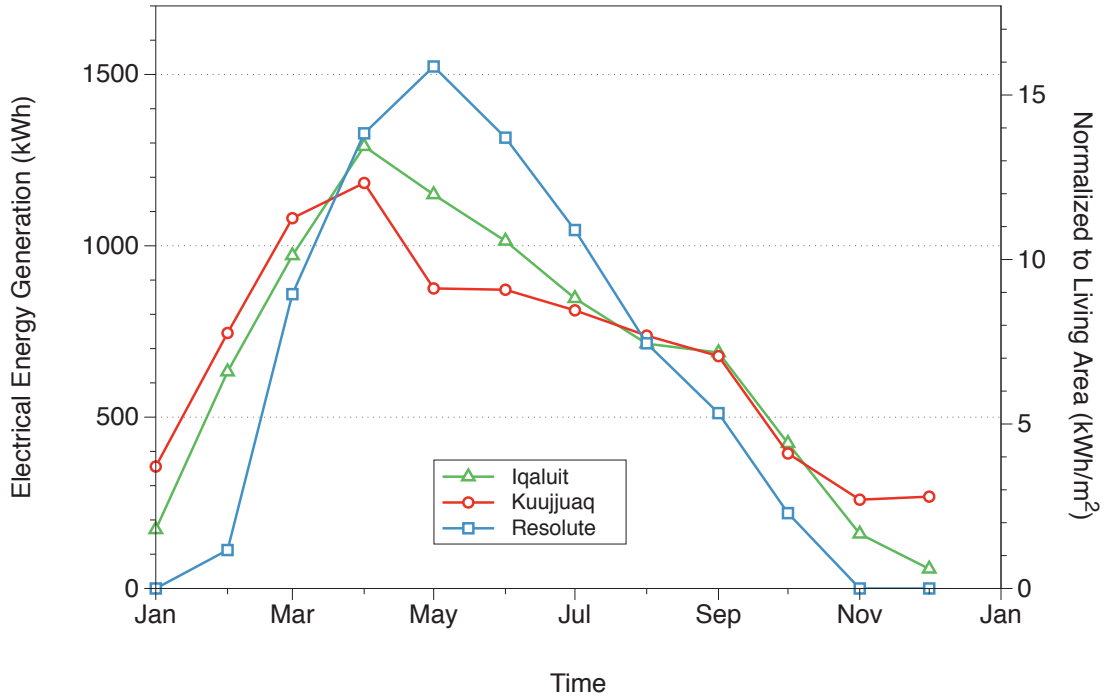


Figure 5.21 Total monthly electrical energy generated with BIPV/T cladding

Figure 5.22 shows the total monthly thermal energy collected by the air passing through the BIPV/T cladding. The curves appear similar to those in Figure 5.21, though the values are different. As with electrical energy generation, the amount of thermal energy collected in winter is low. However, in Iqaluit and Kuujjuaq, more than 5kWh per m² of livable area are generated monthly February through September (March through August for Resolute). The values for total thermal energy collected annually are shown in Table 5.8. In the winter, the heated air is often too cold to be used directly indoors as fresh air. However, the warmed air can be used to offset reheating requirement of fresh air supplied by a heat recover ventilator (HRV). According to ASHRAE 62.1 (ASHRAE, 2016b), if the building had 6 occupants, the required fresh air ventilation rate is 43.8 L/s. Assuming

the HRV effectiveness is 75% and that the supply air would need to be reheated to 22 °C, the total annual energy savings would be as presented in Table 5.8.

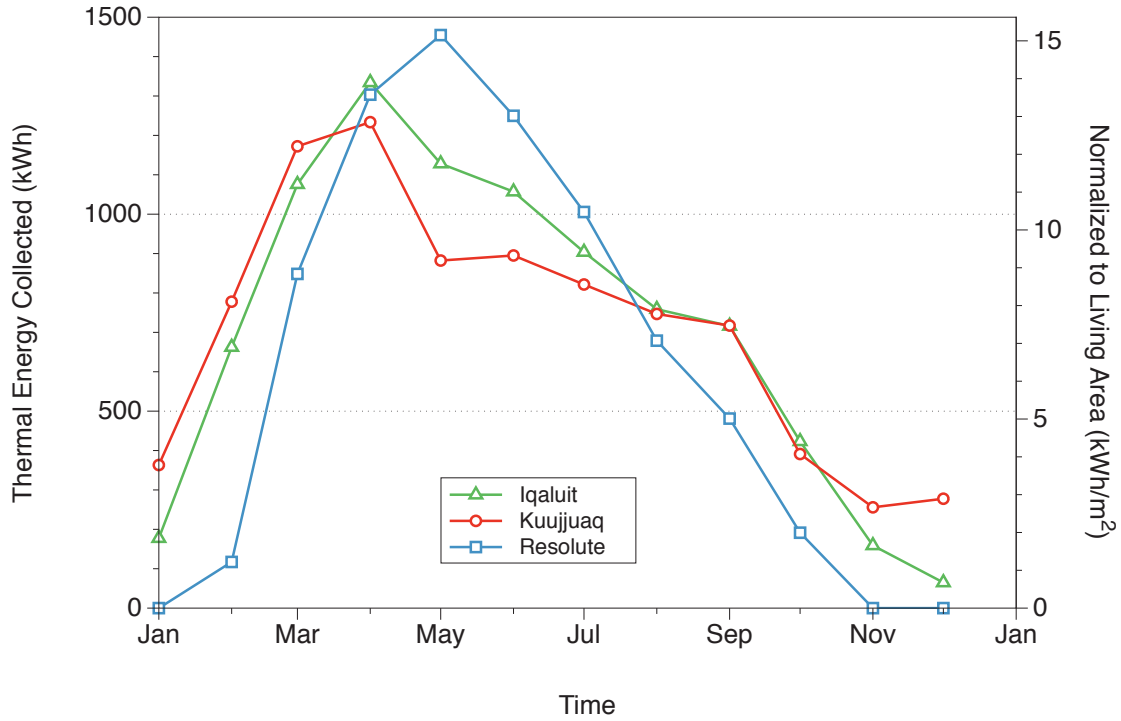


Figure 5.22 Total monthly thermal energy collected from BIPV/T cladding

Table 5.8 Total annual energy values, normalized with living area

Parameter	Iqaluit	Kuujuaq	Resolute
Electricity Generation (kWh/m ²)	84.6	86.1	79.5
Thermal Energy Collected (kWh/m ²)	88.1	88.9	76.4
HRV Reheat Energy Use Reduction using BIPV/T (kWh/m ²)	8.4	7.7	8.2

CHAPTER 6 Conclusion

6.1 SIP Joints

An experiment utilizing a full-scale SIP test hut is conducted to evaluate the thermal and airtightness performance of 8 SIP joints. Temperature sensors embedded in the joints provide the temperature profile in the joints, which is affected by the indoor and outdoor temperatures as well as air leakage. Pressurization and depressurization of the test hut revealed how leaky the joints were. The joints were tested both with and without the tape. By comparing the experimental results with ideal scenarios without air leakage obtained by simulations, the leakiness of the joints can be quantified to some extent. The actual amount of air leakage at each joint cannot be readily calculated using the experimental or simulation results, however.

Overall, it was found that joints formed by the meeting of two envelope elements performed better than those formed by the meeting of three envelope elements. Joints containing two envelope elements had more consistent temperature profiles without pressurization, where the readings from the various instances of each joint type did not differ significantly (up to 3% difference). When subjected to pressure differentials, the temperature profiles of those joints were affected, but not significantly. Except for a few cases, these joints were shown to rely on the tape for airtightness.

The readings from the various instances of joints containing three envelope elements showed large discrepancies in the temperature profile of those joints. Top joints were more susceptible to exfiltration and pressurization of the test hut, while bottom joints

were more susceptible to infiltration and depressurization. These joints also relied heavily on the tape seal, which itself is difficult to apply properly on those joints.

Since air leakage through joints occur as soon as a building is in commission, and Arctic houses are subjected to very large temperature differences, frost accumulation and condensation can happen very easily and pose a significant risk to the integrity of the envelope. In the SIP system tested, all the joints can be improved to be less dependent on the tape seal, though the joints most susceptible to moisture damage are the top joints since air tends to exfiltrate at those locations due to stack effect.

6.2 Attics

The ideal attic design and ventilation strategy for Arctic climates in terms of hygrothermal performance are not yet well understood. The main issue with ventilated attics is the infiltration of fine, blowing snow, while unvented attics are sensitive to air leakage from the indoor spaces. In this study, a full-scale test hut with two attic bays, one unvented and the other ventilated with a fan, is set up inside an environmental chamber and tested under extreme cold climate conditions. Because the duration of the tests was short and condensed, major conclusions cannot be drawn. However, it was found that when air leakage occurs at the bottom of the insulation in the attic, ventilating under winter conditions is not effective as the moisture tends to condense and freeze within the insulation. Even when air is injected directly into the attic air space, there is little capacity to dry the attic in extreme cold conditions. Ventilation proves to be effective under shoulder season and summer conditions, given that the outdoor humidity is lower than that of the attic space. Overall, the ventilated attic performed better than the unvented

attic in the experimental tests, though neither showed significant signs moisture or frost accumulation.

A multi-zone hygrothermal simulation replicating one of the experimental tests was done to verify the computer model. Good agreement ($<1\text{ }^{\circ}\text{C}$ and $<3\%$ RH root mean square error) was found between the simulation and experiment. The model was used to simulate the hygrothermal performance of attic utilizing various ventilation strategies in three Inuit communities: Iqaluit, Kuujjuaq, and Resolute. Table 6.1 summarizes the findings and recommendations for each of the ventilation strategies studied. Unvented attics have a limited capacity to dry out through vapor diffusion, putting them at high risk for mold growth if air leakage is not minimized. Diffusion vents can significantly improve performance, though may not be sufficient if the ceiling is not airtight or in colder communities. All forms of ventilation are found to benefit the attics, provided that snow infiltration is prevented. A low amount of ventilation (1 ACH) applied April through September is found to effectively deter mold growth in all communities studied. Natural ventilation is also highly effective and simple to implement. Attics should receive an annual average of at least 1 ACH to minimize the ability for mold to grow. Natural ventilation, therefore, is the simplest and least expensive method of ensuring healthy attic conditions. Adding a BIPV/T system to a naturally ventilated attic improves performance slightly while generating electrical energy. Combining mechanical ventilation with a BIPV/T system is also highly effective, even if used seasonal and if the majority of the air is bypassed for use elsewhere. The attic can be kept dry while generating a significant amount of electrical energy and supplying pre-heated ventilation air for indoor spaces. Further research on this subject would include investigating other ventilation strategies,

like adaptive ventilation, and also field testing and applications. Because of the extreme cold, air leaking through the ceiling can condense partially within the ceiling insulation before reaching the attic air space. Detailed heat, air, and moisture simulation can provide significant insight into this issue, though field applications and detailed monitoring will be necessary to fully understand the issues.

Table 6.1 Summary of comments for each ventilation strategy

Ventilation Strategy	Comments
Unvented	<ul style="list-style-type: none"> • Sensitive to air leakage • Sensitive to built-in moisture and moisture diffusion from indoor space • Diffusion vents help significantly, more so in warmer Arctic climates • No moving parts • Minimal chance of snow infiltration • Overall, this strategy is reasonably effective in Arctic climates if diffusion vents are implemented, otherwise air leakage rates must be kept very low.
Mechanical Ventilation	<ul style="list-style-type: none"> • Seasonal ventilation effective for deterring mold growth • 1 ACH sufficient to avoid mold growth in wide range of Arctic climates • Higher ventilation rates reduce moisture levels further • Utilizes moving parts (fan, damper, etc.) • Possibility of snow infiltration • Overall, an effective strategy for Arctic climates
Natural Ventilation	<ul style="list-style-type: none"> • Natural ventilation rates, driven by wind, are sufficient to deter mold growth • No moving parts • Possibility of snow infiltration • Benefits from being tried and tested in many communities in Nunavik • Overall, an effective and low-cost strategy for Arctic communities
BIPV/T Natural	<ul style="list-style-type: none"> • Addition of BIPV/T system helps decrease mold index • Generates electricity • Thermal energy cannot be used without fan • No moving parts • Possibility of snow infiltration • Overall, this strategy is effective hygrothermally but does not take full

	advantage of BIPV/T's potential
BIPV/T Mechanical Ventilation	<ul style="list-style-type: none"> • Can provide the lowest moisture levels of all attics and lowest mold index • Seasonal ventilation sufficient to avoid mold growth in wide range of Arctic climates, even if 70% or airflow is bypassed. • Generates useful thermal and electrical energy • Utilizes moving parts • Possibility of snow infiltration • Overall, an effective attic ventilation strategy that also generates useful thermal and electrical energy

6.3 Contributions

The experiments and simulations conducted in this study provide insight into the behavior of the building envelope in extreme cold temperatures. Contributions from this study include:

- Design and implementation of a test procedure for hygrothermal testing of multiple SIP joints and attics in extreme cold temperatures. The experiment showed that the SIP instrumentation method did not interfere with the performance of the joints and provided detailed feedback on the transient and steady state temperature profiles in all joints. The test setup and procedure allowed for a detailed investigation on hygrothermal behaviors in unvented and ventilated attics within a short test period (less than one month).
- Assessment of the performance of 8 SIP joints under large temperature differences and pressure differences. The study identified the weaknesses in the SIP system, the joints most likely to fail in cold climates, and how they can be improved. A comprehensive, multi-joint study on the heat and air performance of SIPs has not been previously performed.
- Experimental assessment of the performance of a ventilated attic and unvented attic in extreme cold climates using an environmental chamber.
- Development and verification of a hygrothermal model using WUFI Plus to simulate hygrothermal conditions in attics. The model is useful for creating

generalized results from long-term simulations, as well as comparing with field testing results.

- Proposal of a novel BIPV/T attic ventilation configuration, where the outlet air is used to ventilate and dry the attic. This configuration allows air heated by the BIPV/T system to facilitate the drying of the attic. Warmer air has a higher capacity to remove moisture, and this study showed the potential for a BIPV/T ventilated attic to achieve high hygrothermal performance, thus improving the durability of the building while generating energy.
- Coupling of the BIPV/T thermal model with hygrothermal simulations. To conduct the hygrothermal simulation incorporating BIPV/T attic ventilation, the BIPV/T outlet conditions are calculated first and used as input in WUFI Plus. This demonstrates the possibility of using various types of methods for ventilation, besides direct ventilation using outdoor air.
- Presented recommendations for attic ventilation strategies suitable for Inuit communities. Existing literature on extreme cold climates presents recommendations for attic designs that have not been evaluated such climates. Long-term simulations accounted for a number attic venting strategies, including BIPV/T ventilation, and a range of air leakage rates to determine the feasibility of each attic ventilation strategy in Arctic climates. An assessment of this scope has not been previously done. The experiments and simulations of this study provide sufficient data to make concrete recommendations for attic ventilation strategies in Arctic climates, and will help in the development of codes and standards.
- The author has co-authored numerous publications including three published journal papers (Wyss et al., 2015; Belleudy et al., 2015; Kayello et al., 2017b) and four conference papers (Kayello et al., 2013; Belleudy et al., 2014; Kayello et al., 2016; Kayello et al., 2017a). The author has also prepared two additional journal papers ready for submission.

6.4 Recommendations for Future Work

For future studies in this field, these recommendations are made:

- Development of a SIP that is insulating and airtight without the use of adhesive tape. This study demonstrated how the SIP system is heavily reliant on adhesive tape for airtightness. Tape is difficult to apply well, especially on edges and corners, and its adhesive strength degrades over time. A durable SIP system should utilize a more robust means of maintaining airtightness, perhaps by relying on compression gaskets.
- Analysis of the effect of air leakage through the SIP joints using detailed HAM models. The flow path in SIP joints is complex and dependent on many uncontrollable variables such as workmanship of tape application. A detailed HAM model is needed to fully visualize the effects of air leakage in the SIP system and can be used to study various designs, minimizing the need for experimental evaluations.
- Experimental and field testing of the BIPV/T attic ventilation system, and verification of simulation results. This novel system presented in this thesis shows much potential for real applications, but must be verified through experimental and field testing.
- Field evaluation of relative hygrothermal performance of proposed attics in extreme cold climates. To verify the results from this study, the attic strategies should be tested side by side such that direct comparisons can be made.
- Inclusion of adaptive mechanical ventilation strategy as part of assessment of attics for the Arctic. This strategy, where an attic is ventilated only when the outdoor humidity level is lower than that of the attics, has great potential for use in all climates zones. Due to limitations of the WUFI Plus software, it was not considered in this study, though its inclusion is warranted.
- Integration of Inuit in the discussion, design, and creation of housing solutions and more. The issues the Inuit face are not one-dimensional nor can they be solved by dissection. Holistic solutions that involve the community are greatly needed. The greater objective of aiding the Inuit in establishing a healthy, sovereign, and free community must not be forgotten, and so every component of the solution must be assessed from this broader perspective.

- Development of a long-term sustainable housing solution that is principally locally sourced. As stated at the beginning of this thesis, the Inuit were living sustainably and self-sufficiently until the last century. The problems they suffer today are a direct consequence of colonialism. A true solution to the housing problem would actually be a part of a greater solution of Inuit decolonization and sovereignty. The Inuit home of the future would therefore be vernacular, perhaps a modernized version of the igloo. The solution must empower the people and minimize their reliance on imported resources.

References

Unread (Green) in medley means added to list and cited in thesis.

Abdou, O. A. (1997). Thermal Performance of an Interlocking Fiber-Reinforced Plastic Building Envelope System. *Journal of Architectural Engineering*, 2(1), 9–14.

Adams, W. A., McMahon, D., & Russell, P. (2013). Sustainable Housing, Transportation and Energy for Remote Communities in the Canadian Arctic. In *EIC Climate Change Technology Conference 2013* (pp. 1–16).

Alev, Ü., & Kalamees, T. (2016). Avoiding mould growth in an interiorly insulated log wall. *Building and Environment*, 105, 104–115.
<http://doi.org/10.1016/j.buildenv.2016.05.020>

Antretter, F., Sauer, F., Schöpfer, T., & Holm, A. (2011). Validation of a Hygrothermal Whole Building Simulation Software. In *12th Conference of International Building Performance Simulation Association* (pp. 1694–1701). Sydney.

ASHRAE. (2013a). *ASHRAE Handbook: Fundamentals 2013*. American Society of Heating, Refrigerating, and Air-Conditioning Engineers. Atlanta, GA.

ASHRAE. (2013b). Standard 169-2013: Climatic Data for Building Design Standards. Atlanta, GA: ASHRAE.

ASHRAE. (2016a). Standard 160-2016: Criteria for Moisture-Control Design Analysis in Buildings. Atlanta, GA: ASHRAE.

- ASTM. (2004). C 177-04 Standard Test Method for Steady-State Heat Flux Measurements and Thermal Transmission Properties by Means of the Guarded-Hot-Plate Apparatus. USA: ASTM International.
- ASTM. (2007). Standard Test Methods for Direct Moisture Content Measurement of Wood and Wood-Base Materials. USA: ASTM International.
- Asiz, A., Smith, I., & Menendez, V. (2008). Air leakage and Moisture Deposition of Prefabricated Light-Frame Wood Building. In *Proceeding of the 10th World Conference on Timber Engineering*. Miyazaki, Japan.
- Athienitis, A. K., Tzempelikos, A., Poissant, Y. (2004). Investigation of the Performance of a Double Skin Façade with Integrated Photovoltaic Panels. In *EuroSun2004 Proceedings*. Freiburg, Germany.
- Baril, D., Fazio, P., & Rao, J. (2013). Field Study of Hygrothermal Performance of Housing in Canadian North. In *EIC Climate Change Technology Conference 2013*. Montreal, QC.
- Barna, L., Claffey, K., Buska, J., Mercer, J., Burnside, J., Haggerty, P., & Crain, R. (2012). Thermal Analysis of an Elevated Building at Summit Station, Greenland. In *Cold Regions Engineering 2012* (pp. 210–220). Quebec, QC.
- Beattie, C., Fazio, P., Zmeureanu, R., & Rao, J. (2015). A Preliminary Study of the Performance of Sensible and Latent Heat Exchanger Cores at the Frosting Limit for use in Arctic Housing. In *6th International Building Physics Conference*,

IBPC 2015 (Vol. 78, pp. 2596–2601). Turin, Italy.

<http://doi.org/10.1016/j.egypro.2015.11.299>

Belleudy, C., Kayello, A., Woloszyn, M., Ge, H., Fazio, P., Chhay, M., & Quenard, D. (2014). A Heat-airflow model for simulating the effects of air leakage on the temperature field in porous insulation. In *Nordic Symposium on Building Physics 2014*. Lund, Sweden. <http://doi.org/10.13140/RG.2.1.1508.0409>

Belleudy, C., Kayello, A., Woloszyn, M., & Ge, H. (2015). Experimental and numerical investigations of the effects of air leakage on temperature and moisture fields in porous insulation. *Building and Environment*, *94*, 457–466. <http://doi.org/10.1016/j.buildenv.2015.10.009>

Broniek, J. (2010). Detailed Modeling Study on How Different Assemblies Affect Comfort Conditions in Zero-Energy House Designs. In *Thermal Performance of the Exterior Envelopes of Whole Buildings XI International Conference* (pp. 1–9). Clearwater, FL: ASHRAE.

Burch, D. M., Lemay, M. R., Rian, B. J., & Parker, E. J. (1984). Experimental Validation of an Attic Condensation Model. *ASHRAE Transactions*, *90*(2).

Burch, D. M., & TenWolde, A. (1993). A Computer Analysis of Moisture Accumulation in the Walls of Manufactured Housing. *ASHRAE Transactions*, *99*(2).

Candanedo, L. M., Athienitis, A., Park, K. (2011) Convective Heat Transfer Coefficients in a Building-Integrated Photovoltaic/Thermal System. *ASME. J. Sol. Energy Eng.* *133*(2):021002-021002-14. doi:10.1115/1.4003145

- Chen, Y., Athienitis, A. K., & Galal, K. (2010). Modeling, design and thermal performance of a BIPV/T system thermally coupled with a ventilated concrete slab in a low energy solar house: Part 1, BIPV/T system and house energy concept. *Solar Energy*, 84(11), 1892–1907. doi:10.1016/j.solener.2010.06.013
- Chen, Y., Fazio, P., Athienitis, A. K., & Rao, J. (2012a). Sustainable Building Design in Cold Regions: High Performance Envelope and Façade-Integrated Photovoltaic/Solar Thermal Systems at High Latitudes. In *Cold Regions Engineering 2012* (pp. 199–209). Quebec, QC: American Society of Civil Engineers. doi:10.1061/9780784412473.020
- Chen, Y., Athienitis, A., & Fazio, P. (2012b). Modelling of High-performance Envelope and Façade Integrated Photovoltaic / Solar Thermal Systems for High-Latitude Applications. In *Proceedings of eSim 2012* (pp. 108–121). Halifax, NS.
- Christian, J. (2007). Panels³. In *Thermal Performance of the Exterior Envelopes of Whole Buildings X International Conference* (pp. 1–13). Clearwater, FL: ASHRAE.
- CMHC. (1993). *Attic Ventilation and Moisture*. Research & Development Highlights: Technical Series 93-201. Canada Mortgage and Housing Corporation. Ottawa, ON.
- CMHC. (2001). Building with Structural Panels — Repulse Bay. *About Your House: North Series I*. Canada Mortgage and Housing Corporation. Ottawa, ON.

- CMHC. (2009). *The Northern Sustainable House: An Innovative Design Process. Research Highlights: Technical Series*. Canada Mortgage and Housing Corporation. Ottawa, ON.
- Collier, P. C. R., & Baker, G. B. (2011). The Influence of Construction Detailing on the Fire Performance of Polystyrene Insulated Panels. *Fire Technology*, 49(2), 195–211. doi:10.1007/s10694-011-0238-5
- COMSOL. (2016). Introduction to COMSOL Multiphysics. COMSOL. *Version: COMSOL 5.2a*.
- Cornick, S. M., Rousseau, M. Z., & Parekh, A. (2009). An Energy Simulation Study of Wall Systems for Canadian Arctic Homes. In *4th International Building Physics Conference*. Istanbul, Turkey.
- Cunningham, M. J. (1993). Moisture transfer in roof sections under cyclic conditions and constant air pressure difference—laboratory and modelling studies. *Building and Environment*, 28(3), 323–332. [http://doi.org/10.1016/0360-1323\(93\)90037-4](http://doi.org/10.1016/0360-1323(93)90037-4)
- Desmarais, G., Derome, D., & Fazio, P. (2000). Mapping of Air Leakage in Exterior Wall Assemblies. *Journal of Thermal Envelope and Building Science*, 24(2), 132–154. <http://doi.org/10.1106/BWH8-9D3J-R939-957E>
- Dutt, G. S. (1979). Condensation in Attics: Are Vapor Barriers Really the Answer? *Energy and Buildings*, 2, 251–258.

- Environment Canada. (2013). *Canadian Climate Normals*. Retrieved January 14, 2014, from http://climate.weather.gc.ca/climate_normals/index_e.html
- Essah, E. A., Sanders, C. H., Baker, P., & Sasic Kalagasidis, A. (2009). Condensation and Moisture Transport in Cold Roofs: Effect of Roof Underlay. *Building Research & Information*, 37(2), 117–128.
- Forest, T. W., & Berg, K. (1993). *Simulations of Attic Ventilation and Moisture*. Department of Mechanical Engineering, Final Report prepared for Canada Mortgage and Housing Corporation. Edmonton, Alberta.
- Forest, T. W., & Walker, I. S. (1992). Attic Ventilation Model. In *Thermal Performance of the Exterior Envelopes of Buildings V Conference*. Clearwater, FL: ASHRAE.
- Forgues, Y. E. (1985). *The Ventilation of Insulated roofs*. National Research Council Canada. Ottawa, ON.
- Fugler, D. W. (1999). Conclusions from Ten Years of Canadian Attic Research. *ASHRAE Transactions*, 105(1).
- Ge, H., Wang, R., & Baril, D. (2018). Field measurements of hygrothermal performance of attics in extreme cold climates. *Building and Environment*, 134, 114–130. <http://doi.org/10.1016/j.buildenv.2018.02.032>
- GN. (2005). *Good Building Practices Guideline*. Government of Nunavut.
- GNT. (2011). *Good Building Practice for Northern Facilities*. Government of Northwest Territories, Department of Public Works and Services. Yellowknife, NT.

- Goldberg, L., Huelman, P., & Bridges, B. (1999). A Preliminary Experimental Assessment of the Comparative Thermal Performance of Attics and Cathedral Ceilings in a Cold Climate. *ASHRAE Transactions*, 105(1).
- Goto, Y., Ghazi Wakili, K., Ostermeyer, Y., Sasic Kalagasidis, A., & Wallbaum, H. (2016). Hygrothermal performance of a vapor-open envelope for subtropical climate, field test and model validation. *Building and Environment*, 110, 55–64. <http://doi.org/10.1016/j.buildenv.2016.09.026>
- Grunewald, J., Nicolai, A., & Zhang, J. (2007). Modeling of Air Convection Effects on Hygrothermal Performance of Vented Roofs. In *Thermal Performance of the Exterior Envelopes of Whole Buildings X International Conference*. Clearwater, FL: ASHRAE.
- Ha, H. K., & Fazio, P. (1978). Flexural Behaviour of Sandwich Floor Assembly. *Building and Environment*, 13(1), 61–67. doi:10.1016/0360-1323(78)90009-4
- Hagentoft, C., & Sasic Kalagasidis, A. (2010). Mold Growth Control in Cold Attics through Adaptive Ventilation: Validation by Field Measurements. In *Thermal Performance of the Exterior Envelopes of Whole Buildings XI International Conference*. Clearwater, FL: ASHRAE.
- Hales, D. G., & Howard, L. (2013). Monitored Performance of Ultra-High Performance Residential Envelopes in the Pacific Northwest Marine Climate. In *Thermal Performance of the Exterior Envelopes of Whole Buildings XII International Conference*. Clearwater, FL: ASHRAE.

- Harderup, L., & Arfvidsson, J. (2013). Moisture Safety in Cold Attics with Thick Thermal Insulation. *Journal of Architectural Engineering*, 19(4), 265–278. doi:10.1061/(ASCE)AE.1943-5568.0000067.
- Hinrichs, H. S. (1962). Comparative Study of the Effectiveness of Fixed Ventilating Louvers. *ASHRAE Transactions*, 68.
- Horvat, M., Gorgolewski, M., & Cuciureanu, A. (2009). Operational and Embodied Impact Placed in Context. In *4th International Building Physics Conference*. Istanbul, Turkey.
- Hukka, A., & Viitanen, H. A. (1999). A mathematical model of mould growth on wooden material. *Wood Science and Technology*, 33, 475–485.
- Janssens, A., & Hens, H. (2003). Interstitial Condensation Due to Air Leakage: A Sensitivity Analysis. *Journal of Building Physics*, 27(1), 15–29. <http://doi.org/10.1177/1097196303027001002>
- Kalamees, T., & Kurnitski, J. (2009). Moisture Convection Performance of External Walls and Roofs. *Journal of Building Physics*, 33(3), 225–247. doi:10.1177/1744259109343502
- Kayello, A., Fazio, P., & Rao, J. (2013). Investigation of the Hygrothermal Performance of a SIP Test Hut with an Unventilated and Ventilated Attic for the Canadian North. In *EIC Climate Change Technology Conference 2013*. Montreal, QC.
- Kayello, A., Athienitis, A., & Ge, H. (2016). Natural Ventilation of Attics Coupled with BIPV/T in Arctic Climates. In *Proceedings of the eSim 2016 Building*

Performance Simulation Conference (pp. 433–443). Hamilton, ON: McMaster University.

Kayello, A., Ge, H., & Athienitis, A. (2017a). Attic Ventilation in Northern Canadian Climates. In *15th Canadian Conference on Building Science and Technology*. Vancouver, BC.

Kayello, A., Ge, H., Athienitis, A., & Rao, J. (2017b). Experimental study of thermal and airtightness performance of structural insulated panel joints in cold climates. *Building and Environment*, *115*, 345–357.
<http://doi.org/10.1016/j.buildenv.2017.01.031>

Kumaran, M. K., Lackey, J. C., Normandin, N., Fitsum, T., & van Reenen, D. (2002). *A Thermal and Moisture Transport Database for Common Building Materials*. ASHRAE Research Project 1018-RP, *Final Report*. National Research Council, Canada.

Langmans, J., Klein, R., & Roels, S. (2012). Hygrothermal risks of using exterior air barrier systems for highly insulated light weight walls: A laboratory investigation. *Building and Environment*, *56*, 192–202.
<http://doi.org/10.1016/j.buildenv.2012.03.007>

Less, B., Walker, I., & Levinson, R. (2016). *A Literature Review of Sealed and Insulated Attics — Thermal, Moisture and Energy Performance*. Berkley, CA.

Lstiburek, J. (2006, April). Understanding Attic Ventilation. *ASHRAE Journal*, (April), 36–45.

- Lstiburek, J. W. (2009, February). Building in Extreme Cold. *ASHRAE Journal*, (February), 56–59.
- Lstiburek, J. W. (2014, April). Cool Hand Luke Meets Attics. *ASHRAE Journal*, (April), 52–57.
- Medina, M., King, J., & Zhang, M. (2008). On the heat transfer rate reduction of structural insulated panels (SIPs) outfitted with phase change materials (PCMs). *Energy*, 33(4), 667–678. doi:10.1016/j.energy.2007.11.003
- Memari, A. (2012). Comparative Study of Multi-hazard Performance of Different Wall Systems Used in Single-Family Dwelling Construction. In *6th Congress on Forensic Engineering* (pp. 1053–1062). San Francisco, CA.
- Minich, K., Saudny, H., Lennie, C., Wood, M., Williamson-Bathory, L., Cao, Z., & Egeland, G. M. (2011). Inuit housing and homelessness: results from the International Polar Year Inuit Health Survey 2007-2008. *International Journal of Circumpolar Health*, 70(5), 520–31. Retrieved from <http://www.ncbi.nlm.nih.gov/pubmed/22152596>
- Mousa, M. A., & Uddin, N. (2012). Structural behavior and modeling of full-scale composite structural insulated wall panels. *Engineering Structures*, 41, 320–334. doi:10.1016/j.engstruct.2012.03.028
- Mousa, M. A., & Uddin, N. (2013). Performance of Composite Structural Insulated Panels after Exposure to Floodwater. *Journal of Performance of Constructed Facilities*, 27(4), 424–436. doi:10.1061/(ASCE)CF.1943-5509.0000306.

- Mullens, M. A., & Arif, M. (2006). Structural Insulated Panels: Impact on the Residential Construction Process. *Journal of Construction Engineering and Management*, 132(7), 786–794. doi:10.1061/ASCE0733-9364(2006)132:7(786) CE
- Newell, T., & Newell, B. (2011, January). Supersealing a House. *ASHRAE Journal*, (January), 54–58.
- Nik, V. M., Sasic Kalagasidis, A., & Kjellström, E. (2012). Assessment of Hygrothermal Performance and Mould Growth Risk in Ventilated Attics in Respect to Possible Climate Changes in Sweden. *Building and Environment*, 55, 96–109. doi:10.1016/j.buildenv.2012.01.024
- NRCC. (1997). *Model National Energy Code of Canada for Buildings 1997*. National Research Council of Canada. Ottawa, ON.
- NRCC. (2010). *National Building Code of Canada 2010*. National Research Council of Canada. Ottawa, ON.
- NRCC. (2011). *National Energy Code of Canada for Buildings 2011*. National Research Council of Canada. Ottawa, ON.
- Ojanen, T. T., & Kumaran, K. (1996). Effect of Exfiltration of a Residential Wall Assembly. *Journal of Building Physics*, 19, 215. doi:10.1177/109719639601900303
- Ojanen, T. T. (2001). Thermal and Moisture Performance of a Sealed Cold-Roof System with a Vapor-Permeable Underlay. In *Thermal Performance of the Exterior Envelopes of Buildings VIII Conference*. Clearwater, FL: ASHRAE.

- Ojanen, T., Viitanen, H., Peuhkuri, R., Lähdesmäki, K., Vinha, J., & Salminen, K. (2010). Mold Growth Modeling of Building Structures Using Sensitivity Classes of Materials. In *Thermal Performance of the Exterior Envelopes of Whole Buildings XI International Conference*. Clearwater, FL: ASHRAE.
- Okamoto, N., Sakai, K., & Ono, H. (2012). Investigation of insulation loss and condensation at the joint of insulation panel. In *10th International Conference on Healthy Buildings* (p. v 3, p 2191–2196). Brisbane, Australia.
- Pallin, S., Kehrer, M., & Miller, W. A. (2013). A Hygrothermal Risk Analysis Applied to Residential Unvented Attics. In *Thermal Performance of the Exterior Envelopes of Whole Buildings XII International Conference*. Clearwater, FL: ASHRAE.
- Panjehpour, M., Ali, A. A. A., & Voo, Y. L. (2013). Structural Insulated Panels: Past, Present, and Future. *Journal of Engineering, Project, and Production Management*, 3(1), 2–8.
- Pankratz, O., & Holm, A. (2004). Designing and Testing a Structural Insulated Panel (SIP) with the Help of Hygrothermal Model. In *Thermal Performance of the Exterior Envelopes of Whole Buildings IX International Conference*. Clearwater, FL: ASHRAE.
- Passive House Institute. (2016). *Criteria for the Passive House, EnerPHit, and PHI Low Energy Building Standard*. Darmstadt, Germany: Passive House Institute.

- PikeResearch (2012). *Building Integrated Photovoltaics - BIPV and BAPV: Market Drivers and Challenges, Technology Issues, Competitive Landscape, and Global Market Forecasts* (Boulder: Navigant).
- Pratinthong, N., Quenard, D., Khedari, J., Bonnebat, C., & Delanoe, R. (2005). Impact of Severe Service Conditions on Hygrothermal Performance of Sandwich Panels. In *10th DBMC International Conference on Durability of Building Materials and Components*. Lyon, France.
- QEC. (2018). *Customer Rates*. Nunavut. Qulliq Energy Corporation.
Retrieved October 22, 2018, from
<https://www.qec.nu.ca/customer-care/accounts-and-billing/customer-rates>
- Quebec. (2018). *Regulation Respecting Energy Conservation in New Buildings*. Quebec.
Retrieved October 22, 2018, from
<http://legisquebec.gouv.qc.ca/en/ShowDoc/cr/E-1.1,%20r.%201>
- Rao, J., Fazio, P., Bartlett, K., & Yang, D.-Q. (2009). Experimental evaluation of potential transport of mold spores from moldy studs in full-size wall assemblies. *Building and Environment*, 44(8), 1568–1577.
<http://doi.org/10.1016/j.buildenv.2008.10.001>
- Roppel, P., Norris, N., & Lawton, M. (2013). Highly Insulated, Ventilated, Wood-Framed Attics in Cool Marine Climates. In *Thermal Performance of the Exterior Envelopes of Whole Buildings XII International Conference* (pp. 1–13). Clearwater, FL: ASHRAE.

- Rose, W. B. (1992). Measured Values of Temperature and Sheathing Moisture Content in Residential Attic Assemblies. In *Thermal Performance of the Exterior Envelopes of Buildings V Conference* (pp. 379–390). Clearwater, FL: ASHRAE.
- Rose, W. B. (1995). The History of Attic Ventilation Regulation and Research. In *Thermal Performance of the Exterior Envelopes of Buildings VI Conference*. Clearwater, FL: ASHRAE.
- Rousseau, M., Manning, M., & Swinton, M. C. (2007). Characterization of Indoor Hygrothermal Conditions in Houses in Different Northern Climates. In *Thermal Performance of Exterior Envelopes of Whole Buildings X International Conference*. Clearwater, FL: ASHRAE.
- Rowley, F. B., Algren, A. B., & Lund, C. E. (1939). Condensation of Moisture and its Relation to Building Construction and Operation. *ASHVE Transactions*, 44(1115).
- Saber, H. H., Maref, W., Elmahdy, H., Swinton, M. C., & Glazer, R. (2012). 3D heat and air transport model for predicting the thermal resistances of insulated wall assemblies. *Journal of Building Performance Simulation*, 5(2), 75–91.
<http://doi.org/10.1080/19401493.2010.532568>
- Saïd, M. N. A. (2006). *Task 2: Literature Review Building Envelope, Heating, and Ventilating Practices and Technologies for Extreme Climates*. Institute for Research in Construction. Ottawa, ON.
- Samuelson, I. (1998). Hygrothermal Performance of Attics. *Journal of Building Physics*, 22(2), 132–146. doi:10.1177/109719639802200206

- Sheltair Scientific Ltd. (1997). *Attic Ventilation and Moisture Control Strategies*. Final Report, Canada Mortgage and Housing Corporation. Ottawa, ON.
- Sherman, M. (1987). Estimation of infiltration from leakage and climate indicators. *Energy and Buildings*, 10(1), 81-86. doi:10.1016/0378-7788(87)90008-9
- Simonson, C. J., Ojanen, T., & Salonvaara, M. (2005). Moisture Performance of an Airtight, Vapor-permeable Building Envelope in a Cold Climate. *Journal of Building Physics*, 28(3), 205–226. <http://doi.org/10.1177/1097196305048628>
- SIPA (Structural Insulated Panel Association). (2002). *SIPA report on the Juneau, Alaska roof issue*. Retrieved January 31, 2014, from <http://www.sips.org/technical-information/sipa-report-on-the-juneau-alaska-roof-issue>
- Slanina, P., & Šilarová, Š. (2009). Moisture transport through perforated vapour retarders. *Building and Environment*, 44(8), 1617–1626. <http://doi.org/10.1016/j.buildenv.2008.10.006>
- Smakosz, Ł., & Tejchman, J. (2014). Evaluation of Strength, Deformability and Failure Mode of Composite Structural Insulated Panels. *Materials & Design*, 54, 1068–1082. doi:10.1016/j.matdes.2013.09.032
- Smith, R. E. (2010). *Prefab Architecture: A Guide to Modular Design and Construction*. Hoboken, NJ: John Wiley & Sons, Inc.
- Statistics Canada. (2008). *Aboriginal Peoples in Canada in 2006: Inuit, Métis and First Nations, 2006 Census*. Ottawa, ON.

- Statistics Canada. (2014). *Census Profile: 2011 Census of Population*. Retrieved January 14, 2014, from <http://www12.statcan.ca/census-recensement/2011/dp-pd/prof/index.cfm?Lang=E>
- Straube, J., Onysko, D., & Schumacher, C. (2002). Methodology and Design of Field Experiments for Monitoring the Hygrothermal Performance of Wood Frame Enclosure. *Journal of Thermal Envelope and Building Science*, 26(2). <http://doi.org/10.1106/109719602028098>
- Taylor, S. B., Manbeck, H. B., Janowiak, J. J., & Hiltunen, D. R. (1997). Modeling Structural Insulated Panel (SIP) Flexural Creep Deflection. *Journal of Structural Engineering*, 123(12), 1658–1665.
- TenWolde, A., & Rose, W. B. (1999). Issues Related to Venting of Attics and Cathedral Ceilings. *ASHRAE Transactions*, 105(1).
- Test, F. L., Lessmann, R. C., Johary, A. A. (1981). Heat Transfer During Wind Flow over Rectangular Bodies in the Natural Environment. ASME. *J. Heat Transfer*. 1981; 103(2), 262-267. doi:10.1115/1.3244451
- Tester, F. (2009). Iglutaasaavut (Our New Homes): Neither “New” nor “Ours” Housing Challenges of the Nunavut Territorial Government. *Journal of Canadian Studies*, 43(2), 137–158
- Thisis, T. K., Barfoed, P., Delpech, P., Gustavsen, A., Hofseth, V., Uvsløkk, S., & Dufresne de Virel, M. (2007). Penetration of Snow Into Roof Constructions—Wind Tunnel Testing of Different Eave Cover Designs. *Journal of Wind*

Engineering and Industrial Aerodynamics, 95(9-11), 1476–1485.

doi:10.1016/j.jweia.2007.02.017

Thirunavukarasu, A., Fazio, P., Ge, H., Athienitis, A. (2015). Performance Assessment Protocol for Pre-Engineered Manufactured Self-Sustaining (PEMaSS) Housing to Remote Regions. In *6th International Building Physics Conference, IBPC 2015*. Turin, Italy.

Tobiasson, W. N., Buska, J. S., & Greatorex, A. R. (2001). Guidelines for Ventilating Attics and Cathedral Ceilings to Avoid Icings at Their Eaves. In *Thermal Performance of the Exterior Envelopes of Buildings VIII Conference*. Clearwater, FL: ASHRAE.

Viitanen, H., & Ojanen, T. T. (2007). Improved Model to Predict Mold Growth in Building Materials. In *Thermal Performance of the Exterior Envelopes of Whole Buildings X International Conference*. Clearwater, FL: ASHRAE.

Walker, I. S., & Forest, T. W. (1995). Field Measurements of Ventilation Rates in Attics. *Building and Environment*, 30(3), 333–347.

Wyss, S. (2011). *Investigation of Hygrothermal Performance of Structural Insulated Panels (SIP) for Northern Canadian Climates*. Master's Thesis. Concordia University.

Wyss, S., Fazio, P., Rao, J., & Kayello, A. (2015). Investigation of Thermal Performance of Structural Insulated Panels for Northern Canada. *Journal of Architectural Engineering*, 21(4), 1–16. doi:10.1061/(ASCE)AE.1943-5568.0000174.

Yang, T., & Athienitis, A. K. (2015). Experimental investigation of a two-inlet air-based building integrated photovoltaic/thermal (BIPV/T) system. *Applied Energy*, *159*, 70–79. doi:10.1016/j.apenergy.2015.08.0

Younes, C., & Abi Shdid, C. (2013). A methodology for 3-D multiphysics CFD simulation of air leakage in building envelopes. *Energy and Buildings*, *65*, 146–158. <http://doi.org/10.1016/j.enbuild.2013.05.050>

Appendix A Complete SIP Joint Results

Steady state temperature values and differences for joint F at -20 and -40 °C

	Sensor	Temperature (°C)			Difference (Max-Min)	Percentage Difference
		F _A	F _B	F _C		
-20 °C	F1	18.26	18.25	18.05	0.22	0.52
	F2	17.58	17.36	17.67	0.30	0.72
	F3	7.23	7.16	7.52	0.36	0.86
	F4	-6.44	-6.36	-6.20	0.24	0.57
	F5	-16.36	-15.70	-16.29	0.66	1.57
	F6	-17.62	-16.97	-16.97	0.65	1.55
-40 °C	F1	17.47	18.72	18.51	1.25	2.02
	F2	16.46	17.34	17.57	1.11	1.80
	F3	2.75	3.97	2.77	1.22	1.97
	F4	-16.40	-15.92	-17.80	1.88	3.04
	F5	-30.51	-30.53	-33.44	2.93	4.72
	F6	-32.94	-32.53	-34.95	2.41	3.89

Steady state temperature values and differences for joint G at -20 and -40 °C

	Sensor	Temperature (°C)		Difference (G _A -G _B)	Percentage Difference
		G _A	G _B		
-20 °C	G1	18.49	18.14	0.35	0.84
	G2	17.36	17.59	-0.23	-0.54
	G3	10.27	9.20	1.07	2.54
	G4	-0.61	-3.03	2.42	5.77
	G5	-14.17	-14.61	0.44	1.06
	G6	-16.10	-17.05	0.95	2.27
-40 °C	G1	18.36	18.73	-0.37	-0.59
	G2	16.50	17.48	-0.97	-1.57
	G3	5.88	5.27	0.61	0.98
	G4	-14.26	-15.45	1.19	1.92
	G5	-29.29	-30.57	1.28	2.06
	G6	-31.61	-34.70	3.09	4.98

Steady state temperature values and differences for joint H at -20 and -40 °C

	Sensor	Temperature (°C)		Difference (H _A -H _B)	Percentage Difference
		H _A	H _B		
-20 °C	H1	18.52	18.21	0.31	0.75
	H2	17.43	17.41	0.03	0.06
	H3	13.02	12.93	0.09	0.21
	H4	9.21	9.24	-0.04	-0.09
	H5	-13.64	-13.91	0.27	0.64
	H6	-17.13	-17.34	0.21	0.50
	H7	-18.02	-18.46	0.44	1.05
-40 °C	H1	19.60	19.90	-0.30	-0.49
	H2	17.56	18.59	-1.04	-1.67
	H3	12.00	12.08	-0.08	-0.13
	H4	7.85	6.49	1.35	2.18
	H5	-24.94	-28.81	3.87	6.23
	H6	-31.98	-34.10	2.11	3.41

	H7	-34.07	-35.74	1.68	2.70
--	-----------	--------	--------	-------------	------

Steady state temperature values and differences for joint I at -20 and -40 °C

	Sensor	Temperature (°C)		Difference (I _A -I _B)	Percentage Difference
		I _A	I _B		
-20 °C	I1	13.36	13.55	-0.19	-0.45
	I2	11.69	13.95	-2.27	-5.39
	I3	-6.23	1.53	-7.76	-18.47
	I4	-13.50	-10.67	-2.84	-6.76
	I5	-17.26	-17.16	-0.10	-0.25
	I6	-18.01	-18.20	0.19	0.44
-40 °C	I1	13.83	14.57	-0.75	-1.20
	I2	9.42	14.20	-4.77	-7.70
	I3	-22.87	-6.90	-15.97	-25.76
	I4	-30.06	-25.27	-4.79	-7.73
	I5	-35.00	-34.60	-0.41	-0.66
	I6	-35.96	-36.13	0.16	0.26

Steady state temperature values and differences for joint J at -20 and -40 °C

	Sensor	Temperature (°C)			Difference (Max-Min)	Percentage Difference
		J _A	J _B	J _C		
-20 °C	J1	14.01	14.23	14.97	0.96	2.29
	J2	14.72	14.82	15.05	0.33	0.78
	J3	3.49	3.49	3.90	0.41	0.98
	J4	-10.10	-9.63	N/A	0.47	1.11
	J5	-17.01	-17.04	-17.77	0.76	1.81
	J6	-17.50	-18.26	-18.53	1.03	2.45
-40 °C	J1	12.42	16.87	15.69	4.45	7.18
	J2	13.22	15.43	14.84	2.21	3.56
	J3	-4.04	-1.95	-1.92	2.12	3.42
	J4	-24.88	-22.81	N/A	2.07	3.33
	J5	-34.62	-34.28	-35.19	0.92	1.48
	J6	-35.18	-36.36	-36.38	1.20	1.94

Steady state temperature values and differences for joint K at -20 and -40 °C

	Sensor	Temperature (°C)		Difference (K _A -K _B)	Percentage Difference
		K _A	K _B		
-20 °C	K1	11.00	12.44	-1.44	-3.42
	K2	8.95	9.48	-0.53	-1.26
	K3	-4.50	-6.07	1.57	3.74
	K4	-13.47	-14.26	0.79	1.88
	K5	-17.91	-17.73	-0.18	-0.43
	K6	-18.54	-19.07	0.53	1.26
-40 °C	K1	5.22	6.93	-1.70	-2.75
	K2	-2.61	2.51	-5.13	-8.27
	K3	-21.24	-20.68	-0.56	-0.91
	K4	-31.06	-31.85	0.79	1.27
	K5	-36.06	-36.25	0.19	0.31
	K6	-36.87	-38.18	1.31	2.11

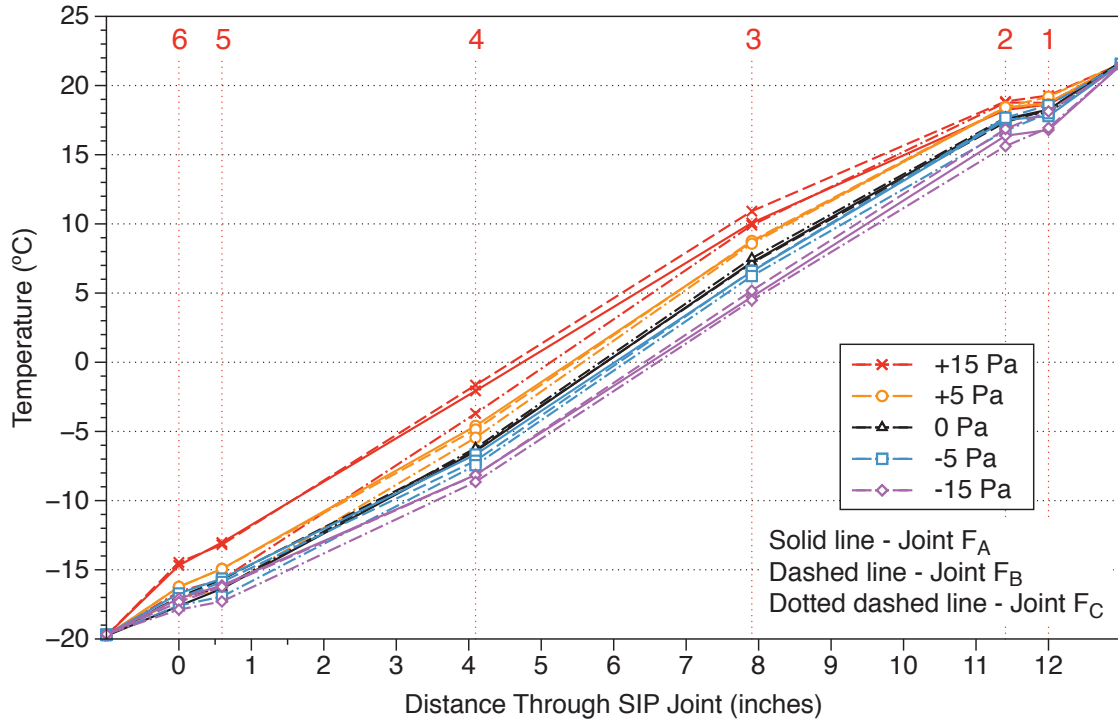
Steady state temperature values and differences for joint L at -20 and -40 °C

Sensor	Temperature (°C)	Difference	Percentage
--------	------------------	------------	------------

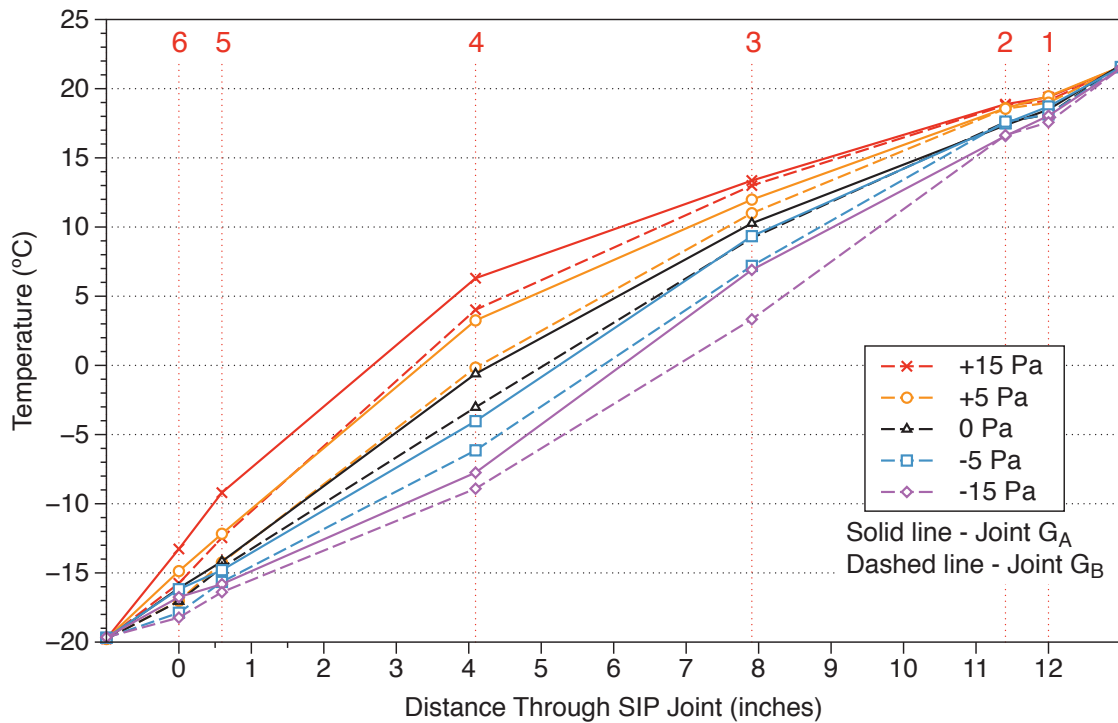
		L_A	L_B	(L_A-L_B)	
-20 °C	L1	17.52	16.31	1.21	2.88
	L2	17.28	15.96	1.32	3.13
	L3	5.74	5.01	0.74	1.75
	L4	-8.36	-8.66	0.31	0.73
	L5	-17.04	-17.43	0.38	0.91
	L6	-17.93	-18.52	0.58	1.39
-40 °C	L1	15.33	16.25	-0.93	-1.49
	L2	14.82	15.20	-0.38	-0.61
	L3	1.06	-0.52	1.59	2.56
	L4	-17.58	-21.06	3.48	5.61
	L5	-32.22	-34.50	2.28	3.67
	L6	-33.94	-36.12	2.18	3.51

Steady state temperature values and differences for joint M at -20 and -40 °C

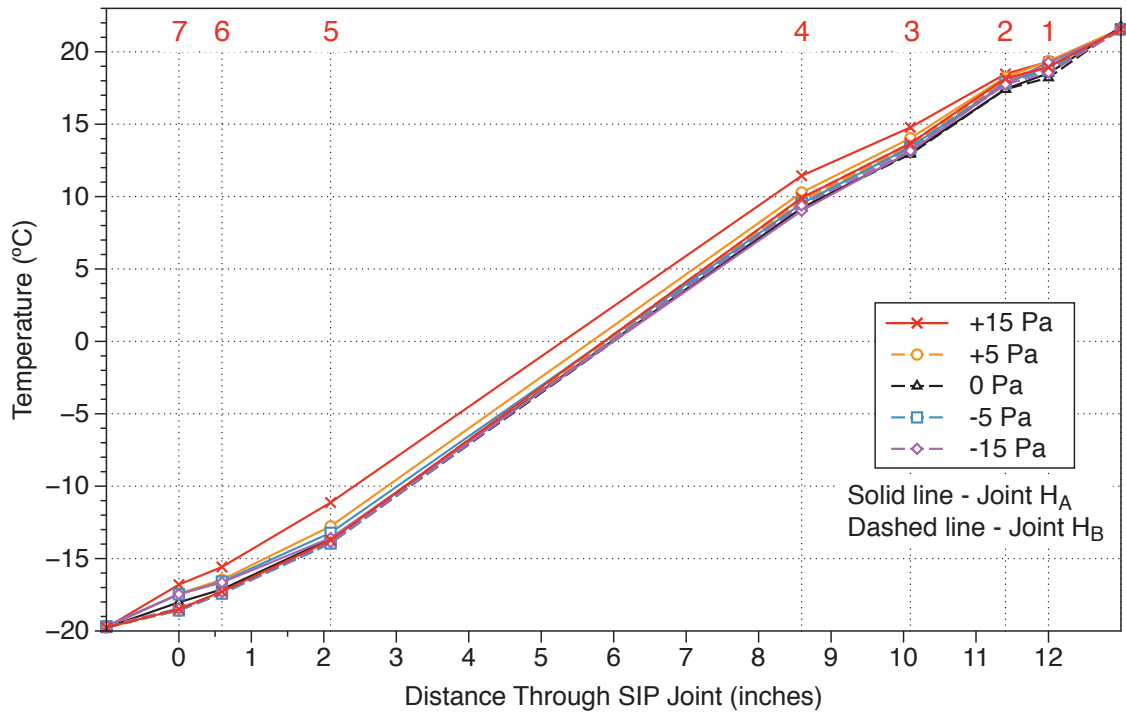
	Sensor	Temperature (°C)		Difference (M_A-M_B)	Percentage Difference
		M_A	M_B		
-20 °C	M1	18.04	16.48	1.56	3.71
	M2	16.89	15.92	0.97	2.31
	M3	10.27	6.96	3.31	7.88
	M4	1.73	-4.29	6.02	14.34
	M5	-13.01	-15.72	2.71	6.45
	M6	-16.17	-17.15	0.98	2.34
-40 °C	M1	15.88	16.26	-0.39	-0.62
	M2	14.17	15.79	-1.63	-2.62
	M3	2.26	6.31	-4.05	-6.54
	M4	-17.76	-5.23	-12.53	-20.21
	M5	-29.73	-28.86	-0.87	-1.40
	M6	-31.88	-33.69	1.80	2.91



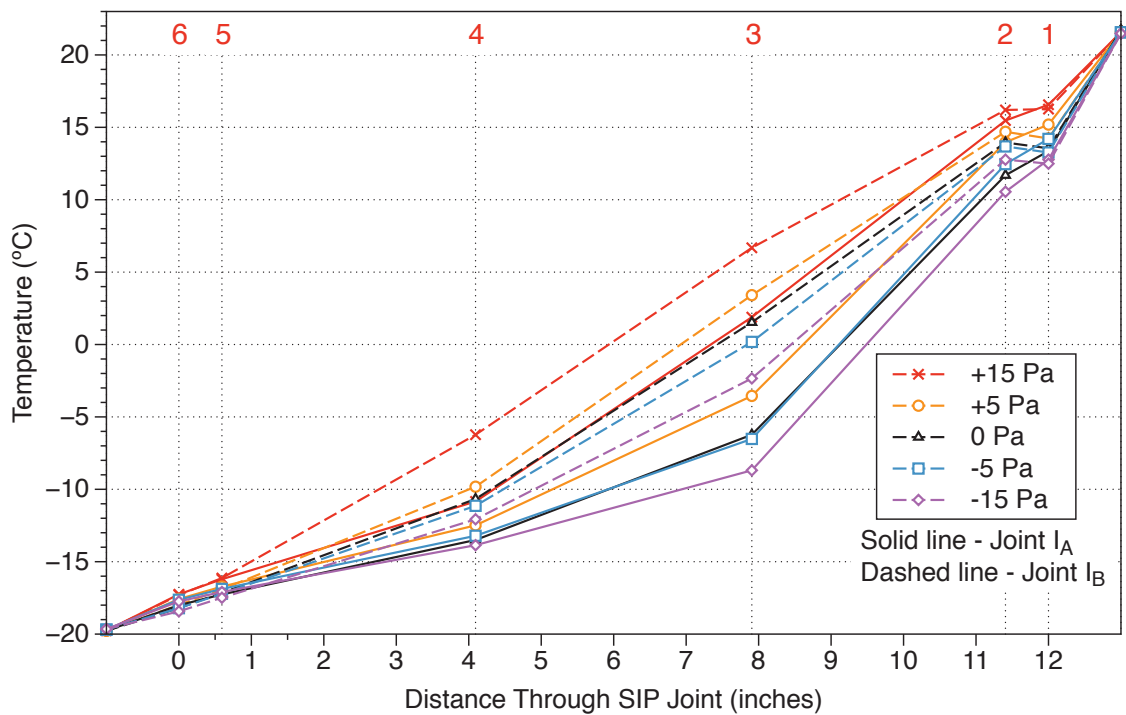
Temperature profile of joint F with -20 °C exterior temperature with tape seal



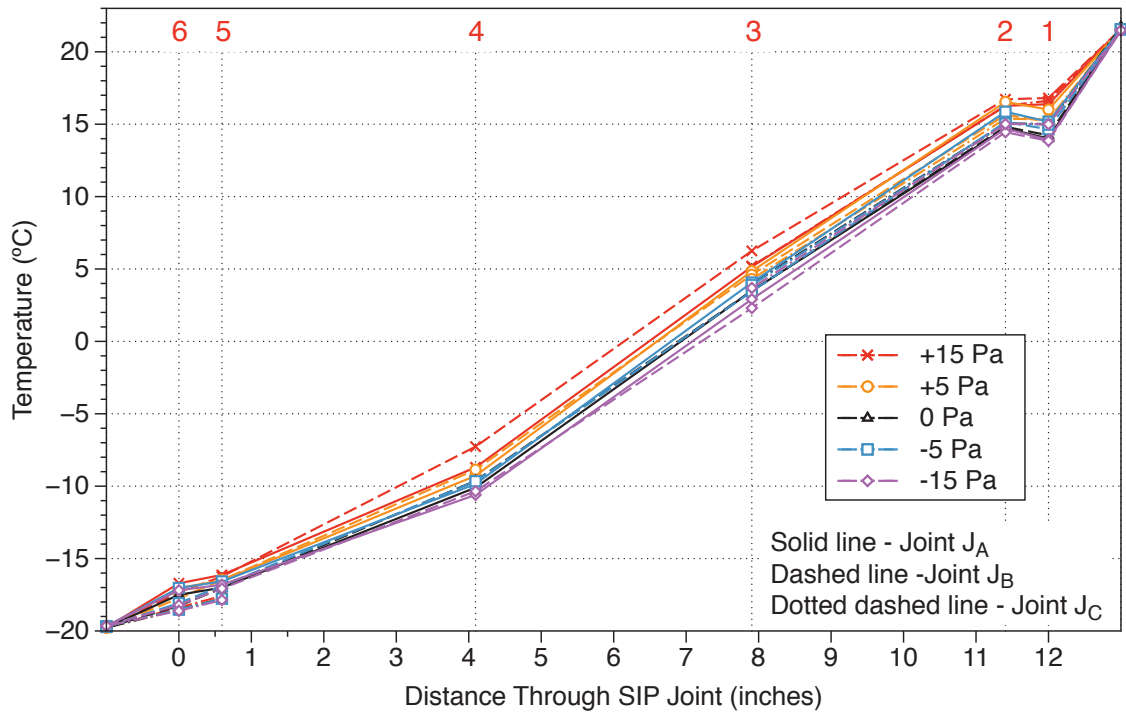
Temperature profile of joint G with -20 °C exterior temperature with tape seal



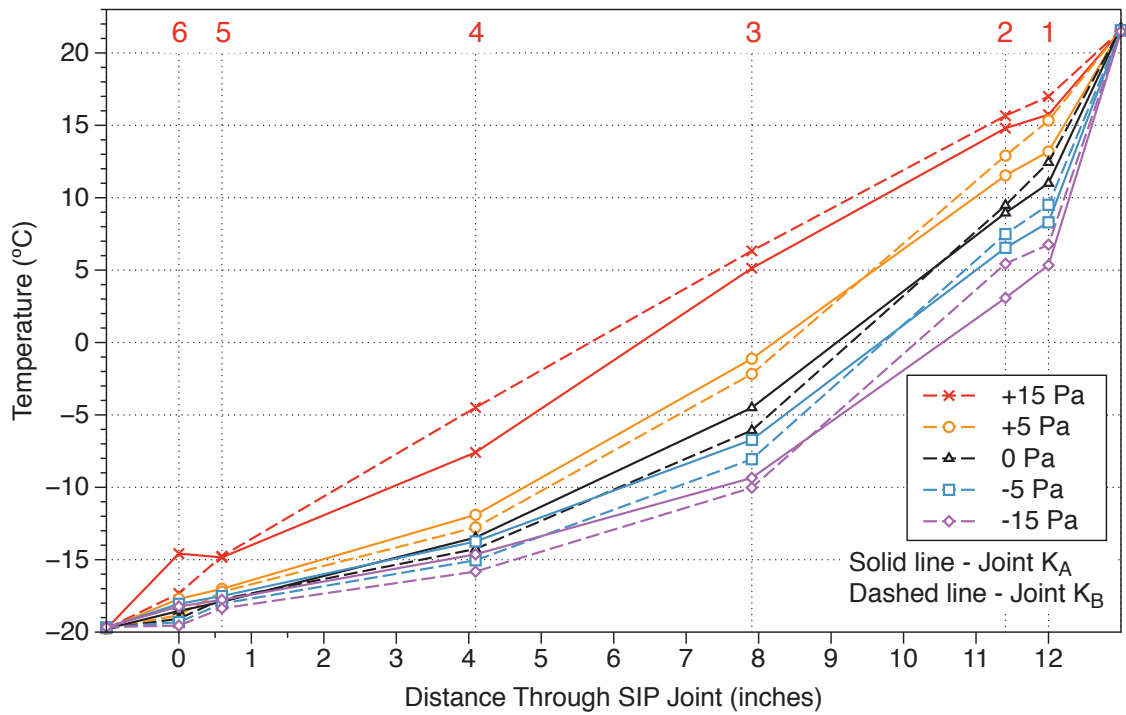
Temperature profile of joint H with -20 °C exterior temperature with tape seal



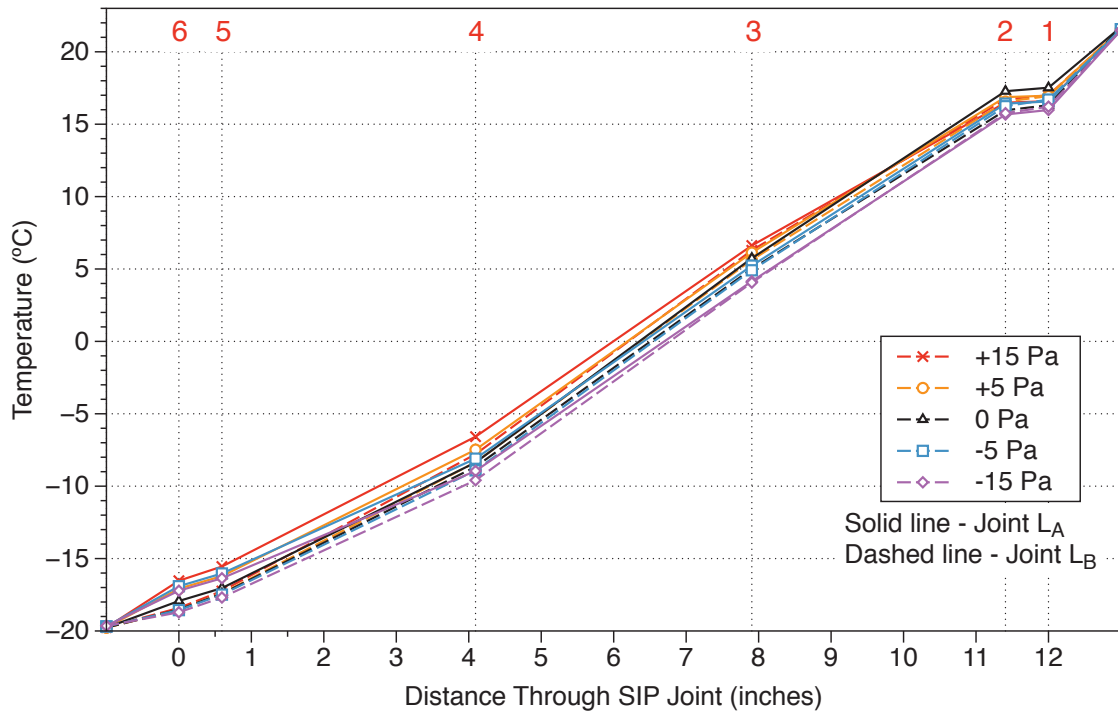
Temperature profile of joint I with -20 °C exterior temperature with tape seal



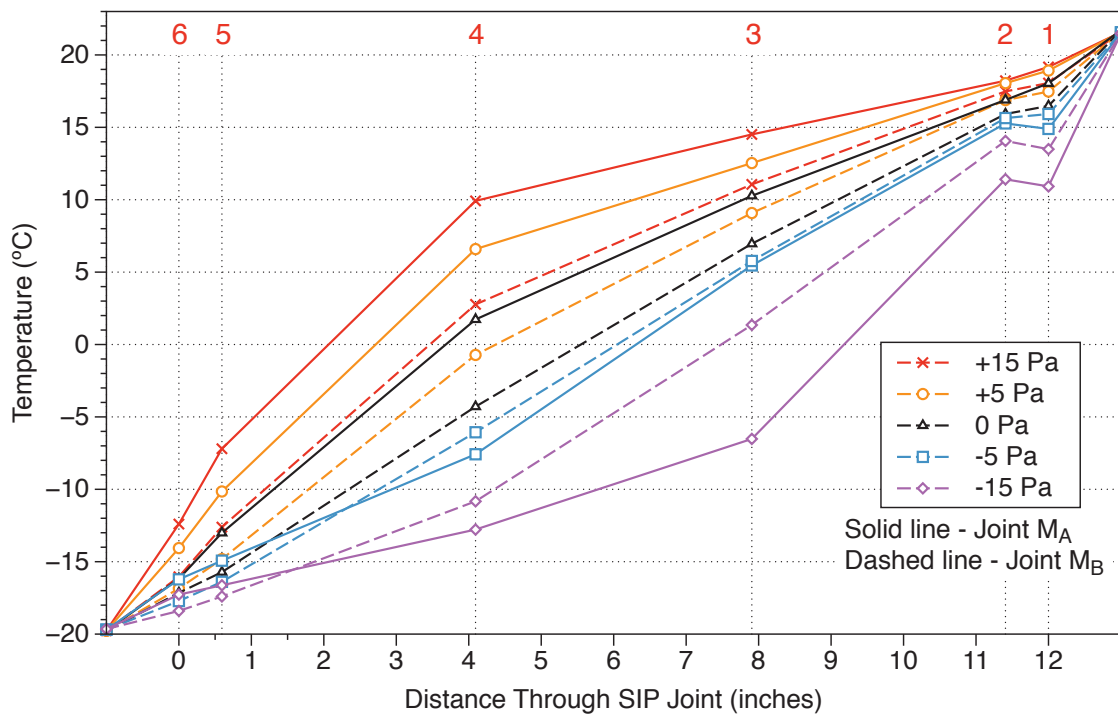
Temperature profile of joint J with -20 °C exterior temperature with tape seal



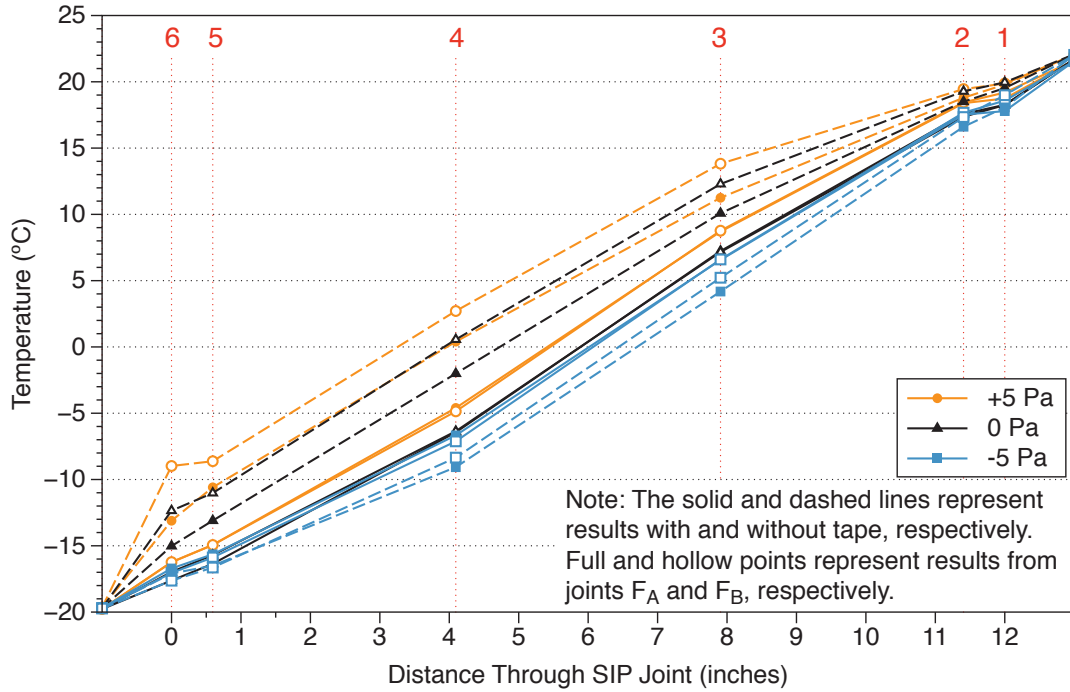
Temperature profile of joint K with -20 °C exterior temperature with tape seal



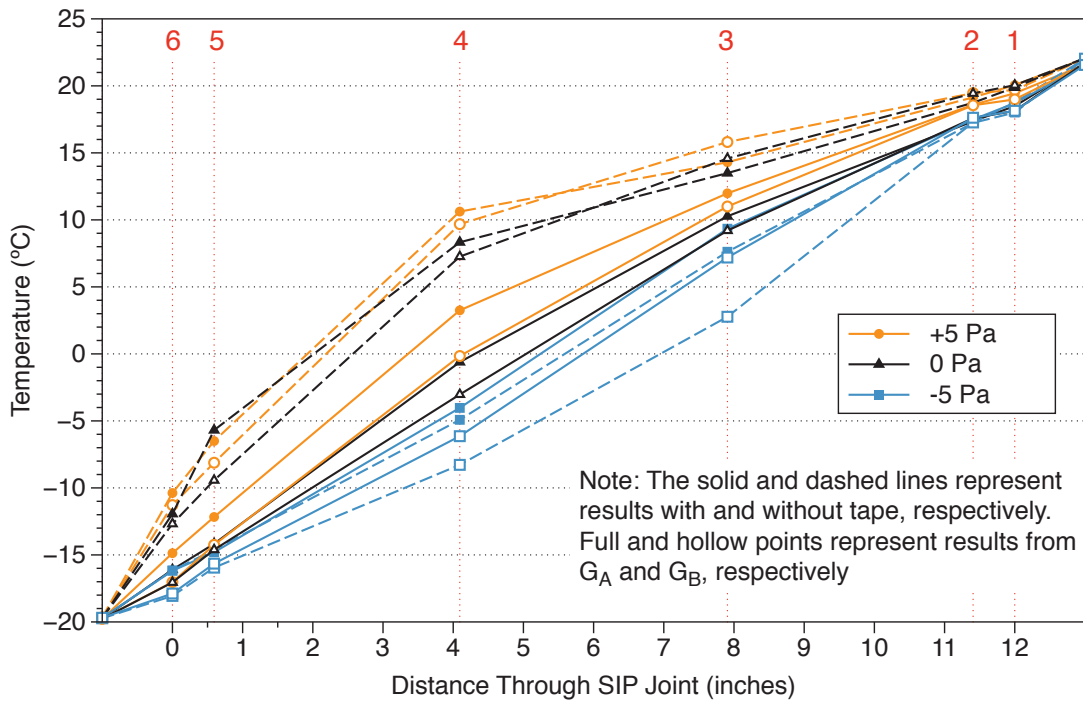
Temperature profile of joint L with -20 °C exterior temperature with tape seal



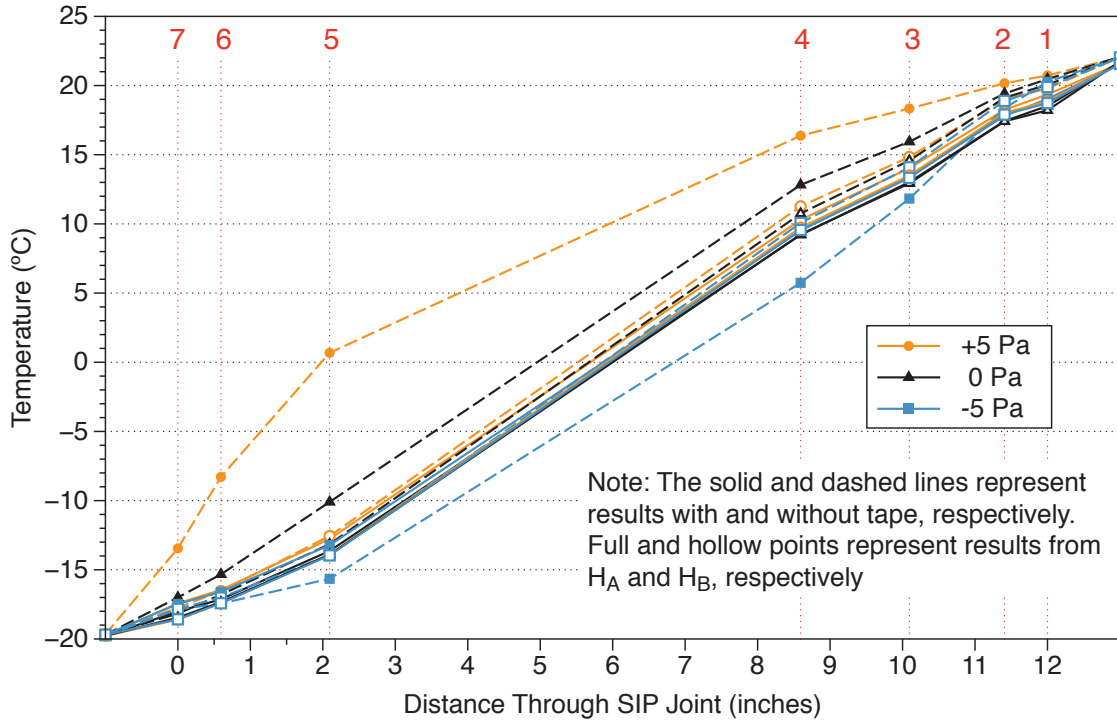
Temperature profile of joint M with -20 °C exterior temperature with tape seal



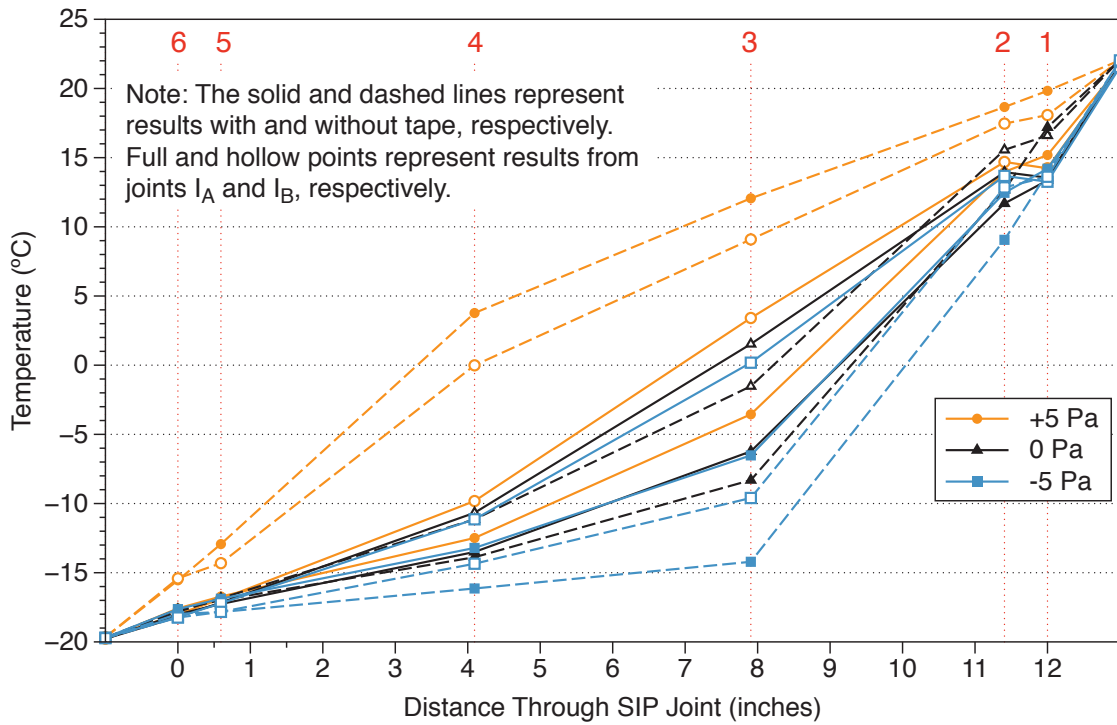
Temperature profile of joint F with -20 °C exterior temperature with and without tape seal



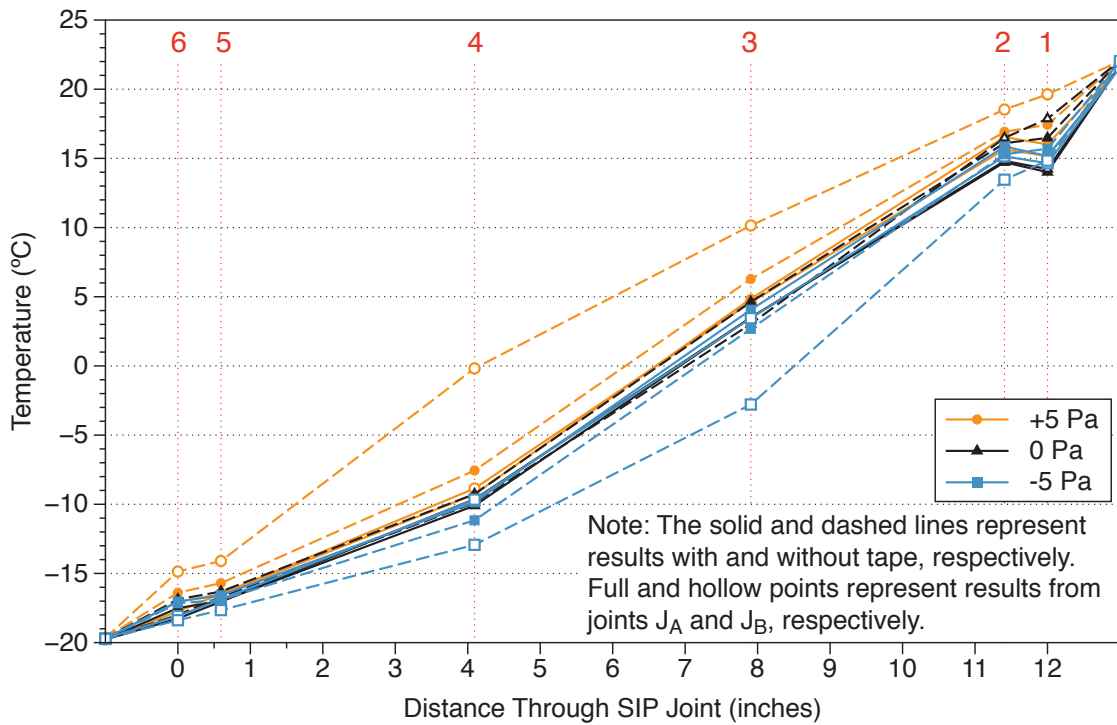
Temperature profile of joint G with -20 °C exterior temperature with and without tape seal



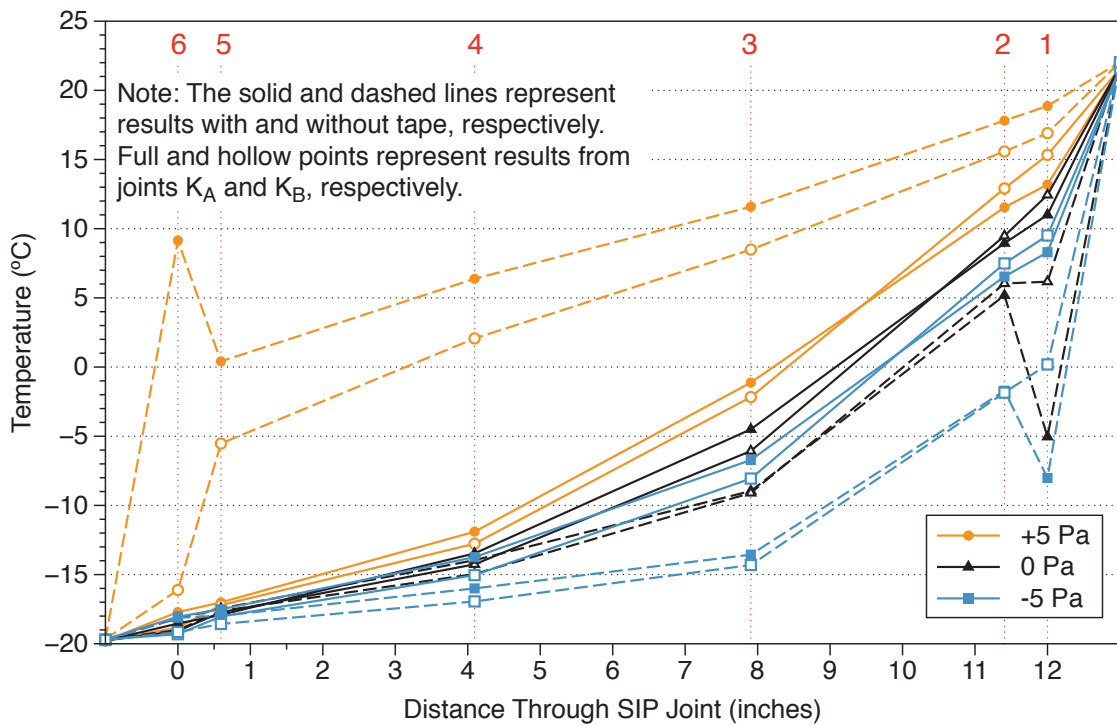
Temperature profile of joint H with $-20\text{ }^\circ\text{C}$ exterior temperature with and without tape seal



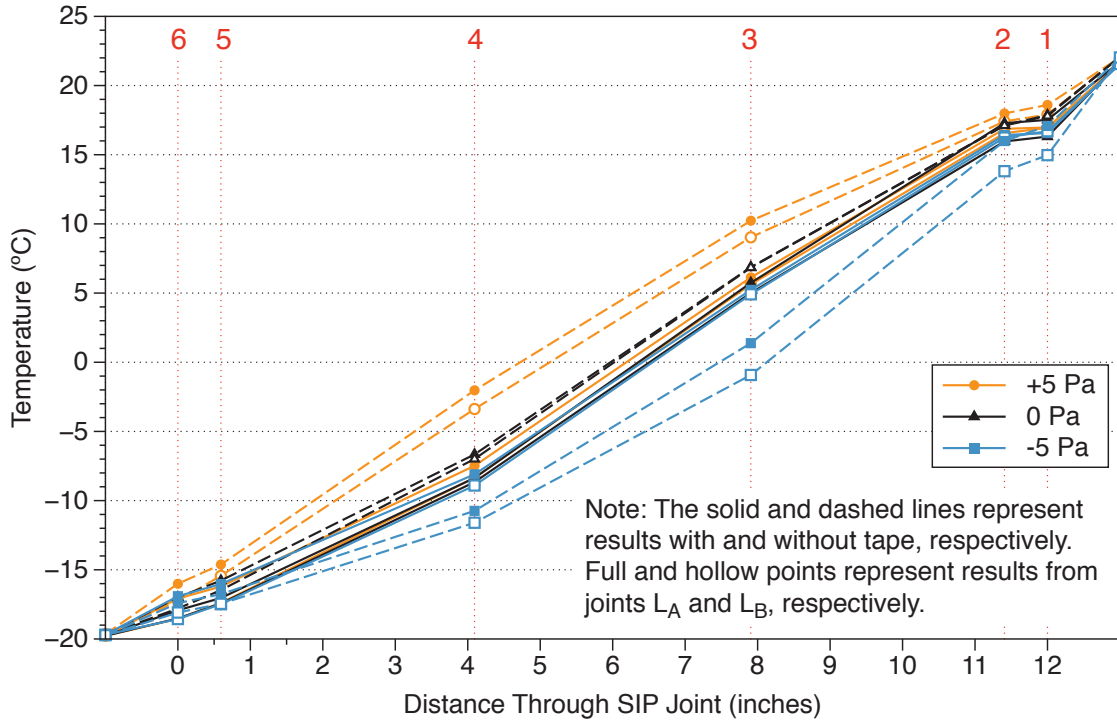
Temperature profile of joint I with $-20\text{ }^\circ\text{C}$ exterior temperature with and without tape seal



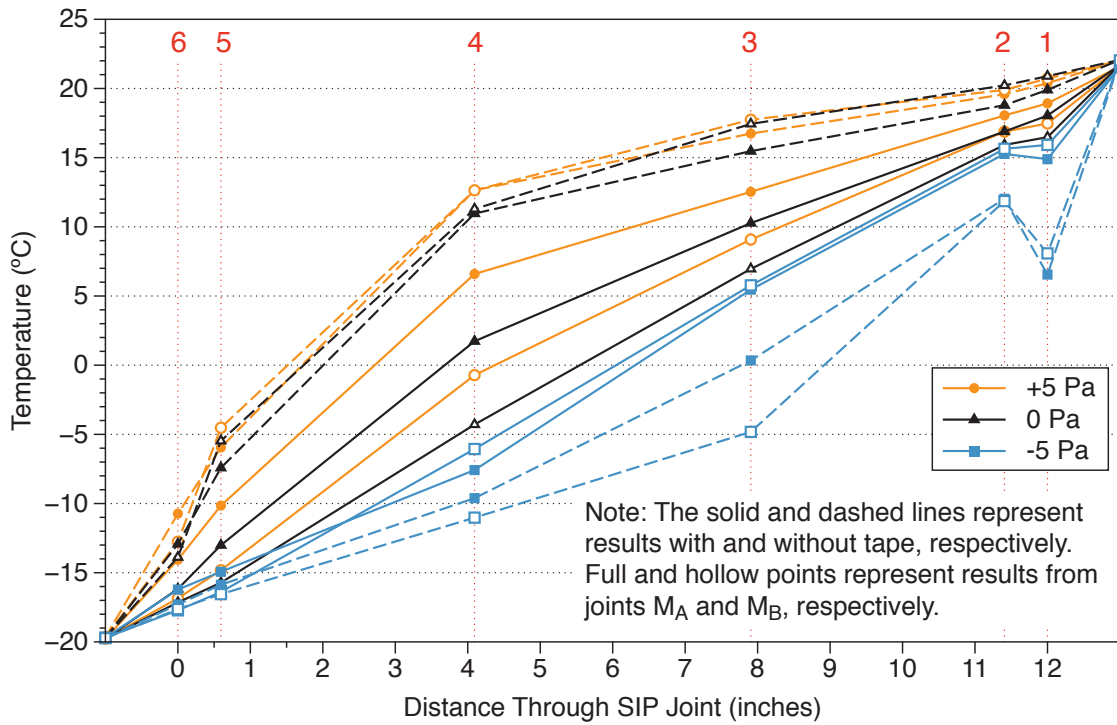
Temperature profile of joint J with -20 °C exterior temperature with and without tape seal



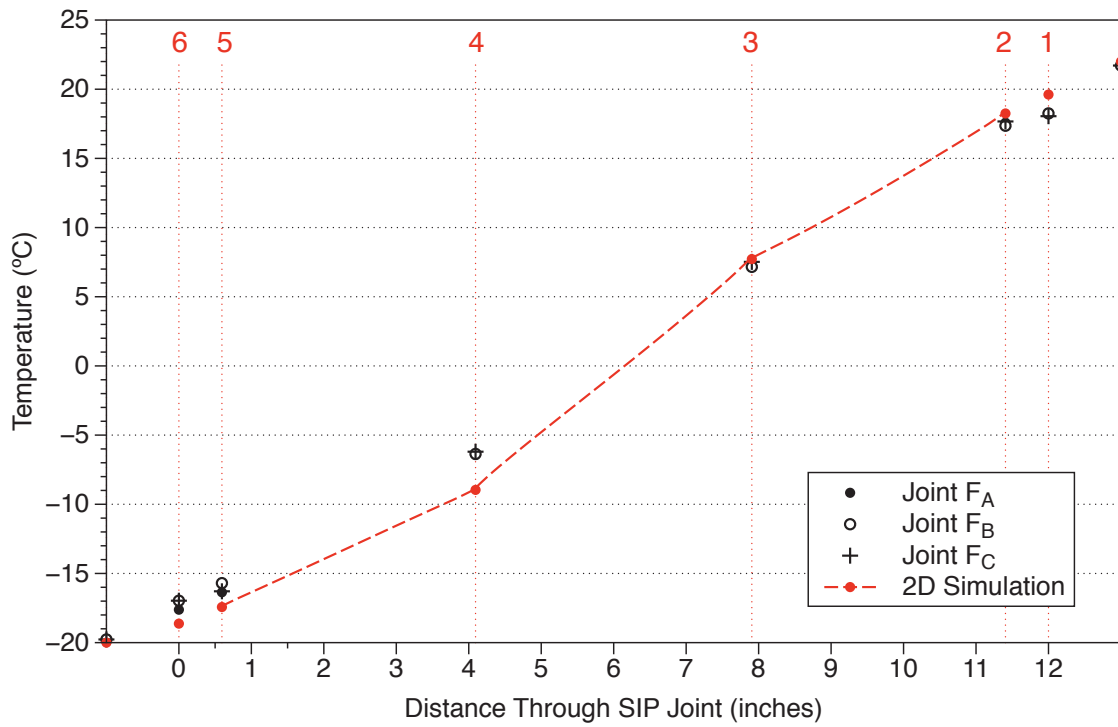
Temperature profile of joint K with -20 °C exterior temperature with and without tape seal



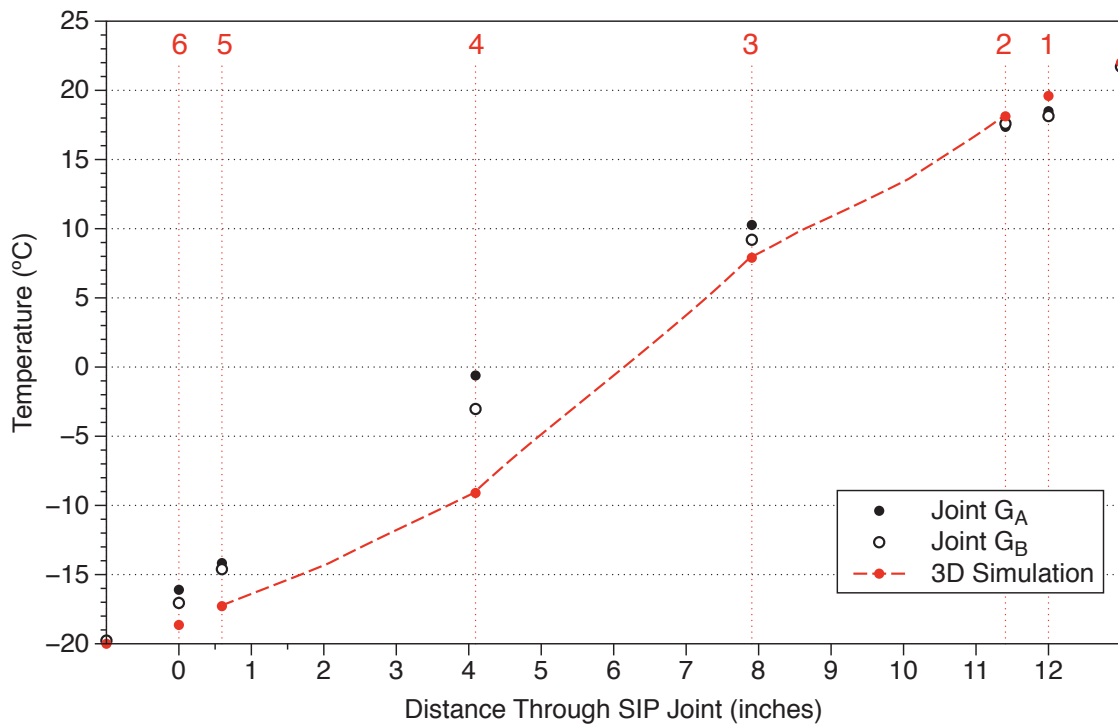
Temperature profile of joint L with -20 °C exterior temperature with and without tape seal



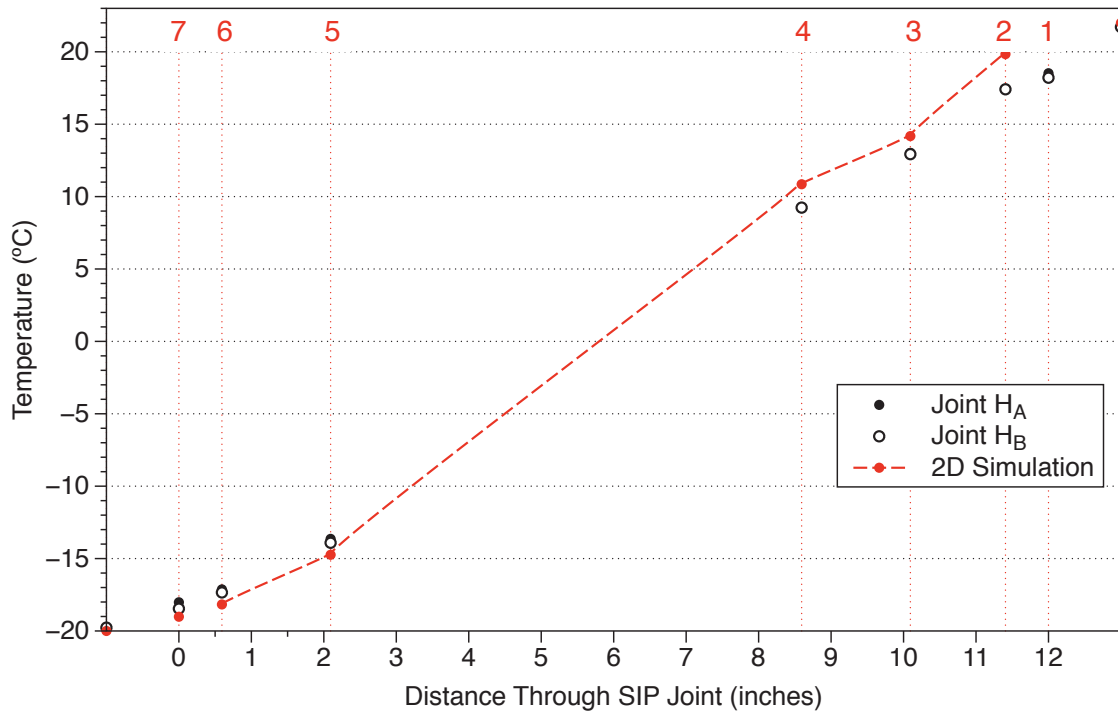
Temperature profile of joint M with -20 °C exterior temperature with and without tape seal



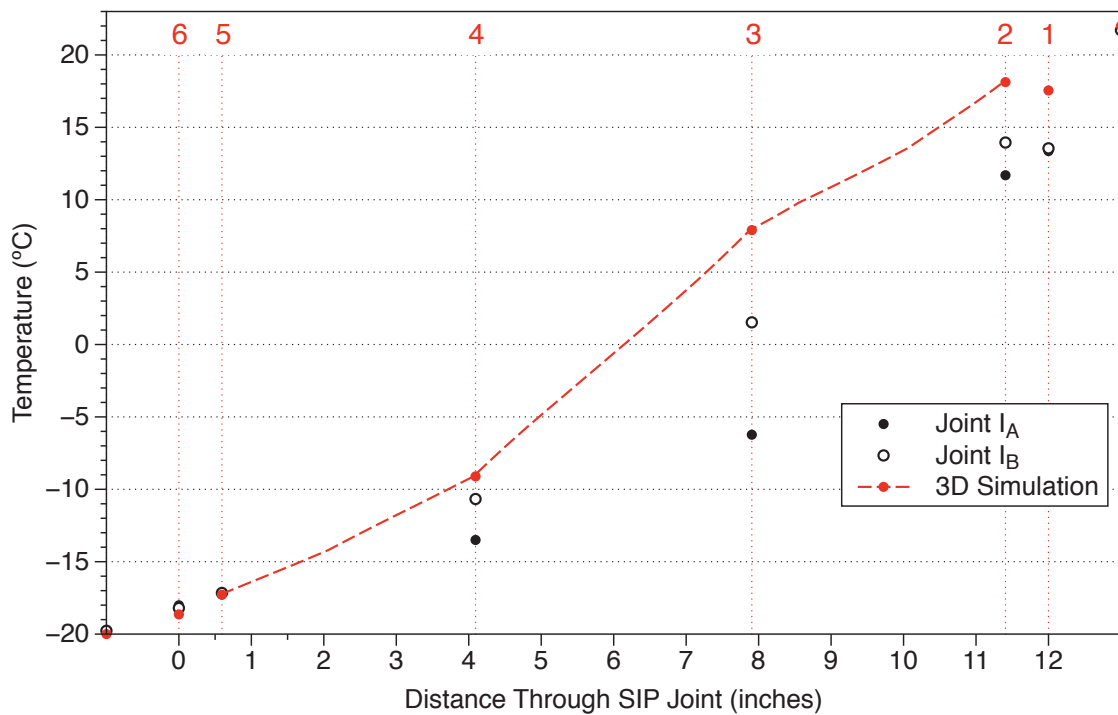
Temperature profile of joint F with values obtained from 2D simulation



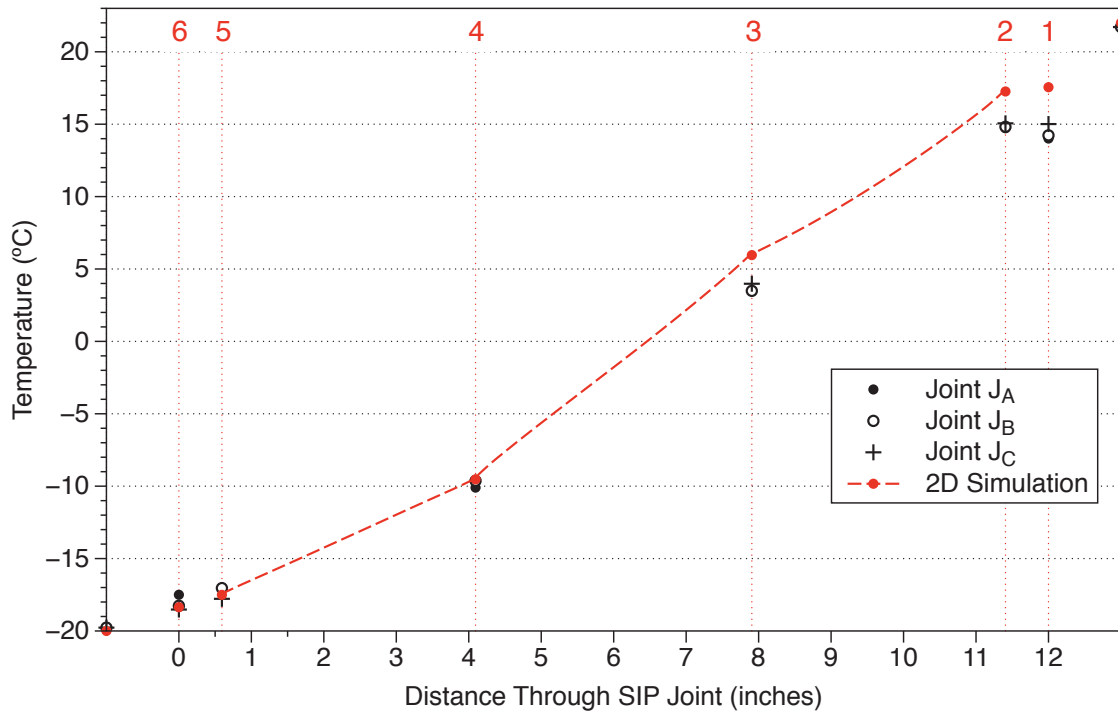
Temperature profile of joint G with values obtained from 3D simulation



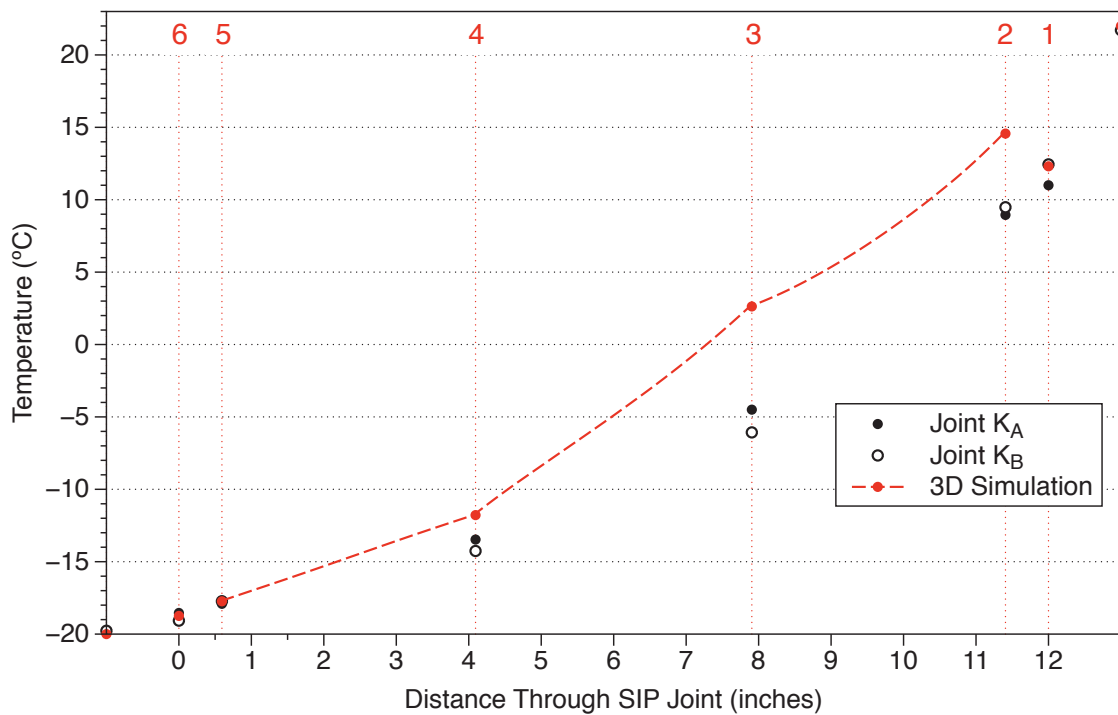
Temperature profile of joint H with values obtained from 2D simulation



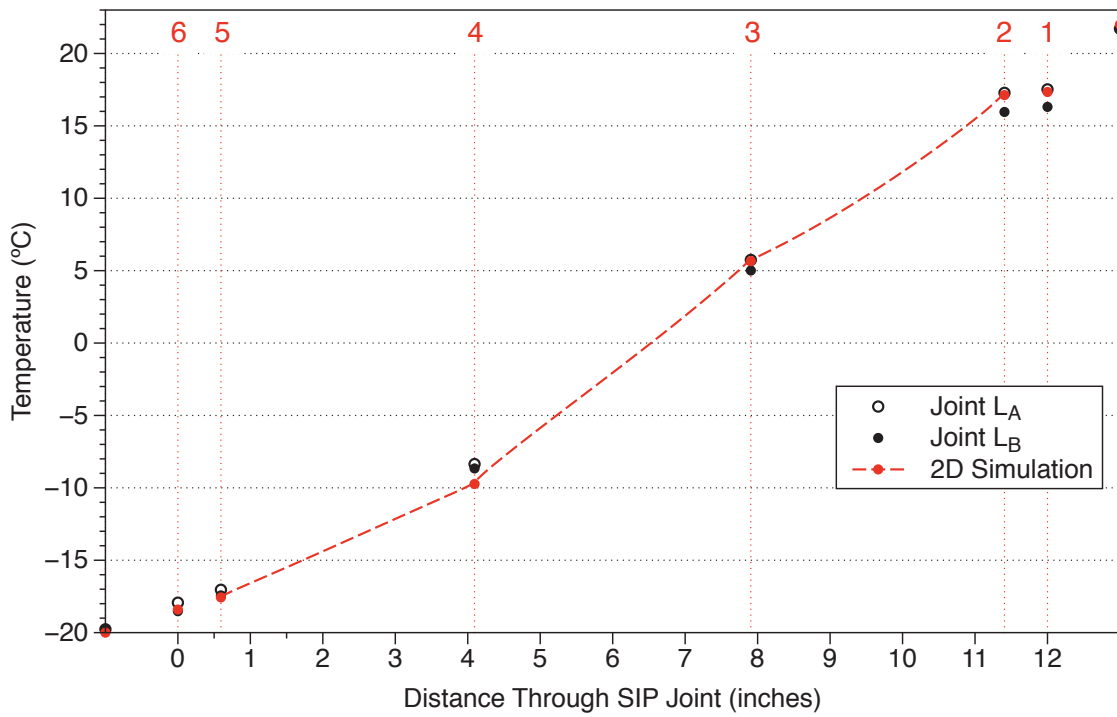
Temperature profile of joint I with values obtained from 3D simulation



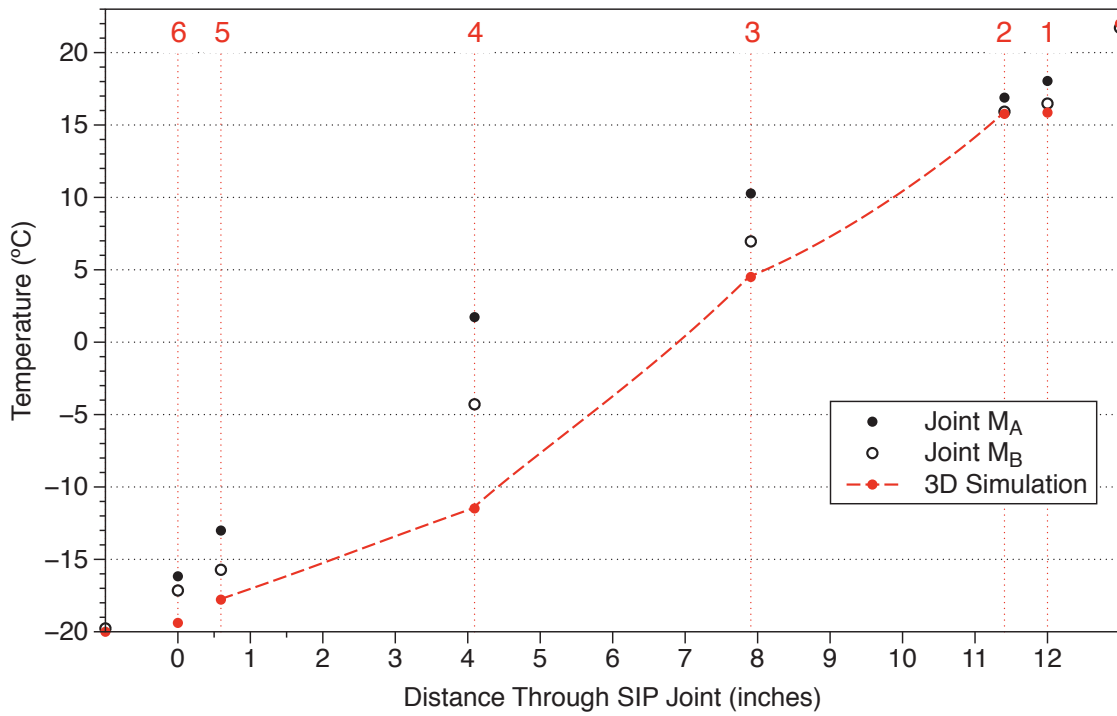
Temperature profile of joint J with values obtained from 2D simulation



Temperature profile of joint K with values obtained from 3D simulation

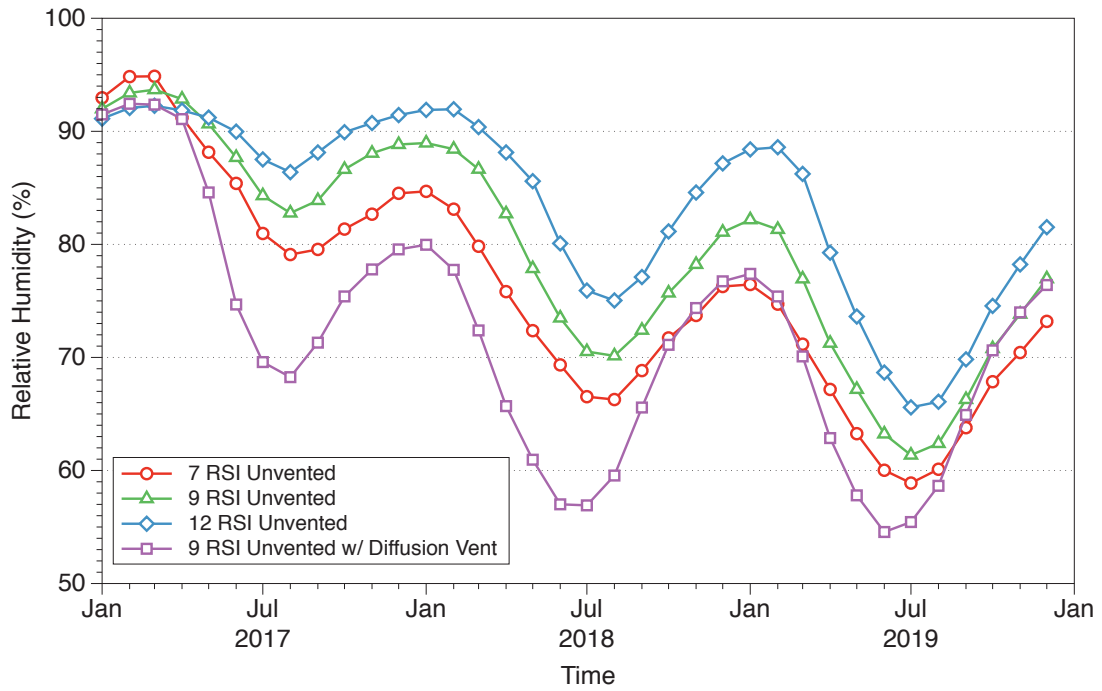


Temperature profile of joint L with values obtained from 2D simulation

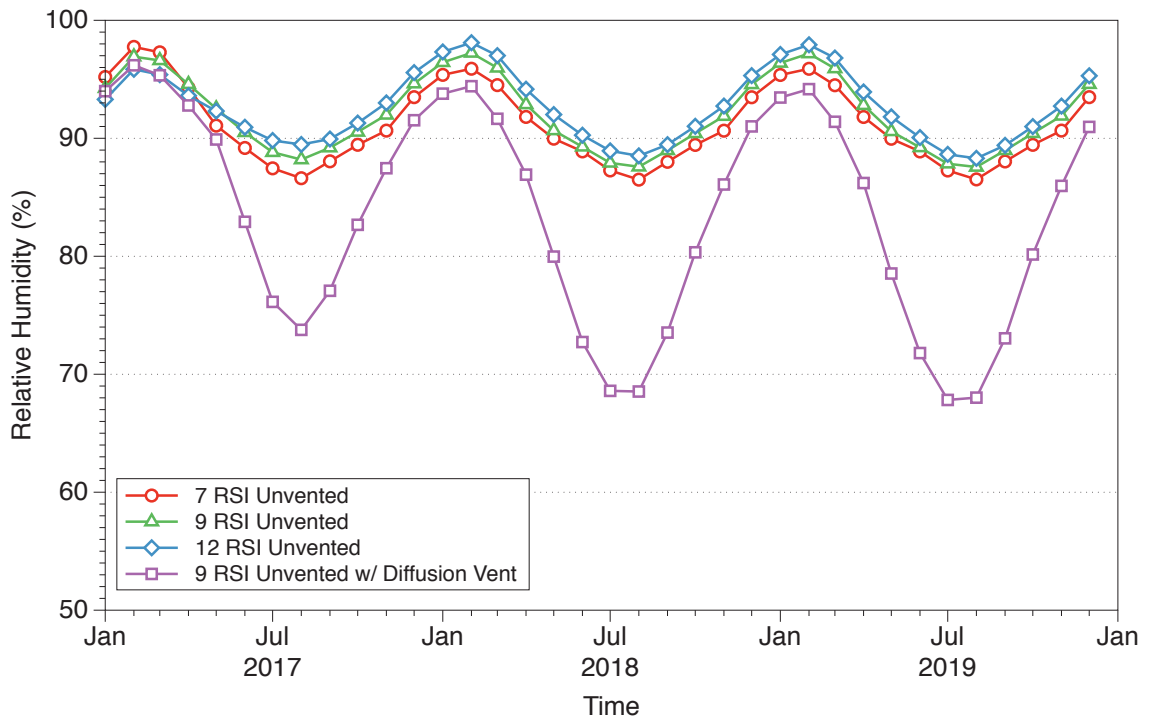


Temperature profile of joint M with values obtained from 3D simulation

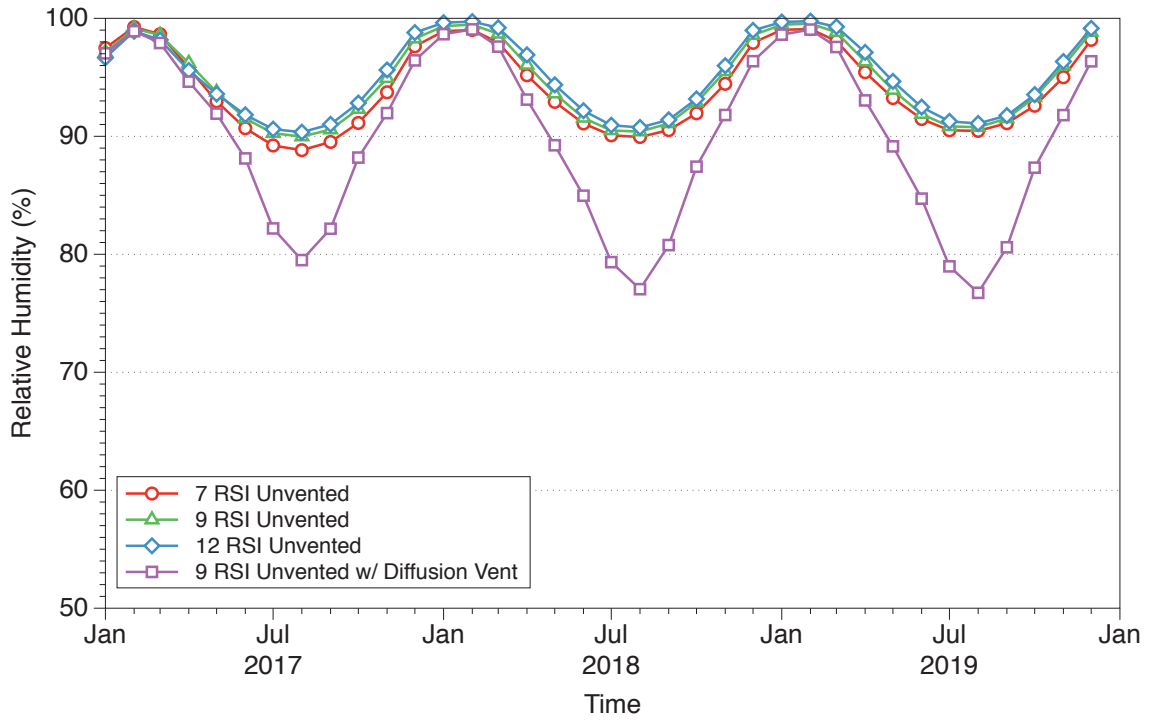
Appendix B Complete Attic Simulation Results



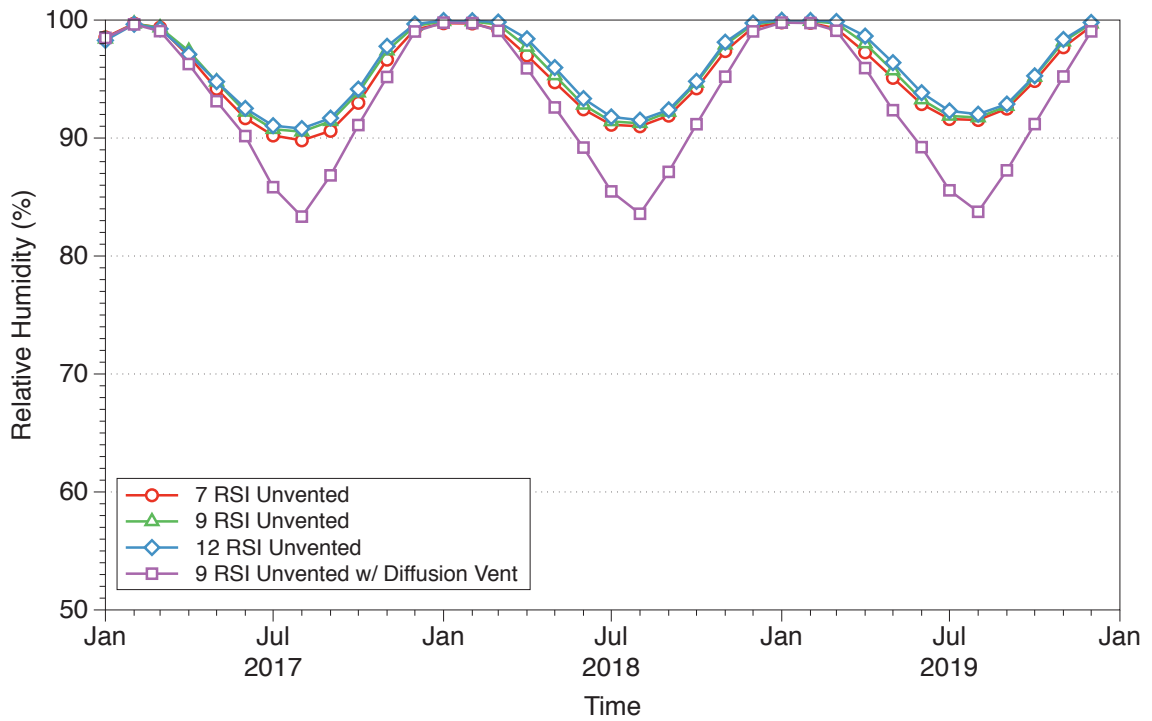
Relative humidity in unvented attics with no air leakage in Iqaluit



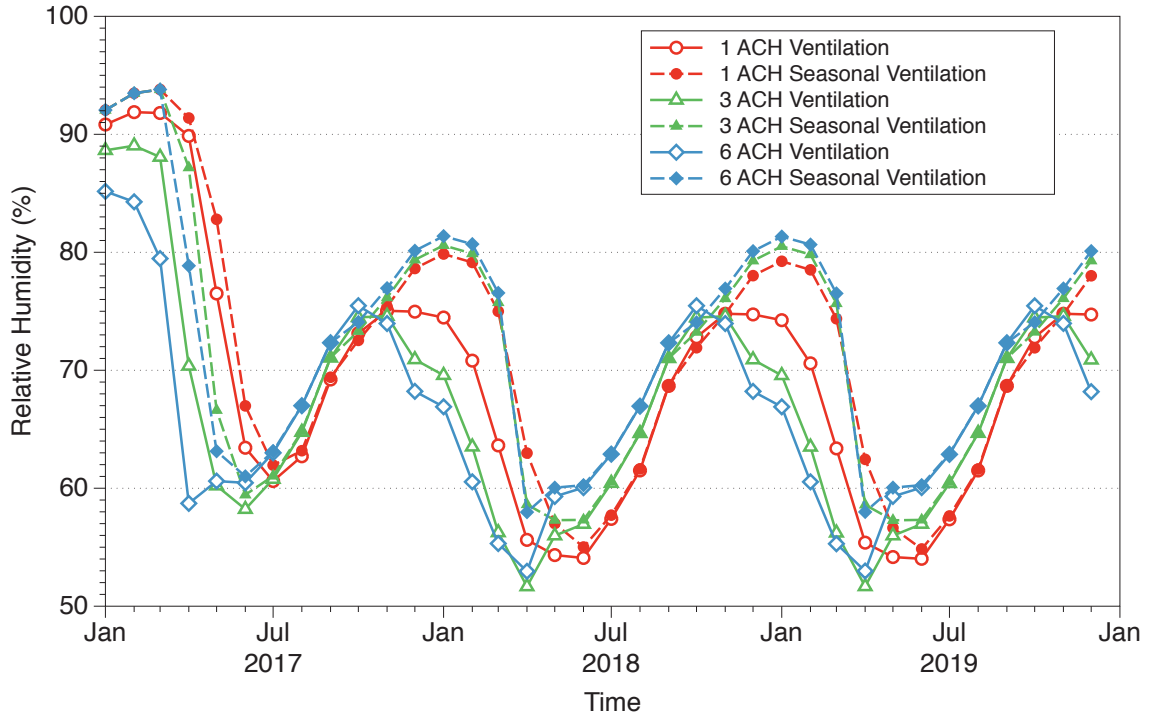
Relative humidity in unvented attics with low air leakage in Iqaluit



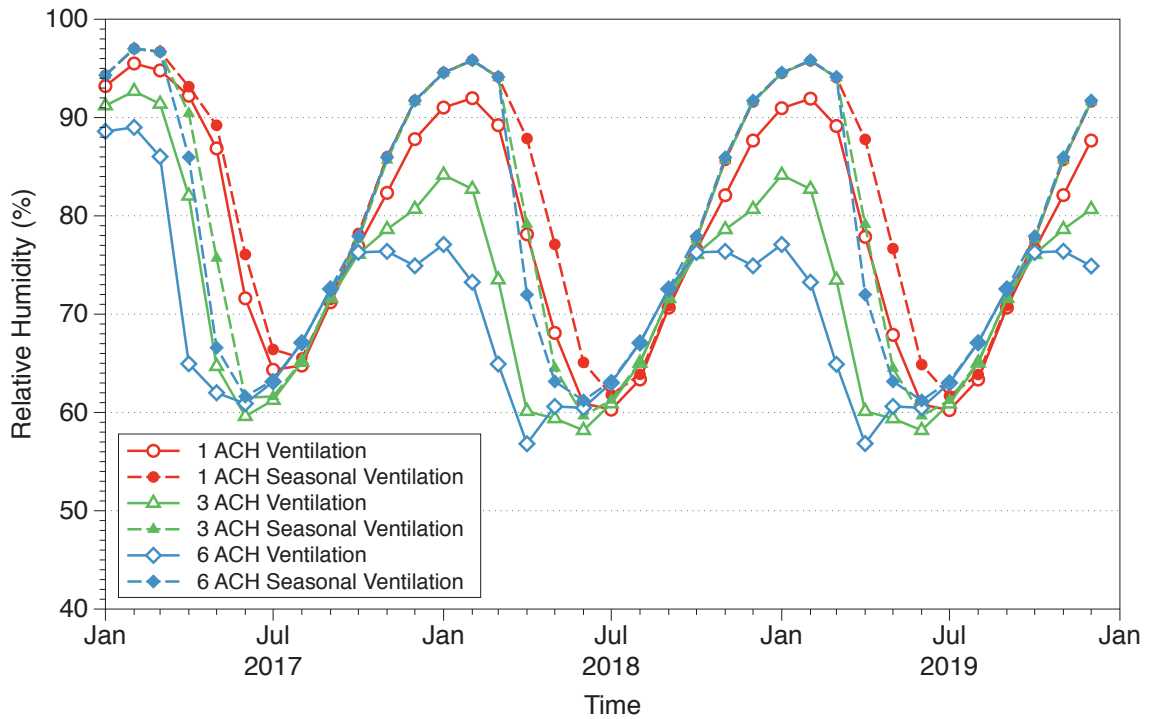
Relative humidity in unvented attics with medium air leakage in Iqaluit



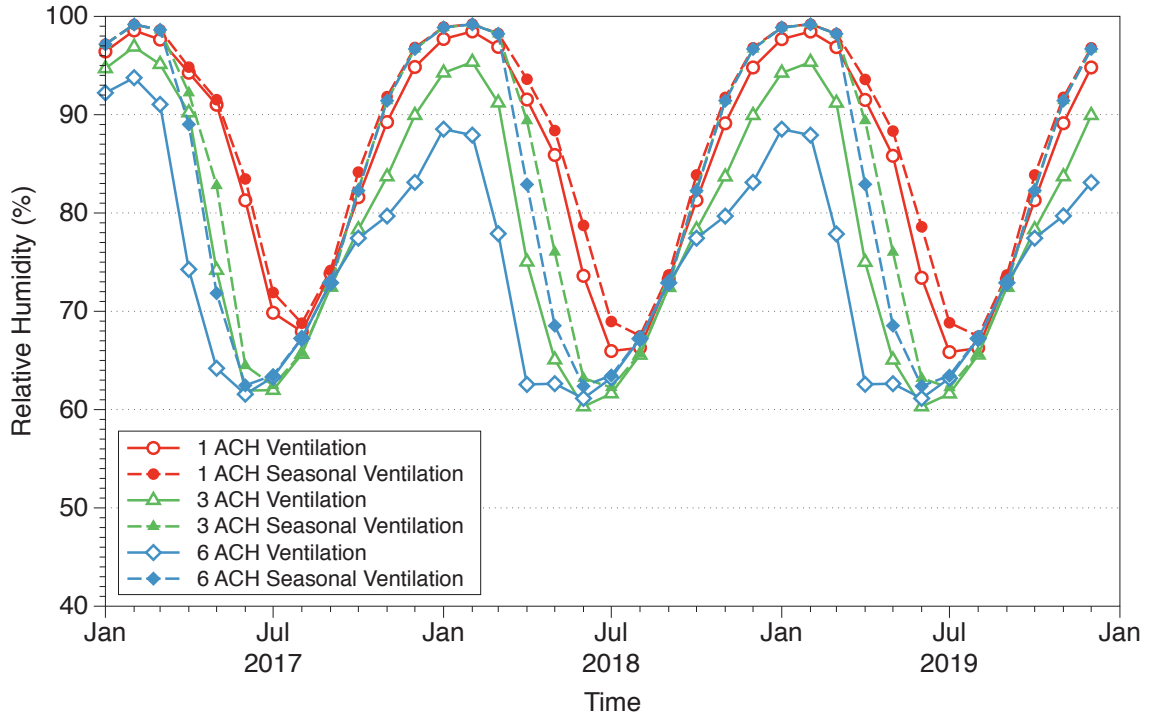
Relative humidity in unvented attics with high air leakage in Iqaluit



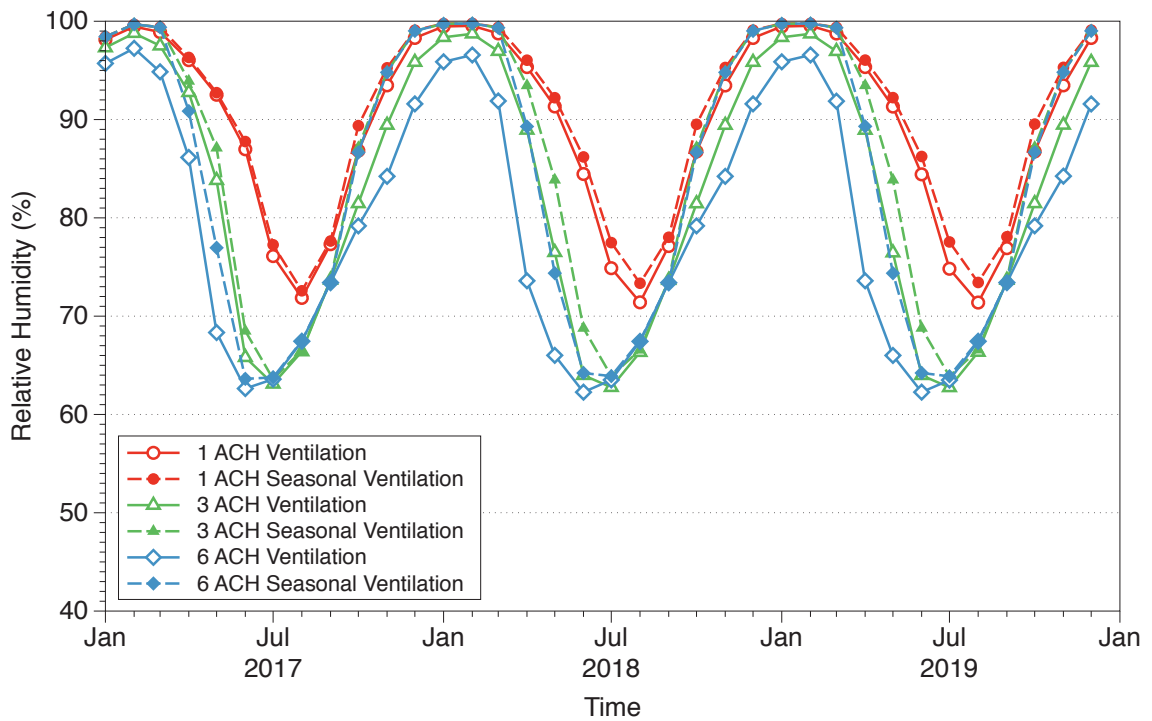
Relative humidity in mechanical ventilated attics with no air leakage in Iqaluit



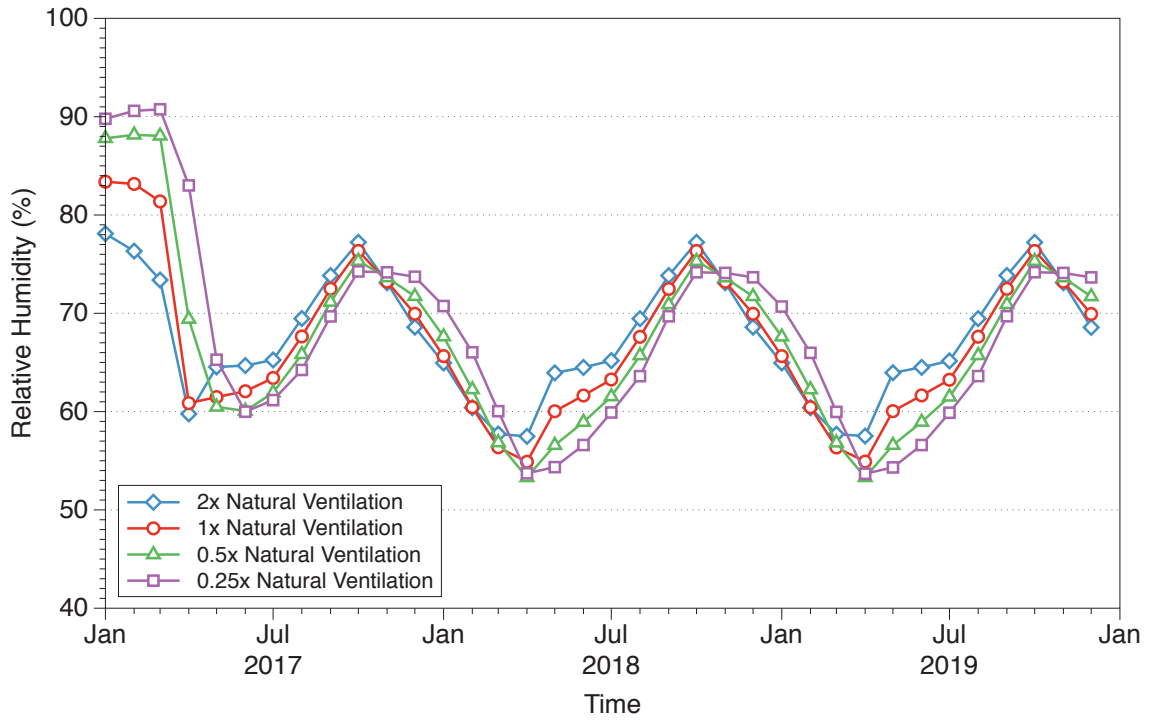
Relative humidity in mechanical ventilated attics with low air leakage in Iqaluit



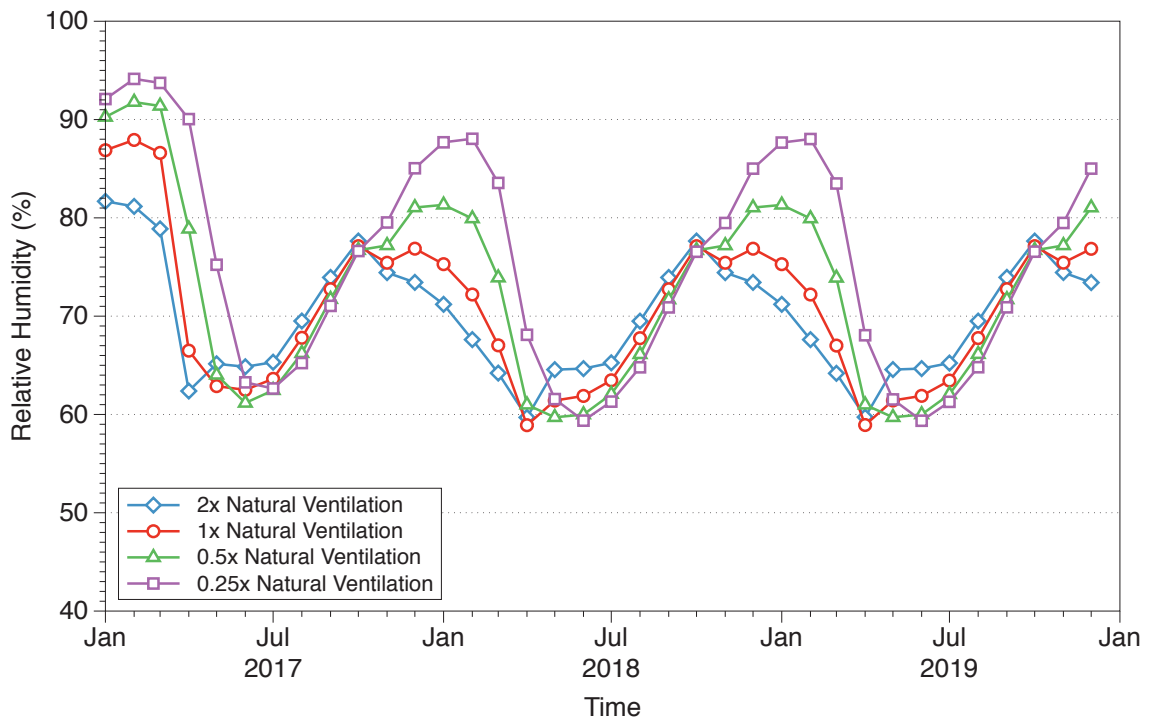
Relative humidity in mechanical ventilated attics with medium air leakage in Iqaluit



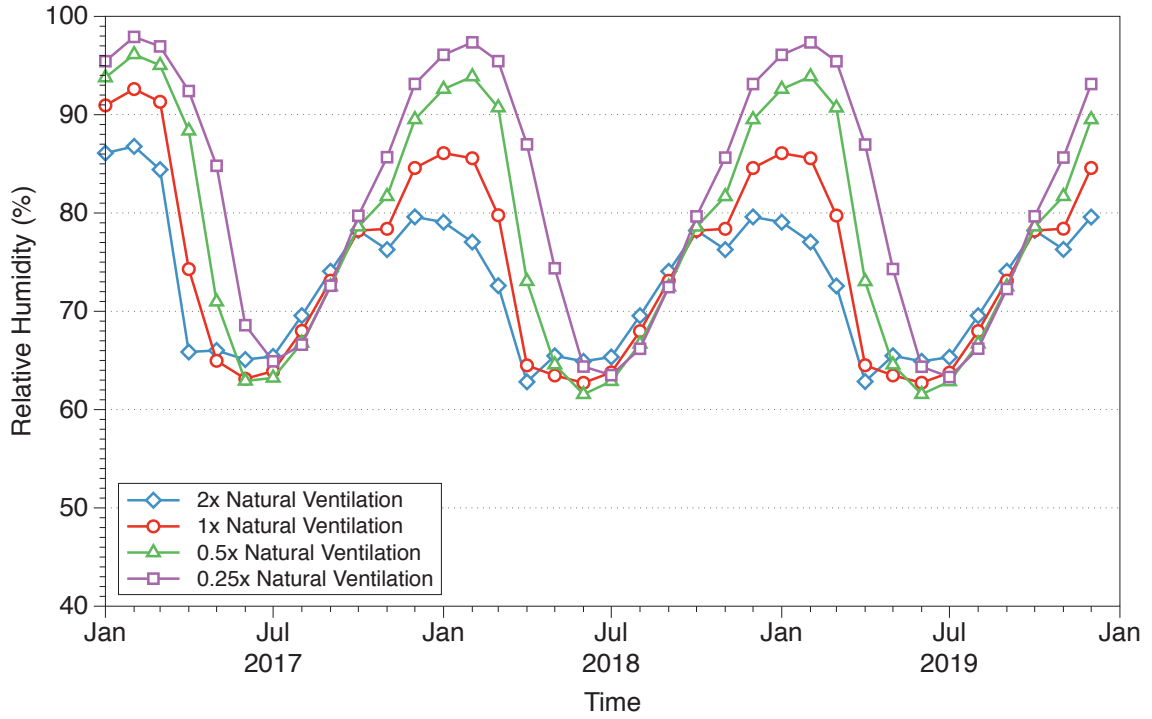
Relative humidity in mechanical ventilated attics with high air leakage in Iqaluit



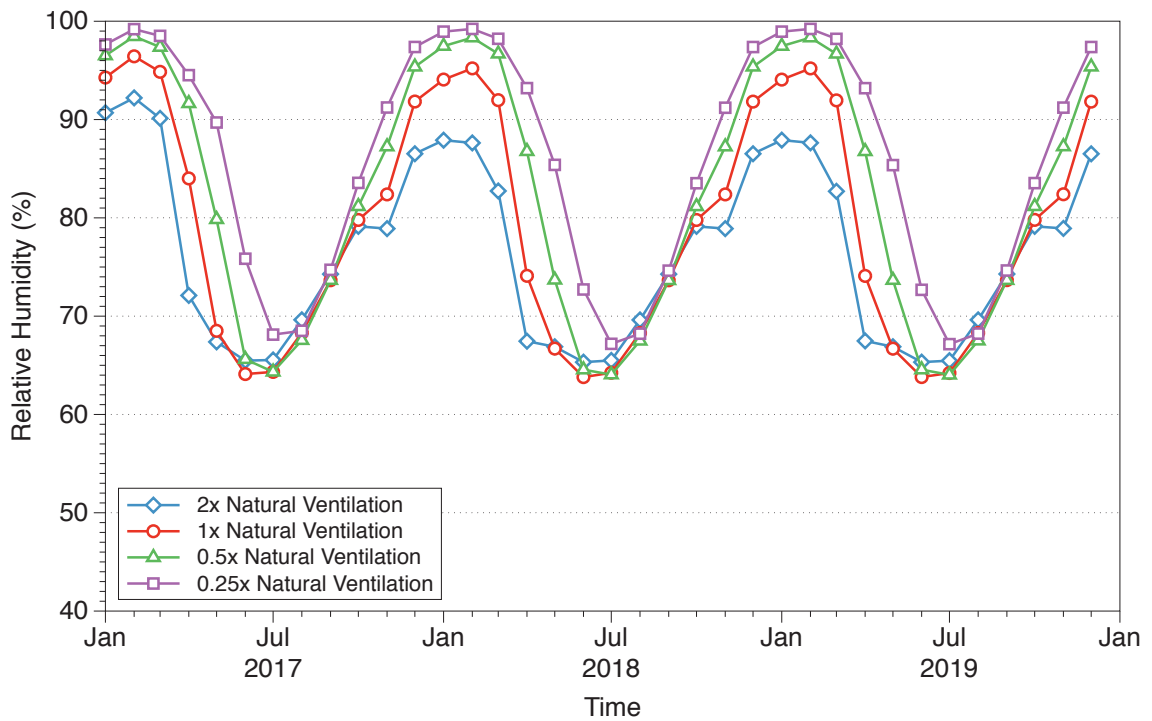
Relative humidity in naturally ventilated attics with no air leakage in Iqaluit



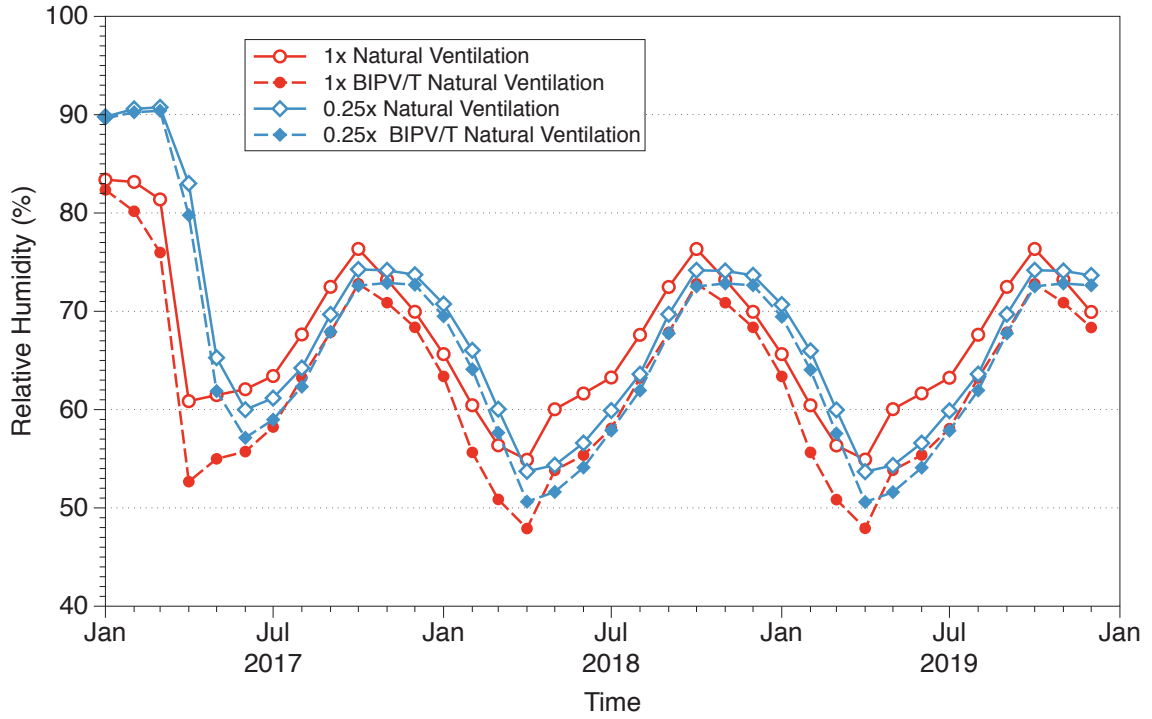
Relative humidity in naturally ventilated attics with low air leakage in Iqaluit



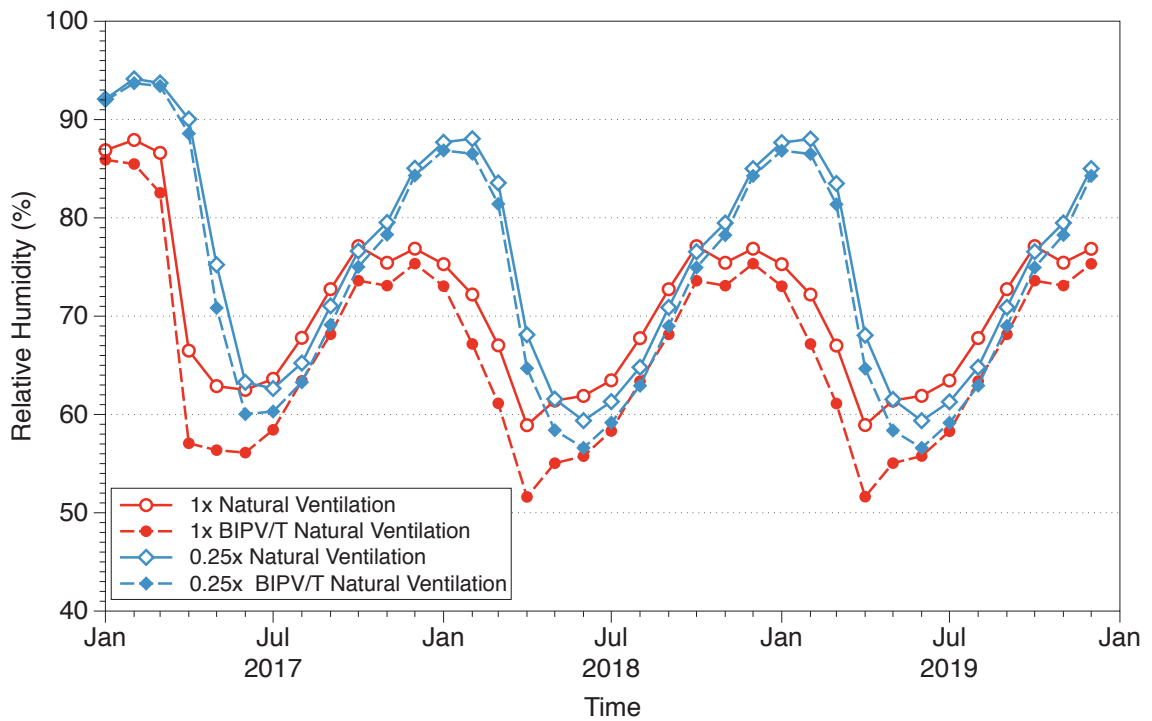
Relative humidity in naturally ventilated attics with medium air leakage in Iqaluit



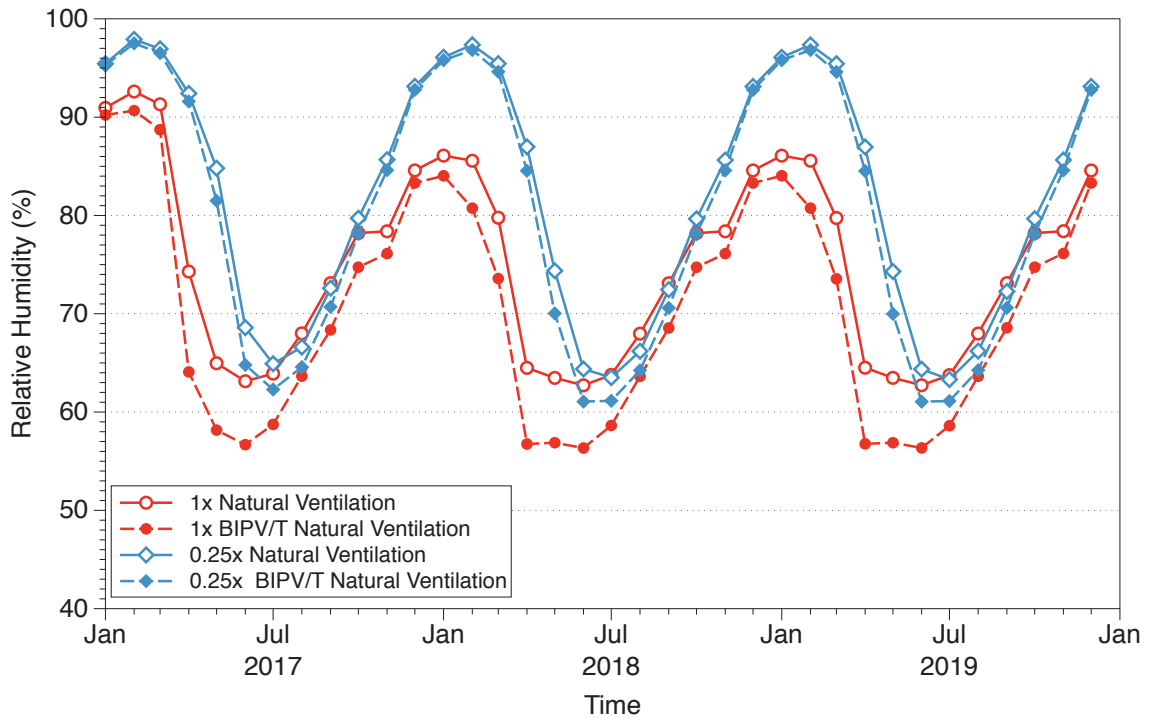
Relative humidity in naturally ventilated attics with high air leakage in Iqaluit



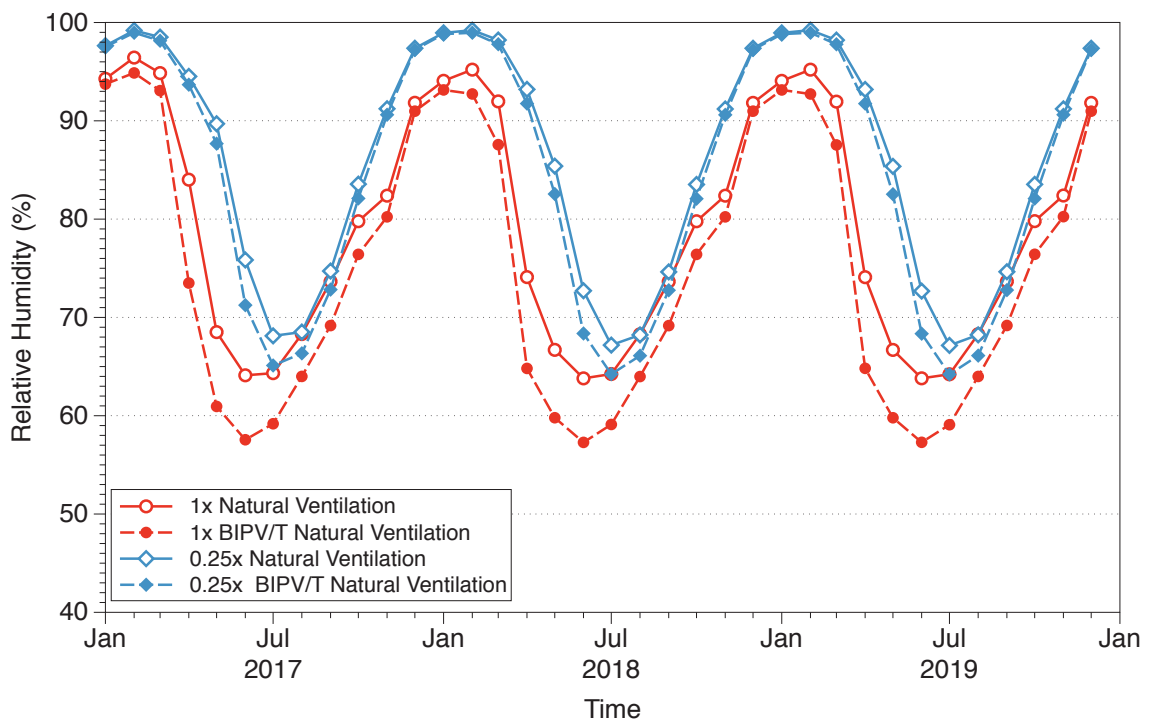
Relative humidity in BIPV/T naturally ventilated attics with no air leakage in Iqaluit



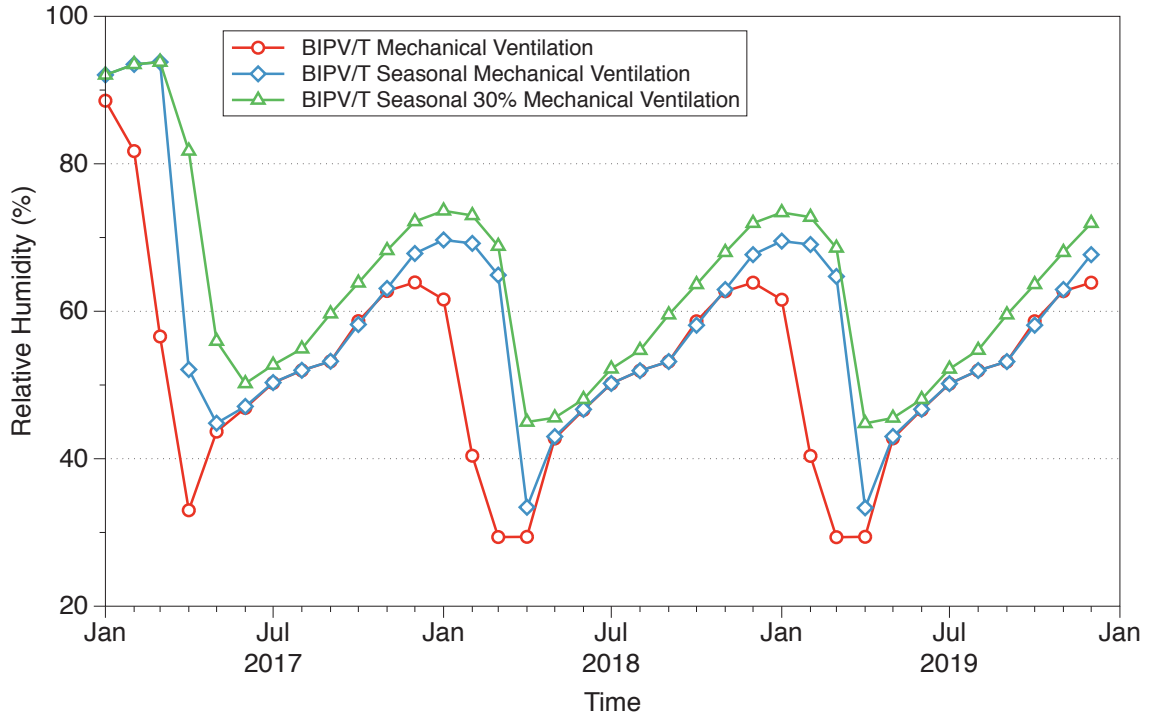
Relative humidity in BIPV/T naturally ventilated attics with low air leakage in Iqaluit



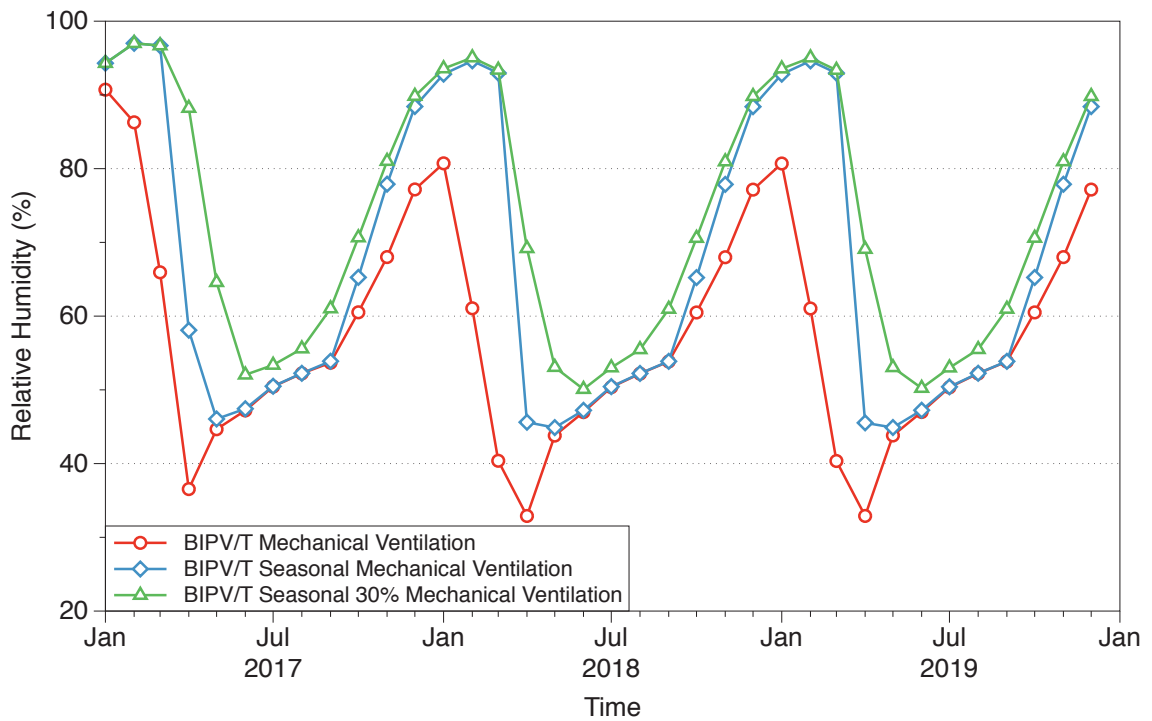
Relative humidity in BIPV/T naturally ventilated attics with medium air leakage in Iqaluit



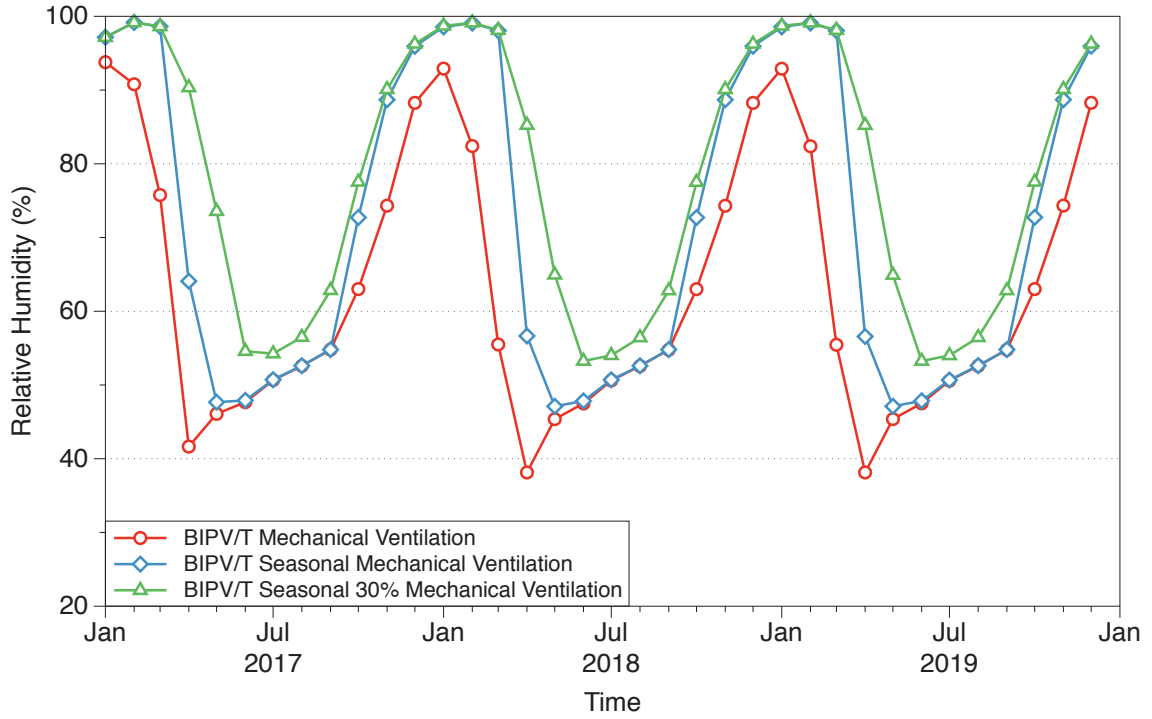
Relative humidity in BIPV/T naturally ventilated attics with high air leakage in Iqaluit



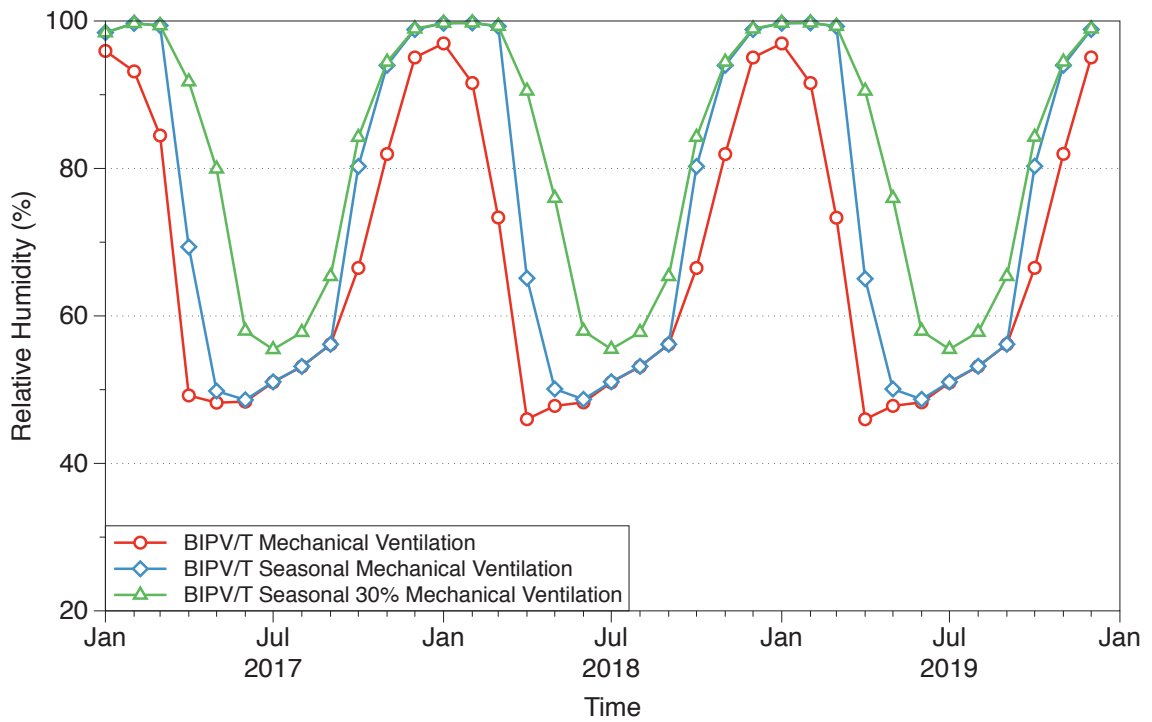
Relative humidity in BIPV/T mechanically ventilated attics with no air leakage in Iqaluit



Relative humidity in BIPV/T mechanically ventilated attics with low air leakage in Iqaluit



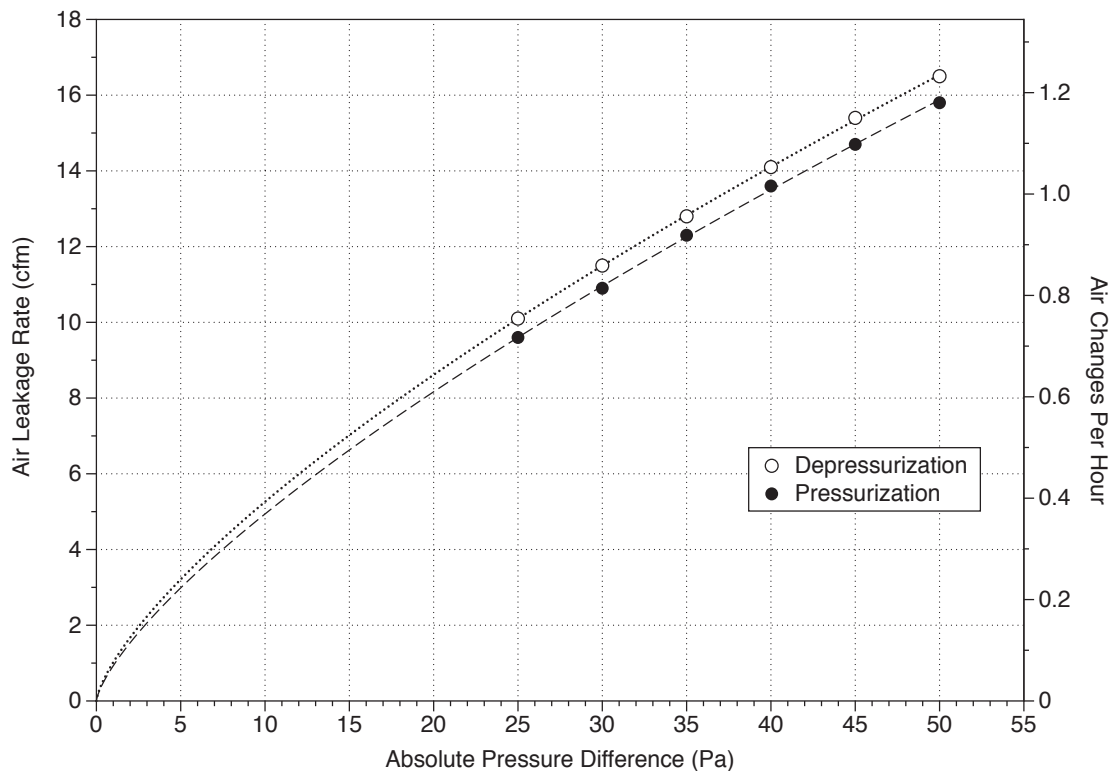
Relative humidity in BIPV/T mechanically ventilated attics with medium air leakage in Iqaluit



Relative humidity in BIPV/T mechanically ventilated attics with high air leakage in Iqaluit

Appendix C Airtightness Tests

An air leakage test using the blower door method is performed on the test hut prior to any testing to ensure airtightness. The test also verified that the sensor wiring in the joints did not affect the airtightness of the test hut. It was found that the hourly air change rate at 50 Pa is 1.18 and 1.23 under pressurization and depressurization, respectively. A full sized house would be expected to have a lower air change rate than those measured for the test hut. The smaller interior air volume to surface area ratio of the test hut is partly responsible for these results. Also, the test hut lacks finishing, which would otherwise contribute to added airtightness.



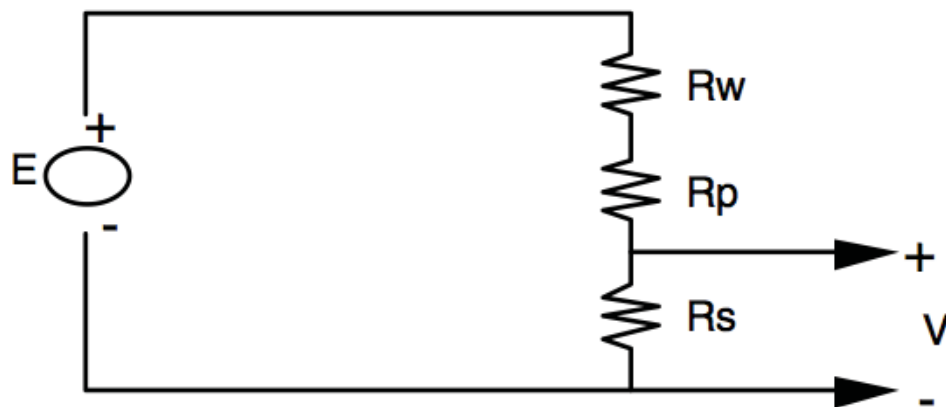
To evaluate the air tightness of the attic space with respect to the outdoors, both the indoor space and the attic space is pressurized and depressurized at 50 Pa. The flow rates required to maintain these pressurized conditions in the attic space are summarized in the following table.

	Depressurization @50 Pa	Pressurization @50 Pa
Attic (6 m³)	0.011 m ³ /s (6.4 ACH)	0.022 m ³ /s (12.9 ACH)

Appendix D Electric MC Measurement Setup

To measure moisture content in wood-based components, home-made moisture content sensors were developed. The setup is based on the methods described by Straube et al. (2002). An Agilent 34970A data acquisition system (DAS) is used to collect the moisture content and temperature readings. The DAS is equipped with a 10 Mohm internal resistor, used to determine the voltage drop across moisture pins. For this project, the moisture pins used are uninsulated steel screws. Readings are done by applying the supply voltage in one direction, then the other. The average of the two readings is the voltage used for calculations. The calculations and programming of the DAS is done using software Keysight VEE.

The method of calculating moisture content is as follows. The electric circuit diagram of the setup is shown below. E is the power source (14.5 V), R_w is the resistance of the wood, R_s is the sensing resistor (10 MOhm), and V is measured voltage drop. In this case, R_p , the protection resistor, is 0 ohm.



Circuit diagram of moisture content sensor system, adopted from Straube et al. (2002)

The electrical resistance of the wood R_w can be calculated using the following equation:

$$R_w = R_s \left(\frac{E}{V} \right) - R_p - R_s$$

Once R_w is obtained, MC_u , the Douglas-Fir moisture content, is calculated.

$$\text{Log}_{10}(MC_u) = 2.99 - 2.113(\text{log}_{10}(\text{log}_{10}(R_w)))$$

To correct for temperature and species, the following equation is used, where MC_c is the corrected moisture content:

$$MC_c = \{[(MC_u + 0.567 - 0.0260 t + 0.000051 t^2)/(0.881(1.0056 t))] - b\}/a$$

t is the temperature of the wood, while a and b are correction factors based on the species of the wood. For this project, the values of a and b were determined by comparing results from gravimetry tests and values from literature. This process is described in the next section.

Calibration

To determine the species corrections for the wood components studied in the experiment, gravimetry measurements are compared with the measured value of MC_u . The gravimetry measurements are done according to ASTM D4442-07 method A (ASTM, 2007). Four samples of each spruce-pine-fir (SPF) wood, plywood and OSB are used. The samples are initially weighed then placed in a 103 °C oven for over 24 hours. The samples are then weighed again to obtain their dry weights. The difference between the initial and

final, dry weight, divided by the dry weight, gives the initial moisture content of the sample.

Before the samples are dried, the MC_u values are measured using the screws and the DAS. For SPF wood, the screws are placed parallel to grain. For plywood, the screws placed parallel to grain of first layer. The temperature of the samples is kept at 21 °C.



The MC_u values are corrected using a number of correction factors obtained from literature (Straube et al., 2002). The corrected values are compared with the gravimetry results, and the correction factors that provide the best results are selected. The table below shows the final selections for the species correction factors.

Wood Component	Species	a	b
SPF Lumber	Northern Alberta Fir	0.985	-1.3
Plywood	Plywood	1.2	0.3666
OSB	OSB	1.1114	0.366

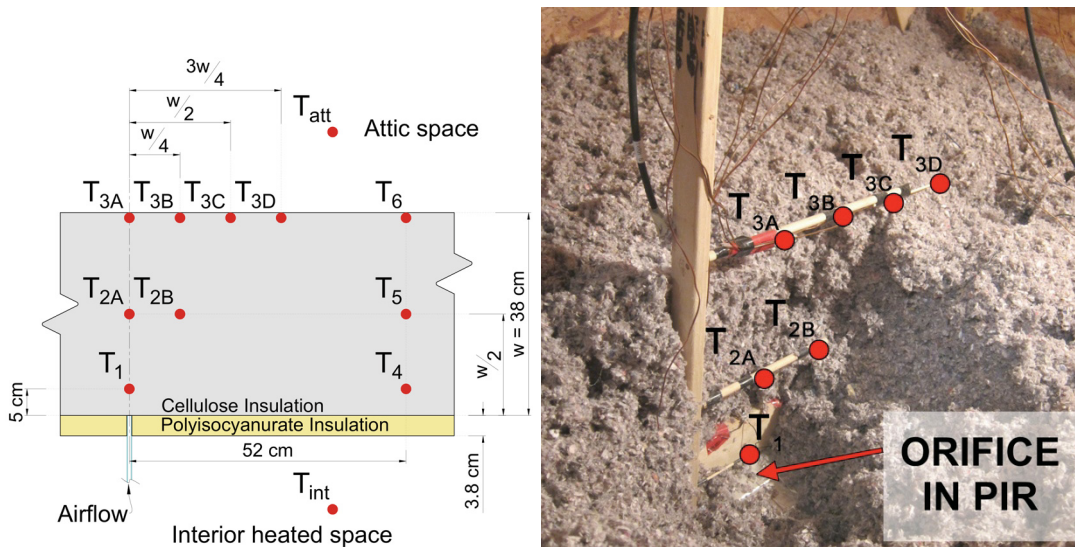
Appendix E Collaboration in Development of Heat-Airflow Model

Airflow Model

For the purpose of validating a heat-airflow model, the test hut was equipped with additional temperature sensors in the ceiling space. Special tests were conducted for this specific purpose.

Instrumentation

The figures below show the location of the temperature and relative humidity sensors in the indoor, ceiling, and attic space.



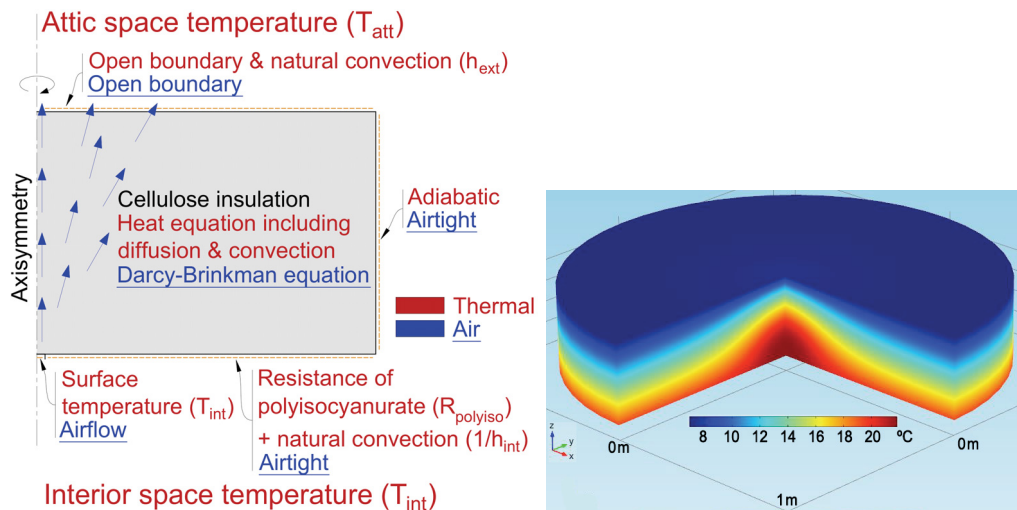
RH/T_{att} and RH/T_{int} are the relative humidity with embedded temperature sensors for the attic and indoor spaces, respectively. A way to indirectly map air leakage through building components is to measure temperature in the vicinity of air leakage path, so the remaining sensors are located within the cellulose insulation at three different heights and at various horizontal distances away from the air leakage orifice in the PIR. T_{3A} and RH/T_6

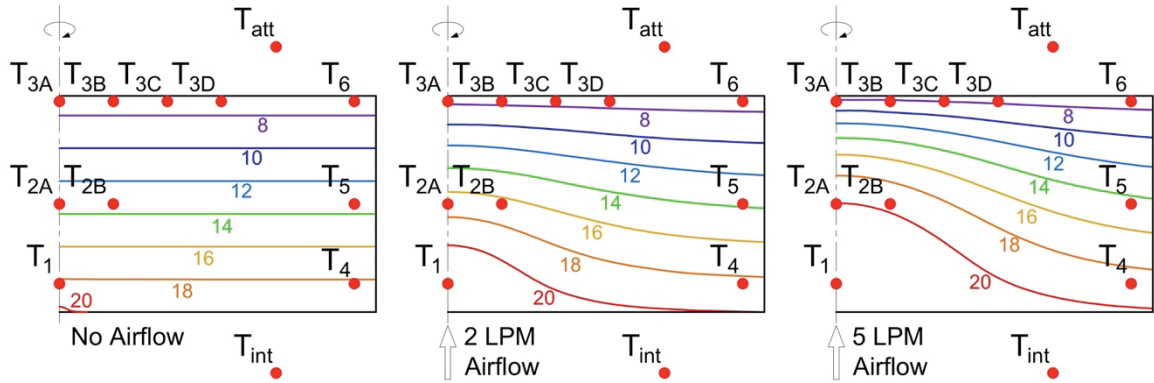
are relative humidity sensors with embedded resistive temperature detectors installed in the top layer of the cellulose. The temperature sensors in the cellulose insulation are supported by a thin wooden structure to ensure proper placement of the sensors without risk of displacement. Horizontal wood members less than 10 mm in diameter support the sensors at each of the three heights in the cellulose insulation; the horizontal members are themselves supported by vertical members at least 100 mm away from the sensors.

Experimental Procedure

The indoor space is maintained at 22_C and 60% relative humidity, while the outdoor space is maintained at 5 °C and 70% relative humidity. Air leakage rates used are 0, 2 and 5 L/min. With the available sampler pumps, it was difficult to ensure constant flow rate below 2 L/min.

The complete details about the heat-airflow model and results obtained can be found in a journal paper published by Belleudy et al. (2015). The figures and table below are a sample the findings from the publication.

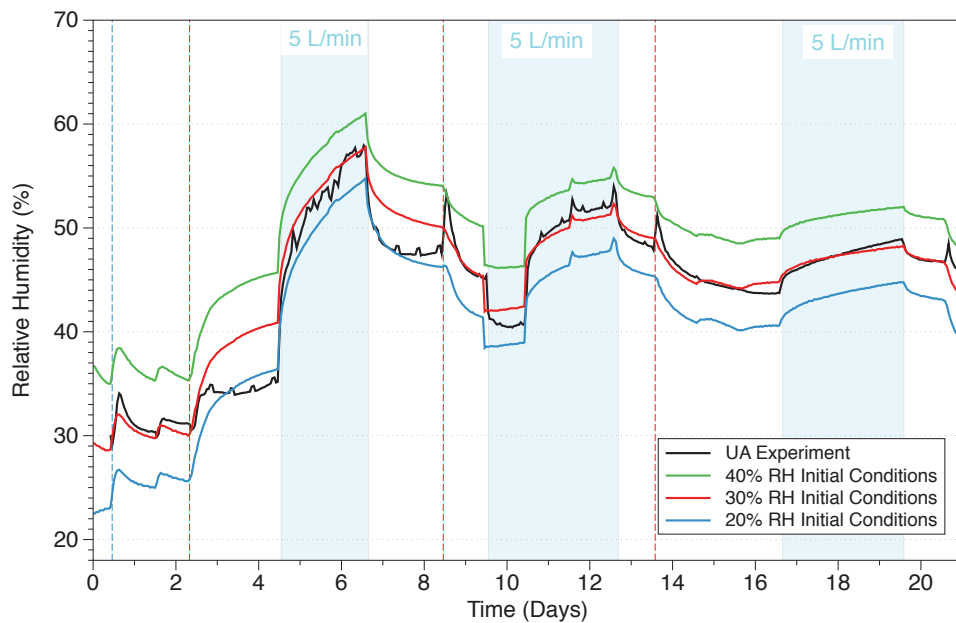




Data Point	Experiment			Simulation		
	No airflow	2 LPM	5 LPM	No airflow	2 LPM	5 LPM
T_{int}	21.9	21.8	21.8	21.9	21.8	21.8
T_1	16.6	20.3	20.8	17.7	21.5	21.8
T_{2A}	12.1	16.1	19.4	13.1	15.9	18.9
T_{2B}	12.1	15.7	19.0	13.1	15.5	18.3
T_{3A}	6.4	6.8	7.9	7.2	7.5	8.0
T_{3B}	6.4	6.6	7.5	7.2	7.5	8.0
T_{3C}	6.4	6.6	7.2	7.2	7.4	7.8
T_{3D}	6.3	6.4	6.8	7.2	7.4	7.6
T_4	16.3	16.9	17.3	17.7	17.9	18.2
T_5	12.0	12.6	13.3	13.1	13.4	13.9
T_6	6.4	6.5	6.6	7.2	7.3	7.4
T_{att}	6.7	6.8	6.8	6.7	6.8	6.8

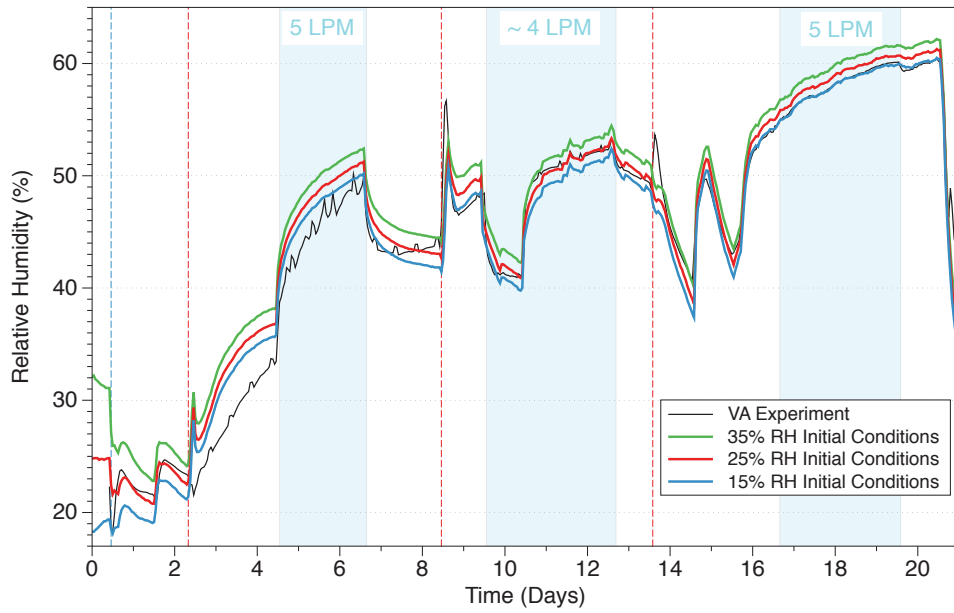
Appendix F Attic Hygrothermal Model Sensitivity Analysis

The WUFI Plus model used to recreate the conditions of the experimental test (Test 2) is highly detailed with many input parameters, most of which were not measured in the experiment. The main known input parameters are the indoor and outdoor temperatures, as well as the initial conditions. Unknown input parameters include material properties, actual air exchange rates between the attics and the outdoor space, and many more. This section provides a sample of the results of a sensitivity analysis performed to compare the effects of varying these parameters.



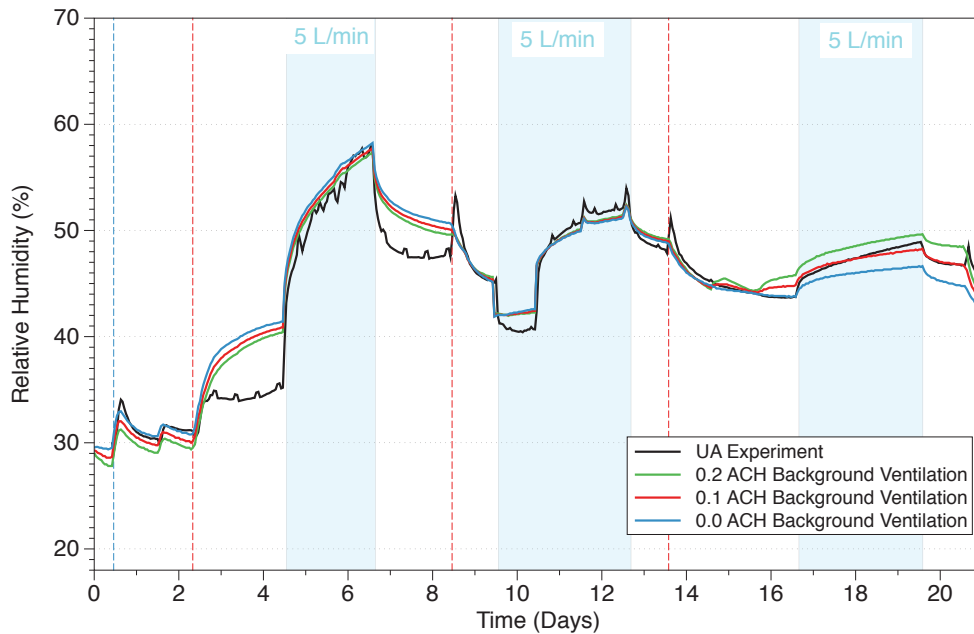
Effect of varying the initial moisture content of UA materials

The unvented attic is highly sensitive to the initial moisture conditions since the moisture is removed from the space mainly by diffusion, which is a very slow process.



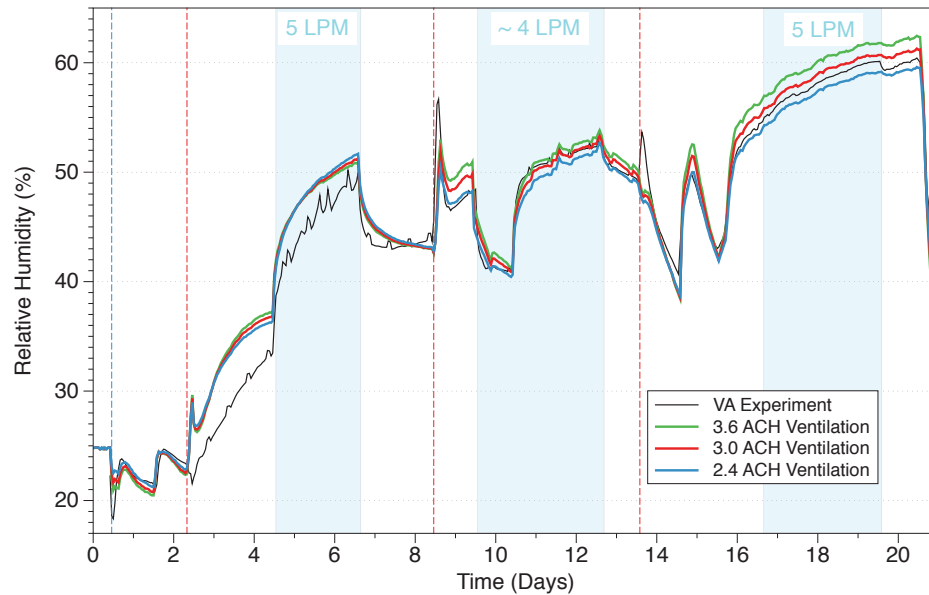
Effect of varying the initial moisture content of VA materials

The ventilated attic, on the other hand is much less affected by changes in the initial moisture content since moisture is readily removed from the space.



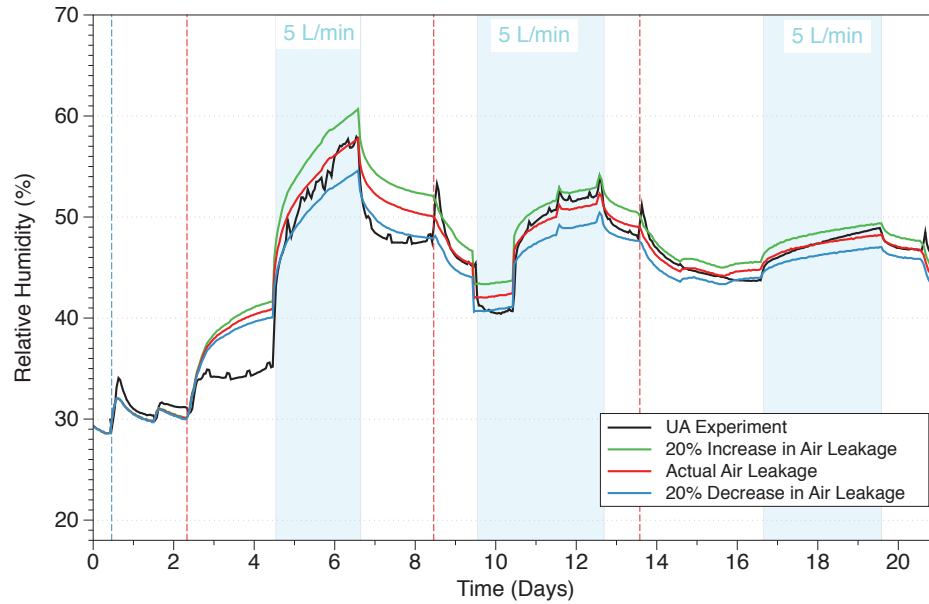
Effect of varying the background ventilation rate of UA

Varying the background, unintentional ventilation by increments of 0.1 ACH in the unvented attic has a slight effect on the RH conditions in the attic. The impact is more pronounced in the warm phase of the test (the last portion), since the humidity ratio in the EC is much higher in that phase. A maximum difference of 3% is observed.



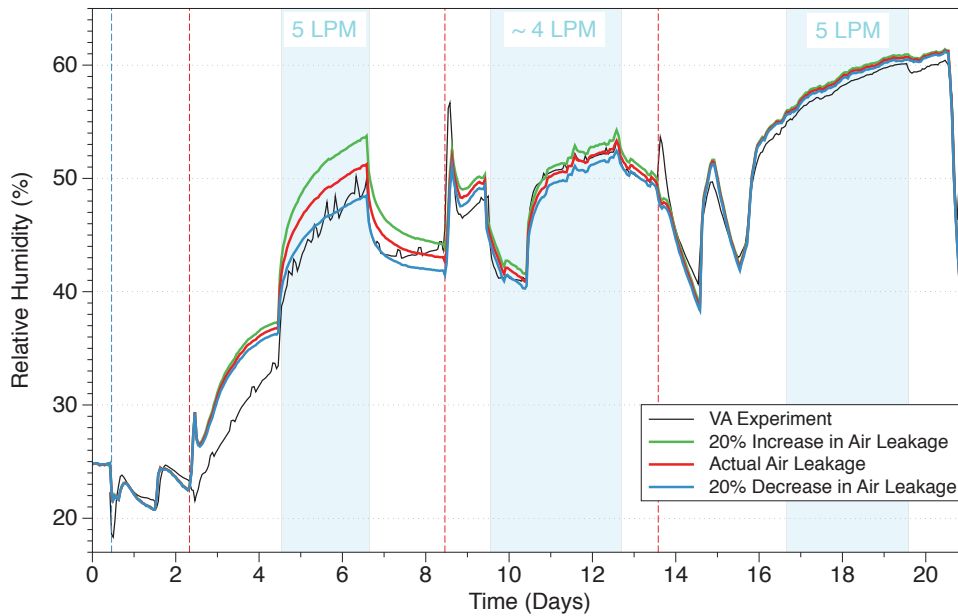
Effect of varying the mechanical ventilation rate of VA

Varying the mechanical ventilation rate in the VA by $\pm 20\%$ (± 0.6 ACH) has a minor effect on the RH conditions. Again, the influence is greatest during the warm phase of the test. A maximum difference of less than 2% is observed.



Effect of varying the air leakage rate in UA

Changing the air leakage rate by $\pm 20\%$ has a notable effect on the RH of the unvented attic. The effect is most pronounced during the coldest (first) phase of the test. A maximum difference of 3% is observed.



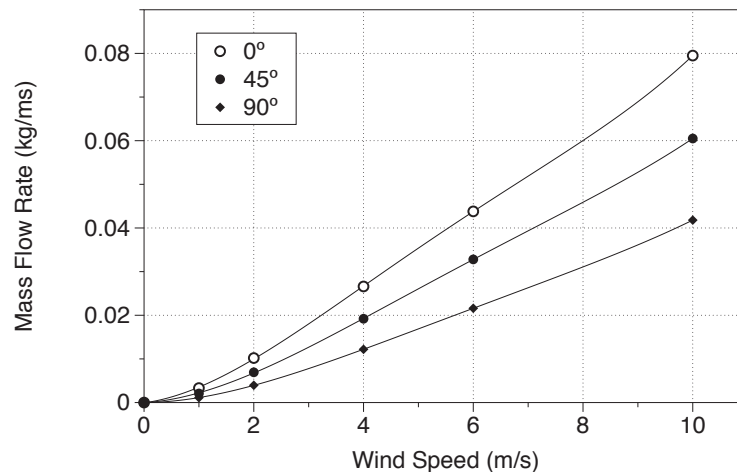
Effect of varying the air leakage rate in VA

Varying the air leakage rate in the ventilated attic has similar effect as with the unvented attic during the first, cold phase of the test, since ventilation has limited capacity to remove moisture. However, in the warmer phases of the test, the effect air leakage rate variation is diminished.

Appendix G Natural Ventilation CFD Analysis Results

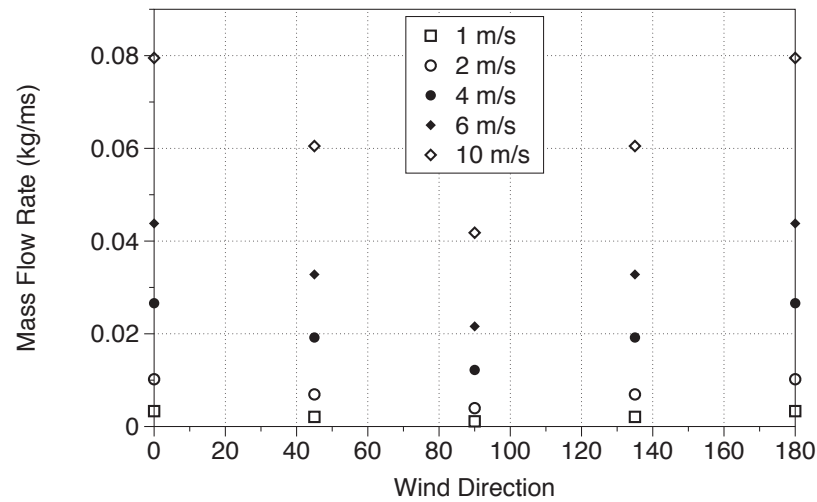
To approximate the rate of natural ventilation of Arctic climates, a computational fluid dynamics (CFD) analysis is performed because of the unique attic ventilation configuration used in the north. The details of the CFD model setup and analysis can be found in Kayello et al. (2016). A brief sample of the results of the study are presented below.

A summary of the ventilation rate results can be found below. The flow rate is in the unit kg/ms because the simulation is in two dimensions. As expected higher wind speeds correspond to higher ventilation rates of the attic space. As the wind direction deviates from normal (0°) to 90° , the ventilation rate decreases. This is understood because the wall openings are on the south and north sides of the house and so winds perpendicular to the opening exhibit less pressure on the openings. This makes the relationship between wind speed and ventilation rate rather interesting.



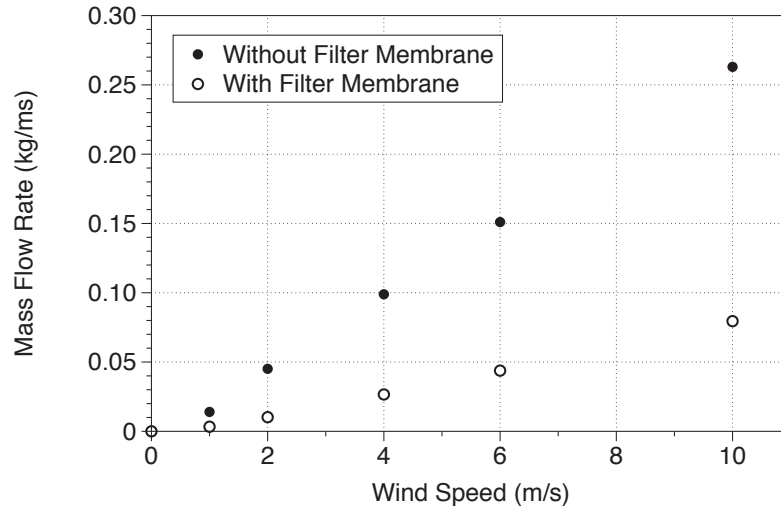
Effect of wind speed and direction on attic ventilation rates

The figure below is a representation of the data where the wind direction is on the x-axis. Considering symmetry, the data is extended to 180°, though it can be further extended to 360°. As can be seen in the figure, the plot points for each wind speed can approximated by sin curves. Therefore, empirical equations can be developed to express the relationship between wind speed, direction, and ventilation rate.



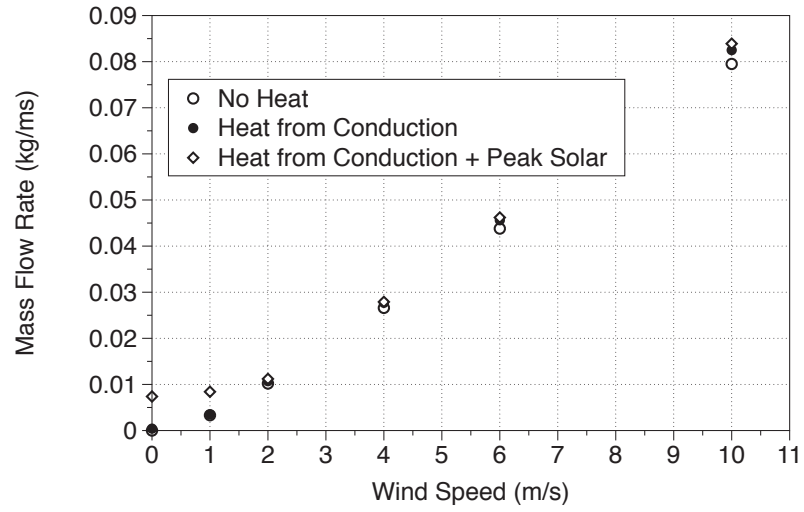
Ventilation rate vs. wind direction

The figure below shows the effect of the porous filter membrane in the wall cavity on the attic ventilation rates. Generally, the ventilation rates are reduced by a factor of 3 with the porous material, based on the assumed characteristics of the material. This is quite significant and can have a significant impact on the hygrothermal performance of an attic.



Effect of porous membrane of ventilation rates

The overall ventilation rates of the attic comparing the effect of considering heat and solar radiation are shown in the figure below. Consistently, accounting for heat transfer in the system increases the ventilation rate in the attic. Adding solar radiation increases it even further. However, in both cases the increase is very marginal if there is wind. If heat conduction is considered without solar radiation, the ventilation rates are also marginally increased. The one interesting condition is when the wind speed is below 2 m/s while heat conduction and solar radiation are considered. The high temperatures achieved in the wall cavity, because of lack of wind, drive the air significantly and a ventilation rate of almost 0.074 kg/ms is observed with no wind and 0.084 kg/ms with 1 m/s wind. This shows that solar driven ventilation should be accounted for at very low wind speeds. However, it must be investigated how often it occurs that the wind speed is low while it is sunny. In Iqaluit, wind speeds lower than 3 m/s overlapping with direct solar radiation higher than 300 W/m^2 occur less 8% of the time.



Effect of heat conduction and solar radiation on ventilation rate